THE ASTROPHYSICAL JOURNAL SUPPLEMENT SERIES, 136:463–535, 2001 October

DISTANCES AND METALLICITIES OF HIGH- AND INTERMEDIATE-VELOCITY CLOUDS

B. P. WAKKER

Department of Astronomy, University of Wisconsin, 475 N. Charter Street, Madison, WI 53706; wakker@astro.wisc.edu
Received 2000 July 26; accepted 2001 March 1

ABSTRACT

A table is presented that summarizes published absorption line measurements for the high- and intermediate-velocity clouds (HVCs and IVCs). New values are derived for N(H I) in the direction of observed probes, in order to arrive at reliable abundances and abundance limits (the H I data are described in Paper II). Distances to stellar probes are revisited and calculated consistently, in order to derive distance brackets or limits for many of the clouds, taking care to properly interpret nondetections. The main conclusions are the following. (1) Absolute abundances have been measured using lines of S II, N I, and O I, with the following resulting values: ~0.1 solar for one HVC (complex C), ~0.3 solar for the Magellanic Stream, ~0.5 solar for a southern IVC, and ~solar for two northern IVCs (the IV Arch and LLIV Arch). Finally, approximate values in the range 0.5–2 solar are found for three more IVCs. (2) Depletion patterns in IVCs are like those in warm disk or halo gas. (3) Most distance limits are based on strong UV lines of C II, Si II, and Mg II, a few on Ca II. Distance limits for major HVCs are greater than 5 kpc, while distance brackets for several IVCs are in the range 0.5–2 kpc. (4) Mass limits for major IVCs are 0.5–8 × 10^5 $M_\odot$, but for major HVCs they are more than 10^6 $M_\odot$. (5) The Ca II/H I ratio varies by up to a factor 2–5 within a single cloud, somewhat more between clouds. (6) The Na I/H I ratio varies by a factor of more than 10 within a cloud, and even more between clouds. Thus, Ca II can be useful for determining both lower and upper distance limits, but Na I only yields upper limits.

Subject headings: Galaxy: halo — ISM: abundances — ISM: clouds — ISM: structure — radio lines: ISM — ultraviolet: ISM

On-line material: machine-readable tables

1. INTRODUCTION

The high- and intermediate-velocity clouds (HVCs and IVCs) consist of gas moving at velocities incompatible with a simple model of differential galactic rotation (Wakker 1991). An operational definition has been that HVCs have velocities larger than ~90 km s^{-1} (positive or negative) relative to the LSR. The definition of IVCs has been less strict. In this paper they are defined as clouds with velocities relative to the LSR between ~40 and 90 km s^{-1}. In a few directions slightly lower velocities are included, if there is a clear connection with gas at higher velocities. This definition excludes many clouds with $|v_{\rm LSR}| < 40$ km s^{-1} that were considered an IVC by other authors, but in most cases these have ill-defined borders and often such velocities can be understood within the framework of differential galactic rotation, after allowing for turbulent velocities of up to 30 km s^{-1}.

The HVCs and IVCs are still poorly understood, although much progress has been made in the most recent decade. They appear to serve as tracers of energetic processes in the Galactic Disk and Halo (as part of a "Galactic Fountain"), but also as an ingredient in the continuing formation of the Galaxy (some are examples of accreting gas). Finally, some may be tidal remnants (most prominently the Magellanic Stream) or isolated clouds in the Local Group. A review of our understanding as of a few years ago was presented by Wakker & van Woerden (1997); an update has already proven necessary (Wakker, van Woerden, & Gibson 1999b). Ever since the discovery of the HVCs (Muller, Oort, & Raimond 1963), it has been clear that the key to a proper understanding lies in using interstellar absorption lines to determine distances (and metallicities) for this class of clouds. Thus, some of the recent progress has come from new models and improved mapping, but most has come from new observations of interstellar absorption lines.

Mapping.—The published HVC all-sky maps (Hulsbosch & Wakker 1988; Bajaja et al. 1985) have proven very useful to understand the properties and statistics of the HVCs. However, both these surveys suffer from low velocity resolution (16 km s^{-1}) and incomplete mapping. The Hulsbosch & Wakker (1988) survey covered the sky north of declination −18° on a 1° grid with a 0.°5 beam, but the southern survey of Bajaja et al. (1985) suffered from lack of coverage (2° grid with a 0.°5 beam) (although Bajaja et al. 1989 mapped selected areas on a 0.°5 grid). IVC maps have only been presented for the "Intermediate-Velocity Arch," a large structure crossing the northern Galactic sky at latitudes greater than 30° (Kuntz & Danly 1996). This paper was based on the data in the "Bell Labs Survey" (Stark et al. 1992), which has a 3° beam and 1 km s^{-1} velocity resolution).

New data sets allow great improvements in mapping, especially for IVCs and southern HVCs. (a) The Leiden-Dwingeloo Survey (LDS) (Hartmann & Burton 1997), covers the sky north of declination −35° on a 0.°5 grid with 1 km s^{-1} velocity resolution. (b) The HVC survey made at the "Instituto Argentina de Radioastronomia" (IAR) (Morras et al. 2000) provides a list of H I components with $|v_{\rm LSR}| > 80$ km s^{-1} for declinations south of −23° on a 0.°5 grid, extracted from spectra with 16 km s^{-1} velocity resolution. (c) The H I Parkes All-Sky Survey (HIPASS) (Staveley-Smith 1997) covers the sky south of declination 0° on a 14.′4 grid with 26 km s^{-1} velocity resolution. (d) The Parkes Narrow Band Survey (Haynes et al. 1999; Brüns, Kerp, & Staveley-Smith 2001) covers the Magellanic Stream (both trailing and leading parts) on a 14.′4 grid with 1 km s^{-1} velocity resolution. This paper presents new IVC maps based on the LDS, and new maps for southern HVCs based on the IAR list. The LDS and both Parkes surveys are further used to construct H I spectra toward HVC and IVC probes.

Models.—Gardiner & Noguchi (1996) presented a modern version of the model in which the Magellanic Stream is formed by tidal stripping. Combined with the observational identification of the predicted leading arm by Lu et al. (1998) and Putman et al. (1998), this has led to a better understanding of the Stream and of which other HVCs could be part of the same tidal feature. Blitz et al. (1999) suggested that the majority of the HVCs are remnants of the formation of the Local Group and are similar to the original building blocks of the Milky Way and the Andromeda Nebula. Braun & Burton (1999) presented a variant of this interpretation, in which only some small HVCs are Local Group clouds. These models contrast with previous ones in which the HVCs/IVCs are generated in a Galactic Fountain (Bregman 1980) or are remnants of the formation of the Milky Way (Oort 1970). It now appears that examples of at least three (and possibly all four) of the proposed origins can be found (see, e.g., Wakker et al. 1999b).

Absorption-line studies.—Metallicities and distances are best determined using absorption-line studies, both in the optical and the ultraviolet. In the future, the optical emission lines of [S II] and Hα may prove useful (Tufte, Reynolds, & Haffner 1998; Bland-Hawthorn & Maloney 1999), but their potential has not yet been realized. Most HVC/IVC metallicity and distance estimates are fairly recent, with half of the relevant papers published since 1994. This is partly due to the availability of the Goddard High Resolution Spectrograph (GHRS), the Space Telescope Imaging Spectrograph (STIS), and the *Far-Ultraviolet Spectroscopic Explorer* (*FUSE*), and partly to an increase in sensitivity of ground-based telescopes. A table of detections of absorptions associated with HVCs was presented by Wakker & van Woerden (1997). Several major discoveries have been made since. This paper aims at summarizing all relevant literature pertaining to deriving distances and metallicities for HVCs and IVCs.

Many of the papers in the literature discuss the implications of absorption-line detections and nondetections for deriving distance brackets or limits. Here a consistent set of criteria was applied to (re)derive these distance brackets and limits. In general, the conclusions agree with the original papers, but some new limits are found, and some are shown to have been in error. For this reanalysis, consistent distances were determined for the stellar probes (see description of col. [5] in the Appendix), and all published equivalent widths and logarithmic column densities were converted to column densities (see description of col. [13]). Further, improved H I data were obtained for almost all sight lines, superseding the published value for directions to probes (see description of cols. [8]–[10]). For about 50% of the probes new Effelsberg H I data were obtained, which are presented in a companion paper (Wakker et al. 2001a, hereafter Paper II). For about 25% of the probes, N(H I) is based on the LDS. The remainder are based on (refitted) published spectra, either of the two new Parkes surveys or (in a small number of cases) on published numbers. These H I column densities were used to rederive absolute and relative (to solar) abundances (see description of cols. [15]–[17]). Finally, a consistent set of criteria was applied to determine the significance of nondetections used to derive lower distance limits (see description of col. [18]).

This paper is organized as follows: first, a general overview is given of the format of the main Table 2 (§ 2). In § 3 a short discussion is given of the abundance results for the individual ions. Section 4 summarizes the derived distance limits, metallicities and abundance patterns for each of the clouds for which relevant information is known, and § 5 presents a final analysis. The values in each column of the main table are described in detail in the Appendix.

2. GENERAL DESCRIPTION OF THE TABLE

Table 1 provides an index to the main table (Table 2), to help find particular clouds or probes. The first part of this table lists the HVC and IVC names and the table page on which results for each cloud can be found. For a number of clouds an abbreviation is given in parentheses [e.g., "(=CHS)"]. This is used in the second part of the index, which lists the clouds seen toward each individual stellar or extragalactic target.

Table 2 lists the published results for all probes of each HVC/IVC, sorted by cloud. Results are given for seven HVC complexes, seven IVC complexes, and 21 smaller HVCs/IVCs. In the complexes a total of 47 cores have been observed. In addition there are 21 unnamed clouds, which often are only seen in absorption. Data are given for 326 different targets (stars and AGNs), with 1078 entries, one for each observation of an ion. Stars less distant than $\sim$0.2 kpc were excluded to avoid including many nearby stars that provide little distance information (i.e., neither upper nor lower limits).

The classical HVCs (A, M, C, H, Anti-Center—see Wakker & van Woerden 1991) are listed first, followed by the GCN and GCP complexes, the Outer Arm, the Magellanic Stream and the smaller HVC complexes. A new HVC complex (complex WE) is introduced here (see § 4.19). Next follow results for the +165, +120, and +65 km s^{-1} clouds projected onto the LMC. Then the classical IVCs (IV Arch, LLIV Arch—see Kuntz & Danly 1996) are listed, followed by other IVC complexes, including three named ones that are introduced in this paper: "K," the "PP Arch," and "gp"—see §§ 4.27, 4.28, and 4.29.

For most clouds the table first gives a summary of measured and expected abundances for each of the ions observed in the cloud. Also, on the first two lines for each cloud, the derived metallicity and upper/lower distance limit are summarized, if known. Details of the method used to derive these limits can be found in the Appendix under the description of columns (4) and (18).

If an abundance was actually measured for a particular ion, that value is listed in column (15) in the cloud summary lines. For the few cases where multiple determinations for one ion were made in the same cloud, the average value is listed (using only the higher quality measurements). A discussion of these abundances is provided in §§ 3 and 4.

Column (16) lists the expected ion abundances in square brackets, but only for ions that are the dominant ionization stage in the diffuse ISM. These values are used to determine whether nondetections are significant and can be used to set a lower distance limit. Expected abundances are derived by assuming an overall abundance level combined with a halo depletion pattern, as given by Savage & Sembach (1996a); see § 3 for a more detailed description. For the highly ionized ions (C IV, N V, O VI, Si IV) a "typical" value is

TABLE 1

Index to Main Table

1........................	A, MI, IV4, WW63	15........................	LMC-HVC @+120 (=LMm)
2........................	MII, CI	16........................	LMC-IVC @+120 (=LMm), @+60 (=LMl)
3........................	CI, CIII, C-south	17........................	LMC-IVC @+60 (=LMl)
4........................	C-extension, C/K, G	18........................	LMC-IVC @+60 (=LMl)
5........................	H	19........................	LMC-IVC @+60 (=LMl)
6........................	AC shell (=ACS) AC0, ACI, ACII, Cohen Stream (=CHS)	20........................	IV7, IV6, IV17, IV11
7........................	CHS, WW507, Other AC, GCN CHS, WW507, Other AC, GCN	21........................	IV9, IV15, Upper IV-Arch (=IVupp), IV24, IV26, IV21, IV19
8........................	GCN, GCP, Outer Arm (=OA), R	22........................	Lower IV-Arch (=IVlow)
9........................	Magellanic Stream (=MS)	23........................	IV spur, LLIV
10........................	Pop. EP, Pop. EN	24........................	LLIV, K
11........................	L, WB, WE, positive-velocity HVCs (=wa/wb)	25........................	PP-Arch (=PP), southern IVCs (=IV south)
12........................	faint HVCs (=fHVC)	26........................	gp
13........................	LMC-HVC @+160 (=LMh)	27........................	Other neg-vel HVCs (=on), Other pos-vel HVCs (=op)
14........................	LMC-HVC @+160 (=LMh), @+120 (=LMm)		

0159+625	H	BR UMa	MI	HD 100340	IV spur, op
0224+671 (4C 67.05)	H	BS 16034−0002	CI	HD 100600	IV spur
0239+108 (4C 10.08)	WW507	BS 16034−0114	CI	HD 100971 (SU Dra)	CIII
0300+470 (4C 47.08)	H	BS 16079−0015	CI, IV15	HD 101075	CIII, IV21
0428+20 (PKS 0428+205)	Other AC	BS 16079−0017	CI	HD 101274	WW187,on,op
0538+498 (3C 147.0)	OA	BS 16086−0123	CI	HD 101714	IV21
0959+68W (FBS0959+685)	C-south	BT Dra	CI, IV15	HD 102383	WW187
1749+096 (4C 09.57)	C-extension	Barnard 29	K	HD 103718	CIII, IV21
1828+487 (3C 380.0)	OA	CTA 21	Other AC	HD 105058	IV4, IV17
1829+29 (4C 29.56)	OA	CTA 102	MS	HD 106420	IV4, IV17
1901+319 (3C 395)	OA	FBS 0959+685(0959+685)	C-south	HD 121800	IV9, IV19
1928+738 (4C 73.18)	OA	Fairall 9	MS	HD 127557	CIII, IV9
2037+511 (3C 418)	OA	Feige 40	IV spur	HD 135485	L
2331+073	MS	Feige 87 (PG 1338+611)	CIII, IV19	HD 137569	on
3C 33	IV-south	Hiltner 190 (LS I +62 200)	H	HD 146813	CI
3C 41	IV-south	Hiltner 198 (LS I +61 251)	H	HD 156110	C-extension,op
3C 75	CHS	HD 108	H	HD 156359	WE
3C 78	CHS	HD 1383	H	HD 173011	GCN
3C 109	Other AC	HD 2619	H	HD 176502	OA
3C 123	ACS	HD 3175	MS	HD 178329	OA
3C 147.0 (0538+498)	OA	HD 10125	H	HD 187350	GCN, GCP
3C 200	wa/wb	HD 12323	H	HD 188350	GCN, GCP
3C 206 (PKS 0837−12)	WB	HD 12567	H	HD 188859	GCP
3C 263.0	CIII	HD 12993	H	HD 189818	OA
3C 351.0	CI	HD 13256	H	HD 203664	gp
3C 380.0 (1828+487)	OA	HD 14069	CHS	HD 203699	IV-south, gp
3C 382	OA	HD 14633	IV-south	HD 205021	OA
3C 386	OA	HD 14947	H	HD 205556	gp
3C 395 (1901+319)	OA	HD 14951	CHS, WW507	HD 212593 (4 Lac)	G, fHVC
3C 418 (2037+511)	OA	HD 15629	H	HD 215733	PP
3C 454.3	MS	HD 16581	IV-south	HD 219188	MS
4C 06.41	wa/wb	HD 16582	Other AC	HD 220172	MS
4C 09.57 (1749+096)	C-extension	HD 17473	CHS, WW507	HD 223987	H
4C 10.08 (0239+108)	WW507	HD 17481	CHS, WW507	HD 225160	H
4C 29.56 (1829+29)	OA	HD 17505	H	HDE 233622(BD +50°1631)	LLIV
4C 33.48	OA, R	HD 17520	H	HDE 233791(AG +53°783)	IVlow
4C 47.08 (0300+470)	H	HD 17907	CHS, WW507	HDE 236894	H
4C 67.05 (0224+671)	H	HD 18059	CHS, WW507	HDE 237844(BD +56°1411)	LLIV
4C 73.18 (1928+738)	OA	HD 18910	CHS, WW507	HDE 241573	ACI, ACII
4 Lac (HD 212593)	G, fHVC	HD 32641 (SAO 76954)	ACI, ACII	HDE 241597	ACI, ACII
AD UMa	A	HD 33090 (SAO 76980)	ACI, ACII	HDE 241882	ACI, ACII
AG +53°783 (HDE 233791)	IVlow	HD 33233 (SAO 76994)	ACI, ACII	HDE 248894	ACS
B2 1607+26	K	HD 33415 (SAO 76016)	ACI, ACII	HDE 252550	AC0
BA 90700003	IVupp	HD 36402 (Sk −67°104)	LMm, LMl	HDE 252605	AC0
BD +10°2179	wa/wb	HD 38268 (Sk −69°243)	LMh, LMm, Lml	HDE 253069	AC0
BD +36°2268 (HZ 25)	IVlow	HD 38282 (Sk −69°246)	LMm, LMl	HDE 255055	ACS
BD +38°2182	MII,IV6,IVlow,op	HD 42904	AC0	HDE 256035	ACS
BD +49°2137	IV4, IV17	HD 45314	ACS	HDE 256725	ACS
BD +50°1631 (HDE 233622)	LLIV	HD 68164	A, LLIV	HDE 269546 (Sk −68°82)	LMm, LMl
BD +56°1411 (HDE 237844)	LLIV	HD 75855	A	HS 0624+6907	OA
BD +59°367	H	HD 76593 (SAO 14733)	A	HZ 22 (PG 1212+369)	IVupp, IV26
BD +62 338	H	HD 77770	A, LLIV	HZ 25 (BD +36°2268)	IVlow
BD +63 253	H	HD 83206	WW63, LLIV, on	H 1821+643	OA
BD +63 985	CIII, IV21	HD 86248	WW211	H. O. +23B (PG 1205+228)	IV spur
BD +67 598	LLIV	HD 87015	IV24	H. O. +41B	IV26
BD +75 306 (SAO 6225)	A	HD 93521	MII,IV6,IVlow,op	H. O. +43B (PG 1205+228)	IV spur
BD +75 310 (SAO 6253)	A	HD 98152	IV26	III Zw 2 (PG 0007+106)	MS

TABLE 1—*Continued*

IU Cas	G	PKS 0003+15	MS	Sk −66°169	LMm
I Zw 18 (Mrk 116)	A	PKS 0103−453	MS	Sk −67°05	LMm, LMl
LH 10 3120	LMm, LMl	PKS 0202+14	CHS	Sk −67°104 (HD 36402)	LMm, LMl
LS I +61 251 (Hiltner 198)	H	PKS 0202−76	MS	Sk −67°120	LMm, LMl
LS I +62 200 (Hiltner 190)	H	PKS 0232−04	fHVC	Sk −67°166	LMh, LMm, LMl
M13 stars	K	PKS 0252−712	MS	Sk −67°169	LMm, LMl
M15 stars	gp	PKS 0407−658	MS	Sk −67°174	LMl
Mrk 106	A, LLIV	PKS 0409−752	MS	Sk −67°250	LMl
Mrk 116 (I Zw 18)	A	PKS 0428+205 (0428+20)	Other AC	Sk −68°82 (HD 269546)	LMm, LMl
Mrk 205	C-south, EN	PKS 0637−75	MS	Sk −68°114 (R 116)	LMl
Mrk 279	C-south	PKS 0837−12 (3C 206)	WB	Sk −68°135	LMh, LMl
Mrk 290	CI	PKS 1136−13	wa/wb	Sk −68°137	LMh
Mrk 501	C-extension, K	PKS 1739+17	C-extension	Sk −69°51	LMh
Mrk 509	GCN, gp	PKS 1741−038	C-extension	Sk −69°52	LMh
Mrk 595	CHS	PKS 1820+17	OA	Sk −69°91	LMm, LMl
Mrk 817	CI	PKS 1923+210	EN	Sk −69°103	LMl
Mrk 876	CI, C-south	PKS 2155−304	GCN	Sk −69°104	LMl
NGC 1705	WW487	PKS 2243−123	MS	Sk −69°106	LMh, LMl
NGC 2808	op	PKS 2251+11	MS	Sk −69°107	LMh, LMl
NGC 2841 UB3	A	PKS 2340−036	MS	Sk −69°195	LMm, LMl
NGC 3783	WW187, on, op	PKS 2344+09	MS	Sk −69°203	LMm, LMl
NGC 7469	MS	PKS 2345−167	MS	Sk −69°204	LMm, LMl
OW Her	C-extension	QSO 1637+574	CI	Sk −69°211	LMh, LMm, LMl
PG 0007+106 (III Zw 2)	MS	QSO 1732+389	C-extension	Sk −69°213	LMm, LMl
PG 0039+048	MS, PP	QSO 2005+403	OA	Sk −69°215	LMm, LMl
PG 0039+134	IV-south	QSO 2200+420	G	Sk −69°216	LMh, LMm, LMl
PG 0043+039	MS	RS Cas	H	Sk −69°220 (R 127)	LMl
PG 0229+064	op	R 116 (Sk −68°114)	LMl	Sk −69°221 (R 128)	LMl
PG 0804+761	LLIV	R 127 (Sk −69°220)	LMl	Sk −69°224	LMm, LMl
PG 0832+675	A, LLIV	R 128 (Sk −69°221)	LMl	Sk −69°225	LMm, LMl
PG 0833+698	LLIV	R 134	LMl	Sk −69°239	LMm, LMl
PG 0859+593	A, LLIV	R 136 (Sk −69°243)	LMh, LMm, LMl	Sk −69°243 (HD 38268)	LMh, LMm, LMl
PG 0906+597	A, LLIV	R 137	LMl	Sk −69°246 (HD 38282)	LMm, LMl
PG 0953+414	fHVC, IVlow	R 139	LMl	Sk −69°247	LMm, LMl
PG 0955+291	IV7, IVlow	R 140	LMl	Sk −69°248	LMl
PG 1008+689	LLIV	SA 12 391	A, LLIV	Sk −69°255	LMl
PG 1116+215	fHVC	SAO 6225 (BD +75 306)	A	Sk −69°270	LMl
PG 1126+468	MI, IV17	SAO 6253 (BD +75 310)	A	Sk −69°274	LMm, LMl
PG 1205+228 (H. O. +23B)	IV spur	SAO 14733 (HD 76593)	A	Sk −69°276	LMh, LMl
PG 1212+369 (HZ 22)	IVupp, IV26	SAO 76016 (HD 33415)	ACI, ACII	Sk −69°282	LMh, LMm, LMl
PG 1213+456	IV4, IV17, IVlow, op	SAO 76954 (HD 32641)	ACI, ACII	Sk −69°289	LMl
PG 1255+546	IV11, IVlow	SAO 76980 (HD 33090)	ACI, ACII	Sk −69°290	LMh, LMm, LMl
PG 1259+593	CIII, IVlow	SAO 76994 (HD 33233)	ACI, ACII	Sk −70°111	LMm, LMl
PG 1338+611 (Feige 87)	CIII, IV19	SN 1981D	on	Sk −70°115	LMl
PG 1351+640	CI, CIII, IV9, IV19	SN 1983N	fHVC, op	Sk −71°3	LMm, LMl
PG 1510+635	CI	SN 1986G	fHVC, op	Sk −71°33a	LMm, LMl
PG 1519+640	CI	SN 1987A	LMh, LMm, LMl	Sk −71°41	LMm, LMl
PG 1619+522	C/K	SN 1991T	wa/wb, fHVC	Sk −71°42	LMm, LMl
PG 1648+536	CI, C-south	SN 1993J	fHVC, LLIV	Sk −71°45	LMm, LMl
PG 1700+518	C-extension	SN 1994D	fHVC	Ton S180	MS
PG 1708+602	C-south	SN 1994I	fHVC	Ton S210	MS
PG 1710+490	C-extension, C/K,op	SN 1998S	IV4, IV17, op	V421 Her	C-extension, op
PG 1718+481	C-extension	SU Dra (HD 100971)	CIII	vZ 1128	on
PG 1722+286	C-extension, K	SW Dra	C-south		
PG 1743+477	C-extension, C/K	Sk −65°40	LMl		
PG 2302+029	MS	Sk −66°28	LMl		
PG 2337+070	MS	Sk −66°118	LMm, LMl		

shown within square brackets in column (13); this serves as a point of comparison for the value observed in the HVC.

The overall abundance is assumed to be near solar, unless shown otherwise in the notes column (col. [20]), on the first line pertaining to the cloud. A number followed by $Z_{\odot}$ in the notes column indicates that the abundance has actually been measured. This is the case for complex MI (0.8 solar), complex CI (0.1 solar), the Magellanic Stream (0.25 solar), the PP Arch (0.5 solar), IV6, IV9, IV19 (1 solar), and the LLIV Arch (1 solar). Parentheses around the abundance indicates clouds where an abundance different from solar is suspected, but not directly proven.

After the cloud summary, the table lists the individual observations relevant for that cloud. In many cases the sight line to a probe intersects more than one cloud, so that one probe may be listed under two, three, or even four different clouds (see Table 1).

Probe	l °	b °	d kpc	z kpc	type	Cld	v_{HI} km/s	N_{HI} 10^{18} cm^{-2}	tel	ion	v_{ion} km/s	N_{ion} 10^{11} cm^{-2}	code	A_{ion} 10^{-9}	A_{ref} 10^{-9}	A/A$_\odot$	D?	Ref	Note
(1)	(2)	(3)	(4)	(5)	(6)	(7)	(8)	(9)	(10)	(11)	(12)	(13)	(14)	(15)	(16)	(17)	(18)	(19)	(20)
Complex A			<9.9	<6.8						OI				4.6E4 ±4.8E4	[74000]	0.062			(0.1$Z_\odot$)
			>4.0	>2.6						NaI									
										SiII				5200 ±4500	[1900]	0.15			
										MgII				>1300	[1400]	>0.034			
										CaII				19 ±5	[22]	0.0087			
Mrk 106	161.14	42.88	—	—	Sey	AVI	−157	38 ±3	WE	MgII	−157	>500	N	>1300		>0.035		87	
										CaII	−157	6.7 ±2.3	N	18 ±6		0.0081		70	
I Zw 18	160.53	44.84	—	—	dIrr	AVI	−170	20 ±1	Ef	OI	−160	9100 ±9600	W	4.6E4 ±4.8E4		0.062		59	1
										SiII	−160	1000 ±900	W	5200 ±4500		0.15		59	
NGC 2841 UB3	166.85	43.81	—	—	QSO	A	−123	0.60 ±0.10	GB	MgII		>0	E	>0		>0		121	f
AD UMa	160.40	43.28	9.9±1.0 t	6.8	RR Lyr	AVI	−158	80 ±1	Ef	CaII	−160	17 ±2	W	21 ±2		0.0096	U	104	
PG 0832+675	147.75	35.01	8.1 a	4.6	PAGB	AIII	−144	30 ±6	WE(	CaII		<2.8	N	<9.3				70)	2
										CaII		<2.7	W	<9.1				94	
PG 0859+593	156.94	39.74	4.0±1.0 a	2.6	HB	AIV	−166	34 ±4	WE	MgII		<23	N	<68			L	87	
SA 12 391	156.95	40.28	1.5±0.2 s	0.97	A0V	AIV	−155	24 ±4	Ef	CaII		<2.4	W	<10				33	3
HD 77770	169.30	41.88	1.3±0.3 t	0.87	B2IV	WW81	−117	4.0 ±1.0	Dw	NaI		<0.44	W	<11				80	4
										CaII		<1.0	W	<26				80	
PG 0906+597	156.22	40.56	0.70±0.20 a	0.46	sdB	AIV	−153	29 ±5	WE	MgII		<12	N	<41			L	87	
BD +75 306	139.02	28.79	0.58±0.06 s	0.28	A2V	AI	−187	182 ±3	ef	NaI		<1.3	S	<0.71				38	5,6
BD +75 310	139.45	29.14	0.50±0.06 s	0.24	A5V	AI	−184	329 ±3	ef	NaI		<1.4	S	<0.42				38	5,7
HD 75855	159.45	39.08	0.45±0.21 p	0.28	B9V	A	−167	6.0 ±1.3	Dw	NaI		<0.74	W	<12				80	
										CaII		<1.8	W	<29				80	
HD 68164	154.62	33.45	0.35±0.13 p	0.19	B9V	A	−187	9.7 ±1.3	Dw	NaI		<0.44	W	<4.5				80	
										CaII		<1.0	W	<11				80	
HD 76593	154.65	38.91	0.22±0.06 p	0.14	A0V	AIV	−180	76 ±15	ef	NaI		<0.29	W	<0.38				33	8
										CaII		<0.69	W	<0.91			l	33	3
Mistaken claims																			
SA 12 391	156.95	40.28	1.5±0.2 s	0.97	A0V	AIV	−155	24 ±4	Ef	CaII	−165	3.0 ±1.0	N	13 ±5		0.0058	U	33	9
Cloud MI										CaII					[22]				
PG 1126+468	157.20	64.71	5.8±0.7 s	5.2	HB	MI	−100	7.5 ±0.5	Ef	CaII		<3.5	N	<47				70	
BR UMa	165.53	66.29	4.7±0.5 s	4.3	RR Lyr	MI	−117	106 ±0.8	Ef	CaII		<12	N	<11				70	
MI ext (IV4)			(<0.8	<0.7)						SiII					[19000]				
			>0.6	>0.5						MgI				6.6 ±1.4		0.00017			
										CaII				3.3 ±0.9	[22]	0.0015			
										FeII				1600 ±80	[7800]	0.051			
										MnII				44 ±11	[87]	0.13			
SN 1998 S	150.75	65.96	—	—	SN	IV4	−87	43 ±2	Ef	MgI	−95.3	2.8 ±0.6	L	6.6 ±1.4		.00017		117	10
										CaII	−95.3	1.4 ±0.4	L	3.3 ±0.9		0.0015		117	
										FeII	−95.3	710 ±20	L	1600 ±80		0.051		117	
										MnII	−95.3	19 ±5	L	44 ±11		0.13		117	
PG 1213+456	141.93	70.44	2.9±0.7 a	2.7	sdB	IV4	−86	2.5 ±0.5	JB	CaII		<1.3	L	<50				93	
BD +49 2137	134.23	67.40	0.80±0.20 a	0.74	HB	IV4	−102	17 ±1	Ef	SiII		>90	N	>530		>0.015	U	83	11,S
										CaII		<0.35	W	<2.1				93	
HD 106420	140.59	68.79	0.55±0.27 p	0.51	B8V	IV4	−110	18 ±1	Ef	SiII		<90	N	<500			L	83	S
HD 105058	141.16	65.80	0.19±0.04 p	0.17	A2V	IV4	−92	27 ±1	Ef	SiII		<90	N	<330			L	83	S
Mistaken claims																			
HD 83206	167.70	46.93	0.90±0.20 t	0.66	B3V	WW63	(−108)	<2.0	Ef	NaI		<0.025	L				X	107	12,13
									(	CaII	−107	0.54	L	>27		>0.012	U	94)	
										CaII	−108.2	0.71	L	>35		>0.016	U	107	

TABLE 2

PUBLISHED RESULTS FOR ALL HV/IV CLOUDS

Probe (1)	l ° (2)	b ° (3)	d kpc (4)	z kpc (5)	type (6)	Cld (7)	v_{HI} km/s (8)	N_{HI} 10^{18} cm^{-2} (9)	tel (10)	ion (11)	v_{ion} km/s (12)	N_{ion} 10^{11} cm^{-2} (13)	code (14)	A_{ion} 10^{-9} (15)	A_{ref} 10^{-9} (16)	A/A$_\odot$ (17)	D? (18)	Ref (19)	Note (20)
Cloud MIII			$<$ 4.0	$<$ 3.5															
BD +38 2182	182.16	62.21	4.0	a 3.5	B3V	MIII	(−93)	<0.50	JB	CII	−85	>600	N	>1.2E5		>0.34	U	57	14
										OI	−85	>1000	N	>2.0E5		>0.27	U	57	
										NaI		<0.33	N					77	15
										SiII	−85	>200	N	>4.0E4		>1.1	U	57	
									(	CaII	−96	1.4 ±0.3	N	>290		>0.13	U	77)	
										CaII	−96	1.4	L	>290		>0.13	U	93	
HD 93521	183.14	62.15	1.9	t 1.7	O9.5V	MIII	(−93)	<0.50	JB	CII		<80	S					57	14,16
										OI		<210	S					57	16
										NaI		<0.33	N					77	15
										SiII		<10	S					57	16
										CaII		<0.90	N					77	15
C I			(> 6.1	> 4.3)						NI				7500 ±3200	[9300]	0.080			0.1$Z_\odot$,17
			> 1.2	> 0.8						NII				>530		>0.0057			
										OVI		[2000]							
										NaI									
										MgII				>0	[1400]	>0			
										SiII					[1900]				
										SiIII				2100		0.060			
										PII				<310	[37]	<0.83			
										SII				1800 ±400	[1900]	0.098			18
										ArI				<350	[120]	<0.095			
										CaII				22 ±1	[22]	0.010			
										FeII				1.6E4 ±6.5E3	[780]	0.50			
										FeIII				<2900		<0.091			
PG 1351+640	111.89	52.02	—	—	QSO	CIA	−115	7.2 ±3.0	Ef	CaII	−118	8.2 ±1.4	N	110 ±50		0.052		79	
Mrk 290	91.49	47.95	—	—	Sey	CIA	−136	92 ±7	WE	SII	−135	1700 ±400	N	1800 ±400		0.098		106	
									(	SII	−135	1700 ±100	N	1900 ±200		0.100		125)	
										CaII	−137	20 ±1	N	21 ±2		0.0098		79	
						C	−105	33 ±5	Ef	CaII	−89	4.1 ±0.9	N	12 ±3		0.0056		79	
Mrk 817	100.30	53.48	—	—	Sey	CIA	−109	31 ±0.9	Ef	SII	−112	1900 ±100	N	6200 ±500		0.33		125	
Mrk 876	98.27	40.38	—	—	QSO	CIB	−133	19 ±0.9	Ef	H_2		<2000	N	<1.1E4				119	
										NI	−133	1000 ±100	N	5400 ±700		0.058		125	
										NI	−133	1400 ±600	N	7500 ±3200		0.080		119	19
										NII	−133	>100	N	>530		>0.0057		119	
										OVI	−133	580 ±110	N					119	20
										SiIII	−133	400	N	2100		0.060		125	
										PII	−133	<58	N	<310				119	
										ArI	−133	<65	N	<350				119	
										FeII	−130	3000 ±1200	N	1.6E4 ±6.5E3		0.50		119	
										FeIII	−130	<550	N	<2900				119	
3C 351.0	90.08	36.38	—	—	QSO	CIB	−129	4.2 ±0.3	Ef	MgII		>0	E	>0		>0		121	f
QSO 1637+574	86.64	40.36	—	—	QSO	CIB	−122	33 ±1	Dw	HI		<74	τ			T_s>140		112	T
										CO		<1.3E4	N	<3.9E4				112	21
BS 16034-0002	91.60	48.86	8.8±1.0 s	6.6	(HB)	CIA	−121	33 ±2	Ef	CaII		<3.0	W	<9.1				114	
BS 16034-0114	89.40	45.07	6.1±0.7 s	4.3	(HB)	CIB	−125	68 ±1	Ef	CaII		<1.5	W	<2.2			l	114	
BS 16079-0017	91.05	46.60	4.8±0.5 s	3.5	(HB)	CIA	−141	31 ±1	Ef	CaII		<3.0	W	<9.7				114	
BS 16086-0123	92.14	47.40	4.5±0.5 s	3.3	(HB)	CIA	−141	36 ±2	Ef	CaII		<3.0	W	<8.3				114	
							−113	7.8 ±1.3	Ef	CaII		<3.0	W	<38				114	
PG 1510+635	100.69	47.28	4.2±0.5 s	3.1	HB	CIA	−114	11 ±1	Ef	CaII		<4.8	N	<42				70	
BS 16079-0015	90.69	46.46	2.4±0.5 s	1.7	(HB)	CIA	−135	35 ±2	Ef	CaII		<2.4	W	<6.8				114	
						C	−105	5.6 ±2.0	Ef	CaII		<2.4	W	<43				114	
BT Dra	99.41	51.21	1.9±0.2 t	1.5	RR Lyr	C	−109	7.9 ±1.1	Ef	NaI		<0.15	W	<1.9				19	
										CaII		<1.2	W	<15				33	3

TABLE 2—*Continued*

Probe	l °	b °	d kpc	z kpc	type	Cld	v_{HI} km/s	N_{HI} 10^{18} cm^{-2}	tel	ion	v_{ion} km/s	N_{ion} 10^{11} cm^{-2}	code	A_{ion} 10^{-9}	A_{ref} 10^{-9}	A/A$_\odot$	D?	Ref	Note
(1)	(2)	(3)	(4)	(5)	(6)	(7)	(8)	(9)	(10)	(11)	(12)	(13)	(14)	(15)	(16)	(17)	(18)	(19)	(20)
PG 1648+536	81.38	39.35	1.2±0.5 a	0.76	sdB	C	−133	12±1	Ef	MgII		<7.9	L	<66			L	60	
										FeII		<100	L	<830			l	60	
PG 1519+640	100.27	46.17	0.70±0.20 a	0.50	sdB	C	−121	8.9±1.6	Ef	NaI		<2.0	L	<22				62	
										MgII		<3.2	L	<36			L	60	
										FeII		<13	L	<140			L	60	
										CaII		<4.0	L	<45				62	
HD 146813	85.71	43.81	0.41±0.13 p	0.28	B8V	CIB	−109	37±2	Ef	SiII		<230	N	<620				50	s,22
Mistaken claims																			
BT Dra	99.41	51.21	1.9±0.2 t	1.5	RR Lyr	CIA	−109	7.9±1.1	Ef	NaI	−110	1.7±0.05	W	22±3		0.011	U	19	23
										CaII	−136	6.0	N	76		0.035	U	33	24
C III										CII				>0	[35000]	>0			0.1$Z_\odot$,25
										NI				4300	[9300]	0.046			
										OI				7.9E4±4.3E4	[74000]	0.11			
										OVI		[2000]							
										NaI									
										MgII				>0	[1400]	>0			
										SiII				5000±2800	[1900]	0.14			
										CaII				18±2	[22]	0.0081			
										FeII				1300±700	[780]	0.041			
PG 1351+640	111.89	52.02	—	—	QSO	CIII	−156	56±2	Ef	CII		>0	E	>0		>0		67	f,26
										SiII		>0	E	>0		>0		67	f,26
										CaII	−163	9.9±1.0	N	18±2		0.0081		79	
PG 1259+593	120.56	58.05	—	—	QSO	CIIIC	−128	84±1	Ef	NI		3600	L	4300		0.046		126	
										OI		6.6E4±3.7E4	L	7.9E4±4.3E4		0.11		126	
										OVI		460±110	L					126	
										SiII		4200±2300	L	5000±2800		0.14		126	
										MgII		>0	E	>0		>0		121	f
										FeII		1100±500	L	1300±600		0.041		126	
3C 263.0	134.16	49.74	—	—	QSO	C	−176	3.0±0.4	Dw	MgII		>0	E	>0		>0		121	f,27
SU Dra	133.45	48.27	0.70±0.10 t	0.52	RR Lyr	CIIIA	−138	31±1	Dw	CaII		<0.58	W	<1.9				33	3,28
BD +63 985	133.74	53.42	0.40±0.10 s	0.32	A5(V)	C	−141	2.3±0.9	Ef	NaI		<0.15	W	<6.4				84	
PG 1338+611	112.54	55.25	0.30±0.10 s	0.25	sdB	C	−126	56±1	Ef	CaII		<3.5	N	<6.2				70	29
HD 127557	109.43	47.13	0.28±0.06 p	0.21	A0V	C	−135	3.5±1.0	Dw	SiII		<90	N	<2600				83	S
HD 101075	135.50	51.13	0.24±0.04 p	0.19	A2IV	C	−149	5.0±0.8	Dw	NaI		<0.24	W	<4.9				84	
HD 103718	134.74	55.33	0.23±0.05 p	0.19	A3V	CIIIA	−130	57±0.8	Dw	NaI		<0.15	W	<0.26				84	
C-south			> 1.2	> 0.8						OVI		[2000]							(0.1$Z_\odot$),30
										NaI				<360		<0.17			
										MgII				3600±1300	[1400]	0.095			
										SII				8100±1900	[1900]	0.43			
										CaII				<580	[22]	<0.27			
										FeII				1.1E4±4.2E3	[780]	0.33			
Mrk 876	98.27	40.38	—	—	QSO	CD	−173	4.4±0.9	Ef	H_2		<2000	N	<4.5E4				119	
										OVI	−175	580±110	N					119	20
										FeII	−175	470±160	N	1.1E4±4.2E3		0.33		119	
Mrk 279	115.04	46.86	—	—	Sey	C	−123	31±5	Ef	SII	−147	2500±400	N	8100±1900		0.43		125	31
Mrk 205	125.45	41.67	—	—	Sey	C	−120	1.2±0.3	Ef	MgII	−147	43±11	W	3600±1300		0.095		75	32
										NaI		<4.3	W	<360				49	
										CaII		<7.0	W	<580				49	
FBS 0959+685	142.46	41.95	—	—	QSO	C	−140	15±4	Dw	MgII		>0	E	>0		>0		121	f,33
PG 1648+536	81.38	39.35	1.2±0.5 a	0.76	sdB	C	−164	17±2	Ef	MgII		<10	L	<60			L	60	
										FeII		<100	L	<600			l	60	
PG 1708+602	89.28	35.91	1.1±0.3 a	0.65	sdB	CD	−189	24±2	Ef	NaI		<1.6	L	<6.5				62	
SW Dra	127.27	47.33	1.0±0.1 t	0.74	RR Lyr	C	−145	25±1	Dw	CaII		<2.3	W	<9.3				33	3

TABLE 2—*Continued*

Probe	l °	b °	d kpc	z kpc	type	Cld	v_{HI} km/s	N_{HI} 10^{18} cm^{-2}	tel	ion	v_{ion} km/s	N_{ion} 10^{11} cm^{-2}	code	A_{ion} 10^{-9}	A_{ref} 10^{-9}	$A/A_\odot$	D?	Ref	Note
(1)	(2)	(3)	(4)	(5)	(6)	(7)	(8)	(9)	(10)	(11)	(12)	(13)	(14)	(15)	(16)	(17)	(18)	(19)	(20)
C-extension										NaI									$(0.1Z_\odot)$,34
										MgII				>0	[1400]	>0			
										SiII					[1900]				
										SII				<2.0E4	[1900]	<1.1			
										CaII				<49	[22]	<0.022			
PG 1700+518	79.02	37.77	—	—	QSO	C	−130	0.60 ±0.10	GB	MgII		>0	E	>0		>0		121	f
PG 1718+481	74.38	34.83	—	—	QSO	C	−133	4.1 ±0.1	GB	MgII		>0	E	>0		>0		121	f
QSO 1732+389	64.03	31.00	—	—	QSO	CeIII	−195	5.4 ±1.3	Dw	HI		<8.7	τ			$T_s>15$		112	T
						CeIII	−151	32 ±1	Dw	HI		<47	τ			$T_s>90$		112	T
Mrk 501	63.60	38.86	—	—	BL Lac	CeI	−116	10 ±1	Ef	SII		<2000	N	<2.0E4				125	
										CaII		<4.9	N	<49				70	
PKS 1739+17	41.35	22.99	—	—	radio	c	−110	29	Ar	HI		<35	τ			$T_s>20$		5	T
4C 09.57	34.93	17.63	—	—	BL Lac	c	−139	15 ±3	Dw	HI		<39	τ			$T_s>90$		112	T,35
										CO		<5500	N	<3.8E4				112	21
						c	−113	26 ±3	Dw	HI		<61	τ			$T_s>110$		112	T
PKS 1741–038	21.60	13.12	—	—	QSO	c	−132	14 ±2	Dw	HI		<48	τ			$T_s>50$		112	T
						c	−86	33 ±2	Dw	HI		<63	τ			$T_s>80$		112	T
										CO		<1.0E4	N	<3.1E4				112	21
V421 Her	64.84	31.60	5.5±0.6 s	2.9	RR Lyr	CeIII	−142	17 ±0.7	Dw	CaII		<5.4	N	<32				70	
OW Her	62.84	24.91	4.4±0.4 s	1.9	RR Lyr	CeIV	−166	73 ±1	Dw	CaII		<17	N	<24				70	
PG 1722+286	51.71	30.57	0.90±0.20 a	0.46	sdOB	C	−162	6.0 ±2.0	ef	NaI		<1.6	L	<26				62	
										CaII		<5.0	L	<84				62	
PG 1743+477	74.41	30.65	0.80±0.30 a	0.41	sdB	C	−145	1.5 ±1.0	Dw	CaII		<4.1	N	<270				70	
HD 156110	70.99	35.71	0.72±0.33 p	0.42	B3Vn	C	−145	8.1 ±0.5	Dw	SiII		<230	N	<2800				50	s
PG 1710+490	75.43	36.08	0.70±0.30 a	0.41	sdB	C	−134	1.9 ±0.7	Dw	NaI		<1.0	L	<53				62	
										CaII		<6.3	L	<330				62	
C/K			> 0.8	> 0.6						NaI									
										MgII					[14000]				
										CaII					[22]				
										FeII					[7800]				
PG 1619+522	80.47	43.96	0.80±0.30 a	0.56	sdB	C/K	−85	4.4 ±0.8	Dw	MgII		<10	L	<230			L	60	
										FeII		<63	L	<1400				60	
PG 1743+477	74.41	30.65	0.80±0.30 a	0.41	sdB	C/K	−88	3.9 ±0.7	Dw	CaII		<4.1	N	<110				70	
PG 1710+490	75.43	36.08	0.70±0.30 a	0.41	sdB	C/K	−94	22 ±0.8	Dw	NaI		<1.0	L	<4.6				62	
										CaII		<6.3	L	<29				62	
Complex G			> 1.3							OI					[740000]				
										MgI									
										MgII					[14000]				
										AlII					[1600]				
										CaII					[22]				
										FeII					[7800]				
QSO 2200+420	92.60	−10.45	—	—	BL Lac	G	−109	18 ±2	Dw	HI		<120	τ			$T_s>450$		112	T
										CO		<7800	N	<4.3E4				112	21
HD 212593	99.90	−6.71	1.3±0.1 t	0.15	B9Iab	G	−107	60 ±8	Ef	OI		<1500	W	<2600			L	42	36
(4 Lac)										MgI		<4.1	W	<6.9				42	
										MgII		<38	W	<64			L	42	
										AlII		<18	W	<30			L	42	
										FeII		<63	W	<110			L	42	
IU Cas	112.69	−9.20	0.90±0.10 s	0.14	RR Lyr	G	−133	22 ±1	Dw	CaII		<9.6	N	<43				70	

TABLE 2—*Continued*

Probe	l	b	d	z	type	Cld	v_{HI}	N_{HI}	tel	ion	v_{ion}	N_{ion}	code	A_{ion}	A_{ref}	$A/A_{\odot}$	D?	Ref	Note
	°	°	kpc	kpc			km/s	10^{18} cm^{-2}			km/s	10^{11} cm^{-2}		10^{-9}	10^{-9}				
(1)	(2)	(3)	(4)	(5)	(6)	(7)	(8)	(9)	(10)	(11)	(12)	(13)	(14)	(15)	(16)	(17)	(18)	(19)	(20)
Complex H – core I			> 5.0							CII					[35000]				(0.1$Z_{\odot}$),37
										OI					[74000]				
										NaI									
										MgII					[1400]				
										CaII					[22]				
0159+625	130.98	1.15	—	—	radio	HI	−199	190	Ws	HI	−199	170	τ	0.92		T_s=47		43	T,38
BD +59 367	131.11	−1.28	5.0±0.6 s	0.11	O9.5I	H	−181	17 ± 5	Ef	MgII		<8.3	N	<49			L	96	
BD +62 338	130.91	1.07	3.5±0.8 t	0.07	B3II	HI	−201	194 ± 1	Ef	MgII		<5.3	N	<2.7			L	96	
HD 10125	128.29	1.82	3.4±0.3 t	0.1	O9.5Ib	HI	−203	42 ± 2	Ef	MgII		<4.1	N	<9.8			L	96	
										CaII		<5.0	L	<12				62	39
						HI	−162	13 ± 2	Ef	MgII		<4.1	N	<32			L	96	
										CaII		<5.0	L	<39				62	
BD +63 253	129.62	2.13	2.3±0.4 t	0.09	B0III	HI	−202	16 ± 2	Ef	CaII		<3.2	L	<20				62	
						HI	−170	9.7 ± 1.2	Ef	CaII		<3.2	L	<33				62	
HD 13256	132.60	−0.64	2.1±0.2 t	0.02	B1Ia	HI	−186	30 ± 1	Dw	CaII		<5.0	L	<16				62	39
LS I +62 200	130.70	1.22	1.9±0.3 s	0.04	B1V	HI	−204	302 ± 2	ef	CaII		<5.0	L	<1.7			l	62	40
LS I +61 251	130.73	0.04	1.8±0.3 s	0	B1V:	HI	−194	95 ± 2	ef	CaII		<5.0	L	<5.3				62	41
HD 12567	130.86	2.56	1.6±0.3 t	0.07	B0.5III	HI	−202	81 ± 2	Ef	CaII		<2.5	L	<3.1				62	
Complex H – core II			> 2.5																(0.1$Z_{\odot}$),42
HD 108	117.93	1.25	2.5±0.2 t	0.05	O6Ia:f	HII	−188	7.7 ± 1.6	Ef	CII		<160	N	<2100			l	96	
										OI		<420	N	<5500			l	96	
										MgII		<5.2	N	<68			L	96	
RS Cas	114.47	0.78	2.0±0.2 t	0.03	Cep	HII	−160	33 ± 2	Dw	CaII		<12	N	<38				70	
HD 225160	117.44	−0.14	1.8±0.4 t	0	O8e	HII	−172	8.4 ± 1.1	Ef	MgII		<4.3	N	<51			L	96	
HD 1383	119.02	−0.89	1.7±0.2 t	0.03	B1II..	H	−160	9.9 ± 1.5	Ef	MgII		<5.4	N	<55			L	96	
HD 223987	116.18	−0.51	1.3±0.1 s	0.01	B1Ib	HII	−163	9.3 ± 3.5	Ef	MgII		<3.8	N	<41			L	96	
Complex H – core III			> 3.6																(0.1$Z_{\odot}$),43
HD 12323	132.91	−5.87	3.6±0.3 t	0.37	O9V	HIII	−145	6.8 ± 1.1	Ef	MgII		<5.1	N	<75			L	96	
HDE 236894	130.83	−3.50	3.4±0.3 t	0.21	O8V	HIII	−184	10 ± 1	Ef	CII		<150	N	<1500			L	96	44
										OI		<390	N	<3900			L	96	
						HIII	−144	12 ± 1	Ef	CII		<150	N	<1300			L	96	
										OI		<390	N	<3300			L	96	
HD 12993	133.11	−3.40	3.4±0.2 t	0.20	O6.5V	HIII	−153	8.0 ± 1.7	Ef	CII		<160	N	<2000			l	96	
										OI		<410	N	<5100			l	96	
Complex H – other			> 2.3																(0.1$Z_{\odot}$),45
4C 67.05	132.13	6.24	—	—	QSO	H	−164	27 ± 2	Dw	CO		<1.4E4	N	<5.2E4				112	21,46
4C 47.08	145.00	−9.86	—	—	BL Lac	H	−120	17 ± 1	Dw	CO		<1.7E4	N	<1.0E5				112	21,47
HD 14947	134.99	−1.74	2.3±0.2 t	0.07	O5f	H	−149	18 ± 1	Ef	CII		<220	N	<1300			L	96	
										OI		<580	N	<3300			L	96	
HD 15629	134.77	1.01	2.1±0.1 t	0.04	O5e	H	−175	13 ± 2	Ef	CII		<220	N	<1800			L	96	48
										OI		<560	N	<4500			l	96	
HD 17520	137.22	0.88	1.7±0.2 t	0.03	O9V	H	−136	13 ± 2	Dw	MgII		<3.1	N	<24			L	96	
HD 2619	120.74	2.49	1.2±0.2 t	0.05	B0.5III	H	−201	16 ± 2	ef	NaI		<2.5	L	<16				62	
										CaII		<2.5	L	<16				62	49
						H	−137	25 ± 2	ef	NaI		<2.5	L	<10				62	
										CaII		<2.5	L	<10				62	
HD 17505	137.19	0.90	1.1±0.1 t	0.02	O6.5V	H	−134	13 ± 4	Dw	MgII		<5.1	N	<40			L	96	

TABLE 2—*Continued*

Probe	l	b	d	z	type	Cld	v_{HI}	N_{HI}	tel	ion	v_{ion}	N_{ion}	code	A_{ion}	A_{ref}	$A/A_{\odot}$	D?	Ref	Note
	°	°	kpc	kpc			km/s	10^{18} cm^{-2}			km/s	10^{11} cm^{-2}		10^{-9}	10^{-9}				
(1)	(2)	(3)	(4)	(5)	(6)	(7)	(8)	(9)	(10)	(11)	(12)	(13)	(14)	(15)	(16)	(17)	(18)	(19)	(20)
AC Shell			(> 1.5)							CaII					[22]				
3C 123	170.58	−11.66	—	—	radio	ACS	−62	230	Ar	HI	−63.9	220	τ	0.96		T_s=832		5	T,50
							−70	230	ab	HI	−70	160	τ	0.70		T_s>360		21	T
							−73.0	16	ab	HI	−73.0	16	τ	1.0		T_s=81		5	T
							−73.1	55	ab	HI	−73.1	55	τ	1.00		T_s=280		21	T
							−57.9	20	ab	HI	−57.9	20	τ	1.0		T_s=562		5	T
							−55.9	1.5	ab	HI	−55.9	1.5	τ	1.00		T_s=57		21	T
							−59.2	13	ab	HI	−59.3	13	τ	1.0		T_s=192		21	T
HDE 256725	192.32	3.36	8.0±2.0 s	0.47	O5V	ACS	−61	33 ±1	Ef	CaII		<1.4	W	<4.3				24	51
HDE 248894	187.89	−2.51	3.0±0.3 s	0.13	O8V	ACS	−56	40 ±2	Ef	CaII		<1.4	W	<3.5				24	
HDE 255055	188.69	3.87	2.6±0.3 s	0.18	O9V	ACS	−81	34 ±1	Dw	CaII		<1.4	W	<4.2				24	
HDE 256035	189.42	4.33	1.5±0.2 s	0.11	O9V	ACS	−79	72 ±1	Dw	CaII		<1.4	W	<2.0			l	24	
HD 45314	196.96	1.52	0.90±0.10 s	0.02	O9V:pe	ACS	−66	100 ±9	Dw	CaII		<0.92	W	<0.90			l	24	
Cloud AC0			(> 0.3)							NaI									
										CaII					[22]				
HDE 252550	179.91	6.25	0.90±0.05 s	0.10	A0V	AC0	−116	37 ±4	Ef	NaI		<0.66	W	<1.8				92	
HDE 253069	179.86	6.74	0.40±0.05 s	0.05	B9V	AC0	−111	120 ±5	Ar	NaI		<0.64	W	<0.53				92	
HD 42904	180.74	6.83	0.30±0.03 s	0.04	A0V	AC0	−114	110 ±5	Ar	NaI		<1.4	W	<1.3				92	
										CaII		<2.0	W	<1.8			l	92	
HDE 252605	180.63	5.89	0.30±0.03 s	0.03	A0V	AC0	−112	150 ±5	Ar	NaI		<1.0	W	<0.67				92	
Cloud ACI			(> 0.4)							NaI									(0.1$Z_{\odot}$)
										CaII					[22]				
HDE 241573	184.37	−11.75	0.40±0.05 s	0.08	B9V	ACI	−203	62 ±4	Ef	NaI		<1.2	W	<1.9				92	
HD 33415	181.69	−10.46	0.36±0.03 p	0.07	A0V	ACI	−187	77 ±9	Dw	CaII		<0.69	W	<0.90			l	33	52,53
HDE 241597	184.70	−11.95	0.30±0.03 s	0.06	A2V	ACI	−205	66 ±3	Ef	NaI		<1.7	W	<2.5				92	
HD 33233	181.47	−10.68	0.30±0.03 s	0.06	A0V	ACI	−187	78 ±10	Dw	CaII		<0.69	W	<0.89			l	33	52,54
HD 33090	181.63	−11.04	0.29±0.09 p	0.06	B5V	ACI	−188	77 ±3	Dw	CaII		<0.69	W	<0.90			l	33	52,55
HD 32641	179.91	−10.73	0.25±0.08 p	0.05	B5V	ACI	−188	66 ±3	Dw	CaII		<0.69	W	<1.1			l	33	52,56
HDE 241882	184.60	−11.37	0.20±0.03 s	0.04	A7V	ACI	−197	155 ±1	Dw	NaI		<1.2	W	<0.78				92	
										CaII		<2.4	W	<1.5			l	92	
Cloud ACII			(> 0.3)							NaI									(0.1$Z_{\odot}$)
										CaII					[22]				
HDE 241573	184.37	−11.75	0.40±0.05 s	0.08	B9V	ACII	−143	30 ±3	Ef	NaI		<1.2	W	<4.1				92	
HD 33415	181.69	−10.46	0.36±0.03 p	0.07	A0V	ACII	−162	24 ±9	Dw	CaII		<0.70	W	<3.0				33	52,53
HDE 241597	184.70	−11.95	0.30±0.03 s	0.06	A2V	ACII	−136	23 ±4	Ef	NaI		<1.6	W	<7.1				92	
HD 33233	181.47	−10.68	0.30±0.03 s	0.06	A0V	ACII	−162	20 ±7	Dw	CaII		<0.70	W	<3.4				33	52,54
HD 33090	181.63	−11.04	0.29±0.09 p	0.06	B5V	ACII	−164	33 ±3	Dw	CaII		<0.70	W	<2.1			l	33	52,55
HD 32641	179.91	−10.73	0.25±0.08 p	0.05	B5V	ACII	−165	21 ±3	Dw	CaII		<0.70	W	<3.3				33	52,56
HDE 241882	184.60	−11.37	0.20±0.03 s	0.04	A7V	ACII	−138	42 ±1	Dw	NaI		<1.2	W	<2.9				92	
										CaII		<8.4	W	<20				92	
Cohen Stream			> 0.3	> 0.2						NaI									
										MgII					[14000]				
										CaII					[22]				
PKS 0202+14	147.93	−44.05	—	—	Sey	CHS	−109	5.3 ±0.5	Ef	HI		<2.3	τ			T_s>50		39	T
3C 75	170.25	−44.91	—	—	radio	CHS	−110	15 ±0.4	Ar	HI		<4.2	τ			T_s>70		39	T
3C 78	174.86	−44.51	—	—	radio	CHS	−97	13 ±0.6	Ar	HI		<1.9	τ			T_s>30		39	T
Mrk 595	164.76	−46.55	—	—	Sey	CHS	−124	27 ±0.9	Ef	NaI		<1.1	N	<4.2				103	
HD 14069	156.66	−49.52	0.30±0.03 s	0.23	A0V	CHS	−111	22 ±2	Ef	NaI		<0.24	W	<1.1				68	
										MgII		<7.4	S	<33			L	68	57
HD 17473	166.54	−45.44	0.30±0.03 s	0.21	A2V	CHS	−127	21 ±1	Ef	NaI		<1.0	W	<5.0				92	
HD 17481	166.39	−45.24	0.30±0.03 s	0.21	A0V	CHS	−114	15 ±1	Ef	NaI		<0.24	W	<1.7				68	58
										MgII		<8.0	S	<55			L	68	57
										CaII		<0.58	W	<4.0				68	58

TABLE 2—*Continued*

Probe	l	b	d	z	type	Cld	v_{HI}	N_{HI}	tel	ion	v_{ion}	N_{ion}	code	A_{ion}	A_{ref}	$A/A_\odot$	D?	Ref	Note
	°	°	kpc	kpc			km/s	10^{18} cm^{-2}			km/s	10^{11} cm^{-2}		10^{-9}	10^{-9}				
(1)	(2)	(3)	(4)	(5)	(6)	(7)	(8)	(9)	(10)	(11)	(12)	(13)	(14)	(15)	(16)	(17)	(18)	(19)	(20)
HD 18059	167.87	−44.21	0.30±0.08 p	0.21	A0V	CHS	−106	3.9 ±0.6	Ef	NaI		<0.30	W	<7.8				92	V
HD 17907	168.50	−45.40	0.25±0.13 p	0.18	B9.5V	CHS	−116	6.6 ±1.1	Ef	NaI		<0.24	W	<3.7				68	58
										MgII		<6.8	S	<100			L	68	57
										CaII		<0.58	W	<8.8				68	58
HD 18910	172.35	−44.73	0.20±0.02 s	0.14	A0V	CHS	−98	13 ±2	Dw	MgII		<8.6	S	<66			L	68	57
HD 14951	157.03	−45.99	0.18±0.03 p	0.13	B7IV	CHS	−119	6.1 ±4.9	Dw	NaI		<0.24	W	<4.0				68	58
										MgII		<6.8	S	<110			L	68	57
										CaII		<0.58	W	<9.5				68	58
Cloud WW507			> 0.3	> 0.2						NaI									(0.1$Z_\odot$)
										MgII					[1400]				
										CaII					[22]				
4C 10.08	161.87	−43.40	—	—	radio	WW507	−335	130 ±0.8	Ef	HI		<92	τ			T_s>320		112	T,59
HD 17473	166.54	−45.44	0.30±0.03 s	0.21	A2V	WW507	−274	15 ±0.9	Ef	NaI		<1.1	W	<7.3				92	
HD 17481	166.39	−45.24	0.30±0.03 s	0.21	A0V	WW507	−276	50 ±1	Ef	NaI		<0.50	W	<1.0				92	
										MgII		<7.3	S	<14			L	68	57
										CaII		<0.58	W	<1.1			l	68	58
HD 18059	167.87	−44.21	0.30±0.08 p	0.21	A0V	WW507	−277	4.0 ±0.9	Ef	NaI		<0.30	W	<7.6				92	
HD 17907	168.50	−45.40	0.25±0.13 p	0.18	B9.5V	WW507	−270	2.9 ±0.9	Ef	NaI		<0.24	W	<8.4				68	58,V
									(	NaI		<0.29	W	<10				92)	
										MgII		<5.6	S	<190			l	68	57
										CaII		<0.58	W	<20				68	58
HD 18910	172.35	−44.73	0.20±0.02 s	0.14	A0V	WW507	−247	5.8 ±2.1	Dw	MgII		<7.2	S	<120			L	68	57
HD 14951	157.03	−45.99	0.18±0.03 p	0.13	B7IV	WW507	−320	2.8 ±0.9	Dw	NaI		<0.24	W	<8.7				68	58,V
										MgII		<5.3	S	<190			l	68	57
										CaII		<0.58	W	<21				68	58
Other AC clouds																			
PKS 0428+205	176.81	−18.56	—	—	radio	WW363	−110	5.0 ±0.6	Ar	HI		<1.6	τ			T_s>20		39	T,60
3C 109	181.83	−27.78	—	—	Sey	WW418	−222	14 ±0.5	Ar	HI		<1.7	τ			T_s>20		39	T
CTA 21	166.64	−33.60	—	—	radio	WW468	−121	2.0 ±0.4	Ar	HI		<2.0	τ			T_s>40		39	T,
HD 16582	170.76	−52.21	0.20±0.03 p	0.16	B2IV	WW525	−203	7.3 ±1.2	Dw	SiII		<230	N	<3200				50	s,61
Complex GCN																			
Mrk 509	35.97	−29.86	—	—	Sey	(WW419)	−283	20 ±20	md	CII	−283	430 ±340	L	2100 ±2700		0.0060		110	62,63
										CIV	−283	>1600	L					110	
										NI		<380	L	<1900				110	
										NV		<150	L					110	
										OVI	−280	910 ±80	L					118	64
										SiII		<100	L	<500				110	
										SiIII	−283	>150	L	>770		>0.022		110	
										SiIV	−283	>280	L					110	
										SII		<850	L	<4300				110	
										SIII		<2300	L	<1.1E4				110	
							−227	2.2 ±2.2	md	CII		<310	L	<1.4E4				110	
										CIV	−227	>480	L					110	
										NI		<250	L	<1.1E4				110	
										NV		<95	L					110	
										OVI	−210	1800 ±200	L					118	64
										SiII		<69	L	<3100				110	
										SiIII	−227	25 ±17	L	1100 ±1400		0.032		110	
										SiIV		<85	L					110	
										SII		<660	L	<3.0E4				110	
										SIII		<2600	L	<1.2E5				110	

TABLE 2—*Continued*

Probe	l °	b °	d kpc	z kpc	type	Cld	v_{HI} km/s	N_{HI} 10^{18} cm^{-2}	tel	ion	v_{ion} km/s	N_{ion} 10^{11} cm^{-2}	code	A_{ion} 10^{-9}	A_{ref} 10^{-9}	A/A$_\odot$	D?	Ref	Note
(1)	(2)	(3)	(4)	(5)	(6)	(7)	(8)	(9)	(10)	(11)	(12)	(13)	(14)	(15)	(16)	(17)	(18)	(19)	(20)
PKS 2155–304	17.73	−52.25	—	—	BL Lac	(GCN)	−256	20 ±20	md(	CIV	−260	420 ±30	L					55)	63,65
										CIV	−256	320 ±50	L					110	
										NV		<110	L					110	
										OVI	−250	330 ±30	L					118	64
										SII		<1600	L	<7900				110	
							−140	20 ±20	md	CIV	−140	320 ±50	L					110	
										NV		<140	L					110	
										OVI	−140	680 ±60	L					118	64
										SiII	−140	54 ±16	L	270 ±280		0.0076		110	
										SII		<1300	L	<6600				110	
HD 173011	21.18	−3.51	1.1	t 0.07	B0.5V	WW302	−208	3.3 ±0.8	Dw	CaII		<2.4	W	<72				1	
HD 187350	38.67	−13.42	0.32±0.14	p 0.07	B1Vne	WW345	−231	6.3 ±0.7	Dw	CaII		<2.3	W	<37				1	
HD 188350	40.55	−13.92	0.11±0.01	p 0.03	A0III	WW345	−211	1.0 ±0.5	Dw	CaII		<1.2	W	<120				1	V
Complex GCP			(> 0.3	> 0.1)						CaII					[22]				
HD 187350	38.67	−13.42	0.32±0.14	p 0.07	B1Vne	GP	+99	299 ±3	Dw	CaII		<2.3	W	<0.78			l	1	
HD 188859	40.92	−14.43	0.11±0.01	p 0.03	A0V	GP	+95	200 ±6	Dw	CaII		<1.2	W	<0.59			L	1	
HD 188350	40.55	−13.92	0.11±0.01	p 0.03	A0III	GP	+90	200 ±10	Dw	CaII		<1.2	W	<0.59			L	1	
Outer Arm										CIV		[1600]							
										NV		[350]							
										OVI		[2000]							
										MgII				>0	[14000]	>0			
										CaII					[22]				
PKS 1820+17	46.07	14.36	—	—	radio	OA	−68	55	Ar	HI		<51	τ			T_s>20		5	T
3C 386	46.97	10.55	—	—	radio	OA	−73	102 ±0.4	Ar	HI		<57	τ			T_s>940		39	T
4C 29.56	57.51	16.88	—	—	QSO	OA	−97	29 ±0.5	Ar	HI		<16	τ			T_s>290		39	T,66
						OA	−71	40 ±0.5	Ar	HI		<40	τ			T_s>460		39	T
3C 382	61.31	17.45	—	—	Sey	OA	−87	13 ±0.5	Ar	HI		<30	τ			T_s>390		39	T
3C 395	63.03	11.76	—	—	QSO	OA	−84	110	Ar	HI	−73	39	τ	0.36		T_s=55		5	T,67
										HI	−73	3.7	τ	0.034		T_s=38		112	T
4C 33.48	66.39	8.37	—	—	radio	OA	−81	180 ±8	Ef	HI		<170	τ			T_s>140		5	T
QSO 2005+403	76.83	4.29	—	—	QSO	OA	−118	122 ±0.3	Dw	HI	−121	100	τ	0.86		T_s=147		112	T
3C 380.0	77.23	23.50	—	—	QSO	OA	−110	93 ±1	Dw	HI		<190	τ			T_s>570		112	T,68
3C 418	88.82	6.03	—	—	QSO	OA	−116	130 ±20	Dw	HI		<320	τ			T_s>620		112	T,69
H 1821+643	94.00	27.42	—	—	QSO	OA	(−213)	<3.0	Ef	CIV	−213	120 ±30	N					76	70
										OVI	−210	1000 ±200	L					118	64
						OA	−128	3.3 ±0.5	Ef	CIV	−120	610 ±110	N					76	71
										NV		<420	N					76	
						OA	−87	8.5 ±0.7	Ef	CIV	−70	600 ±160	N					76	
										NV		<350	N					76	
										MgII		>0	E	>0		>0		121	f
4C 73.18	105.63	23.54	—	—	QSO	OA	−121	33 ±2	GB	MgII		>0	E	>0		>0		121	f,72
										HI		<0.0	τ			T_s>110		112	T
HS 0624+6907	145.71	23.35	—	—	QSO	OA	−100	20 ±2	Ef	MgII		>0	E	>0		>0		121	f,73
3C 147.0	161.64	10.20	—	—	QSO	OA	−121	32 ±4	Dw	HI		<0.0	τ			T_s>2000		21	T,74
										HI		<53	τ			T_s>410		112	T
HD 178329	72.15	14.98	0.63±0.22	p 0.16	B3V	OA	−93	83 ±2	Dw	CaII		<1.2	W	<1.4			l	1	
HD 189818	91.18	14.36	0.40	t 0.10	B5V	OA	−131	47 ±2	Dw	CaII		<1.9	W	<4.0				1	
HD 176502	70.88	16.00	0.29±0.05	p 0.08	B3V	OA	−91	45 ±2	Dw	CaII		<1.2	W	<2.6				1	
HD 205021	107.54	14.03	0.18±0.02	p 0.04	B1III	OA	−119	104 ±1	Dw	CaII		<0.46	W	<0.44			L	1	
Complex R																			
4C 33.48	66.39	8.37	—	—	radio	R	−128	29 ±2	Ef	HI	−128	5.8	τ	0.20		T_s=69		5	T

TABLE 2—*Continued*

Probe (1)	l ° (2)	b ° (3)	d kpc (4)	z kpc (5)	type (6)	Cld (7)	v_{HI} km/s (8)	N_{HI} 10^{18} cm^{-2} (9)	tel (10)	ion (11)	v_{ion} km/s (12)	N_{ion} 10^{11} cm^{-2} (13)	code (14)	A_{ion} 10^{-9} (15)	A_{ref} 10^{-9} (16)	A/A$_\odot$ (17)	D? (18)	Ref (19)	Note (20)
Magellanic Stream										CIV		[1600]							0.25$Z_\odot$
										NV		[350]							
										OVI		[2000]							
										NaI				<2.5		<0.0012			
										MgII				3600 ±700	[3600]	0.095			75
										SiII				>440	[4800]	>0.012			
										SII				6200 ±400	[4700]	0.33			
										CaII				27 ±2	[22]	0.012			
										FeII				2000 ±800	[1900]	0.062			
3C 454.3	86.11	−38.18	—	—	QSO	MS	−365	1.1 ±0.1	GB	MgII	−375	300 ±130	W	2.7E4 ±1.2E4		0.72		121	76
CTA 102	77.44	−38.58	—	—	QSO	WW485	−323	3.0 ±0.2	Ar	HI		<0.18	τ			T$_s$>10		39	T
PKS 2251+11	82.78	−41.94	—	—	QSO	MS	−363	4.9 ±0.1	GB	MgII	−304	240 ±190	W	4900 ±3800		0.13		121	76
PKS 0003+15	107.32	−45.33	—	—	QSO	WW509	−326	0.90 ±0.10	GB	MgII	−290	93 ±46	W	1.0E4 ±5.3E3		0.27		121	76
NGC 7469	83.10	−45.47	—	—	Sey	MS	−333	3.1 ±0.6	Ef	MgII	−340	70 ±9	N	2300 ±500		0.059		122	76
										OVI	−300	4200 ±700	L					118	64
PKS 2344+09	97.50	−50.13	—	—	QSO	MS	−372	4.3 ±0.1	GB	MgII	−332	280 ±300	W	6600 ±7100		0.17		121	76
PG 2302+029	78.46	−50.23	—	—	QSO	MS	−324	4.1 ±0.1	GB	MgII	−310	150 ±50	W	3600 ±1300		0.094		121	76
2331+073	91.90	−50.56	—	—	radio	MS	−338	28 ±1	Dw	HI		<54	τ			T$_s$>50		112	T
III Zw 2	106.98	−50.63	—	—	Sey	MS	(−350)	<1.5	Dw	MgII	−350	100 ±10	N	>6800		>0.18		122	77
PKS 2243–123	53.87	−57.07	—	—	QSO	(MS)	(−335)	<0.70	GB	MgII	−335	130 ±90	W	>1.8E4		>0.48		121	76
PG 0043+039	120.22	−58.67	—	—	QSO	WW532	−366	1.3 ±0.1	GB	MgII	−388	140 ±70	W	1.1E4 ±5.3E3		0.28		121	76
PKS 2340–036	85.40	−61.15	—	—	QSO	MS	−277	4.1 ±0.1	GB	MgII	−310	130 ±30	W	3100 ±900		0.081		121	76
PKS 2345–167	65.56	−71.90	—	—	QSO	MS	−174	11 ±1	Dw	HI		<5.7	τ			T$_s$>10		112	T
										CO		<1.4E4	N	<1.3E5				112	21
PKS 0103–453	295.04	−71.82	—	—	radio	MS	101	9.7 ±0.8	PK	HI		<11	τ			T$_s$>50		44	T
Ton S180	139.00	−85.07	—	—	QSO	MS	(−150)	<3.0	Dw	OVI	−150	1900 ±300	L					118	
Ton S210	224.97	−83.16	—	—	QSO	MS	(−175)	<3.0	Ef	OVI	−175	1300 ±300	L					118	
Fairall 9	295.07	−57.83	—	—	QSO	MS	+190	89 ±1	PK	CIV		<410	W					66	78
										NV		<510	W					66	
										NaI		<2.2	W	<2.5				8	79
									(	SiII	+195	>1500	N	>1700		>0.047		66)	τ
										SiII	+176	>390	N	>440		>0.012		122	
										SII		5500 ±400	N	6200 ±400		0.33		122	
										CaII	+193	24 ±2	W	27 ±2		0.012		8	79
							+149	14 ±0.8	PK(	SII		<3900	W	<2.8E4				66)	
										SII	+142	1100 ±400	N	7700 ±3100		0.41		122	
							+194	75 ±1	PK(	SII		<3500	W	<4600				66)	
									(	SII	+193	4500 ±400	N	5900 ±500		0.32		122)	
PKS 0252–712	290.02	−42.88	—	—	radio	MS	+218	80 ±2	PK	HI		<41	τ			T$_s$>460		44	T
							+257	80 ±2	PK	HI		<41	τ			T$_s$>460		44	T
PKS 0407–658	278.64	−40.88	—	—	radio	MS	+258	9.4 ±1.6	PK	HI		<11	τ			T$_s$>480		44	T
PKS 0202–76	297.55	−40.04	—	—	QSO	MS	+148	114 ±3	PK	HI		<170	τ			T$_s$>40		44	T
PKS 0409–752	288.98	−36.13	—	—	radio	MS	+200	124 ±2	PK	HI		<59	τ			T$_s$>670		44	T
							+243	147 ±3	PK	HI		<59	τ			T$_s$>670		44	T
PKS 0637–75	286.37	−27.16	—	—	QSO	MS	+245	31 ±0.9	PK	MgII	+254	>1300	W	>4300		>0.11		74)	76,τ
										MgII	+254	>1300	W	>4200		>0.11		121	76,τ
										FeII	+200	610 ±240	W	2000 ±800		0.062		99	76
HD 219188	83.03	−50.17	2.3±0.2 t	1.8	B0.5II	MS	−273	3.3 ±0.6	Ef	SiII		<230	N	<7000				50	s
HD 3175	306.22	−53.96	1.6±0.2 t	1.3	B5III	MS	+168	26 ±0.5	PK	CaII		<4.9	W	<19				30	V
						WW524	+104	8.3 ±0.9	PK	CaII		<4.8	W	<58				30	
PG 0039+048	118.59	−57.64	1.1±0.4 a	0.93	sdB	WW532	−367	27 ±2	Ef	NaI		<1.6	L	<5.8				62	
PG 2337+070	93.71	−51.49	0.80±0.30 a	0.63	sdB	MS	−313	27 ±1	Ef	NaI		<1.3	L	<4.7				62	
HD 220172	68.10	−62.65	0.80±0.10 t	0.71	B3Vn	MS	−235	2.0 ±0.3	Dw	SiII		<230	N	<1.1E4				50	s

TABLE 2—*Continued*

Probe (1)	l ° (2)	b ° (3)	d kpc (4)	z kpc (5)	type (6)	Cld (7)	v_{HI} km/s (8)	N_{HI} 10^{18} cm^{-2} (9)	tel (10)	ion (11)	v_{ion} km/s (12)	N_{ion} 10^{11} cm^{-2} (13)	code (14)	A_{ion} 10^{-9} (15)	A_{ref} 10^{-9} (16)	A/A$_\odot$ (17)	D? (18)	Ref (19)	Note (20)
Population EP			> 0.4	> 0.2						CI				270 ±170		0.00075			0.25$Z_\odot$
										CIV		[1600]							
										NI				>4000	[23000]	>0.043			
										NII				>1100		>0.012			
										NV		[350]							
										NaI				<3.6		<0.0018			
										SiII				>1100	[4800]	>0.031			
										AlII				<1500	[410]	<0.51			
										SII				4500 ±1300	[4700]	0.24			
										PII				<140	[93]	<0.36			
										PIII				<490	[93]	<1.3			
										ArI				<2100	[300]	<0.59			
										FeII				1000 ±200	[1900]	0.032			
										CaII				67 ±8	[22]	0.031			
NGC 1705	261.08	−38.74	—	—	Gal	WW487	+287	1.7 ±0.4	PM	SiII	+260	290 ±50	W	1.7E4 ±5.0E3		0.48		91	
										SiII	+260	1700 ±800	W	1.0E5 ±5.0E4		2.9		91	
										SiII	+260	1800 ±800	W	1.0E5 ±5.5E4		2.9		91	
										SII	+260	<4500	W	<2.6E5				101	
										AlII	+260	<26	W	<1500				101	
										FeII	+260	<460	W	<2.7E4				101	
NGC 3783	287.46	22.95	—	—	Sey	WW187	+240	83 ±9	AP	H_2	+241	6.9E5 ±1.6E5	L	8.3E5 ±2.1E5				127	
										CI	+236	220 ±140	W	270 ±170		.00075		64	
										CIV		<330	W					64	
										NI	+240	>3300	L	>4000		>0.043		127	
										NII	+240	>930	L	>1100		>0.012		127	
										NV		<330	W					64	
										NaI		<3.0	N	<3.6				22	
									(	SiII	+231	>930	W	>1100		>0.031		64)	80,τ
										SiII	+240	4400 ±1000	L	5300 ±1300		0.15		127	τ
									(	SII	+236	4000 ±1600	W	4800 ±2000		0.26		64)	81
										SII	+236	3700 ±1000	N	4500 ±1300		0.24		100	
										PII	+240	<110	L	<140				127	
										PIII	+240	<410	L	<490				127	
										ArI	+240	<1800	L	<2100				127	
										FeII	+240	850 ±100	N	1000 ±200		0.032		100	
										CaII	+241	56 ±3	N	67 ±8		0.031		22	
NGC 2808	282.19	−11.25	8.9	1.7	GC	WW621	+275	2.2 ±0.9	PM	CaII		<5.9	W	<270				8	
HD 86248	264.59	18.11	7.6±1.7 t	2.4	B3II	WW211	+201	7.6 ±3.0	GB	SiII		<230	N	<3000				50	s,82
HD 102383	290.10	19.97	0.80±0.10 t	0.27	B6Vne	WW187	+230	2.0 ±0.3	PK	CaII		<5.5	W	<280				25	
HD 101274	287.47	22.94	0.40±0.03 s	0.16	A0V	WW187	+244	83 ±9	AP	CaII		<5.4	W	<6.5			l	25	
Population EN																			
Mrk 205	125.45	41.67	—	—	Sey	WW84	−202	8.0 ±5.0	WE	NaI		<4.4	W	<55				49	83
										MgII	−209	61 ±17	W	770 ±530		0.020		75	
										CaII		<7.1	W	<89				49	
PKS 1923+210	55.56	2.26	—	—	radio	WW274	(−198)	<2.5	Dw	HCO^+	−198	4.3	N	>170				115	

TABLE 2—*Continued*

Probe	l	b	d	z	type	Cld	v_{HI}	N_{HI}	tel	ion	v_{ion}	N_{ion}	code	A_{ion}	A_{ref}	$A/A_{\odot}$	D?	Ref	Note
	°	°	kpc	kpc			km/s	10^{18} cm^{-2}			km/s	10^{11} cm^{-2}		10^{-9}	10^{-9}				
(1)	(2)	(3)	(4)	(5)	(6)	(7)	(8)	(9)	(10)	(11)	(12)	(13)	(14)	(15)	(16)	(17)	(18)	(19)	(20)
Complex L			> 0.2	> 0.1															
HD 135485	347.31	35.46	0.18±0.04	p 0.1	B5IIIp	WW132	−98	5.1	WJ	CII		<70	N	<1400			L	78	84
										OI		<200	N	<3900			L	78	
										SiII		<10	N	<200			L	78	
Mistaken claims																			
HD 135485	347.31	35.46	0.18±0.04	p 0.1	B5IIIp	WW132	−98	5.1	WJ	CaII	−98	1.8 ±0.3	W	34 ±5		0.016	U	58	84,85
										CaII	−127	1.9 ±0.3	W	37 ±6		0.017	U	58	
Complex WB										NaI									
										CaII				280 ±120	[22]	0.13			
PKS 0837–12	237.17	17.43	—	—	QSO	WW225	+112	7.9 ±3.2	Ef	CaII	+106	22 ±3	N	280 ±120		0.13		48	86
HD 76510	241.02	19.75	1.3	t 0.44	B1V	WW225	+100	10 ±5	Dw	NaI	+98	<1.5	N	<15				54	
										CaII	+98	<1.5	N	<15			l	54	
Complex WE			< 13	< 3.2															
HD 156359	328.68	−14.52	13±2	t 3.2	O9.7II	WW364	(+110)	<2.0	VE	CII	+112	290 ±100	W	>1.5E4		>0.042	U	45	87,W
										NV	+128	58 ±22	N					71	
										MgII	+112	20 ±3	W	>1000		>0.027	U	45	W
										SiII	+106	20 ±6	W	>990		>0.028	U	45	W
										SiIII	+106	14 ±3	W	>690		>0.019	U	45	W
										FeII	+115	51 ±14	W	>2600		>0.079	U	45	W
Small positive-velocity clouds																			
3C 200	193.95	32.60	—	—	radio	WW137	+97	14	Ar	HI		<14	τ			T_s>20		5	T
BD +10 2179	235.21	54.44	4.0	r 3.3	Bp	WW29	+88	5.7 ±0.4	Ef	SiII		<230	N	<4000				50	s
4C 06.41	241.11	52.65	—	—	QSO	WW34	+91	2.6 ±0.3	Dw	MgII		>0	E	>0		>0		121	f
PKS 1136–13	277.53	45.43	—	—	QSO	WW62	+100	<1.0	Ef	MgII		>0	E	>0		>0		121	f
SN 1991 T	292.61	65.19	—	—	SN		+113	2.9 ±0.1	HC	CaII		<0.46	W	<16				47	88
HD 212593	99.90	−6.71	1.3±0.1	t 0.15	B9Iab	100–7	+106	5.0 ±0.2	WJ	OI	+110	2.5E4 ±2.0E4	L	5.0E5 ±4.0E5		0.68	U	42	89
(4 Lac)										MgII	+100	3200 ±2200	L	6.3E4 ±4.3E4		1.7	U	42	τ
										MgI	+100	5.0 ±1.2	L	100 ±20		0.0026	U	42	
										AlII	+106	63 ±38	L	1300 ±800		0.42	U	42	
										FeII	+105	400 ±90	L	8000 ±1900		0.25	U	42	

TABLE 2—*Continued*

Probe	l °	b °	d kpc	z kpc	type	Cld	v_{HI} km/s	N_{HI} 10^{18} cm^{-2}	tel	ion	v_{ion} km/s	N_{ion} 10^{11} cm^{-2}	code	A_{ion} 10^{-9}	A_{ref} 10^{-9}	A/A$_\odot$	D?	Ref	Note
(1)	(2)	(3)	(4)	(5)	(6)	(7)	(8)	(9)	(10)	(11)	(12)	(13)	(14)	(15)	(16)	(17)	(18)	(19)	(20)
HVCs with low or no H I																			
SN 1994 I	104.84	68.56	—	—	SN		(+250)	<2.5	Ef	NaI	+246	3.2 ± 1.5	L	>130		>0.062		73	90
										NaI	+272	0.79 ± 0.18	L	>32		>0.016		73	
										NaI	+301	1.3 ± 0.3	L	>50		>0.025		73	
SN 1993 J	142.15	40.92	—	—	SN		(+125)	<6.0	ef	NaI	+125	48	N	>800		>0.39		61	91
										KI	+122	0.55	N	>9.2		>0.068		61	
										CaI	+122	0.10	N	>1.7		>.00076		61	
										CaII	+125	17	N	>280		>0.13		61	
							(+140)	<6.0	ef	CIV	+140	400	L					53	
										NaI	+140	29	N	>480		>0.24		61	
										MgI	+140	20	L	>330		>0.0087		53	
										AlII	+140	100	L	>1700		>0.55		53	
										AlIII	+140	200	L	>3300		>1.1		53	
										SiII	+140	2500	L	>4.2E4		>1.2		53	τ
										SiIV	+140	250	L					53	
										KI	+140	0.35	N	>5.8		>0.043		61	
										CaI	+140	0.10	N	>1.7		>.00076		61	
										CaII	+140	2.6	N	>43		>0.020		61	
										FeII	+140	1600	L	>2.6E4		>0.82		53	
							(+230)	<6		MgII	+231	40 ± 16	N	>670		>0.018		63	
PKS 0232–04	174.46	−56.16	—	—	QSO		(+275)	<0.70	GB	MgII	+275	>540	W	>7.7E4		>2.0		121	76
PG 0953+414	179.78	51.71	—	—	QSO		(−150)	<2.0	Ef	CII	−149	350 ± 60	L	>1.8E4		>0.050		128	
										SiII	−152	32 ± 5	L	>1600		>0.046		128	
										SiIII	−148	35 ± 7	L	>1800		>0.050		128	
										AlII	−145	8.9 ± 3.6	L	>450		>0.15		128	
							(+130)	<2.0	Ef	CII	+126	210 ± 30	L	>1.1E4		>0.030		128	
										SiIII	+131	43 ± 9	L	>2100		>0.060		128	
PG 1116+215	223.36	68.21	—	—	QSO		(+200)	<0.70	GB	CII	+200	>0	N	>0		>0		98	
										SiII	+200	>0	N	>0		>0		98	
										MgII	+267	90 ± 48	W	>1.3E4		>0.34		121	76,W
SN 1994 D	290.15	70.14	—	—	SN		+204	1.6 ± 0.5	Ef	CaII	+204	1.7 ± 0.3	L	100 ± 40		0.047		69	92
							(+214)	<2.5	Ef	NaI	+214	1.4 ± 0.2	L	>57		>0.028		73	
										CaII	+216	3.4 ± 0.4	L	>140		>0.062		69	
							(+234)	<2.5	Ef	NaI	+234	1.5 ± 0.2	L	>59		>0.029		73	
										CaII	+232	13 ± 1	L	>500		>0.23		69	
							(+252)	<2.5	Ef	NaI	+254	0.50 ± 0.08	L	>20		>0.0098		73	
										CaII	+254	3.5 ± 0.4	L	>140		>0.065		69	
SN 1991 T	292.61	65.19	—	—	SN		(+250)	<0.30	HC	CaII	+215	0.74 ± 0.12	N	>250		>0.11		47	88
										CaII	+263	1.1 ± 0.1	N	>370		>0.17		47	
SN 1986 G	309.54	19.40	—	—	SN	WW219	+245a	2.8 ± 1.2	PK	NaI	+233	1.3 ± 0.05	W	46 ± 20		0.023		31	93,V
										CaII	+233	4.3 ± 0.3	W	150 ± 70		0.070		31	
						WW219	+245b	4.0 ± 1.2	PK	NaI	+254	2.4 ± 0.05	W	60 ± 18		0.030		31	
										CaII	+254	6.2 ± 0.3	W	150 ± 50		0.070		31	
SN 1983 N	314.54	31.95	—	—	SN		(+250)	<6.0	Dw	CaII	+248	1.6 ± 1.4	W	>27		>0.012		20	94,W

TABLE 2—*Continued*

Probe	l	b	d	z	type	Cld	v_HI	N_HI	tel	ion	v_ion	N_ion	code	A_ion	A_ref	A/A⊙	D?	Ref	Note
	°	°	kpc	kpc			km/s	10^{18} cm^{-2}			km/s	10^{11} cm^{-2}		10^{-9}	10^{-9}				
(1)	(2)	(3)	(4)	(5)	(6)	(7)	(8)	(9)	(10)	(11)	(12)	(13)	(14)	(15)	(16)	(17)	(18)	(19)	(20)
HVC on LMC @+160 km s^{-1}			< 50							CI				<590		<0.0017			
										NaI				<5.9		<0.0029			
										MgI				110 ±20		0.0029			
										MgII				2.3E4 ±2.7E3	[14000]	0.61			
										AlII				930 ±170	[1600]	0.31			
										SiII				1.8E4 ±5.4E3	[19000]	0.50			
										PII				<1.2E4	[370]	<31			
										ClI				<930		<5.0			
										KI				<2.9		<0.022			
										CaI				0.87 ±0.11		0.00040			
										CaII				40 ±10	[22]	0.018			95
										TiII				<150	[21]	<1.7			
										CrII				<290	[150]	<0.61			
										MnII				74 ±21	[87]	0.22			
										FeII				8700 ±1800	[7800]	0.27			
										NiII				<590	[260]	<0.33			
										ZnII				<93	[42]	<2.1			
SN 1987 A	279.70	−31.94	50 g	26	SN		+165	5.4	AB	CI		<32	L	<590				109	96
										NaI		<0.32	N	<5.9				109	
										MgI	+165	6.0 ±1.1	L	110 ±20		0.0029	U	109	
									(	MgII	+171	400 ±190	L	7400 ±3500		0.19	U	34)	
										MgII	+165	1300 ±100	L	2.3E4 ±2.7E3		0.61	U	109	
									(	AlII	+171	55 ±13	L	1000 ±200		0.34	U	34)	
										AlII	+165	50 ±9	L	930 ±170		0.31	U	109	
									(	SiII	+171	500 ±120	L	9300 ±2200		0.26	U	34)	
										SiII	+165	950 ±290	L	1.8E4 ±5.4E3		0.50	U	109	
										PII		<630	L	<1.2E4				109	
										ClI		<50	L	<930				109	
										KI		<0.16	L	<2.9				109	
									(	CaI	+168.6	0.043 ±0.003	N	0.80 ±0.06		.00036	U	26)	
										CaI	+165	0.047 ±0.006	N	0.87 ±0.11		.00040	U	109	
									(	CaII	+165.4	2.1	W	39		0.018	U	27)	W
									(	CaII	+169.9	2.8 ±0.01	N	52 ±0.2		0.024	U	26)	
										CaII	+165	2.8 ±0.3	N	52 ±6		0.024	U	109	
										TiII		<7.9	L	<150				109	
									(	CrII		<10	L	<190				34)	
										CrII		<16	L	<290				109	
									(	MnII		<10	L	<190				34)	
										MnII	+165	4.0 ±1.1	L	74 ±21		0.22	U	109	
									(	FeII	+171	400 ±110	L	7400 ±2100		0.23	U	34)	
										FeII	+165	470 ±100	L	8700 ±1800		0.27	U	109	
									(	NiII		<79	L	<1500				34)	
										NiII		<32	L	<590				109	
										ZnII		<5.0	L	<93				109	
Sk–67 166	277.84	−32.49	50 g	27	O4If+		(+170)	<2.0	PR	CaII	+175	3.6	W	>180		>0.081	U	40	97,W
Sk–68 135	279.26	−31.77	50 g	26	On9.7Ia		+170	2.0 ±1.0	PR	CaII	+150	7.4	W	370		0.17	U	40	97,W
Sk–68 137	279.20	−31.73	50 g	26	O3III(f*)		+170	2.0 ±1.0	PR	CaII	+160	3.6	W	180		0.081	U	40	97,W
Sk–69 51	281.02	−35.07	50 g	29	B1		+170*a*	11 ±1	PR	CaII	+155	11	W	110		0.050	U	40	97
							+170*b*	9.5 ±1.0	PR	CaII	+180	10	W	110		0.048	U	40	97
Sk–69 52	281.23	−35.02	50 g	29	B2Ia		+170	20 ±1	PR	CaII	+160	7.4	W	37		0.017	U	40	97,W
Sk–69 106	280.44	−33.30	50 g	27	B0:					CaII	+150	3.6	W				U	23	97,W
Sk–69 107	280.42	−33.27	50 g	27	O9.5Ib					CaII	+150	3.6	W				U	23	97,W
Sk–69 211	279.85	−31.86	50 g	26	B9Ia		+165	6.5 ±1.0	PI	CaII	+169.6	4.4 ±0.3	L	67 ±11		0.031	U	52	
Sk–69 216	279.83	−31.77	50 g	26	Be		+164	5.6	PI	CaII	+169.7	5.5 ±0.5	L	98 ±9		0.045	U	52	
Sk–69 276	279.96	−31.37	50 g	26	B0Iab					CaII	+165.7	8.7 ±0.3	N				U	85	

TABLE 2—*Continued*

Probe	l	b	d	z	type	Cld	v_{HI}	N_{HI}	tel	ion	v_{ion}	N_{ion}	code	A_{ion}	A_{ref}	A/A$_{\odot}$	D?	Ref	Note
	°	°	kpc	kpc			km/s	10^{18} cm^{-2}			km/s	10^{11} cm^{-2}		10^{-9}	10^{-9}				
(1)	(2)	(3)	(4)	(5)	(6)	(7)	(8)	(9)	(10)	(11)	(12)	(13)	(14)	(15)	(16)	(17)	(18)	(19)	(20)
Sk–69 243=R136	279.47	−31.69	50 g	26	OB+WN5-6		+155	5.8 ±1.0	Pk(	CaII	+149	2.0	W	34		0.016	U	6)	98,W
(HD 38268)										CaII	+141.6	1.5 ±0.6	L	26 ±11		0.012	U	52	
Sk–69 282	279.34	−31.38	50 g	26	B1.5					CaII	+176.2	2.7 ±0.1	N				U	85	
										TiII	+173.8	1.5 ±0.9	N				U	85	
Sk–69 290	279.29	−31.31	50 g	26	B0.5					CaII	+182.0	4.2 ±1.1	N				U	85	
HVC on LMC @+120 km s^{-1}			< 50							CI				<400		<0.0011			
										CIV		[1600]							
										OI				2.2E5 ±9.0E4	[740000]	0.30			99
										NaI				0.75 ±0.38		0.00037			
										MgI				400 ±200		0.011			100
										MgII					[14000]				
										AlII				1200 ±200	[1600]	0.39			
										AlIII				54 ±37		0.018			
										SiII				1.8E4 ±5.5E3	[19000]	0.51			
										SiIV		[440]							
										PII				<7900	[370]	<21			
										SII				5.0E4 ±3.0E5	[19000]	2.7			101
										ClI				<630		<3.4			
										KI				<2.5		<0.018			
										CaI				<0.050		<.000023			
										CaII				31 ±14	[22]	0.014			102
										TiII				<99	[21]	<1.2			
										CrII				<200	[150]	<0.41			
										MnII				63 ±33	[87]	0.18			
										FeII				2.0E4 ±1.5E4	[7800]	0.62			103
										NiII				<400	[260]	<0.22			
										ZnII				<63	[42]	<1.4			
SN 1987 A	279.70	−31.94	50 g	26	SN		+122	8.0	AB	CI		<32	L	<400				109	96
										NaI	+122	0.060 ±0.030	N	0.75 ±0.38		.00037	U	109	
										MgI	+122	8.9 ±1.0	L	110 ±10		0.0029	U	109	
									(	MgII	+129	400 ±190	L	5000 ±2400		0.13	U	34)	
										MgII	+122	1700 ±200	L	2.1E4 ±2.9E3		0.55	U	109	
									(	AlII	+129	50 ±12	L	630 ±150		0.21	U	34)	
										AlII	+122	93 ±19	L	1200 ±200		0.39	U	109	
									(	SiII	+129	400 ±90	L	5000 ±1200		0.14	U	34)	
										SiII	+122	1400 ±400	L	1.8E4 ±5.5E3		0.51	U	109	
										PII		<630	L	<7900				109	
										ClI		<50	L	<630				109	
										KI		<0.20	L	<2.5				109	
									(	CaI		<.0070	N	<0.087			l	26)	
										CaI		<.0040	N	<0.050			l	109	
									(	CaII	+125.7	3.3	W	41		0.019	U	27)	W
										CaII	+122	4.6 ±0.2	N	57 ±3		0.026	U	109	
										TiII		<7.9	L	<99				109	
									(	CrII		<10	L	<120				34)	
										CrII		<16	L	<200				109	
									(	MnII		<10	L	<120				34)	
										MnII	+122	5.0 ±2.6	L	63 ±33		0.18	U	109	
									(	FeII	+129	600 ±260	L	7500 ±3200		0.23	U	34)	
										FeII	+122	720 ±200	L	9100 ±2500		0.28	U	109	
									(	NiII		<79	L	<990				34)	
										NiII		<32	L	<400				109	
										ZnII		<5.0	L	<63				109	

TABLE 2—*Continued*

Probe (1)	l ° (2)	b ° (3)	d kpc (4)	z kpc (5)	type (6)	Cld (7)	v_{HI} km/s (8)	N_{HI} 10^{18} cm^{-2} (9)	tel (10)	ion (11)	v_{ion} km/s (12)	N_{ion} 10^{11} cm^{-2} (13)	code (14)	A_{ion} 10^{-9} (15)	A_{ref} 10^{-9} (16)	A/A$_\odot$ (17)	D? (18)	Ref (19)	Note (20)
							+120–	14	AB	CIV		270 ±30	L					37	104
							+190			AlIII		7.6 ±5.2	L	54 ±37		0.018	U	37	
										SiIV		59 ±7	L					37	
Sk–66 118	277.00	−32.66	50 g	27	B2Ia					CIV	+130	>300	N					81	
Sk–66 169	276.60	−32.11	50 g	27	O9.7Ia					NaI	+108	11 ±3	W				U	8	W
Sk–67 05	278.89	−36.33	50 g	30	O9.7Ib		+133	2.2 ±1.0	Pk	NaI		<2.3	W	<100				8	98,105,W
Sk–67 104	277.76	−33.04	50 g	27	WC5+O9		+120	5.8	Pk	H_2	+131	3200	L	5.5E4		000055	U	124	98
(HD 36402)										OI	+131	1.6E4 ±1.2E4	L	2.7E5 ±2.0E5		0.37	U	124	
										MgI	+131	20 ±12	L	340 ±210		0.0090	U	124	
										MgII	+131	1600 ±1300	L	2.7E4 ±2.3E4		0.72	U	124	τ
										SiII	+131	4000 ±3000	L	6.9E4 ±5.1E4		1.9	U	124	τ
										SII	+131	5000 ±3000	L	8.6E4 ±5.2E4		4.6	U	124	
										FeII	+131	1600 ±1200	L	2.7E4 ±2.0E4		0.84	U	124	
Sk–67 120	277.70	−32.89	50 g	27	O8III:		+113	8.8 ±1.0	PI	CaII	+130	6.1	W	69		0.032	U	40	97
Sk–67 166	277.84	−32.49	50 g	27	O4If+		+130	3.0 ±1.0	PR	H_2	+120	5000	L	1.7E5		.00017	U	124	
										OI	+125	7100 ±3400	L	2.4E5 ±1.4E5		0.32	U	124	
										MgI	+125	18 ±8	L	590 ±340		0.016	U	124	
										MgII	+125	630 ±590	L	2.1E4 ±2.1E4		0.55	U	124	
										SiII	+125	2000 ±1500	L	6.7E4 ±5.4E4		1.9	U	124	τ
										SII	+125	7100 ±3400	L	2.4E5 ±1.4E5		13	U	124	
										CaII	+120	4.8	W	160		0.073	U	40	97,W
										FeII	+125	1300 ±800	L	4.2E4 ±2.9E4		1.3	U	124	
Sk–67 169	277.15	−32.54	50 g	27	B1Ia		+104	4.6 ±1.0	Pk	CIV	+145	70	N					81	98
Sk–68 82	279.32	−32.78	50 g	27	B3I+WN		+122	12 ±1	Pk(	H_2	+120	2.9E4 ±7.0E3	N	2.4E5 ±6.0E4				105)	98
(HD 269546)										H_2	+118	3.6E4 ±6.7E3	L	3.0E5 ±6.0E4				124	
										OI	+118	1.6E4 ±1.2E4	L	1.3E5 ±9.7E4		0.17	U	124	
										NaI		<1.2	W	<10				12	W
										MgI	+118	63 ±47	L	510 ±390		0.013	U	124	
										SiII	+118	1.3E4 ±9.4E3	L	1.0E5 ±7.7E4		2.9	U	124	τ
										SII	+118	4500 ±3300	L	3.6E4 ±2.7E4		2.0	U	124	
										CaII	+123	24 ±2	W	200 ±20		0.089	U	12	W
									(	FeII	+120	2000 ±1000	L	1.6E4 ±7.8E3		0.50	U	105)	
										FeII	+118	2500 ±1900	L	2.0E4 ±1.5E4		0.63	U	124	τ
Sk–69 91	280.69	−33.36	50 g	27	B0.7Ia					CaII		<5.4	W					8	W
Sk–69 195	279.67	−31.99	50 g	26	B2:		+122	8.0	AB	NaI		<1.6	L	<20				52	
Sk–69 203	279.66	−31.95	50 g	26	B0.7Ia		+122	8.0	AB	NaI		<0.63	L	<7.9				52	
										CaII	+122	8.3 ±0.8	L	100 ±10		0.048	U	52	
Sk–69 204	279.92	−31.92	50 g	26	B1		+115	7.7	PI	NaI		<0.42	L	<5.4				52	
Sk–69 211	279.85	−31.86	50 g	26	B9Ia		+115	7.6	PI	NaI		<0.52	L	<6.9				52	
							+115*a*	4.7	PI	CaII	+107.1	3.2 ±0.3	L	68 ±6		0.031	U	52	
							+115*b*	2.9	PI	CaII	+129.4	2.0 ±0.3	L	68 ±10		0.031	U	52	
Sk–69 213	279.60	−31.88	50 g	26	B1Ia		+116	7.3	PI	NaI		<0.32	L	<4.3				52	
Sk–69 215	279.52	−31.88	50 g	26	O-B0		+116	7.1	PI	NaI		<0.32	L	<4.5				52	
Sk–69 216	279.83	−31.77	50 g	26	Be		+112	7.5	PI	NaI		<0.42	L	<5.6				52	
										CaII		<2.2	L	<30				52	
Sk–69 224	279.61	−31.82	50 g	26	B0		+115	7.2	PI	NaI		<0.42	L	<5.8				52	
										CaII		<5.4	L	<75				52	
Sk–69 225	279.68	−31.81	50 g	26	B8I		+114	7.3	PI	NaI		<0.63	L	<8.6				52	
Sk–69 239	279.48	−31.72	50 g	26	A0I		+111	6.1	Pk	NaI		<0.21	L	<3.4				52	
										CaII		<1.3	L	<22				52	

TABLE 2—*Continued*

Probe	l °	b °	d kpc	z kpc	type	Cld	v_{HI} km/s	N_{HI} 10^{18} cm^{-2}	tel	ion	v_{ion} km/s	N_{ion} 10^{11} cm^{-2}	code	A_{ion} 10^{-9}	A_{ref} 10^{-9}	A/A$_\odot$	D?	Ref	Note
(1)	(2)	(3)	(4)	(5)	(6)	(7)	(8)	(9)	(10)	(11)	(12)	(13)	(14)	(15)	(16)	(17)	(18)	(19)	(20)
Sk–69 243=R136	279.47	−31.69	50 g	26	OB+WN5-6		+111	6.1	Pk	NaI		<0.32	L	<5.2				52	98
(HD 38268)									(	CaII	+123	1.2	W	19		0.0087	U	6)	W
										CaII	+121.6	1.3 ±0.6	L	21 ±10		0.0097	U	52	
Sk–69 246	279.39	−31.67	50 g	26	WN7		+111	6.1 ±1.0	Pk	NaI		<0.32	L	<5.2				52	98
(HD 38282)										CaII		<1.3	L	<22				52	
										FeII	+130	320	L	5200		0.16	U	3	
Sk–69 247	279.93	−31.61	50 g	26	A0Ia+		+105	7.4	Pk	NaI		<0.52	L	<7.1				52	106
							+105*a*	3.0	Pk	CaII	+121.7	1.2 ±0.5	L	40 ±17		0.018	U	52	
							+105*b*	4.4	Pk	CaII	+135.3	1.8 ±0.5	L	40 ±11		0.018	U	52	
Sk–69 274	280.25	−31.35	50 g	26	B2.5Ia		+110	5.0 ±1.0	PR	CaII	+110	2.3	W	47		0.021	U	40	97,W
Sk–69 282	279.34	−31.38	50 g	26	B1.5					CaII	+112.9	3.3 ±0.1	N				U	85	
Sk–69 290	279.29	−31.31	50 g	26	B0.5					CaII	+105.7	2.8 ±1.1	N				U	85	
Sk–70 111	280.49	−31.31	50 g	26	B0.5Ia					CaII	+117.7	5.4 ±0.1	N				U	85	
Sk–71 3	282.82	−34.25	50 g	28	pec		+125	2.7 ±1.0	Pk(	NaI	+144	6.4 ±0.9	W	240 ±90		0.12	U	8)	98,W
										NaI		<2.5	W	<93				12	W
									(	CaII	+139	35 ±3	W	1300 ±500		0.59	U	8)	W
										CaII	+126	52 ±3	W	1900 ±700		0.89	U	12	W
Sk–71 33a	281.85	−32.19	50 g	27	B5Ia					CaII	+120	4.8	W				U	23	97,W
Sk–71 41	281.91	−32.07	50 g	27	O8.5I		+112	11 ±1	Pk	CaII	+120	2.3	W	22		0.010	U	23	97,W
Sk–71 42	281.87	−32.06	50 g	27	B1Iab		+112	11 ±1	Pk	NaI		<0.99	W	<9.2				12	98,W
									(	CaII	+132	26	W	240		0.11	U	12)	W
										CaII	+130	3.6	W	33		0.015	U	23	97,W
Sk–71 45	281.86	−32.02	50 g	27	O4If		+112	11 ±1	Pk	CaII	+120	2.3	W	22		0.010	U	23	97,W
LH 10:3120	277.19	−36.06	50 g	29	O5.5V					H_2	+120	1.0E4	L				U	124	
										OI	+122	1.0E4	L				U	124	
										SiII	+122	400	L				U	124	
										SII	+122	1.3E4	L				U	124	
										FeII	+122	1600	L				U	124	
IVC on LMC @+65 km s^{-1}			< 50							CI				340 ±130		0.00095			
										CII				>6.0E4	[350000]	>0.17			
										CIV		[1600]		8600					
										NV		[350]		<2600					
										OI				1.0E5 ±2.0E4	[740000]	0.13			
										NaI				11 ±1		0.0054			107
										MgI				390 ±50		0.010			
										MgII				2.6E4	[14000]	0.68			
										AlII					[1600]				108
										SiII				3.5E4 ±2.0E4	[19000]	0.99			109
										SiIII				>2600		>0.073			
										SiIV		[440]							
										PII				<9700	[370]	<26			
										SII				>1.9E4	[19000]	>1.00			
										ClI				<770		<4.1			
										KI				<3.9		<0.029			
										CaI				0.31 ±0.06		0.00014			
										CaII				100 ±70	[22]	0.046			110
										TiII				<120	[21]	<1.4			
										CrII				930 ±170	[150]	1.9			
										MnII				390 ±70	[87]	1.1			
										FeII				3.3E4 ±6.0E3	[7800]	1.0			111
										NiII				2200 ±800	[260]	1.2			
										ZnII				40 ±24	[42]	0.91			

TABLE 2—*Continued*

Probe	l	b	d	z	type	Cld	v_{HI}	N_{HI}	tel	ion	v_{ion}	N_{ion}	code	A_{ion}	A_{ref}	$A/A_\odot$	D?	Ref	Note
	°	°	kpc	kpc			km/s	10^{18} cm^{-2}			km/s	10^{11} cm^{-2}		10^{-9}	10^{-9}				
(1)	(2)	(3)	(4)	(5)	(6)	(7)	(8)	(9)	(10)	(11)	(12)	(13)	(14)	(15)	(16)	(17)	(18)	(19)	(20)
SN 1987 A	279.70	−31.94	50 g	26	SN		+65	6.5	AB	CI	+65	22 ±8	L	340 ±130		.00095	U	109	96
										OI	+70	>1.0E4	L	>1.5E5		>0.21	U	34	
									(	NaI	+64.6	0.69	W	11		0.0052	U	27)	W
									(	NaI	+74.8	0.097	W	1.5		.00073	U	27)	W
									(	NaI	+64.5	0.50 ±0.08	N	7.7 ±1.2		0.0038	U	36)	
										NaI	+65	0.74 ±0.07	N	11 ±1		0.0056	U	109	
										MgI	+65	25 ±3	L	390 ±50		0.010	U	109	
										AlII	+70	>500	L	>7700		>2.6	U	34	τ
									(	SiII	+70	>1200	L	>1.8E4		>0.52	U	34)	τ
										SiII	+65	4800 ±800	L	7.4E4 ±1.2E4		2.1	U	109	
										PII		<630	L	<9700				109	
										ClI		<50	L	<770				109	
										KI		<0.25	L	<3.9				109	
									(	CaI	+65.3	0.016	W	0.25		.00011	U	27)	W
									(	CaI	+64.3	0.022 ±0.003	N	0.34 ±0.05		.00015	U	26)	
										CaI	+65	0.020 ±0.004	N	0.31 ±0.06		.00014	U	109	
									(	CaII	+60.8	8.7 ±0.004	W	130 ±0.06		0.061	U	27)	W
									(	CaII	+64.5	8.3 ±0.01	N	130 ±0.2		0.058	U	26)	
									(	CaII	+73.5	2.3 ±0.01	W	36 ±0.2		0.017	U	27)	W
									(	CaII	+83.6	1.8 ±0.01	W	28 ±0.2		0.013	U	26)	W
										CaII	+65	15 ±0.3	N	230 ±5		0.11	U	109	
										TiII		<7.9	L	<120				109	
									(	CrII	+70	30 ±13	L	450 ±190		0.95	U	34)	
										CrII	+65	60 ±11	L	930 ±170		1.9	U	109	
									(	MnII	+70	30 ±13	L	460 ±200		1.4	U	34)	
										MnII	+65	25 ±5	L	390 ±70		1.1	U	109	
									(	FeII	+70	>1500	L	>2.3E4		>0.72	U	34)	
										FeII	+65	2600 ±500	L	4.0E4 ±8.3E3		1.2	U	109	
									(	NiII	+70	170 ±40	L	2600 ±600		1.5	U	34)	
										NiII	+65	140 ±50	L	2200 ±800		1.2	U	109	
									(	ZnII		<2.0	L	<31				34)	
										ZnII	+65	2.6 ±1.5	L	40 ±24		0.91	U	109	
Sk–65 40	276.76	−34.02	50 g	28	B3Ia		+60	<2.0	Pk	CaII		<1.2	W					12	98,W
Sk–66 28	277.27	−36.06	50 g	29	WC6+O8					CaII	+70	3.6	W				U	35	97,W
Sk–66 118	277.00	−32.66	50 g	27	B2Ia					CIV	+73	>1000	N					81	
Sk–67 05	278.89	−36.33	50 g	30	O9.7Ib		+45	4.9 ±1.0	Pk	NaI	+57	3.4 ±0.8	W	70 ±22		0.034	U	8	98,105,W
							+45−	7.1 ±1.0	Pk	OI	+75	7400	W	1.0E5		0.14	U	10	W
							+133			AlII	+70	30	W	430		0.14	U	10	W
										FeII		>1300	L	>1.8E4		>0.55	U	10	
Sk–67 104	277.76	−33.04	50 g	27	WC5+O9		+52	4.8	Pk	H_2	+60	4000	L	8.3E4		000083	U	124	98
(HD 36402)										CII	+90	>7000	N	>1.5E5		>0.41	U	11	
										CIV	+90	1000	N					11	
										NV		<300	N					11	
									(	OI	+90	>5000	L	>1.0E5		>0.14	U	10)	
									(	OI	+90	>1.0E4	L	>2.1E5		>0.28	U	11)	
										OI	+70	1.8E4 ±1.3E4	L	3.7E5 ±2.8E5		0.50	U	124	
										MgI	+70	20 ±14	L	420 ±280		0.011	U	124	
									(	MgII	+90	>630	L	>1.3E4		>0.35	U	10)	
									(	MgII	+90	3000	N	6.2E4		1.6	U	11)	τ
										MgII	+70	320 ±280	L	6600 ±5800		0.17	U	124	
									(	AlII	+90	>130	L	>2600		>0.87	U	10)	
										AlII	+90	150	N	3100		1.0	U	11	
									(	SiII	+90	>3200	L	>6.6E4		>1.9	U	10)	τ
									(	SiII	+90	3500	N	7.3E4		2.1	U	11)	τ
										SiII	+70	1000 ±700	L	2.1E4 ±1.4E4		0.59	U	124	τ

TABLE 2—*Continued*

Probe (1)	l ° (2)	b ° (3)	d kpc (4)	z kpc (5)	type (6)	Cld (7)	v_{HI} km/s (8)	N_{HI} 10^{18} cm^{-2} (9)	tel (10)	ion (11)	v_{ion} km/s (12)	N_{ion} 10^{11} cm^{-2} (13)	code (14)	A_{ion} 10^{-9} (15)	A_{ref} 10^{-9} (16)	A/A$_\odot$ (17)	D? (18)	Ref (19)	Note (20)
										SiIII	+90	>300	N	>6300		>0.18	U	11	
										SiIV	+90	300	N					11	
										SII	+70	2000 ±1200	L	4.2E4 ±2.5E4		2.2	U	124	
									(	FeII	+90	>2500	L	>5.2E4		>1.6	U	10)	τ
									(	FeII	+90	2500	N	5.2E4		1.6	U	11)	τ
										FeII	+70	1600 ±1100	L	3.3E4 ±2.3E4		1.0	U	124	
Sk–67 120	277.70	−32.89	50 g	27	O8III:		+51	3.9 ±1.0	PI	CaII	+70	7.4	W	190		0.086	U	40	97
Sk–67 166	277.84	−32.49	50 g	27	O4If+		(+60)	<2.0	PR	H_2	+60	4000	L	>2.0E5		>.00020	U	124	
										OI	+61	1.0E4 ±9.4E3	L	>5.0E5		>0.67	U	124	
										MgI	+61	7.9 ±5.9	L	>400		>0.010	U	124	
										MgII	+61	2000 ±1900	L	>1.0E5		>2.6	U	124	τ
										SiII	+61	1000 ±700	L	>5.0E4		>1.4	U	124	τ
										SII	+61	6300 ±6100	L	>3.2E5		>17	U	124	
										CaII	+60	4.8	W	>240		>0.11	U	40	97,W
										FeII	+61	2500 ±1500	L	>1.3E5		>3.9	U	124	τ
Sk–67 169	277.15	−32.54	50 g	27	B1Ia		(+70)	<2.0	Pk	CIV	+73	600	N					81	98
Sk–67 174	277.91	−32.44	50 g	27	O8V					NaI	+87	2.0	W				U	7	97,W
Sk–67 250	277.96	−31.37	50 g	26	O7.5II(f)					CaII	+67	17	W				U	14	97,W
Sk–68 82	279.32	−32.78	50 g	27	B3I+WN		+50	1.6 ±1.0	Pk	H_2	+60	4.5E4 ±3.6E4	L	2.8E6 ±2.8E6		0.0028	U	124	98
(HD 269546)										OI	+56	2000 ±1400	L	1.2E5 ±1.2E5		0.17	U	124	
										NaI	+67	7.6 ±0.6	W	470 ±300		0.23	U	12	W
										MgI	+56	40 ±38	L	2500 ±2900		0.065	U	124	
										MgII	+56	71 ±60	L	4400 ±4600		0.12	U	124	
										SiII	+56	4000 ±2700	L	2.5E5 ±2.3E5		7.0	U	124	τ
										SII	+56	1.6E4 ±7.6E3	L	1.0E6 ±7.8E5		53	U	124	
										CaII	+58	41 ±2	W	2600 ±1600		1.2	U	12	W
										FeII	+56	3200 ±2400	L	2.0E5 ±1.9E5		6.1	U	124	τ
Sk–68 114=R116	278.89	−32.36	50 g	27	B1Iae					NaI	+45.8	<0.24	W					18	W
Sk–68 135	279.26	−31.77	50 g	26	On9.7Ia		(+60)	<2.0	PR	CaII	+60	4.8	W	>240		>0.11	U	40	97,W
Sk–69 91	280.69	−33.36	50 g	27	B0.7Ia				(	CaII		<5.4	W					8)	W
Sk–69 103	280.42	−33.27	50 g	27	WC5+OB					CaII	+70	2.3	W				U	23	97,W
Sk–69 104	279.91	−33.38	50 g	28	O6Ib(f)					SiII	+60	170	W				U	10	W
Sk–69 106	280.44	−33.30	50 g	27	B0:					CaII	+80	3.6	W				U	23	97,W
Sk–69 107	280.42	−33.27	50 g	27	O9.5Ib					CaII	+70	2.3	W				U	23	97,W
Sk–69 195	279.67	−31.99	50 g	26	B2:		+65	10	AB	NaI	+61.8	0.45 ±1	L	4.5 ±10		0.0022	U	52	
Sk–69 203	279.66	−31.95	50 g	26	B0.7Ia		+65	10	AB(	NaI	+64.4	0.20 ±0.08	N	2.0 ±0.8		.00098	U	36)	
									(	NaI	+73.7	0.70 ±0.08	N	7.0 ±0.8		0.0034	U	36)	
										NaI	+73.7	0.69 ±0.14	L	6.9 ±1.4		0.0034	U	52	
										CaII	+64.6	6.7 ±0.5	W	67 ±5		0.031	U	52	W
Sk–69 204	279.92	−31.92	50 g	26	B1		+57	8.8	PI	NaI	+61.3	0.79 ±0.14	L	9.0 ±1.6		0.0044	U	52	
Sk–69 211	279.85	−31.86	50 g	26	B9Ia		+57	8.5	PI (	NaI	+64.0	3.1 ±0.08	N	36 ±0.9		0.018	U	36)	
										NaI	+64.0	3.1 ±0.1	L	36 ±2		0.018	U	52	
							+57a	7.8	PI	CaII	+64.8	31 ±0.3	L	400 ±4		0.18	U	52	
							+57b	0.74	PI	CaII	+79.2	3.0 ±0.3	L	400 ±40		0.18	U	52	
Sk–69 213	279.60	−31.88	50 g	26	B1Ia		+64	6.8	PI	NaI		<0.32	L	<4.7				52	
Sk–69 215	279.52	−31.88	50 g	26	O-B0		+66	5.9	PI	NaI		<0.32	L	<5.4				52	
Sk–69 216	279.83	−31.77	50 g	26	Be		+55	7.8	PI	NaI	+64.4	1.7 ±0.09	L	22 ±1		0.011	U	52	
							+55a	4.2	PI	CaII	+66	20 ±0.5	L	490 ±10		0.22	U	52	
							+55b	2.1	PI	CaII	+91.4	10 ±0.5	L	490 ±20		0.22	U	52	
							+54c	1.6	PI	CaII	+100.5	7.9 ±0.5	L	480 ±30		0.22	U	52	
Sk–69 220=R127	279.96	−31.80	50 g	26	OIafpe		+53	8.2	PI	NaI	+46.7	0.99 ±0.10	W	12 ±1		0.0059	U	18	W
Sk–69 221=R128	279.96	−31.79	50 g	26	B2Ia		+52	8.2	PI	NaI	+47.6	1.6 ±0.1	W	19 ±1		0.0095	U	18	W

TABLE 2—*Continued*

Probe (1)	l ° (2)	b ° (3)	d kpc (4)	z kpc (5)	type (6)	Cld (7)	v_{HI} km/s (8)	N_{HI} 10^{18} cm^{-2} (9)	tel (10)	ion (11)	v_{ion} km/s (12)	N_{ion} 10^{11} cm^{-2} (13)	code (14)	A_{ion} 10^{-9} (15)	A_{ref} 10^{-9} (16)	A/A$_\odot$ (17)	D? (18)	Ref (19)	Note (20)
Sk–69 224	279.61	−31.82	50 g	26	B0		+63	6.5	PI	NaI		<0.42	L	<6.4				52	
										CaII		<5.4	L	<83				52	
Sk–69 225	279.68	−31.81	50 g	26	B8I		+61	7.0	PI	NaI		<0.63	L	<9.0				52	
Sk–69 239	279.48	−31.72	50 g	26	A0I		+70	1.5	Pk	NaI		<0.21	L	<14				52	98
									(	CaII	+40	2.3	W	160		0.072	U	23)	97,W
							+70a	0.75	Pk	CaII	+55.2	2.7 ±0.3	L	360 ±40		0.16	U	52	
							+70b	0.75	Pk	CaII	+67.0	3.0 ±0.3	L	390 ±40		0.18	U	52	
R 134	279.46	−31.67	50 g	26	WN6		+70	1.5 ±1.0	Pk	CaII		<2.3	W	<160				23	97,W
R 137	279.45	−31.68	50 g	26	B0.5Ia:		+70	1.5 ±1.0	Pk	CaII		<2.3	W	<160				23	97,W
R 139	279.45	−31.68	50 g	26	WN7/Of		+70	1.5 ±1.0	Pk	CaII	+60	2.3	W	160		0.072	U	23	97,W
R 140	279.45	−31.68	50 g	26	WN6		+70	1.5 ±1.0	Pk	CaII	+60	2.3	W	160		0.072	U	23	97,W
Sk–69 243=R136	279.47	−31.69	50 g	26	OB+WN5-6		+70	1.5 ±1.0	Pk	NaI		<0.32	L	<21				52	98
(HD 38268)									(	CaII	+70	2.8	W	190		0.086	U	6	W
									(	CaII		<2.3	W	<160				23)	97,W
									(	CaII	+100	3.6	W	240		0.11	U	40)	97,W
										CaII	+58.4	1.2 ±0.6	L	80 ±67		0.037	U	52	
Sk–69 246	279.39	−31.67	50 g	26	WN7		+70	1.5 ±1.0	Pk	NaI		<0.32	L	<21				52	98
(HD 38282)									(	CaII	+62	4.3 ±1.2	W	290 ±210		0.13	U	12)	W
									(	CaII		<2.3	W	<160				23)	97,W
										CaII	+67.5	1.3 ±0.3	L	86 ±61		0.039	U	52	
										SiII	+60	170	W	1.1E4		0.31	U	10	W
										FeII	+60	400	L	2.7E4		0.82	U	10	
Sk–69 247	279.93	−31.61	50 g	26	A0Ia+		+45	7.1 ±1.0	Pk	NaI		<0.52	L	<7.4				52	106
							+45a	3.8	Pk	CaII	+65.8	1.7 ±0.5	L	45 ±13		0.020	U	52	
							+45b	3.3	Pk	CaII	+76.3	1.5 ±0.5	L	45 ±15		0.020	U	52	
Sk–69 248	279.47	−31.65	50 g	26	WN7		+70	1.5 ±1.0	Pk	CaII	+60	2.3	W	160		0.072	U	23	97,W
Sk–69 255	279.81	−31.53	50 g	26	WC5+OB		+45	7.1	Pk	CaII	+71.1	2.2 ±0.2	N	31 ±3		0.014	U	85	
Sk–69 270	279.42	−31.44	50 g	26	B2.5Ia		(+60)	<2.0	PR	CaII	+60	10	W	>500		>0.23	U	40	97,W
Sk–69 274	280.25	−31.35	50 g	26	B2.5Ia		+45	7.1	PR	CaII		<0.35	W	<4.9			l	85	W
										TiII		<1.8	W	<25				85	W
Sk–69 276	279.96	−31.37	50 g	26	B0Iab					CaII	+75.7	4.0 ±0.2	N				U	85	
Sk–69 282	279.34	−31.38	50 g	26	B1.5					CaII	+76.3	3.1 ±0.1	N				U	85	
										TiII	+82.6	2.0 ±0.9	N				U	85	
Sk–69 289	279.93	−31.27	50 g	26	B0.7Ia		(+60)	<2.0	PR	CaII	+60	7.4	W	>370		>0.17	U	40	97,W
Sk–69 290	279.29	−31.31	50 g	26	B0.5					CaII	+73.8	5.1 ±1.1	N				U	85	
										TiII	+65.0	7.8 ±3.1	N				U	85	
										TiII	+87.7	7.7 ±3.1	N				U	85	
Sk–70 111	280.49	−31.31	50 g	26	B0.5Ia					CaII	+58.0	20 ±0.2	N				U	85	
Sk–70 115	280.48	−30.70	50 g	26	O6.5III		+55	<2.0	Pk	CaII	+55.5	8.3 ±0.1	N	>420		>0.19	U	85	98
										TiII		<3.5	W					85	W
Sk–71 3	282.82	−34.25	50 g	28	pec		+61	2.0 ±1.0	Pk(	NaI	+70	1.5 ±0.5	W	74 ±45		0.036	U	8)	98,W
										NaI	+71	2.0 ±0.5	W	100 ±56		0.049	U	12	W
									(	CaII	+68	5.4 ±1.9	W	270 ±170		0.12	U	8)	W
										CaII	+75	8.7 ±1.3	W	430 ±230		0.20	U	12	W
Sk–71 33a	281.85	−32.19	50 g	27	B5Ia					CaII	+70	3.6	W				U	23	97,W
Sk–71 41	281.91	−32.07	50 g	27	O8.5I		+66	6.2 ±1.0	Pk	CaII	+70	2.3	W	38		0.017	U	23	97,98,W
Sk–71 42	281.87	−32.06	50 g	27	B1Iab		+66	6.2 ±1.0	Pk	NaI		<0.99	W	<16				12	98,W
									(	CaII	+71	27	W	440		0.20	U	12)	98,W
										CaII	+70	3.6	W	57		0.026	U	23	97,W
Sk–71 45	281.86	−32.02	50 g	27	O4If		+66	6.2 ±1.0	Pk	CaII	+80	3.6	W	57		0.026	U	23	97,98,W
LH 10:3120	277.19	−36.06	50 g	29	O5.5V					H_2	+60	1.0E4	L				U	124	
										SiII	+51	320	L				U	124	
										SII	+51	1.0E4	L				U	124	
										FeII	+51	320	L				U	124	

TABLE 2—*Continued*

Probe	l °	b °	d kpc	z kpc	type	Cld	v_{HI} km/s	N_{HI} 10^{18} cm^{-2}	tel	ion	v_{ion} km/s	N_{ion} 10^{11} cm^{-2}	code	A_{ion} 10^{-9}	A_{ref} 10^{-9}	A/A$_\odot$	D?	Ref	Note
(1)	(2)	(3)	(4)	(5)	(6)	(7)	(8)	(9)	(10)	(11)	(12)	(13)	(14)	(15)	(16)	(17)	(18)	(19)	(20)
Upper IV Arch: IV14, IV13, IV7, IV16, IV6, IV5, IV17, IV11, IV12, IV9, IV15, IV8, IV10																			
IV7			$<$ 5.0	$<$ 3.9															
PG 0955+291	199.89	51.94	5.0±0.6	s 3.9	B5V	IV7	−64	8.0 ±3.0	Ef	CaII	−64	1.8	L	23		0.010	U	93	112
IV6			$<$ 1.9	$<$ 1.7						CI*				720 ±690		0.0020			1$Z_\odot$
			$>$ 0.4	$>$ 0.4						CIV		[1600]							
										NaI				1.6		0.00080			
										MgII				2.7E4 ±2.8E4	[14000]	0.72			
										SiII				3.3E4 ±3.2E4	[19000]	0.94			
										SII				3.8E4 ±3.6E4	[19000]	2.1			
										SIII				3500 ±3700		0.19			
										SiIV		[440]							
										CaII				30	[22]	0.014			
										TiII				39 ±38	[21]	0.46			
										MnII				180 ±170	[87]	0.52			
										FeII				1.4E4 ±1.3E4	[7800]	0.42			
BD +38 2182	182.16	62.21	4.0	a 3.5	B3V	IV6	(−73)	<0.50	JB	NaI	−74	0.25	L	>50		>0.025	U	93	113
										CaII	−73	1.3	L	>250		>0.12	U	93	
HD 93521	183.14	62.15	1.9	t 1.7	O9.5V	IV6	−65	3.2 ±3.0	GB	CI*	−66.3	23 ±5	L	720 ±690		0.0020	U	56	
										CIV	−67	240	N					51	
										NaI	−64.8	0.052	L	1.6		.00080	U	107	
										MgII	−66.3	870 ±370	L	2.7E4 ±2.8E4		0.72	U	56	114
										SiII	−66.3	1100 ±200	L	3.3E4 ±3.2E4		0.94	U	56	
										SII	−66.3	1200 ±90	L	3.8E4 ±3.6E4		2.1	U	56	
										SIII	−66.3	110 ±60	L	3500 ±3700		0.19	U	56	
										SiIV	−60	820	N					51	
									(	CaII	−66.3	1.1 ±0.1	L	36 ±34		0.016	U	56)	
										CaII	−65.6	0.95	L	30		0.014	U	107	
										TiII	−66.3	1.3 ±0.3	L	39 ±38		0.46	U	56	
										MnII	−66.3	5.6 ±0.8	L	180 ±170		0.52	U	56	
										FeII	−66.3	440 ±40	L	1.4E4 ±1.3E4		0.42	U	56	
HD 98152	171.46	66.38	0.40±0.10	t 0.37	A0V	IV6	−72	37 ±5	Ef	SiII		<90	N	<250			L	83	S
IV17			$<$ 0.8	$<$ 0.7						MgI				36		0.00094			
			$>$ 0.6	$>$ 0.5						SiII				>190	[19000]	>0.0055			
										CaII				16 ±10	[22]	0.0073			
										MnII				130	[87]	0.39			
SN 1998 S	150.75	65.96	—	—	SN	IV17	−54	102 ±1	Ef	MgI	−59	36	N	36		.00094		117	10,115
										CaII	−59	27	N	26		0.012		117	
										MnII	−59	140	N	130		0.39		117	
PG 1126+468	157.20	64.71	5.8±0.7	s 5.2	HB	IV17	−63	78 ±0.6	Ef	CaII	−70	12	W	16		0.0071	U	70	116
PG 1213+456	141.93	70.44	2.9±0.7	a 2.7	sdB	IV17	−61	24 ±1	JB	CaII		<1.3	L	<5.2				93	
BD +49 2137	134.23	67.40	0.80±0.20	a 0.74	HB	IV17	−53	46 ±1	Ef	SiII		>90	N	>190		>0.0055	U	83	11,S
							−53a	29 ±1	Ef	CaII	−63	1.2	L	4.3		0.0020	U	93	
							−53b	18 ±1	Ef	CaII	−76	0.76	L	4.3		0.0020	U	93	
HD 106420	140.59	68.79	0.55±0.27	p 0.51	B8V	IV17	−59	39 ±1	Ef	SiII		<90	N	<230			L	83	S
HD 105058	141.16	65.80	0.19±0.04	p 0.17	A2V	IV17	−57	75 ±0.9	Ef	SiII		<90	N	<120			L	83	S
IV11			($>$ 0.8	$>$ 0.7)						SiII					[19000]				
PG 1255+546	120.91	62.68	0.80±0.30	a 0.71	sdB	IV11	−81	4.5 ±0.3	Dw	SiII		<90	N	<2000			l	83	S

TABLE 2—*Continued*

Probe (1)	l ° (2)	b ° (3)	d kpc (4)	z kpc (5)	type (6)	Cld (7)	v_{HI} km/s (8)	N_{HI} 10^{18} cm^{-2} (9)	tel (10)	ion (11)	v_{ion} km/s (12)	N_{ion} 10^{11} cm^{-2} (13)	code (14)	A_{ion} 10^{-9} (15)	A_{ref} 10^{-9} (16)	A/A$_\odot$ (17)	D? (18)	Ref (19)	Note (20)
IV9			< 2.1	< 1.6						CIV		[1600]							1$Z_\odot$
			> 0.3	> 0.2						SiII				<290	[19000]	<0.0083			
										SiIV		[440]							
										SII				1.5E4 ±2.2E2	[19000]	0.78			
										CaII				7.5	[22]	0.0034			
PG 1351+640	111.89	52.02	—	—	QSO	IV9	−74	15 ±1	Ef	CaII		<50	N	<340				79	117
HD 121800	113.01	49.76	2.1±0.3 t	1.6	B1.5V	IV9	−71	72 ±0.7	Ef	CIV	−79	360 ±40	N					129	
										SiIV	−79	140 ±40	N					129	
										SII	−69	1.1E4 ±1.2E2	N	1.5E4 ±2.2E2		0.78	U	129	118
										CaII	−71	5.4	N	7.5		0.0034	U	58	
HD 127557	109.43	47.13	0.28±0.06 p	0.21	A0V	IV9	−71	98 ±1	Dw	SiII		<90	N	<92			L	83	S
							−58	31 ±2	Dw	SiII		<90	N	<290			L	83	S
IV15										CaII					[22]				
BS 16079-0015	90.69	46.46	2.4±0.5 s	1.7	(HB)	IV15	−72	5.7 ±1.5	Ef	CaII		<2.4	W	<41				114	
Upper IV Arch (off cores)																			
BA 90700003	114.19	30.08	4.2 a	2.1		IVa	−88	8.6 ±0.5	Dw	SiII		>90	N	>1000		>0.029	U	83	S,119
PG 1212+369	159.93	77.72	2.7±0.4 a	2.6	sd(B2)	IVa	(−96)	<3.0	Ef	CaII	−96	0.95	L	>32		>0.015	U	93	120
							(−76)	<3.0	Ef	CaII	−76	0.76	L	>25		>0.012	U	93	
							(−66)	<3.0	Ef	CaII	−66	2.0	L	>68		>0.031	U	93	
							(−57)	<3.0	Ef	CaII	−57	3.5	L	>120		>0.053	U	93	
BT Dra	99.41	51.21	1.9±0.2 t	1.5	RR Lyr	IVa	−79	5.2 ±1.1	Ef	CaII	−83	8.0	N	150		0.070	U	33	121
Lower IV Arch: IV22, IV24, IV18, IV26, IV21, IV19, IV25, IV23, IV27, IV20																			
IV24			> 0.5	> 0.4															
HD 87015	211.17	51.48	0.49±0.19 p	0.38	B2.5IV	IV24	−41	57 ±2	Ef	NaI		<0.13	L	<0.22				93	
										SiII		<230	N	<400			L	50	s
									(	CaII		<1.2	W	<2.0				2)	
										CaII		<0.20	L	<0.35			L	93	
IV26			< 2.7	< 2.6						NaI				0.57		0.00028			
			> 0.4	> 0.4						SiII				>54	[19000]	>0.0015			
										CaII				4.6	[22]	0.0021			
H.O.+41B	144.63	75.06	3.1 r	3.0	B5V	IV26	−36	166 ±1	JB	NaI	−50	0.95	L	0.57		.00028	U	93	
										SiII		>90	N	>54		>0.0015	U	83	S
										CaII	−53	7.6	L	4.6		0.0021	U	93	
PG 1212+369	159.93	77.72	2.7±0.4 a	2.6	sd(B2)	IV26	−29	154 ±2	Ef	CaII	−41	17	L	11		0.0049	U	93	120
HD 98152	171.46	66.38	0.40±0.10 t	0.37	A0V	IV26	−54	28 ±4	Ef	SiII		<90	N	<320			L	83	S
IV21			< 0.4	< 0.3						NaI				1.2		0.00057			
BD +63 985	133.74	53.42	0.40±0.10 s	0.32	A5V	IV21	−47	85 ±2	Ef	NaI	−45	0.99	W	1.2		.00057	U	84	
HD 101714	135.93	52.78	0.30±0.10 s	0.24	A5V	IV21	−48	105 ±1	Dw	NaI		<0.15	W	<0.14				84	
HD 101075	135.50	51.13	0.24±0.04 p	0.19	A2IV	IV21	−47	189 ±1	Dw	NaI		<0.24	W	<0.13				84	
HD 103718	134.74	55.33	0.23±0.05 p	0.19	A3V	IV21	−46	96 ±1	Dw	NaI		<0.15	W	<0.15				84	
IV19			< 2.1	< 1.6						SiII				>900	[19000]	>0.025			
										SII				1.5E4 ±7.6E3	[19000]	0.81			
										CaII				25 ±10	[22]	0.011			
PG 1351+640	111.89	52.02	—	—	QSO	IV19	−47	105 ±2	Ef	CaII	−46	39 ±0.8	N	37 ±1		0.017		79	117
HD 121800	113.01	49.76	2.1±0.3 t	1.6	B1.5V	IV19	−37	10 ±5	Ef	SiII		>90	N	>900		>0.025	U	83	S
										SII	−37	1500 ±100	N	1.5E4 ±7.6E3		0.81	U	129	118
										CaII	−57	1.3	N	13		0.0059	U	58	
PG 1338+611	112.54	55.25	0.30±0.10 s	0.25	sdB	IV19	−52	124 ±4	Ef	CaII		<3.5	N	<2.8				70	29

TABLE 2—*Continued*

Probe	l °	b °	d kpc	z kpc	type	Cld	v_{HI} km/s	N_{HI} 10^{18} cm^{-2}	tel	ion	v_{ion} km/s	N_{ion} 10^{11} cm^{-2}	code	A_{ion} 10^{-9}	A_{ref} 10^{-9}	A/A$_\odot$	D?	Ref	Note
(1)	(2)	(3)	(4)	(5)	(6)	(7)	(8)	(9)	(10)	(11)	(12)	(13)	(14)	(15)	(16)	(17)	(18)	(19)	(20)
Lower IV Arch (off cores)																			
PG 1259+593	120.56	58.05	—	—	QSO	IVa	−54	30 ± 1	Ef	NI		1.2E4 ± 9.5E3	L	4.1E4 ± 3.2E4		0.44		126	
										OI		2.0E5 ± 1.5E5	L	6.7E5 ± 5.1E5		0.91		126	
										OVI		480 ± 160	L					126	
										SiII		5400 ± 2700	L	1.8E4 ± 9.2E3		0.51		126	
										ArI		350 ± 270	L	1200 ± 900		0.33		126	
										FeII		3600 ± 1500	L	1.2E4 ± 5.0E3		0.38		126	
PG 0953+414	179.78	51.71	—	—	QSO	IVa	−47	23 ± 1	Ef	SII	−40	4800 ± 800	L	2.1E4 ± 3.6E3		1.1		128	
PG 0955+291	199.89	51.94	5.0±0.6 a	3.9	B5V	IVa	−45	15 ± 3	Ef	CaII	−45	5.5	L	36		0.016	U	93	112
BD +38 2182	182.16	62.21	4.0 a	3.5	B3V	IVa	−53*a*	9.5 ± 0.1	JB	NaI	−56	0.58	L	6.1		0.0030	U	93	
										CaII	−58	5.2	L	55		0.025	U	93	
							−53*b*	34 ± 0.1	JB	NaI	−44	1.7	L	4.9		0.0024	U	93	
										CaII	−44	19	L	55		0.025	U	93	
BD +36 2268	153.37	79.56	3.7±0.7 s	3.6	B2V	IVa	−47*a*	22 ± 1	Ef	NaI		<0.13	L	<0.58				93	122
										CaII	−56	3.4	L	16		0.0071	U	93	
							−47*b*	37 ± 1	Ef	NaI		<0.13	L	<0.34				93	
										CaII	−44	5.8	L	16		0.0071	U	93	
PG 1213+456	141.93	70.44	2.9±0.7 a	2.7	sdB	IVa	−40	27 ± 1	JB	CaII		<1.3	L	<4.6				93	
HD 93521	183.14	62.15	1.9 t	1.7	O9.5V	IVa	−57.8	22 ± 3	GB	H_2	−62	3200 ± 1900	L	1.4E4 ± 9.0E3				116	
										CI*	−57.8	120 ± 8	L	540 ± 80		0.0015	U	56	
										NaI	−57.4	0.35	L	1.6		.00079	U	107	
										MgII	−57.7	1300 ± 500	L	6200 ± 2500		0.16	U	56	114
										SiII	−57.7	4400 ± 300	L	2.0E4 ± 3.1E3		0.56	U	56	
										SII	−57.7	3200 ± 100	L	1.4E4 ± 2.1E3		0.78	U	56	
										SIII	−57.7	130 ± 70	L	590 ± 320		0.032	U	56	
									(	CaII	−55	6.1 ± 0.4	N	28 ± 4		0.013	U	16)	
									(	CaII	−57	7.2	L	33		0.015	U	93)	
										CaII	−59.1	1.7	L	7.9		0.0036	U	107	
										CaII	−56.2	2.6	L	12		0.0055	U	107	
									(	TiII	−55	5.4 ± 0.7	N	25 ± 5		0.29	U	16)	
									(	TiII	−57.7	2.8 ± 0.4	L	13 ± 2		0.15	U	56)	
										TiII	−59.1	6.3	L	29		0.34	U	107	
										MnII	−57.7	17 ± 14	L	78 ± 66		0.23	U	56	
										FeII	−57.7	2600 ± 2200	L	1.2E4 ± 1.0E4		0.36	U	56	
							−51.2	16 ± 3	GB	CI*	−51.2	48 ± 10	L	300 ± 90		.00085	U	56	
										NaI	−54.6	0.13	L	0.80		.00039	U	107	
										MgII	−51.2	1600 ± 600	L	1.0E4 ± 4.0E3		0.26	U	56	114
										SiII	−51.2	3900 ± 400	L	2.5E4 ± 5.5E3		0.69	U	56	
										SII	−51.2	3400 ± 200	L	2.1E4 ± 4.3E3		1.2	U	56	
										SIII	−51.2	510 ± 80	L	3200 ± 800		0.17	U	56	
									(	CaII	−51.2	1.2 ± 0.2	L	7.8 ± 1.8		0.0036	U	56)	
										CaII	−49.5	3.7	L	24		0.011	U	107	
									(	TiII	−51.2	1.5 ± 0.5	L	9.8 ± 3.5		0.12	U	56)	
										TiII	−52.5	0.20	L	1.3		0.015	U	107	
										MnII	−51.2	14 ± 1	L	89 ± 19		0.26	U	56	
										FeII	−51.2	910 ± 60	L	5800 ± 1200		0.18	U	56	
							−38.8	7.6 ± 3.0	GB	CI*	−38.8	37 ± 8	L	490 ± 220		0.0014	U	56	
										MgII	−38.8	1000 ± 700	L	1.4E4 ± 1.0E4		0.36	U	56	114
										SiII	−38.8	1300 ± 90	L	1.7E4 ± 7.0E3		0.49	U	56	
										SII	−38.8	1000 ± 200	L	1.4E4 ± 5.9E3		0.74	U	56	
										SIII	−38.8	140 ± 110	L	1800 ± 1600		0.098	U	56	
									(	CaII	−40	2.4 ± 0.4	N	32 ± 14		0.014	U	16)	
									(	CaII	−39	3.7	L	49		0.022	U	93)	
										CaII	−38.8	2.8 ± 0.2	L	37 ± 15		0.017	U	56	

TABLE 2—*Continued*

Probe	l °	b °	d kpc	z kpc	type	Cld	v_{HI} km/s	N_{HI} 10^{18} cm^{-2}	tel	ion	v_{ion} km/s	N_{ion} 10^{11} cm^{-2}	code	A_{ion} 10^{-9}	A_{ref} 10^{-9}	A/A$_\odot$	D?	Ref	Note
(1)	(2)	(3)	(4)	(5)	(6)	(7)	(8)	(9)	(10)	(11)	(12)	(13)	(14)	(15)	(16)	(17)	(18)	(19)	(20)
									(	TiII	−40	0.80 ±0.40	N	11 ±7		0.12	U	16)	
										TiII	−38.8	0.50 ±0.43	L	6.6 ±6.3		0.077	U	56	
										MnII	−38.8	5.9 ±1.2	L	77 ±35		0.23	U	56	
										FeII	−38.8	600 ±30	L	7900 ±3200		0.25	U	56	
PG 1255+546	120.91	62.68	0.80±0.30 a	0.71	sdB	IVa	−51	75 ±0.3	Dw	SiII		<90	N	<120			L	83	S
HDE 233791	154.53	56.65	0.48±0.70 a	0.40	HB	IVa	−50	39 ±0.6	Ef	NaI	−51	1.7	L	4.5		0.0022	U	93	123
							−50*a*	11 ±0.6	Ef	CaII	−66	>2.0	L	>18		>0.0081	U	93	
							−50*a*	27 ±0.6	Ef	CaII	−52	4.9	L	18		0.0082	U	93	
IV Spur			< 2.1	< 2.1						SiII				>200	[19000]	>0.0056			
			> 0.3	> 0.3						CaII				22	[22]	0.0099			
										FeII				>0	[7800]	>0			
HD 100340	258.85	61.23	3.0 a	2.6	B1V	Sp	−70	7.3 ±2.0	Dw(	CaII	−64	1.1	N	15		0.0069	U	58)	124
										CaII	−63	1.6	L	22		0.0099	U	113	
										FeII	−55	>0	N	>0		>0	U	86	
Feige 40	245.37	63.62	2.9±0.4 t	2.6	B4V	Sp	−52	45 ±3	Dw	SiII		>90	N	>200		>0.0056	U	83	S,125
PG 1205+228	235.56	79.12	2.1 a	2.1	sdB	S1	−42	137 ±4	Ef	SiII		>90	N	>66		>0.0019	U	83	S,126
HD 100600	239.18	69.47	0.30±0.05 t	0.28	B4V	S1	−40	86 ±1	Ef	SiII		<90	N	<110			L	83	S
										CaII		<0.60	N	<0.70			L	58	
LLIV Arch			< 1.8	< 1.2						CIV		[1600]							$1Z_\odot$
			(> 0.9	> 0.6)						NI				5.2E4 ±2.1E4	[93000]	0.55			
										NII				7100 ±3400		0.076			
										OI				7.6E5 ±4.2E5	[740000]	1.0			
										NaI				2.4		0.0012			
										MgI				44		0.0012			
										MgII				>750	[14000]	>0.020			
										AlII				280	[1600]	0.092			
										AlIII				<44		<0.015			
										SiII				1.4E4 ±4.9E3	[19000]	0.39			
										SiIV		[440]							
										PII				470 ±130	[370]	1.3			
										ArI				1200 ±200	[1200]	0.32			
										FeII				7000 ±800	[7800]	0.21			
										FeIII				270 ±60		0.0084			
										CaII				13 ±1	[22]	0.0059			
										ZnII				70 ±21	[42]	1.6			
SN 1993 J	142.15	40.92	—	—	SN	LLIV1	−50	70 ±10	Ef	CIV	−50	>2000	L					53	127
										NaI	−50	1.7	N	2.4		0.0012		61	
										MgI	−50	32	L	45		0.0012		53	
										SiII	−50	7900	L	1.1E4		0.32		53	τ
										SiIV	−50	630	L					53	
										AlII	−50	200	L	290		0.094		53	
										AlIII		<32	L	<45				53	
										FeII	−50	2500	L	3600		0.11		53	τ
										CaII	−53	9.9	N	14		0.0065		61	
										ZnII	−50	50 ±15	L	72 ±24		1.6		53	
PG 0804+761	138.28	31.03	—	—	QSO	LLIV	−58	35 ±1	Ef	H_2	−55	5100 ±3800	L	1.5E4 ±1.1E4				123	
										NI	−55	1.8E4 ±7.1E3	L	5.2E4 ±2.1E4		0.55		123	
										NII	−55	2500 ±1200	L	7100 ±3400		0.076		123	
										OI	−55	2.6E5 ±1.5E5	L	7.6E5 ±4.2E5		1.0		123	
										SiII	−55	4800 ±1700	L	1.4E4 ±4.9E3		0.39		123	
										PII	−55	160 ±50	L	470 ±130		1.3		123	
										ArI	−55	400 ±60	L	1200 ±200		0.32		123	
										FeII	−55	2400 ±300	L	7000 ±800		0.21		123	
										FeIII	−55	93 ±22	L	270 ±60		0.0084		123	

TABLE 2—*Continued*

Probe	l °	b °	d kpc	z kpc	type	Cld	v_{HI} km/s	N_{HI} 10^{18} cm^{-2}	tel	ion	v_{ion} km/s	N_{ion} 10^{11} cm^{-2}	code	A_{ion} 10^{-9}	A_{ref} 10^{-9}	$A/A_\odot$	D?	Ref	Note
(1)	(2)	(3)	(4)	(5)	(6)	(7)	(8)	(9)	(10)	(11)	(12)	(13)	(14)	(15)	(16)	(17)	(18)	(19)	(20)
PG 0832+675	147.75	35.01	8.1 a	4.6	PAGB	LLIV	−55	92 ± 2	Ef	CaII	−57	13	L	14		0.0062	U	94	
PG 0859+593	156.93	39.74	4.0±1.0 a	2.6	HB	LLIV3	−52	53 ± 3	WE	MgII	−50	>400	N	>750		>0.020	U	87	
PG 0833+698	145.00	34.50	3.4 a	1.9	PAGB	LLIV	−75	24 ± 0.8	Ef	CaII	−67	2.9	L	12		0.0056	U	94	
							−37	77 ± 1	Ef	CaII	−45	1.9	L	2.5		0.0011	U	94	
PG 1008+689	141.27	42.29	1.8±0.2 s	1.2	HB	LLIV1	−45a	34 ± 0.6	Ef	CaII	−51	4.6	L	13		0.0062	U	94	
							−45b	24 ± 0.6	Ef	CaII	−41	3.2	L	13		0.0062	U	94	
SA 12 391	156.95	40.28	1.5±0.2 s	0.97	A0V	LLIV3	−52	88 ± 2	Ef	CaII		<2.3	W	<2.6				33	
BD +67 598	146.34	40.62	0.90±0.10 s	0.59	A0V	LLIV1	−54	88 ± 2	Dw	CaII		<0.93	W	<1.1			l	61	128
PG 0906+597	156.22	40.56	0.70±0.20 a	0.46	sdB	LLIV3	−50	110 ± 5	WE	MgII		<12	N	<11			L	87	
HD 68164	154.62	33.45	0.35±0.13 p	0.19	B9V	LLIV4	−50	78 ± 1	Dw	CaII		<1.0	W	<1.3				80	V
LLIV Arch extension			< 0.9	< 0.6						NaI				4.2		0.0020			$1Z_\odot$
										MgII				>1500	[14000]	>0.040			
										SiII				>730	[19000]	>0.021			
										CaII				14 ± 3	[22]	0.0064			
										TiII				9.5	[21]	0.11			
Mrk 106	161.14	42.88	—	—	Sey	LLIVe	−39	26 ± 3	WE	MgII	−40	>400	N	>1500		>0.040		87	
HDE 233622	168.17	44.23	4.4±0.6 t	3.1	B1.5V	LLIVe	−40	32 ± 0.7	Ef	NaI		<0.16	W	<0.51				94	129
										SiII	−44	>230	N	>730		>0.021	U	50	s
										CaII	−44	4.4	L	14		0.0063	U	94	
										TiII	−42	3.0	N	9.5		0.11	U	72	
							−62	<5.0	Dw	CaII	−62	1.4	L	>28		>0.013	U	94	
HDE 237844	158.60	47.06	2.4±0.4 t	1.8	B3V	LLIVe	−40	20 ± 0.9	Ef	NaI		<0.12	W	<0.61				94	129
										CaII	−47	3.5	L	17		0.0079	U	94	
HD 77770	169.30	41.88	1.2±0.3 t	0.80	B2IV	LLIVe	−38	31 ± 1	Dw	NaI	−37	1.3	N	4.2		0.0020	U	80	4
										CaII	−37	4.2	N	14		0.0062	U	80	
HD 83206	167.70	46.93	0.90±0.20 t	0.66	B3V	LLIVe	−40	16 ± 0.6	Ef(	NaI		<0.025	L	<0.16				107)	12
										CaII	−34.2	1.4	L	9.1		0.0042	U	107	
Complex K			< 6.8	< 4.5						NaI				20 ± 15		0.0098			
										MgII				>0	[14000]	>0			
										SII				<3.7E4	[19000]	<2.0			
										CaII				89	[22]	0.041			
Mrk 501	63.60	38.86	—	—	BL Lac	K	−83	5.6 ± 0.7	Ef	SII		<2000	N	<3.6E4				125	
										CaII	−80	5.0	W	89		0.041		70	
B2 1607+26	44.17	46.20	—	—	radio	K	−60	10 ± 0.3	Ar	HI		<5.3	τ			T_s>80		39	T
M 13 II-67	59.06	40.97	6.8 g	4.5	K2Ib	K	−69	18 ± 3	JD	NaI	−69	7.9 ± 3.8	L	45 ± 23		0.022	U	88	
M 13 III-73	58.96	40.96	6.8 g	4.5		K	(−68)	<6.0	JD	NaI		<0.50	L					88	
M 13 II-34	59.06	40.94	6.8 g	4.5		K	−70	10 ± 3	JD	NaI		<0.50	L	<5.0				88	
M 13 III-33	58.97	40.93	6.8 g	4.5	B2p	K	(−65)	<6.0	JD	MgII		>0	N	>0		>0	U	15	
(Barnard 29)										CaII		11 ± 3	L	>190		>0.085	U	88	
M 13 L 598	58.99	40.91	6.8 g	4.5		K	−68	18 ± 3	JD	NaI	−69	2.5 ± 0.7	L	14 ± 5		0.0069	U	88	
M 13 III-56	58.97	40.91	6.8 g	4.5		K	(−68)	<6.0	JD	NaI		<0.40	L					88	
M 13 L 629	59.00	40.90	6.8 g	4.5		K	−70	18 ± 3	JD	NaI		<0.50	L	<2.8				88	
M 13 V-15	58.98	40.89	6.8 g	4.5		K	−70	13 ± 3	JD	NaI		<0.63	L	<5.0				88	
M 13 I-48	59.04	40.88	6.8 g	4.5	K0Ib	K	−72	10 ± 3	JD	NaI	−72	1.3 ± 0.4	L	13 ± 5		0.0062	U	88	
M 13 IV-25	58.94	40.87	6.8 g	4.4		K	(−68)	<6.0	JD	NaI		<0.50	L					88	
PG 1722+286	51.71	30.57	0.90±0.20 a	0.46	sdOB	K	−84	15 ± 2	ef	NaI		<4.0	L	<27				62	
										CaII		<5.0	L	<33				62	

TABLE 2—*Continued*

Probe (1)	l ° (2)	b ° (3)	d kpc (4)	z kpc (5)	type (6)	Cld (7)	v_{HI} km/s (8)	N_{HI} 10^{18} cm^{-2} (9)	tel (10)	ion (11)	v_{ion} km/s (12)	N_{ion} 10^{11} cm^{-2} (13)	code (14)	A_{ion} 10^{-9} (15)	A_{ref} 10^{-9} (16)	A/A$_\odot$ (17)	D? (18)	Ref (19)	Note (20)
PP Arch			< 1.1	< 0.9															$0.5Z_\odot$
HD 215733	85.16	−36.35	2.7±0.4	s 1.6	B1II	PP	−92	2.8 ±0.7	GB	CII*	−93	11 ±9	L	390 ±350		0.0011	U	90	130
										SiII	−93	110 ±8	L	3900 ±1000		0.11	U	90	
										SII	−93	87 ±26	L	3100 ±1200		0.17	U	90	
										CaII	−93	0.36 ±0.05	L	13 ±4		0.0059	U	90	
										FeII	−93	51 ±1	L	1800 ±500		0.057	U	90	
							−56	78 ±0.7	GB	CII*	−56	340 ±50	L	440 ±70		0.0012	U	90	131
										CIV	−66.0	14 ±8	L					90	
										MgII	−56	1800 ±400	L	2300 ±500		0.062	U	90	114
										SiII	−56	4800 ±700	L	6200 ±900		0.17	U	90	
										SII	−56	4600 ±300	L	5900 ±400		0.32	U	90	
										CaII	−56	6.5 ±1.5	L	8.3 ±1.9		0.0038	U	90	
										CrII	−56	27 ±5	L	35 ±6		0.072	U	90	
										MnII	−56	13 ±3	L	17 ±4		0.051	U	90	
										FeII	−56	1400 ±100	L	1900 ±200		0.057	U	90	
										ZnII	−56	7.9 ±1.5	L	10 ±2		0.23	U	90	
							−43	20 ±0.7	GB	CI	−43	47 ±6	L	240 ±30		.00068	U	90	131
										CI*	−43	14 ±6	L	71 ±29		.00020	U	90	
										CI**	−43	6.3 ±4.7	L	32 ±24		000091	U	90	
										CII*	−43	480 ±70	L	2500 ±400		0.0069	U	90	
										CII*	−43	480 ±70	L	2500 ±400		0.0069	U	90	
										CIV	−38.9	370 ±40	L					90	
										MgI	−43	5.9 ±2.8	L	30 ±14		.00079	U	90	
										MgII	−43	1900 ±1000	L	9500 ±5100		0.25	U	90	114
										SiII	−43	5200 ±1000	L	2.7E4 ±5.1E3		0.76	U	90	
										SiIV	−38.9	66 ±12	L					90	
										SII	−43	4300 ±600	L	2.2E4 ±3.1E3		1.2	U	90	
										CaII	−43	10 ±2	L	51 ±12		0.023	U	90	
										TiII	−45	4.3 ±2.0	N	22 ±10		0.26	U	16	
										CrII	−43	35 ±7	L	180 ±40		0.37	U	90	
										MnII	−43	17 ±4	L	87 ±18		0.26	U	90	
										FeII	−43	1700 ±200	L	8900 ±1300		0.28	U	90	
										ZnII	−43	8.3 ±1.5	L	43 ±8		0.95	U	90	
PG 0039+048	118.59	−57.64	1.1±0.4	a 0.93	sdB	PP	−47	110 ±10	Ef	NaI	−47	18	W	16		0.0079	U	62	
Southern IVCs																			
HD 203699	65.64	−24.92	0.80±0.10	t 0.34	B2.5IVn		−30	37 ±5	Ef	CaII	−42	2.0	N	5.5		0.0025	U	58	
PG 0039+134	119.54	−49.05	1.7±0.4	a 1.3	He-sdO		−46	23 ±3	ef	NaI		<11	N	<49				62	
3C 33	129.45	−49.31	—	—	Sey		−43	15 ±0.4	Ar	HI		<17	τ			T_s>350		39	T
3C 41	131.38	−29.07	—	—	radio		−53	40 ±0.4	Ar	HI		<14	τ			T_s>450		39	T
HD 14633	140.78	−18.20	2.5±0.2	t 0.78	O8.5V		−82	7.7 ±1.2	Dw	NaI		<0.020	L	<0.26				107	
										CaII	−77.0	0.41	L	5.3		0.0024	U	107	
										NaI		<0.025	L	<0.33				107	
										CaII	−72.5	0.74	L	9.6		0.0044	U	107	
										NaI		<0.025	L	<0.33				107	
										CaII	−63.8	2.2	L	29		0.013	U	107	
HD 16581	169.69	−51.41	0.30	p 0.23	B9V		−64	2.3 ±0.5	Ef	CaII		<5.0	N	<220				58	
										TiII		<1.7	N	<74				58	

TABLE 2—*Continued*

Probe (1)	l ° (2)	b ° (3)	d kpc (4)	z kpc (5)	type (6)	Cld (7)	v_{HI} km/s (8)	N_{HI} 10^{18} cm^{-2} (9)	tel (10)	ion (11)	v_{ion} km/s (12)	N_{ion} 10^{11} cm^{-2} (13)	code (14)	A_{ion} 10^{-9} (15)	A_{ref} 10^{-9} (16)	A/A$_{\odot}$ (17)	D? (18)	Ref (19)	Note (20)
Complex gp			< 4.3	< 2.0						NaI				20		0.0098			
			> 0.8	> 0.3						KI				4.9		0.036			
										SiII				>0	[19000]	>0			
										SII				1.6E4 ±8.2E3	[19000]	0.88			
										CaII				38	[22]	0.018			
										FeII				>0	[7800]	>0			
Mrk 509	35.97	−29.86	—	—	Sey		+60	25 ±1	Ef	NaI	+62.9	2.6 ±0.5	L	10 ±2		0.0051		13	98
										SiII	+59	>0	N	>0		>0		13	
										SII	+60	4000 ±2000	N	1.6E4 ±8.2E3		0.88		120	132
										CaII	+59	18 ±3	L	74 ±14		0.034		25	133
										FeII	+59	>0	N	>0		>0		13	
M 15	65.01	−27.31	10	g 4.6	GC		+69	47 ±0.8	Ef	NaI	+68	6.0 ±0.7	W	13 ±1		0.0063	U	8	V
										CaII	+61	32 ±4	W	69 ±10		0.031	U	8	
M 15 IV-38	65.00	−27.33	10	g 4.6	AGB		+69	49 ±1	Ef(	NaI	+60	7.5	W	15		0.0075	U	4)	134,V
									(	NaI	+59	11	W	22		0.011	U	41)	
										NaI	+67	9.6	W	20		0.0096	U	102	
										KI		<0.40	L	<0.82				102	
M 15 K 027	64.89	−27.28	10	g 4.6	HB		+70	54 ±1	Ef	CaII	+59	14 ±9	W	27 ±17		0.012	U	108	134,V
M 15 K 048	65.01	−27.31	10	g 4.6	HB		+69	50 ±1	Ef	CaII	+69	25 ±16	W	51 ±33		0.023	U	108	134,V
M 15 K 064	64.97	−27.27	10	g 4.6	HB		+70	53 ±1	Ef	CaII	+64	28 ±18	W	53 ±33		0.024	U	108	134,V
M 15 K 080	65.01	−27.31	10	g 4.6	HB		+69	47 ±1	Ef	CaII	+57	9.4 ±9.7	W	20 ±21		0.0091	U	108	134,V
M 15 K 084	65.01	−27.31	10	g 4.6	HB		+69	47 ±1	Ef	CaII	+60	6.4 ±7.2	W	14 ±15		0.0062	U	108	134,V
M 15 K 127	64.89	−27.36	10	g 4.6	HB		+69	44 ±1	Ef	CaII	+65	11 ±8	W	25 ±19		0.011	U	108	134,V
M 15 K 143	65.00	−27.28	10	g 4.6	HB		+70	51 ±1	Ef	CaII	+61	13 ±9	W	25 ±17		0.011	U	108	134,V
M 15 K 144 = II-75	65.00	−27.27	10	g 4.6	AGB		+70	51 ±1	Ef(	NaI	+61	16	W	31		0.015	U	4)	134,V
									(	NaI	+58	21	W	40		0.020	U	41)	
										NaI	+67	20	W	38		0.019	U	102	
										KI	+68	2.5	L	4.9		0.036	U	102	
M 15 K 154 = III-9	64.98	−27.29	10	g 4.6	HB		+70	52 ±1	Ef	CaII	+66	41 ±37	W	79 ±73		0.036	U	108	134,V
M 15 K 239	65.02	−27.28	10	g 4.6	HB		+69	48 ±1	Ef	CaII	+63	21 ±11	W	43 ±24		0.020	U	108	134,V
M 15 K 258	65.01	−27.29	10	g 4.6	HB		+69	50 ±1	Ef	CaII	+80	14 ±9	W	29 ±19		0.013	U	108	134,V
M 15 K 267	65.02	−27.31	10	g 4.6	HB		+69	50 ±1	Ef	CaII	+80	9.4 ±8.0	W	19 ±16		0.0086	U	108	134,V
M 15 K 341	65.05	−27.27	10	g 4.6	HB		+68	42 ±1	Ef	NaI	+56	8.6	W	20		0.0100	U	41	134,V
M 15 K 996	65.05	−27.33	10	g 4.6	HB		+69	46 ±1	Ef	NaI	+70	12 ±4	W	26 ±9		0.013	U	25	134,V
										CaII	+69	20	L	44		0.020	U	25	
M 15 N1	65.01	−27.31	10	g 4.6			+69	50 ±1	Ef	CaII	+63	14 ±9	W	29 ±19		0.013	U	108	134,V
M 15 S1	64.91	−27.18	10	g 4.6			+70	54 ±1	Ef	NaI	+54	8.1	W	15		0.0074	U	41	134,V
M 15 S4	65.01	−27.31	10	g 4.6			+69	50 ±1	Ef	NaI	+57	5.5	W	11		0.0055	U	41	134,V
M 15 S7	64.93	−27.37	10	g 4.6			+69	44 ±1	Ef	NaI	+59	9.7	W	22		0.011	U	41	134,V
M 15 S8	65.02	−27.31	10	g 4.6			+69	50 ±1	Ef	NaI	+56	7.1	W	14		0.0070	U	41	134,V
M 15 NW core	65.01	−27.31	10	g 4.6			+69	50 ±1	Ef	NaI	+68	5.0	N	10		0.0049	U	111	134,135
M 15 SE core	65.01	−27.31	10	g 4.6			+69	50 ±1	Ef	NaI	+68	>80	N	>160		>0.079	U	111	134,135
HD 203664	61.93	−27.46	4.3±0.4	t 2.0	B0.5III		+65	2.2 ±0.4	JB(	NaI	+70	1.7	N	77		0.038	U	65)	
									(	CaII	+81	9.0	N	410		0.19	U	58)	
									(	CaII	+69	5.0	N	230		0.10	U	65)	
									(	CaII	+70	10	L	450		0.21	U	102)	
							+65a	1.1	JB	NaI	+80.2	1.4 ±0.07	N	120 ±6		0.059	U	82	
										CaII	+80.0	5.0 ±0.5	N	440 ±40		0.20	U	82	
							+65b	0.53	JB	NaI	+75.2	0.16 ±0.06	N	30 ±11		0.015	U	82	
										CaII	+75.2	2.4 ±0.4	N	450 ±80		0.20	U	82	
							+65c	0.53	JB	NaI		<0.25	N	<47				82	
										CaII	+69.8	2.4 ±0.6	N	440 ±110		0.20	U	82	
HD 203699	65.53	−24.92	0.80±0.10	t 0.34	B2.5IV		+76	10 ±1	Ef(	CaII		<1.4	W	<13				65)	
										CaII		<0.40	L	<3.8			l	102	
HD 205556	60.02	−32.62	0.40±0.10	s 0.22	B9V		+57	2.1 ±0.6	JB	CaII		<1.4	W	<67				65	

TABLE 2—*Continued*

Probe	l °	b °	d kpc	z kpc	type	Cld	v_{HI} km/s	N_{HI} 10^{18} cm^{-2}	tel	ion	v_{ion} km/s	N_{ion} 10^{11} cm^{-2}	code	A_{ion} 10^{-9}	A_{ref} 10^{-9}	$A/A_{\odot}$	D?	Ref	Note
(1)	(2)	(3)	(4)	(5)	(6)	(7)	(8)	(9)	(10)	(11)	(12)	(13)	(14)	(15)	(16)	(17)	(18)	(19)	(20)
Other Negative-Velocity IVCs																			
HD 137569	21.87	51.93	0.60±0.30 t	0.47	B5IIIp		(−43)	<4.0	GB	CaII	−43	1.7	N	>42		>0.019	U	58	
SN 1981 D	240.21	−56.70	—	—	SN		−35	6.6 ±3.0	PM	CaII	−43	6.2	L	93		0.043		25	136
NGC 3783	287.46	22.95	—	—	Sey					NaI	−39	7.0	N					22	
										CaII	−39	14 ±2	N					22	
HD 101274	287.47	22.94	0.40±0.03 s	0.16	A0V					CaII	−48	10	L				U	25	
Mistaken claims																			
M 3 vZ1128	42.50	78.68	9.7 g	9.5	PAGB	K	(−70)	<3.0	Dw	CII	−70	>1000	N	>3.3E4		>0.094	U	17	137
HD 83206	167.70	46.93	0.90±0.20 t	0.66	B3V		(−80)	<2.0	Ef (	NaI		<0.24	W					94)	12,13,W
										NaI		<0.025	L					107	
									(	CaII	−80	0.58	L	>29		>0.013	U	94)	
										CaII	−79.8	0.42	L	>21		>0.0095	U	107	
Other Positive-Velocity IVCs																			
V421 Her	64.84	31.60	5.5±0.6 s	2.9	RR Lyr		+61	2.9 ±0.6	Dw	CaII		<5.4	N	<190				70	
HD 156110	70.99	35.71	0.72±0.33 p	0.42	B3Vn		+43	12 ±4	Dw	SiII		<230	N	<1900				50	s
PG 1710+490	75.43	36.08	0.70±0.30 a	0.41	sdB		+43	7.1 ±0.9	Dw	NaI	+43	1.7	W	23		0.011	U	62	
										CaII	+43	2.6	W	37		0.017	U	62	
PG 1213+456	141.93	70.44	2.9±0.7 a	2.7	sdB		+51	3.8 ±0.4	JB	CaII		<11	N	<290				93	
SN 1998 S	150.75	65.96	—	—	SN		(+48)	<3.0	Ef	FeII	+47.8	190 ±20	L	>6200		>0.19		117	
PG 0229+064	162.56	−48.29	0.70±0.30 s	0.52	sdB		(+82)	<3.0	Ef	NaI	+82	2.9	W	>98		>0.048	U	62	W
BD +38 2182	182.16	62.21	4.0 a	3.5	B3V		+38	2.4 ±0.04	JB	CaII		<0.23	W	<9.6				93	V
HD 93521	183.14	62.15	1.9 t	1.7	O9.5V		+38	3.0 ±0.1	JB	SiII		<6.9	S	<230			L	56	
										CaII		<0.23	W	<7.7				93	
HD 100340	258.85	61.23	3.0 a	2.6	B1V		+45	4.8 ±0.3	GB	NaI		<0.20	L	<4.2				113	
							+73	<1.5	GB(	CaII	+73	1.5	N	>100		>0.046	U	58)	
										CaII	+77	1.7	L	>120		>0.053	U	113	
NGC 2808	282.19	−11.25	8.9 g	1.7	GC	WW339	+76	124 ±1	PM	CaII		<5.9	W	<4.8				8	
NGC 3783	287.46	22.95	—	—	Sey				(	CaII	+52	13	L					25)	
										CaII	+64	18 ±2	N					22	
HD 86248	264.59	18.11	7.6±1.7 t	2.4	B3II					CaII		6.3 ±1.0	N				U	54	
HD 101274	287.47	22.94	0.40±0.03 s	0.16	A0V		+60	103 ±0.5	PM	CaII	+37	10	L	9.7		0.0044	U	25	
SN 1986 G	309.54	19.40	—	—	SN					CaII	+97	1.9	N					31	
SN 1983 N	314.54	31.95	—	—	SN		+30	8.0 ±3.0	Dw(	CaII	+43	6.3	N	79		0.036		20)	
										CaII	+42	4.1	L	51		0.023		25	

TABLE 2—*Continued*

NOTE.—Table 2 is available in machine-readable form in the electronic edition of the *Astrophysical Journal Supplement*.

TABLE 3

SOLAR AND HALO ION ABUNDANCES

Ion	log $A_\odot$	$A_\odot$ (ppb)	log δ[a]	δ[a]	A(halo) (ppb)	IP[b](Produce)	IP (Destroy)
C I	−3.45	350000	−3.15	0.0007[c]	240−280[c]		11.26
C II	−3.45	350000	−0.41	0.39[a]	140000	11.26	24.38
C IV	−3.45	350000			($N = 1.6 \times 10^{14}$)[d]	47.89	64.49
N I	−4.03	93000	−0.07	0.85[a]	79000		14.53
N II	−4.03	93000	−1.20	0.068[c]	5500−7100[c]	14.53	29.60
N V	−4.03	93000			($N = 3.5 \times 10^{13}$)[d]	77.47	97.89
O I	−3.13	740000	0.00	1.0[a]	740000		13.62
O VI	−3.13	740000			($N = 2.0 \times 10^{14}$)[d]	113.90	138.12
Na I	−5.69	2000	−2.30	0.005[a]	1.2−240[c]		5.14
Mg I	−4.42	38000	−2.50	0.003[c]	6.6−390[c]		7.65
Mg II	−4.42	38000	−0.42	0.38[a]	14000	7.65	15.04
Al II	−5.52	3000	−0.27	0.53[a]	1600	5.99	18.83
Al III	−5.52	3000			($N = 3.3 \times 10^{12}$)[d]	18.83	28.45
Si II	−4.45	35000	−0.27	0.53[a]	19000	8.15	16.35
Si III	−4.45	35000	−1.00	0.1[a]	3500	16.35	33.49
Si IV	−4.45	35000			($N = 4.4 \times 10^{13}$)[d]	33.49	45.14
P II	−6.43	370	0.00	1.0[a]	370	10.49	19.73
S II	−4.73	19000	0.00	1.0[a]	19000	10.36	23.33
S III	−4.73	19000	−1.00	0.1[c]	590−3500[c]	23.33	34.83
Cl II	−6.73	190				12.97	23.81
Ar I	−5.44	3600	−0.48	0.33[a]	1200		15.76
K I	−6.87	135	−1.40	0.04[c]	<0.8−>9.2[c]		4.34
Ca I	−5.66	2200	−3.30	0.0005[c]	<0.05−>1.7[c]		6.11
Ca II	−5.66	2200	−2.00	0.01[c]	2.5−570[c]	6.11	11.87
Ti II	−7.07	85	−0.45	0.35[c]	30	6.82	13.58
Cr II	−6.32	480	−0.50	0.32[a]	150	6.77	16.50
Mn II	−6.47	340	−0.59	0.26[a]	87	7.44	15.64
Fe II	−4.49	32000	−0.62	0.24[a]	7800	7.79	16.18
Fe III	−4.49	32000	−1.50	0.03[c]	270−>2900[c]	16.18	30.65
Zn II	−7.35	45	−0.03	0.93[a]	42	9.39	17.96

[a] δ is the product of depletion onto dust and ionization fraction typical for halo gas, as derived by Savage & Sembach 1996a.

[b] IP stands for ionization potential.

[c] Value derived in this paper; for nondominant ions a range is given for the abundances, and an average for the value of δ.

[d] Average column density toward the galactic pole, from Sembach & Savage (1992 and Savage et al. 2000b.

3. NOTES ON ION ABUNDANCES

3.1. *General Remarks*

3.1.1. *Organization*

In this section, some general remarks are given to accompany the discussion of results for most of the observed ions below. The symbol A refers to the abundance of the element, while δ is used to refer the ratio (observed abundance in the gas)/(solar abundance). Savage & Sembach (1996a, § 7) define δ in this way, but call it "depletion," implying that the gaseous abundances appear lower than solar because most of the element's atoms sit in dust grains. However, with this definition δ really refers to the combination of depletion and ionization, as both depletion onto dust grains and the presence of different ionization stages can make the elemental abundance in the gas appear lower than the intrinsic abundance. Here we will use δ to stand for the observed relative abundance in the gas, i.e., the product of depletion onto dust and ionization.

Below, some general remarks are given concerning reference abundances, oscillator strengths, complications due to ionization, and comparisons of different measurements of the same ion in the same cloud. A correlation between ion abundances and H I column density was found, which is summarized. Then, a summary is given of absorption by H I, which yields the kinetic (spin) temperature. Early results on molecular hydrogen are listed. Next, dominant ions of undepleted ions are discussed, which yield intrinsic abundances. This is followed by a discussion of dominant ions of depleted elements, which yield depletion patterns and insight into the presence (and composition) of the dust, Then, results for nondominant ions are summarized. Finally, the highly ionized ions are described. A more detailed discussion of the numerical results for each cloud is presented in § 4.

3.1.2. *Reference Abundances*

Reference abundances are summarized in Table 3, following Savage & Sembach (1996a). This table lists the Solar System (meteoritic) abundances of the element, as given by Anders & Grevesse (1989) (with photospheric updates for C, N, and O from Grevesse & Noels 1993), the depletion × ionization (assuming a halo-like pattern, as given by Savage & Sembach 1996a), the resulting expected halo abundance (in parts per billion, ppb), and the ionization potential of the previous and next ionization stage (i.e., the energy required to produce and destroy the ion).

Solar System abundances are used as a reference because these are comparatively well determined. However, as Savage & Sembach (1996a) point out, abundances in nearby

B stars tend to be 0.15–0.25 dex lower. Since B stars have formed recently, they may be a better reference for the local ISM. ISM abundances may also show inhomogeneities between individual open clusters. Such differences mostly influence the interpretation of depletion patterns and the composition of dust.

Meyer, Jura, & Cardelli (1998) determined from a set of high-quality measurements that the typical gaseous abundance of oxygen in nearby low-velocity gas is about 320,000 ppb, or 0.4 solar. They also argued that dust contains at most 180,000 ppb of oxygen, so that the total oxygen abundance in the nearby ISM is about 0.66 solar. This is similar to the value derived for nearby B stars. The suggested explanations are that (a) the early solar system was enriched by a supernova, (b) the ISM has recently been diluted by metal-poor gas, or (c) the Sun has moved outward from the Galactic center since it formed. This abundance difference is mostly important when using a depletion pattern to derive the composition of dust particles. Further, if the local ISM indeed has intrinsic abundances below solar, this has some bearing on understanding the origin of relatively nearby intermediate-velocity halo gas, which appears to have solar abundance (as derived from sulfur, see §§ 4.24, 4.26, 4.27, and 4.28).

For nondominant ions, the results listed in Table 2 were used to derive fiducial values for HVCs/IVCs. This pertains to C I, N II, Na I, Mg I, S III, K I, Ca I, Ca II, and Fe III. Table 3 shows the range of abundances found in the HVCs and IVCs for these elements [in the column labeled A(halo)]. An average value is given for δ. These abundances clearly can vary by a large amount, which is not unexpected considering that they depend on the detailed physical conditions in a cloud (temperature, density, radiation field).

Rarely are there complementary data for other ionization stages for clouds where nondominant ions were measured. And in cases where both kinds of ions have been measured, usually no analysis of physical conditions has been done—the exceptions being HD 93521 (Spitzer & Fitzpatrick 1993), HD 215733 (Fitzpatrick & Spitzer 1997), SN 1987A (Welty et al. 1999), and PG 0804+761 (Richter et al. 2001a).

3.1.3. *Oscillator Strength Issues*

To convert the observed amount of absorption into a column density, it is necessary to know the oscillator strength or f-value of the line. For papers published since 1990, most authors take f-values from the list of Morton (1991). No attempt was made to correct column densities in older papers or papers where a different source was used for the f-values. In general, differences tend to be relatively small ($<20\%$), although there are exceptions. Still, this is an extra source of systematic uncertainty in the tabulated column densities. If a paper gave the column density, this was used in Table 2, independent of the actual f-value and method used to derive this column density.

If a paper gave an equivalent width, this was converted to a column density as described in the Appendix under column (13). The f-value was then taken from the compilation of Verner, Barthel, & Tytler (1994), which claims to be a digitized update of the Morton (1991) list. For Si II λ1260, Si II λ1304, Si II λ1526, Ar I $\lambda\lambda$1048, 1066, Cr II $\lambda\lambda$2056, 2062, 2066, and Zn II $\lambda\lambda$2026, 2062 updated values were taken from Savage & Sembach (1996a), while for Mg II $\lambda\lambda$1239, 1240 updated values were found by Fitzpatrick & Spitzer (1997). Further, for the Fe II lines between 1121 and 1144 Å, new f-values were determined experimentally from *FUSE* spectra by Howk et al. (2000).

However, for some lines the f-values that Verner et al. (1994) give are rather different than those given by Morton (1991). In particular, the ratio Verner/Morton is 0.95 for S II $\lambda\lambda$1250, 1253, 1259, 2.88 for N I $\lambda\lambda$1134.16, 1134.41, 1134.98, and 1.22 for N I $\lambda\lambda$1199.54, 1200.22, 1200.71. These differences are unexplained. However, for the case of N I the Morton values appear more reliable. This conclusion is based on comparing the relative equivalents widths predicted for the N I λ1134 and N I λ1200 triplets with the high-quality measurements made by Howk, Savage, & Fabian (1999) for the sight line to μ Col.

Morton (2001) present a new compilation of f-values. These may differ from the previously published values, sometimes by as much as a factor 2. However, such differences mostly pertain to far-UV lines in the wavelength range observed by *FUSE*. In the publications using such data, the new f-values have been used.

3.1.4. *Ionization Issues*

Note that the numbers in the table give the ratio N(ion)/N(H I). That is, they do *not* include a correction for hydrogen ionization. In fact, only for a few sight lines was a study of ionization possible. Toward HD 93521 (Spitzer & Fitzpatrick 1993) and HD 215733 (Fitzpatrick & Spitzer 1997) $N(H^+)/N$(H I) does not seem to be high in the IVCs studied. However, toward Mrk 509 Sembach et al. (1999) find that N(C IV) > N(C II), which suggests almost completely ionized gas. Also, toward Mrk 876 (Murphy et al. 2000) $N(H^+)$ appears to dominate in the complex C component. In contrast, toward Mrk 290 (complex C; Wakker et al. 1999a) and PG 0804+761 (LLIV Arch; Richter et al. 2001a) $N(H^+)/N$(H I) ~ 0.2, while toward HD 215733 hydrogen ionization appears negligible (Fitzpatrick & Spitzer 1997). Clearly, ionization issues are important in general, but usually they cannot be addressed with the existing data.

3.1.5. *Multiple Measurements in One Cloud*

For a few ions multiple determinations were made within the same cloud. This is the case for both Na I and Ca II in the IV Arch (§ 4.24), complex gp (§ 4.29) and the +65 km s^{-1} IVC toward the LMC (§ 4.23). Further, Ca II is seen in several sight lines on complex A (§ 4.1), complex C (§ 4.3), the LLIV Arch (§ 4.26) and the HVCs toward the LMC.

These values are compared later in this section (§§ 3.5 and 3.6). There it is shown that in general Na I can vary by a factor of more than 10 within a single cloud and by a factor up to 100 for any given H I column density. Ca II is more constant, varying by a factor 2–5 within a single cloud, and a factor less than 10 at any given N(H I).

Multiple measurements were also made for S II in complex C, for Mg II in the Magellanic Stream, and for O I, Mg II, S II, and Fe II in the +120 km s^{-1} HVC toward the LMC. These are discussed under the subsection pertaining to each cloud (§§ 4.3, 4.14, and 4.23).

Figure 1 presents scatter plots of the H I column density versus the ion column density for the clouds with multiple determinations.

3.2. *A Correlation between Ion Abundances and* N(H I)

Previous studies of the depletion in the ISM have found that the abundance of elements such as Mg II, P II, Cl II, Mn II, Fe II, Ca II, and Ti II correlates with the average density of H I in the sight line (calculated as N(H I) divided

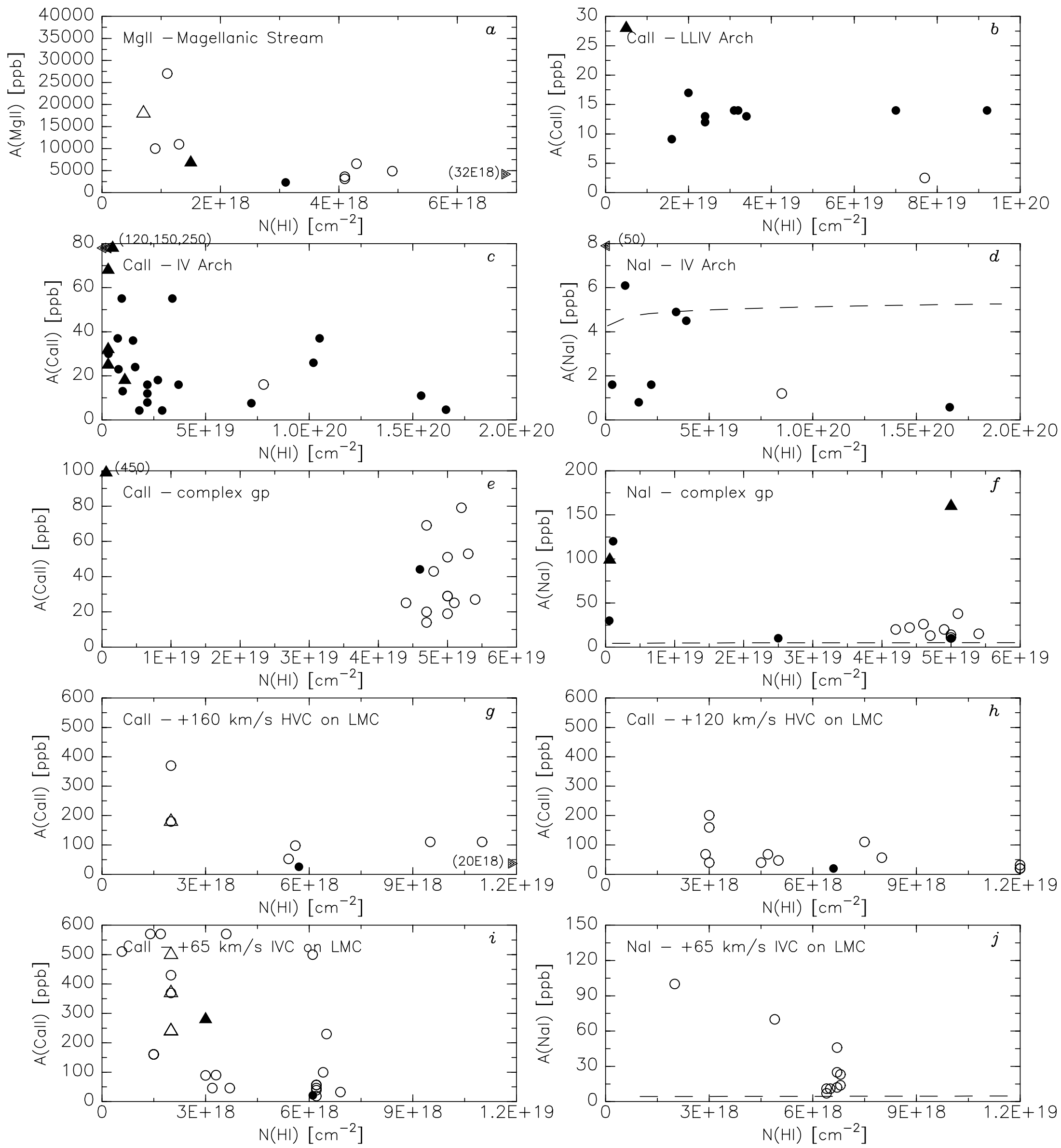

FIG. 1.—Scatter plots of [N(ion)/N(H I)] vs. N(H I) for the ions for which multiple determinations exist in a single cloud. Circles indicate actual measurements, triangles show lower limits. Closed symbols show measurements where both the H I and the ion column density were carefully measured. Open symbols refer to measurements where only the equivalent width was given, or where the H I data were interpolated (in the case of LMC stars). Note that three Ca II limits in the IV Arch and one in complex gp are off-scale. Most of the scatter at high N(H I) may be due to fine structure in N(H I), or to variations in depletion/ionization fraction. The scatter at low N(H I) is probably due to the ionization of hydrogen in the case of Mg II or to low dust content in the case of Ca II (see Wakker & Mathis 2000).

by the distance to the background star) (e.g., Jenkins, Savage, & Spitzer 1986; Crinklaw, Federman, & Joseph 1994).

In these studies of nearby, low-velocity gas the lowest observed H I column density is $\sim 10^{20}$ cm^{-2}. As HVC and IVC components stand out in velocity, it is possible to measure abundances in clouds with much lower column density, down to 10^{18} cm^{-2}. However, it is not possible to derive an average volume density since the cloud's distances and depths are not known. Instead, the gaseous abundances of Mg II, Mn II, Ca II, Ti II, and Fe II in HVCs/IVCs (from this paper) and low-velocity gas (from Jenkins et al. 1986 and Crinklaw et al. 1994) were plotted against H I column density (rather than against average H I volume density).

Unexpectedly, significant correlations were found. The high column density low-velocity gas and the low column density high-velocity gas lie on the same curves. Least-squares fits yield a rms scatter of 0.3–0.4 dex around the mean, for N(H I) between 10^{18} and 10^{22} cm^{-2}. These results are presented in detail in a separate paper (Wakker & Mathis 2000) and have implications for the density structure of the ISM and for understanding the formation and destruction of dust. Here the fit results are used to predict abundances at a given N(H I); these predictions are compared to the actual observed values to help understand the observed abundance patterns.

3.3. H I 21 cm *Absorption*

21 cm H I absorption is seen in only four HVCs/IVCs. The radio continuum source showing absorption in complex H is unidentified but is probably extragalactic

(Wakker, Vijfschaft, & Schwarz 1991). The derived spin temperature of 50 K is typical for cold gas. As N(H I, absorption) $\sim N$(H I, emission), there appears to be no warm H I in the very core of complex H.

Three H I absorption components associated with the Anti-Center shell are seen in the spectrum of 3C 123 (Payne, Salpeter, & Terzian 1980; Kulkarni, Dickey, & Heiles 1985), although only one emission component can be discerned. The column density of the broad (30 km s^{-1}) absorption component is similar to that of the emission column density, suggesting the presence of mostly warm ($T > 200$ K) gas. One might argue that the feature sampled by 3C 123 is unconnected with the main AC Shell feature that runs at $b \sim 7°$ from $l = 170°$ to $l = 200°$ (see Fig. 8), so a separate measurement of T_s in the main feature would be useful.

Relatively many radio continuum sources lie projected onto the Outer Arm, and H I absorption is seen toward two of those (3C 395 and QSO 2005+403—Payne et al. 1980 and Akeson & Blitz 1999), yielding a spin temperature of $\sim$50 and $\sim$150 K, respectively, i.e., typical values for Galactic H I. In several other background sources the lack of H I absorption sets lower limits of 300–1000 K, although a few of these may be Galactic sources in front of the Outer Arm. This deserves a more thorough study.

Payne et al. (1980) reported H I absorption associated with cloud R in the spectrum of 4C 33.48, which is probably an extragalactic radio source. The derived spin temperature is 69 K. The ratio of absorption to emission H I column density is only $\sim$0.2, suggesting that most of the H I is warm.

In all other cases where observations have been made, 21 cm H I absorption was not found. This often implies lower limits to the temperature of more than 20 K, which is not a very interesting limit. However, lower limits of 70 K or more have been found for complex C (Akeson & Blitz 1999), the Cohen Stream (Colgan, Salpeter, & Terzian 1990), the Magellanic Stream (Payne et al. 1980; Colgan et al. 1990; Mebold et al. 1991; Akeson & Blitz 1999) and complex K (Colgan et al. 1990).

3.4. *Molecular Hydrogen*

The study of H_2 in HVCs and IVCs is in its infancy. Attempts to detect molecular gas in HVCs using CO emission have always been unsuccessful (see Wakker et al. 1998). However, H_2 is easy to detect in ultraviolet absorption, as is shown by the recent *ORFEUS* (Orbiting and Retrievable Far and Extreme Ultraviolet Spectrometer) and *FUSE* instruments. H_2 has now been found in two HVCs and three IVCs.

The first detection was that in the *ORFEUS* spectrum of Sk $-68°82$ for the $+120$ km s^{-1} cloud projected on the LMC (Richter et al. 1999). This was also measured by Bluhm et al. (2001) and yields a ratio for $N(H_2)/N$(H I) of $3.0 \pm 0.6 \times 10^{-5}$, with N(H I) $= 12 \times 10^{18}$ cm^{-2}. However, toward the star Sk $-68°80$ (less than an arcmin away) P. Richter (2000, private communication) finds no H_2, showing large variations on small scales in this cloud. The $+60$ km s^{-1} cloud toward the LMC also contains H_2, with a fraction of 5×10^{-3}, although N(H I) is only $\sim 10^{18}$ cm^{-2}.

Murphy et al. (2000) reported a limit of $N(H_2)/N$(H I) $< 10^{-5}$, for complex C, where N(H I) $= 19 \times 10^{18}$ cm^{-2}. H_2 in the IV arch was found in the *ORFEUS* spectrum of HD 93521 (Gringel et al. 2000), where N(H I) $= 37 \times 10^{18}$ cm^{-2} and $N(H_2)/N$(H I) $= 0.8 \pm 0.5 \times 10^{-5}$. H_2 in the LLIV arch was detected by Richter et al. (2001a), in the *FUSE* spectrum of PG 0804+761. The $N(H_2)/N$(H I) ratio there is 1.5×10^{-5}, with N(H I) $= 35 \times 10^{18}$ cm^{-2}. H_2 is also found in the $+240$ km s^{-1} HVC seen in the spectrum of NGC 3783 (cloud WW187), where N(H I) $= 83 \times 10^{18}$ cm^{-2} and $N(H_2)/N$(H I) $= 0.8 \pm 0.2 \times 10^{-3}$ (Sembach et al. 2001).

Thus, high- and intermediate-velocity molecular hydrogen has been found, with molecular fractions that are not atypical for the amount of hydrogen in the sight line. This requires the presence of dust in the detected IVCs/HVCs, which is also suggested by the depletion pattern of these particular clouds. The only nondetection is toward complex C, where a smaller absolute amount of dust is expected because this cloud has low metallicity. However, it is unclear whether the sensitivity was sufficiently high to detect H_2 at the low H I column density. Further studies with *FUSE* show H_2 in all sight lines with an IVC, but not toward HVCs other than the Magellanic Stream.

3.5. *Dominant Ions of lightly Depleted Elements*

Intrinsic abundances can be determined or estimated using lines of N I, O I, P II, S II, and Zn II. That these elements are (almost) completely in the gas phase is an expectation based on measurements of low-velocity gas (Savage & Sembach 1996a). Results have been reported for seven clouds, as summarized below.

First, for HVC complex A an abundance of about 0.1 solar is suggested by the O I λ1302 absorption seen toward I Zw 18 (Kunth et al. 1994). However, this measurement is based on a strong line, the error in the equivalent width is large and the component structure complicates matters further (see also § 4.1).

For complex C abundances were measured in two sight lines with high N(H I) ($\sim 90 \times 10^{18}$ cm^{-2}—Mrk 290 and PG 1259+593), two with intermediate N(H I) ($\sim 30 \times 10^{18}$ cm^{-2}—Mrk 817 and Mrk 279) and one with relatively low N(H I) ($\sim 20 \times 10^{19}$ cm^{-2}—Mrk 876).

A value of 0.09 ± 0.02 solar was measured for sulfur toward Mrk 290 (Wakker et al. 1999a), which was corrected for 20% H ionization (based on a measurement of Hα emission) and for H I small-scale structure. Richter et al. (2001b) find O I/H I $= 0.11^{+0.13}_{-0.08}$ solar toward PG 1259+593. O I is a particularly useful ion as it has an ionization potential similar to that of H I and its ionization is strongly coupled to that of hydrogen through a charge-exchange reaction (Sofia & Jenkins 1998).

Toward Mrk 876 Murphy et al. (2000) found N(N I)/N(H I) ~ 0.08 solar and N(Ar I)/N(H I) < 0.1 solar. N I and H I have similar ionization potential and the nitrogen ionization also tends to couple to that of hydrogen, although not as strongly as that of oxygen. Argon is a noble gas, and therefore probably undepleted. However, Ar I has a larger photoionization cross section than H I and is not coupled to H I. It is therefore more easily ionized than H I and in a situation where neutral and (photo-) ionized gas are mixed, Ar I can appear deficient. In the sight line toward Mrk 876 Murphy et al. (2000) further find that N(Fe II)/N(H I) ~ 0.5 solar. To reconcile this with the N I abundance requires a large H^+/H I ratio.

For two other complex C probes (Mrk 817, Mrk 279) Gibson et al. (2001) found N(S II)/N(H I) $= 0.3$–0.4 solar. However, in neither of these directions has H I small-scale structure or ionization been taken into account. Ionization probably is important, since if photoionization is responsible for the H^+, $N(H^+)$ should not vary by more than a factor ~ 2 across the face of the cloud. Since, in the sight line toward Mrk 290 $N(H^+)$ is $\sim 2 \times 10^{19}$ cm^{-2}, and toward Mrk 817 and Mrk 279 N(H I) is $\sim 3 \times 10^{19}$ cm^{-2}, the ionization correction could easily be a factor 2, bringing the S^+ abundances in line with those found toward Mrk 290.

Two sulfur abundance measurements exist for the Magellanic Stream: 0.33 solar (Fairall 9, Gibson et al. 2000) and 0.25 solar (NGC 3783, Lu et al. 1998). Ionization corrections have not yet been addressed, but they are expected to be minimal as N(H I) is high and the gas is far from both the Galaxy and the LMC. Note that toward NGC 3783 a 1′ resolution map of the H I small-scale structure resulted in a 50% correction of N(H I) (and thus the S^+ abundance) relative to a measurement with a large beam (Lu et al. 1998).

For three sight lines through the IV Arch S II/H I ratios have been derived, resulting in values of 0.78 solar for IV9/IV19 (HD 121800, Howk et al. 2001), 0.8 and 1.2 solar for off-core components at -58 and -51 km s^{-1} (HD 93521, Spitzer & Fitzpatrick 1993), and 1.1 solar toward PG 0953+414 (Fabian et al. 2001). Further, O I/H I is found to be 0.9 ± 0.7 solar toward PG 1259+593.

PG 0804+761 gives the best estimate of abundances in the LLIV Arch (Richter et al. 2001a). N(O I)/N(H I) is ~ 1 solar, while N(N I)/N(H I) is ~ 0.6 solar. The fact that N(P II)/N(H I) ~ 1.3 solar is interpreted as evidence that 20% of the H is in the form of H^+, as P^+ can coexist with H^+ as well as with H I, whereas O I becomes ionized when H I gets ionized. This is supported by the value of 1.6 ± 0.4 solar for Zn^+ (which behaves like P^+) found from SN 1993J. The lower N I/H I ratio may be interpreted as evidence for partial ionization (following Sofia & Jenkins 1998), which is further supported by the low ratio N(Ar I)/N(H I) ~ 0.3.

Toward HD 215733 Fitzpatrick & Spitzer (1997) decomposed the H I spectrum based on the absorption components. This results in components at -92 km s^{-1} with N(S II)/N(H I) = 0.17 solar, at -56 km s^{-1} with N(S II)/N(H I) = 0.32 solar and at -43 km s^{-1} with N(S II)/N(H I) = 1.2 solar. The latter two are part of what is defined in this paper as the "PP Arch" (see § 4.28). The combined abundance is 0.5 solar. In both components Zn II absorption is also seen, yielding abundances of 0.23 and 0.95 solar, 0.37 solar when combined. Ionization appears to be unimportant as Fitzpatrick & Spitzer (1997) derive a low electron column density, but the complex component structure hampers the interpretation. Still, the measurements are consistent with an intrinsic abundance of ~ 0.5 solar for the PP Arch.

Penton, Stocke, & Shull (2000) fitted three components to the S II $\lambda\lambda$1250, 1253, and 1259 lines in a GHRS spectrum of Mrk 509. One of these is at $+60$ km s^{-1} and is associated with complex gp. This spectrum is also shown (but not measured) by Sembach et al. (1999). Penton et al. (2000) give equivalent widths of 58, 85, and 30 mÅ for the three sulfur lines. The S II λ1259 line is strongly blended with Si II λ1260, and thus unreliable. The better view of the spectrum presented by Sembach et al. (1999) shows that the equivalent width must be about half the value given by Penton et al. (2000). Therefore, to calculate the S II column density, values of 29 and 42 mÅ were used. Using the H I line width of 29 km s^{-1} seen in this direction, these equivalent widths imply an average S II/H I ratio of 0.8 solar. Since N(H I) is small (24.5×10^{18} cm^{-2}), a large correction for H^+ is quite possible, and the intrinsic abundance of complex gp remains unknown. However, this result strongly suggests that the abundance of complex gp is within a factor 2 of solar.

3.6. *Dominant Ions of Depleted Elements*

C II, Mg II, Si II.—Several depleted ions have very strong lines, reaching an optical depth of 3 for clouds with standard depletion patterns and solar abundances at quite low column densities ($\sim 2 \times 10^{18}$ cm^{-2} for C II λ1334, $\sim 10^{18}$ cm^{-2} for Mg II λ2796 and Si II λ1260). These lines are therefore very useful for determining distance limits, but in general they are less useful for determining depletion patterns.

C II λ1334 is clearly detected in many clouds and has been used to derive a lower distance limit for complex H. Unresolved Mg II $\lambda\lambda$2796, 2803 absorption has been seen in many AGNs observed with the FOS, as described by Savage et al. (2000a). Mg II λ2796 is the main line used to derive lower distance limits for complexes A (Wakker et al. 1996a), C (de Boer et al. 1994), H (Wakker et al. 1998), the Cohen Stream and WW507 (Kemp et al. 1994), and the LLIV Arch (Wakker et al. 1996a), while Si II is the main ion used to derive limits for IV4, IV6, IV9, IV11, IV17, IV19, IV24, IV26, and the IV spur (Kuntz & Danly 1996).

For a few sight lines with low N(H I), Mg II λ2796 has been used to derive the Mg II abundance: for complex C and cloud WW84 using Mrk 205 (Bowen, Blades, & Pettini 1995b), and for 11 sight lines through the Magellanic Stream (see § 4.14). Mg II $\lambda\lambda$1239, 1240 has been measured toward SN 1987A (Welty et al. 1999), HD 93521 (Spitzer & Fitzpatrick 1993) and HD 215733 (Fitzpatrick & Spitzer 1997).

Al II, Al III, Cl I.—These ions are difficult to observe, and thus data exist only for three sight lines: 4 Lac (Bates, Catney, & Keenan 1990), SN 1993J (de Boer et al. 1993) and SN 1987A (Welty et al. 1999).

Ti II, Cr II, Mn II, Ni II.—These elements have weak lines and are rarely seen. In fact, Cr II and Ni II have only been found toward the IVC toward the LMC and in the PP Arch (Welty et al. 1999; Fitzpatrick & Spitzer 1997), while Ti II and Mn II are also seen in the IVC toward the LMC (Caulet & Newell 1996) and several IV Arch cores (Albert 1983; Albert et al. 1993; Spitzer & Fitzpatrick 1993; Lipman & Pettini 1995; Fitzpatrick & Spitzer 1997; Lehner et al. 1999a, Bowen et al. 2000).

Fe II.—This is the most useful ion for obtaining an indication of the presence and amount of dust in HVCs/IVCs, as it has many strong lines in the UV, with a large range of oscillator strengths. Sembach & Savage (1996) found that the depletion of Fe is maximal in cold disk gas (typically $\delta \sim 0.01$), less in warm disk gas ($\delta \sim 0.1$), and least in halo gas ($\delta \sim 0.2$). Higher gaseous abundances were not observed in the sight lines studied, which was interpreted by Sembach & Savage (1996) as evidence for a hard-to-destroy iron core of the dust particles.

High- and intermediate-velocity Fe II absorption has been seen in many clouds: complex C (Murphy et al. 2000; Richter et al. 2001b), the Magellanic Stream (Jannuzi et al. 1998; Savage et al. 2000a), WW187 (Lu et al. 1998), HVC 100−7+100 (Bates et al. 1990), the HVCs/IVCs toward the

LMC (Savage & de Boer 1979, 1981; Welty et al. 1999; Richter et al. 1999), IV4 (Bowen et al. 2000), IV6 (Spitzer & Fitzpatrick 1993), the LLIV Arch (de Boer et al. 1993; Richter et al. 2001a), and the PP Arch (Fitzpatrick & Spitzer 1997).

For clouds where an undepleted element was also measured the ratio with Fe II can be derived and the depletion of Fe can be derived. This results in (Fe/N) > 5 solar for complex C (Mrk 876—Murphy et al. 2000; ionization corrections are likely to be large in this sight line, however); (Fe/N) < 1 solar and (Fe/O) = 0.37 ± 0.26 solar in complex C (PG 1259+593—Richter et al. 2001b); (Fe/S) = 0.19 ± 0.07 solar in the Magellanic Stream proper (PKS 0637−75 combined with Fairall 9—Jannuzi et al. 1998 and Gibson et al. 2000). (Fe/S) = 0.13 ± 0.05 solar in the leading arm (NGC 3783—Lu et al. 1998); (Fe/O) ∼ 0.4 solar in the IV Arch (PG 1259+593—Richter et al. 2001b); (Fe/S) ∼ 0.2 solar in the IV Arch (HD 93521—Spitzer & Fitzpatrick 1993); (Fe/O) ∼ 0.27 solar and (Fe/P) ∼ 0.2 solar in the LLIV Arch (PG 0804+762—Richter et al. 2001a), and (Fe/S) ∼ 0.2 solar in the PP Arch (HD 215733—Fitzpatrick & Spitzer 1997).

Thus, the Magellanic Stream and three of the major IVCs appear to have Fe depletions of about a factor 5, which is similar to the typical halo value derived by Savage & Sembach (1996a). Note, however, that the IVC results for HD 93521 and HD 215733 were used to arrive at this typical value. Note also that Wakker & Mathis (2000) show that the apparent depletion of Fe II depends on N(H I). It is thus unclear whether the high Fe/S ratios in HVCs/IVCs are due to environmental conditions or to the fact that the HVC/IVC H I column densities are relatively low.

3.7. *Nondominant Ions*

Several nondominant ions have been seen. These are discussed individually below, in order to derive a reference value for incorporation in Table 3.

C I.—For this ion an abundance has been found for clouds WW187 (NGC 3783, 280 ± 180 ppb—Lu, Savage, & Sembach 1994a) and the PP Arch (HD 215733, 240 ± 30 ppb—Fitzpatrick & Spitzer 1997). Both values are about 0.2% of the reference C II abundance. C I was also seen in the +65 km s^{-1} IVC in the SN 1987A sight line (Welty et al. 1999), with an abundance of 340 ± 130 ppb [however, N(H I) is comparatively uncertain].

N II.—The *FUSE* bandpass contains the N II λ1083 line, which is a good complement to the N I triplets at 1134 and 1199 Å. An analysis of the PG 0804+761 sight line yields an N II/N I ratio ∼0.15 (Richter et al. 2001a). Only a lower limit to N II is found for complex C toward Mrk 876 (Murphy et al. 2000).

Mg I.—This ion has been measured toward HVC 100−7+110 (4 Lac, 100 ± 20 ppb—Bates et al. 1990), IV4 (SN 1998S, 6.6 ± 1.4 ppb—Bowen et al. 2000), the +120 and +60 km s^{-1} clouds toward the LMC (Bluhm et al. 2001, with large errors but showing large variations), IV17 (SN 1998S, 36 ppb—Bowen et al. 2000), LLIV1 (SN 1993J, 44 ppb—de Boer et al. 1993), and the PP Arch (HD 215733, 30 ± 14 ppb—Fitzpatrick & Spitzer 1997). These values are 0.04%–0.7% of the reference for A(Mg II). The approximate values for the clouds in the SN 1987A sight line are slightly higher (110, 110, and 390 ppb, Welty et al. 1999). Since each of the listed clouds has near-solar abundance (see §§ 4.23 and 4.24), there clearly are large variations in the relative Mg I abundance.

Only for the +165 and +122 km s^{-1} LMC clouds and the PP Arch has an Mg II abundance also been measured directly. The resulting Mg I/Mg II ratios are 0.5%, 0.5%, and 0.3%, respectively.

Si III.—The 1206 Å line of Si III is very strong, so that all six detections only give lower limits to the Si^{+2} abundance: in complex C (Mrk 876—Gibson et al. 2001), WW487 (NGC 1705—Sahu & Blades 1997), complex GCN (Mrk 509—Sembach et al. 1995b, 1999), complex WE (HD 156359—Sembach, Savage, & Massa 1991), the −150 km s^{-1} and +130 km s^{-1} clouds against PG 0953+414 (Fabian et al. 2001), and the +65 km s^{-1} IVC toward the LMC (Sk −67°104—Savage & Jeske 1981).

S III.—This ion has only been seen in the three IVCs toward HD 93521, where the S III/S II ratios are 0.11, 0.04, and 0.15 (Spitzer & Fitzpatrick 1993).

K I.—This ion has weak optical lines. It was detected toward SN 1993J at +122 and +140 km s^{-1} with abundances of >9.2 and >5.8 ppb (Vladilo et al. 1993, 1994). It was also detected in complex gp in the spectrum of M15 K144, with an abundance of 4.9 ppb (Kennedy et al. 1998), which is about 5% of the solar K abundance. However, Kennedy et al. (1998) did not detect K I toward the star M15 IV-38, with a limit of 0.82 ppb, suggesting large variations in the K I abundance on small scales.

Ca I.—Like K I, Ca I has weak optical lines and was found toward SN 1993J at +122 and +140 km s^{-1} (Vladilo et al. 1993, 1994). The abundance is more than 1.7 ppb for both clouds. For the +165 and +65 km s^{-1} clouds toward SN 1987A approximate abundances of 0.87 and 0.31 ppb were found, whereas for the +120 km s^{-1} cloud an upper limit of 0.05 ppb was set (Magain 1987; Vidal-Madjar 1987; Welty et al. 1999).

Fe III.—The *FUSE* bandpass contains the Fe III λ1122 line, which is a good complement to the many Fe II lines. The analysis of the PG 0804+761 sight line gives an Fe III/Fe II ratio ∼0.03 for the LLIV Arch.

3.8. Na I

3.8.1. Na I *Detections*

In low-velocity gas, an average Na I abundance of ∼5 ppb is seen, although the range is large (more than a factor 10 either way). Only one cataloged HVC has been detected in Na I absorption: cloud WW219 toward SN 1986G (d'Odorico et al. 1989) yields A(Na I) = 50 ± 10 ppb. High-velocity Na I has been searched for in only two stars known to be sufficiently distant. Yet, it was not detected toward BD +38°2182 (MIII—Keenan et al. 1995) and HD 83206 (WW63—Lehner et al. 1999a). Four extragalactic probes give upper limits: <4 ppb (Mrk 595, Cohen Stream—Kemp & Bates 1998), <55 ppb (Mrk 205, WW84—Bowen, Blades, & Pettini 1995a), <2.5 ppb (Fairall 9, Magellanic Stream—Songaila & York 1981), and <3.7 ppb (NGC 3783, cloud WW187—West et al. 1985). Considering the large observed range for N(Na I) in low-velocity gas, these limits clearly are not very significant.

Detections of Na I at high velocity have been reported for some extreme-positive velocity gas, in all but one case for directions where no H I was detected: SN 1993J (Vladilo et al. 1993, 1994), SN 1994D and SN 1994I (Ho & Filippenko 1995, 1996) give A(Na I) > 20 to >800 ppb. In all these cases the rather large abundances and low value of N(H I) suggest that the gas is mostly ionized.

For the $+65$ km s^{-1} IVC toward the LMC, Na I abundances in directions with $N(\mathrm{H\ I}) > 5 \times 10^{18}$ cm^{-2} vary by a factor of more than 10 ($<$7–70 ppb; see Fig. 1*f*). The highest abundances ($>$70 ppb) occur for two directions with low N(H I) (Sk $-68°82$ and Sk $-71°03$—Songaila & York 1981 and Songaila, Cowie, & York 1981).

In the IV Arch Na I detections exist for cores IV6, IV21, and IV26, as well as in some off-core probes (Benjamin et al. 1996; Ryans et al. 1997a; Lehner et al. 1999a). Abundances range from 0.57 ppb to 6.1 ppb, i.e., inside the range typical for low-velocity gas (Fig. 1*h*). One higher value ($>$50 ppb for BD $+38°2182$, Ryans et al. 1997a) is associated with a low value for N(H I), in which case ionization issues may be important.

The two measurements in the LLIV Arch yield normal abundances of 2.4 and 4.2 ppb (SN 1993J—Vladilo et al. 1993, 1994, HD 77770—Welsh, Craig, & Roberts 1996).

Toward several stars in M13 that probe complex K, Shaw et al. (1996) determined N(H I) at 1′ resolution and found that Na I was not always detected toward stars with similar N(H I), giving limits $A < 5$ ppb, while the detections range from 13 ppb to 45 ppb.

Detections associated with complex gp toward eight stars in M15 yield abundances between 10 and 40 ppb (Morton & Blades 1986; Langer, Prosser, & Sneden 1990; Kennedy et al. 1998; Fig. 1*j*). Meyer & Lauroesch (1999) found a change from 10 to more than 160 ppb over several arcminutes in M15. These values were derived using N(H I) as measured at 9′.1 resolution and interpolated between nine beams placed at 5′ intervals. When probed in the sight line toward HD 203664, this IVC shows three absorption components with an average abundance of 77 ppb (Ryans, Sembach, & Keenan 1996). Finally, toward Mrk 509 $A(\mathrm{Na\ I}) = 10$ ppb (York et al. 1982).

Thus, for the IV and LLIV Arch, A(Na I) tends to be similar to that in low-velocity gas, whereas for the IVC toward the LMC and complex gp it is higher. Further, within a single cloud the measured abundance can vary by a factor of more than 10.

3.8.2. *Correlation between A*(Na I) *and N*(H I)

Figure 2*a* shows the correlation between A(Na I) and N(H I) for the high- and intermediate-velocity detections. The mostly horizontal straight line is the relation claimed by Ferlet, Vidal-Madjar, & Gry (1985b) for low-velocity H I (log $N(\mathrm{Na\ I}) = 1.04$ log N(H I)—9.09), while the dotted lines show the 1 σ spread in that relation (0.5 in the log). Note that this relation is supposed to correlate N(Na I) with the combined atomic and molecular column density, not just the neutral hydrogen column density. For HVCs and IVCs, $N(\mathrm{H_2})$ is relatively low, so $N(\mathrm{H}) \sim N(\mathrm{H\ I})$. This correlation is often used to infer N(H I) from a measurement of N(Na I). For instance, Ho & Filippenko (1995) stated that the Na I column density for the $+243$ km s^{-1} component seen in the spectrum of SN 1994D implies that N(H I) should be $\sim 6 \times 10^{19}$ cm^{-2}.

However, the N(Na I) versus N(H I) relation is not as well defined as it has been made out to be, and here it is shown to be invalid for the HVC/IVC gas. Also, Welty, Hobbs, & Kulkarni (1994, § 4.3) pointed out that below $N(\mathrm{H\ I}) = 10^{19}$ cm^{-2} the relation was defined from five points, three of which they showed to be inaccurate. Welty et al. (1994) also point out that Ferlet et al. 1985b) mixed Na I/H I ratios derived for individual components with velocity-integrated values, which is invalid if the abundance versus N(H) relation is not linear. Finally, the spread in the nominal relation is large: for any given value of N(Na I), the predicted value of N(H I) has a range of at least a factor 100.

In the case of the HVCs/IVCs, a direct observation of N(H I) toward SN 1994D shows that $N(\mathrm{H\ I}) < 2.5 \times 10^{18}$ cm^{-2} (Paper II), a factor 25 lower than would be inferred from N(Na I). For the HVC/IVC points in Figure 2*a* the formal fit shows a nonlinear correlation, but the 1 σ range of log N(Na I) at any given value of log N(H I) is ± 1, even larger than the ± 0.5 shown by Ferlet et al. (1985b) for low-velocity gas. Thus, for any given N(H I) there is a range of about a factor 100 in the Na I column density, rather than the factor 10 for low-velocity gas. In conclusion, for high- and intermediate-velocity gas N(Na I) is an even worse predictor of N(H I) than it is for low-velocity gas.

3.9. Ca II

3.9.1. Ca II *Abundances in HVCs*

The most important nondominant ion is Ca II. HVCs and IVCs have H I column densities in the range a few 10^{18} to 10^{20} cm^{-2}, and the Ca II abundance then tends to be 10–100 ppb, which corresponds to a logarithmic value for the product depletion $\times$ ionization (log δ) of -1.3 to -2.3. Ca II has been detected in many different clouds, HVCs as well as IVCs, often in multiple sight lines through the same cloud. It is therefore possible to check the constancy of its abundance across a cloud. So far, assuming constant Ca II abundance appears to be reasonable, although it may be even better to calculate a predicted value for A(Ca II) using the observed correlation between A(Ca II) and N(H I) (see Wakker & Mathis 2000). This correlation can also be seen in Figure 2*b*, which shows N(Ca II) versus N(H I).

Ca II is detected in the following HVCs: complex A (Mrk 106—Schwarz, Wakker, & van Woerden 1995; AD UMa—van Woerden et al. 1999a), complex C (Mrk 290 and PG 1351+640—Wakker et al. 1996a), cloud MIII (BD $+38°2182$—Ryans et al. 1997a), cloud IV4 (SN 1998S—Bowen et al. 2000), complex WB (PKS 0837$-$12—Robertson et al. 1991), the Magellanic Stream (Fairall 9—Songaila 1981, NGC 3783—West et al. 1985), and cloud WW219 (SN 1986G—d'Odorico et al. 1989). For eight components with $N(\mathrm{H\ I}) = 30\text{–}90 \times 10^{18}$ cm^{-2} six Ca II abundances are in the range 12–27 ppb, while a high value of 69 ppb is found toward NGC 3783 and a low value of 3.3 ± 0.9 ppb is found toward SN 1998S in IV4. The latter may be low because IV4 shows a disklike (i.e., more depleted) pattern, rather than the halo-like pattern seen in other HVCs (see § 4.2). The A(Ca II)–N(H I) correlation (Wakker & Mathis 2000) predicts a range of 8–18 ppb for the H I column densities in these components.

In five lower column density components (N(H I) $< 8 \times 10^{18}$ cm^{-2}) the values are higher, 110–290 pbb, where the A(Ca II)–N(H I) correlation predicts a range of 53–440 ppb for the observed H I column densities.

Within a single complex multiple determinations are within a factor 2.5 of each other (18/21 ppb in complex A, 21/12/18 ppb in complex C, 27/69 ppb in the Magellanic Stream). However, the H I column densities in these directions are also within a factor 2 of each other, so that the abundances are expected to be similar.

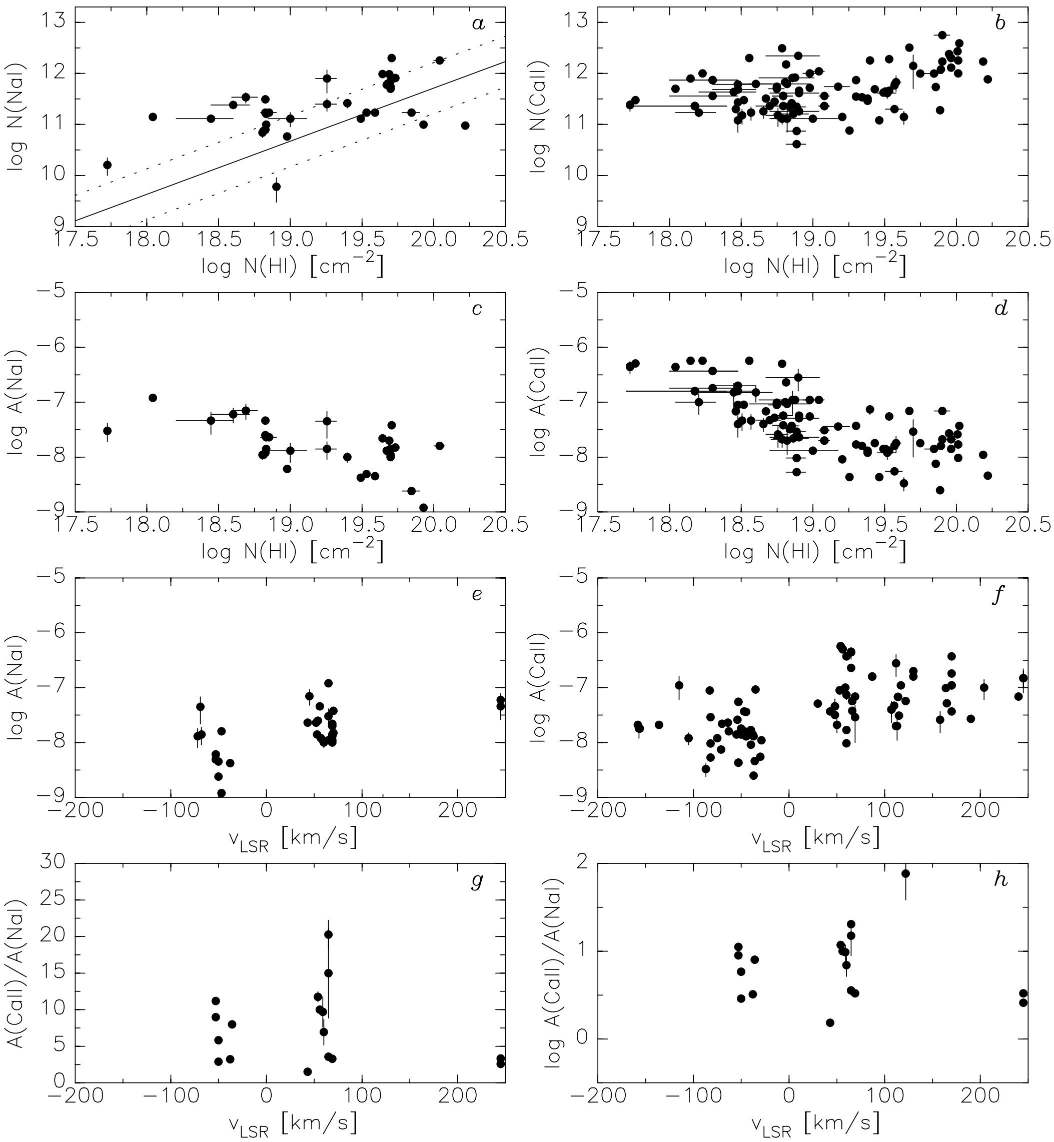

FIG. 2.—Correlations for Na I and Ca II. (*a*, *b*): log *N*(Na I) and log *N*(Ca II) vs. log *N*(H I). The straight line in panel (*a*) shows the relation claimed by Ferlet et al. (1985a, 1985b). The dotted line indicates the 1 σ spread in that relation. (*c*, *d*) log *A*(Na I) and log *A*(Ca II) vs. $v_{\rm LSR}$; *A*(Ca II) appears to be higher in positive-velocity clouds, but this may be biased by the fact that many of these directions have low *N*(H I). (*e*, *f*) ratio of *A*(Ca II) and *A*(Na I) vs. $v_{\rm LSR}$, showing that above $|v_{\rm LSR}| = 50$ km s^{-1} there is no obvious Routly-Spitzer effect.

Ca II absorption without associated high-velocity H I was seen toward four extragalactic supernovae (SN 1983N—d'Odorico, Pettini, & Ponz 1985; SN 1991T—Meyer & Roth 1991; SN 1993J—Vladilo et al. 1993, 1994; SN 1994D—King et al. 1995) and two stars (BD $+38°2182$—Keenan et al. 1995 and HD 83206—Lehner et al. 1999a). Note that Lehner et al. (2001) conclude that the absorptions toward HD 83206 actually are stellar S I linesThis sets lower limits to *A*(Ca II) of >27 to >500 ppb. In all cases, the H I column density must be very low ($<$few 10^{18} cm^{-2}), so the limit on the abundance is below (and thus consistent with) the value predicted from the *A*(Ca II)–*N*(H I) relation that is discussed by Wakker & Mathis (2000).

3.9.2. Ca II *Abundances in HVCs/IVCs toward the LMC*

Many detections exist toward the HVCs/IVC toward the LMC. If the H I column densities toward the background stars were more reliable, this cloud would provide an ideal testing ground to look for abundance variations. However, many H I column densities are interpolated between three directions (see item PI in the description of col. [10]), or based on using a ruler on the plots of Wayte (1990) (item PR). Still, some patterns do emerge, see Figs. 1*g*, 1*h*, and 1*i*). Excluding two discrepant values from Songaila et al. (1981), in the two HVCs (at $+165$, and $+120$ km s^{-1}) the abundance range is about a factor 5 (26–110 ppb and 20–100 ppb, respectively), when *N*(H I) $> 4.5 \times 10^{18}$ cm^{-2}, while for sight lines with lower *N*(H I) the typical abundances are higher (180–370 ppb and 160–1300 ppb, respectively). The pattern in the IVC is similar, but with higher values. *A*(Ca II) ranges from 31 to 230 ppb for *N*(H I) $> 4.5 \times 10^{18}$ cm^{-2}, with two outliers at 400 and 480 ppb [both have interpolated *N*(H I)], and from 80 to 430 ppb at lower *N*(H I). This cloud shows an unusual depletion pattern for all the other elements (see Welty et al. 1999), which may indicate that unusual processes are going on.

3.9.3. Ca II *Abundances in IVCs*

Many detections exist in the IV Arch (Fig. 1*c*) (Wesselius & Fejes 1973; Albert 1983; Songaila et al. 1985, 1988; Spitzer & Fitzpatrick 1993; Albert et al. 1993; Schwarz et al. 1995; Wakker et al. 1996b; Ryans et al. 1997a; Lehner et al. 1999a; Ryans et al. 1999; van Woerden et al. 1999b; Bowen et al. 2000).

Within a single core some variations exist: 16/26 ppb in IV17, 13/37 ppb in IV19, 4.6/11 ppb in IV26. Between cores the variations are larger: 30 ppb in IV6, 23 ppb in IV7, 7.5 ppb in IV9. Outside cores the range is 8–55 ppb. Clearly, variations are about a factor 5. However, this relatively small range may be an artifact of the small range in *N*(H I), as for 15 out of 19 cases the observed value is within a factor 3 of the value predicted by the *A*(Ca II)–*N*(H I) relation discussed by Wakker & Mathis (2000). One of the exceptions is BD $+49°2137$ where two Ca II components are seen, but only one H I component can be measured.

Abundances in the LLIV Arch have been measured toward eight different background probes (Fig. 1*b*) (Vladilo et al. 1993, 1994; Welsh et al. 1996; Ryans et al. 1997b; Lehner et al. 1999a), and tend to lie in the narrow range of 12–17 ppb (with two outliers at 9 and 2.5 ppb; for the latter the derived H I column density is probably affected by the spectral decomposition). Thus, variations appear to be very small, and on average the value is lower than in other clouds. This is consistent with the warm-disk–like depletion pattern for this object (§ 4.26). The values predicted from the *A*(Ca II)–*N*(H I) relation discussed in § 3.6 lie in the range 9–26 ppb, i.e., the low Ca II abundance may also be due to the relatively high H I column densities seen in the LLIV Arch.

A cloud where future work will allow a study of small-scale variations in *A*(Ca II) is complex gp (see § 4.29), which is probed by the globular cluster M15 (Fig. 1*e*). Meyer & Lauroesch (1999) found that toward M15 the Na I abundance varies from 10 to 160 ppb (i.e., a factor 16) on a scale of a few arcsec. Lehner et al. (1999b) measured *N*(Ca II) toward 12 stars but did not provide a detailed H I map. *N*(H I) was measured at nine positions with Effelsberg and interpolated to the stellar positions. This results in abundances of 20–55 ppb. The same IVC is also seen toward Mrk 509 [*A*(Ca II) = 74 ppb; York et al. 1982] and toward HD 203664, where *N*(H I) is very low (2.2×10^{18} cm^{-2}), and the Ca II abundance is correspondingly high (440 ppb; Ryans et al. 1996). The *A*(Ca II)–*N*(H I) relation (Wakker & Mathis 2000) predicts values that are a factor ~ 3 lower, i.e., the Ca II abundance in complex gp is relatively high compared to expectations.

3.9.4. *Correlations between N*(Na I), *N*(Ca II) *and Velocity*

For the IVCs and HVCs no evidence exists for a correlation between velocity and Na I (or Ca II) column density (Figs. 2*c* and 2*d*). For low-velocity gas, Routly & Spitzer (1952) found that the column density ratio *N*(Ca II)/*N*(Na I) increases with LSR velocity. Vallerga et al. (1993) show that the effect occurs when studying nearby (<100 pc), low-velocity (<20 km s^{-1}) gas, while Sembach & Danks (1994) find a correlation of this ratio with the deviation velocity (the difference between the observed LSR velocity and the maximum velocity that is expected from a simple model of galactic rotation), but only for gas with LSR velocities below 50 km s^{-1}. This effect is usually interpreted as showing that Ca is less depleted at higher peculiar velocities. Figures 2*e* and 2*f* show that the Ca II/Na I column density ratio does not depend on velocity for sight lines through IVCs and HVCs. This is not entirely unexpected since for the HVCs/IVCs the LSR velocity is not a good measure of the peculiar velocity relative to their surroundings. Further, it should be noted that components at higher velocity tend to have lower column density. Wakker & Mathis (2000) showed that on average the abundance of Na I is independent of *N*(H I), whereas *A*(Ca II) is larger at lower *N*(H I). Thus, the Ca II/Na I ratio depends on *N*(H I), which tends to be lower at higher velocity.

3.9.5. *Implications of the* Na I *and* Ca II *Results*

Na I varies by a factor of more than 10 within clouds and by an even larger factor between clouds. Ca II also shows a large range (a factor >100), although at any given H I column density the range is more like a factor 10), and within any given cloud the range is a factor up to ~ 5.

These results can be used to derive a safety factor for interpreting the significance of a nondetection of Na I or Ca II. This is discussed in more detail in the Appendix, under the description of column (18). In summary, H I small-scale structure requires a safety factor ~ 2. For both Na I and Ca II the depletion is uncertain by a factor ~ 2.5. The ionization is uncertain by a factor ~ 2 for Ca II, ~ 5 for Na I. Finally, if the ion abundance in the cloud has to be assumed (rather than being measured toward another probe), a final factor ~ 2 is needed.

Thus, in practice nondetections of Na I never result in a lower limit to a cloud distance, as the combined safety factor needs to be 25–50. Since at an abundance of 4.6 ppb τ(Na I D2) is 0.022 (*N*(H I)/10^{19}), a significant nondetection requires a spectrum with S/N > 1000–2000 [10^{19}/*N*(H I)]. Thus, although Na I tends to be the easiest interstellar line to observe, it is hard to determine upper limits to HVC/IVC distances and not useful for determining lower limits. None of the published nondetections can be considered to give a significant lower distance limit.

Ca II gives much stronger absorption than Na I (τ(Ca II K) is 0.13 (*N*(H I)/10^{19}) for a standard abundance of 22 ppb). Thus, a spectrum with S/N > 75–100 [10^{19}/*N*(H I)] can yield a lower distance limit. However, it remains necessary to derive *A*(Ca II) for any given cloud. Also, such S/N ratios are difficult to achieve for the more distant, fainter stars that will be needed to derive distances to HVCs.

3.10. *Highly Ionized Species*

For the high-ionization ions (C IV, N V, Si IV), the results of Sembach & Savage (1992) were used to provide fiducial values for the column density. They found that, on average, *N*(C IV) = 1.6×10^{14} cm^{-2} toward the Galactic pole. Averages for the other ions follow from the average ratios they give, yielding 3.5×10^{13} cm^{-2} for N V, and 4.4×10^{13} cm^{-2} for Si IV.

Preliminary results for halo O VI were presented by Savage et al. (2000b), showing column densities in the range $1–7 \times 10^{14}$ cm^{-2}. The polar value (the average of N sin *b*) is about 2×10^{14} cm^{-2}.

C IV.—High-velocity C IV is observed in the Outer Arm (H 1821+643—Savage, Sembach, & Lu 1995), complex GCN (Mrk 509 and PKS 2155−304—Bruhweiler et al. 1993; Sembach et al. 1999), in the +65 and +120 km s^{-1} IVCs toward the LMC (Savage & Jeske 1981; Savage et al. 1989; Bomans et al. 1996), IV6 (HD 93521—Spitzer & Fitzpatrick 1992), IV9/IV19 (HD 121800—Howk et al. 2001), LLIV1 (SN 1993J—de Boer et al. 1993), and the PP Arch (HD 215733—Fitzpatrick & Spitzer 1997). The more reliable determinations have column densities in the range 2.4–6.0 $\times$ 10^{13} cm^{-2}, i.e., a factor 3–6 below the typical value though the Galactic halo. Higher values exist toward Mrk 509 ($>1.6 \times 10^{14}$ cm^{-2}) and SN 1993J ($>2 \times 10^{14}$ cm^{-2}).

N V.—N V was observed but not detected toward five AGNs with high-velocity gas in the sight line (H 1821+643—Savage et al. 1995; Fairall 9—Lu et al. 1994b; NGC 3783—Lu et al. 1994a; Mrk 509 and PKS 2155−304—Sembach et al. 1999), although the upper limits are only 1–5 $\times$ 10^{13} cm^{-2}, i.e., comparable to the total amount through the Galactic halo. A small amount of high-velocity N V was found in complex WE, toward HD 156359, with a column density of 5.8 $\times$ 10^{12} cm^{-2} (Sembach, Savage, & Lu 1995a).

O VI.—Sembach et al. (2000) found high-velocity O VI absorption associated with complex C (Mrk 876), complex GCN (toward Mrk 509 and PKS 2155−304), the Magellanic Stream (three sight lines) and the Outer Arm (H 1821+643), with column densities that are a significant fraction of the total O VI column density in these directions. Note: Further study with *FUSE* shows high-velocity O VI in $\sim$50 out of 100 observed sight lines, associated with both complex C and the Magellanic Stream, as well as away from directions with high-velocity H I.

Si IV.—High-velocity Si IV was found toward Mrk 509 (Sembach et al. 1999) and SN 1993J (de Boer et al. 1993) with column densities of $\sim$2.5 $\times$ 10^{13} cm^{-2}. Intermediate-velocity Si IV has been detected toward IV6 (HD 93521—Spitzer & Fitzpatrick 1992), LLIV1 (SN 1993J—de Boer et al. 1993), the PP Arch (HD 215733—Fitzpatrick & Spitzer 1997), and the +65 and +120 km s^{-1} HVC toward the LMC (Savage & Jeske 1981; Savage et al. 1989). The measured column densities range from 5.9 to 82 $\times$ 10^{12} cm^{-2}, where for low-velocity gas values between 50 and 100 $\times$ 10^{12} cm^{-2} are typical for the galactic latitude range of the probes.

4. NOTES ON INDIVIDUAL CLOUDS

In this section, some remarks are made concerning the metallicity and distance determinations for each listed cloud. For about half the clouds a map is presented that shows the positions of the probes relative to the H I. Further, for 18 clouds the pattern of abundances is plotted in Figure 3, where it is compared to the standard patterns for cool disk, warm disk and halo gas.

An estimated mass range is given for most of the clouds, using the observed distance range. For the HVCs the mass is based on the integrated flux measured by Hulsbosch & Wakker (1988). The flux, S, is converted to an H I mass ($M_{\rm HI} = 0.236$ (S/Jy km s^{-1}) (D/1 kpc)^2 $M_\odot$. In the case of IVCs, a column density map is made using the LDS survey, and this is summed over an irregular region outlining the cloud. Since each beam represents an area $A = 7.25 \times 10^{38}$ cm^2 at a distance of 1 kpc, the sum is multiplied by $Am_{\rm H}/M_\odot$ to obtain the cloud mass at a distance of 1 kpc. In both cases, a (hopefully typical) factor 1.2 is included to account for ionized hydrogen, and a factor 1.39 is included to account for helium.

4.1. *Complex A*

This is the only HVC for which a distance bracket is known: 4.0–9.9 kpc, which implies a mass of 0.3–2 $\times$ 10^6 $M_\odot$. Figure 4 shows the velocity field and probe positions. The bracket is based on the stars AD UMa (van Woerden et al. 1999a) and PG 0859+593 (Wakker et al. 1996a). The nondetection of Ca II in PG 0832+675 (d = 8.1 kpc) is not significant, the limit being only a factor 2 below the value measured toward Mrk 106 and AD UMa. Note: The *FUSE* spectrum of PG 0832+675 yields a significant nondetection for C II, O I, and Fe II.

Welsh et al. (1996) did not detect Ca II and Na I toward three stars (HD 77770, HD 75755, and HD 68164), and claimed to derive a lower limit of 1 kpc from this result. However, this provides a clear example of the difficulties of interpreting nondetections, as all their limits are similar to the values observed in more distant targets. They are thus not significant in terms of setting a lower distance limit.

The metallicity of complex A has not yet been determined, due to a lack of known UV-bright background probes. O I λ1302 and Si II λ1304 associated with complex A were seen in the spectrum of I Zw 18 by Kunth et al. (1994). The low flux of that galaxy makes the measured equivalent widths of 310 $\pm$ 100 mÅ and 110 $\pm$ 75 mÅ rather uncertain. The derived abundances of course depend on the assumed line width and component structure. The most likely case is that the absorption width is comparable to the H I line width of 53 km s^{-1}. Then the O I abundance is $0.06^{+0.07}_{-0.03}$ times solar. If a two-component structure is assumed, with two equal lines with the same intrinsic width, the derived O I abundance is $0.09^{+0.3}_{-0.06}$ solar (for widths of 20 km s^{-1}) to $0.05^{+0.05}_{-0.02}$ solar (for widths of 30 km s^{-1}). Thus, for reasonable assumptions, the implied O I abundance of complex A is most likely to be on the order of 0.05–0.1 solar, though the uncertainty is large.

Combined with the Mg II and Ca II abundances, a halo-like depletion pattern is suggested for complex A (Fig. 3*a*). It is clear, however, that better measurements at higher angular and spectral resolution are needed to confirm this.

4.2. *Complex M*

Complex M consists of several clouds. These have similar velocities but they are not connected. Whether these clouds are spatially close or only close in position on the sky is an open question, though the former seems most likely. The different clouds in the complex are discussed separately below. Figure 5 shows the positions of the probe stars.

Cloud MI has the most negative velocities (< -100 km s^{-1}), and lies at longitudes $l > 150°$; it was also classified as IV2 by Kuntz & Danly (1996). The Ca II nondetections in Schwarz et al. (1995) turn out to be not significant, so no distance limits are known. Its mass is 4 $\times$ 10^3 (D/1 kpc)^2 $M_\odot$.

Tufte et al. (1998) observed Hα and [S II]λ6716 emission associated with cloud MI (see Wakker & van Woerden 1991), in the direction of the brightest H I emission in cloud MI. So far, this is the only observation of [S II] emission in a HVC or IVC. The observed [S II]/Hα ratio is 0.64 $\pm$ 0.14. This can be used to constrain the metallicity of cloud MI. To do this three assumptions are needed: (a) what is the geometry? (b) what is the temperature? and (c) what is the fraction of S^{+2}? It is most likely that toward the bright H I core the cloud has a neutral core surrounded by a fully

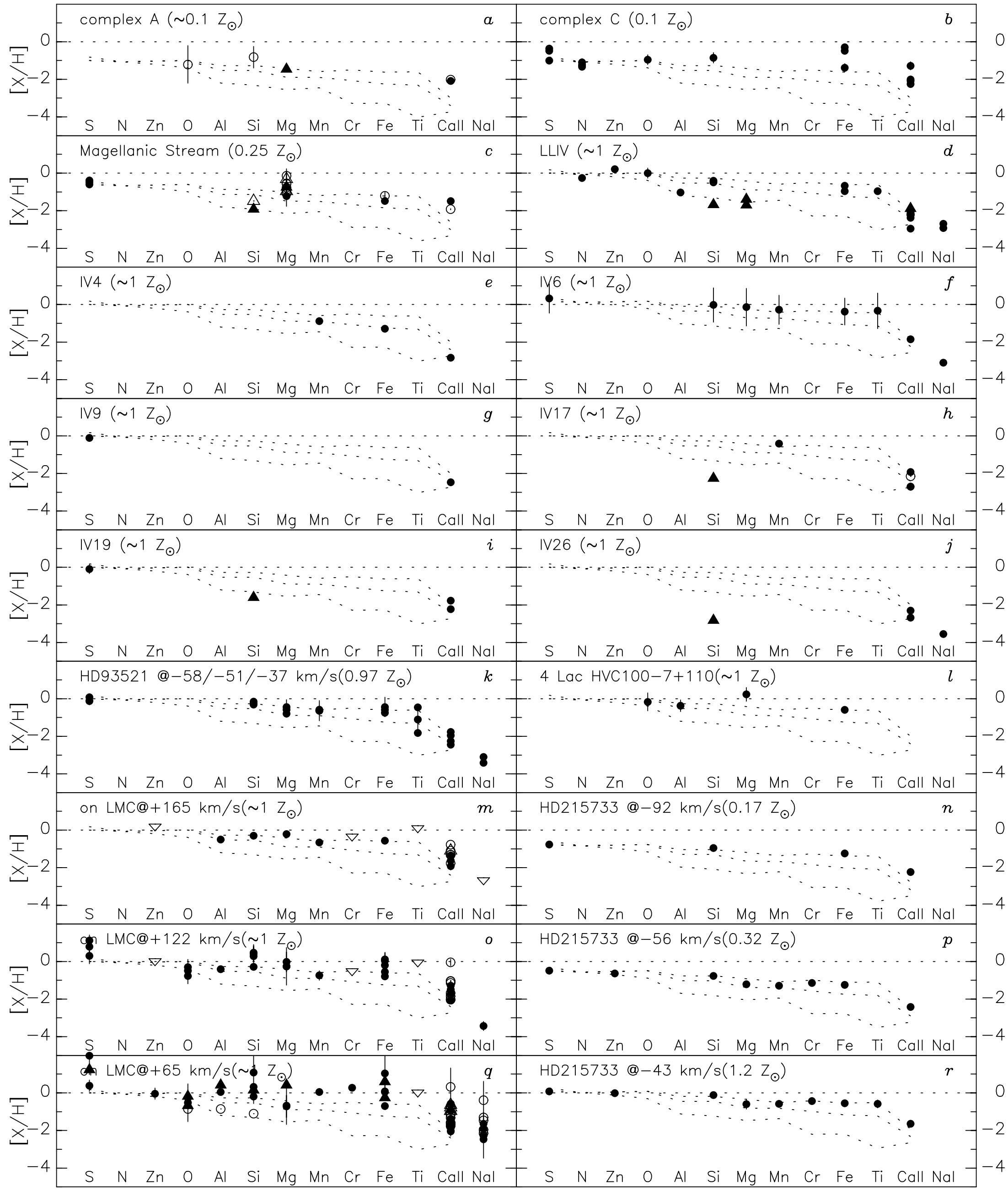

FIG. 3.—Abundance [i.e., N(ion)/N(H I)] patterns in 18 selected HVCs/IVCs where multiple elements have been measured. The elements are ordered in terms of decreasing reference abundance in halo gas. The dotted lines shows the patterns for cool disk, warm disk, and halo gas (Savage & Sembach 1996a), shifted by the overall metallicity. The latter is given in parentheses after the cloud name and is derived from the results for undepleted elements. Note that the halo pattern was *derived* from the IVCs in the direction of HD 93521 and HD 215733. Error bars are usually smaller than the size of the dots. Closed circles show good measurements. Open circles indicate only the equivalent width was published. Downward-pointing open triangles indicate an upper limit. Upward-pointing closed triangles indicate lower limits.

ionized envelope. A temperature in the range 6000–10,000 K is suggested by the systematic study of Hα and [S II] emission at heights up to 1 kpc above the Perseus arm (Haffner et al. 1999). They also find that $N(S^{+2})/N(S^{+})$ lies in the range 0.3–0.7. With this range of parameters, the S^{+} abundance of cloud MI has a most likely value of $\sim$0.8 solar but is only restricted to lie in the range 0.4–1.8 times solar. That is, a metallicity of $\sim$0.1 solar such as that found for complex C (see § 4.3) is excluded, and the most likely value is consistent with the idea that complex M is part of the IV Arch, for which near solar metallicity has been found (see § 4.24).

Toward lower longitudes, the velocity of MI changes to ~ -80 km s^{-1}. This part was classified as IV4 by Kuntz & Danly (1996) and is probably part of the IV Arch (see § 4.24). Behind IV4 lies SN 1998S, which was observed by Bowen et al. (2000). The Ca II, Mn II, and Fe II abundances (3.3, 44, and 1600 ppb) are more like those in warm disk gas (6.9, 42, and 1800 ppb) than like in halo gas (69, 87, and 7800 ppb) (see also Fig. 3*e*). The same can be said for the

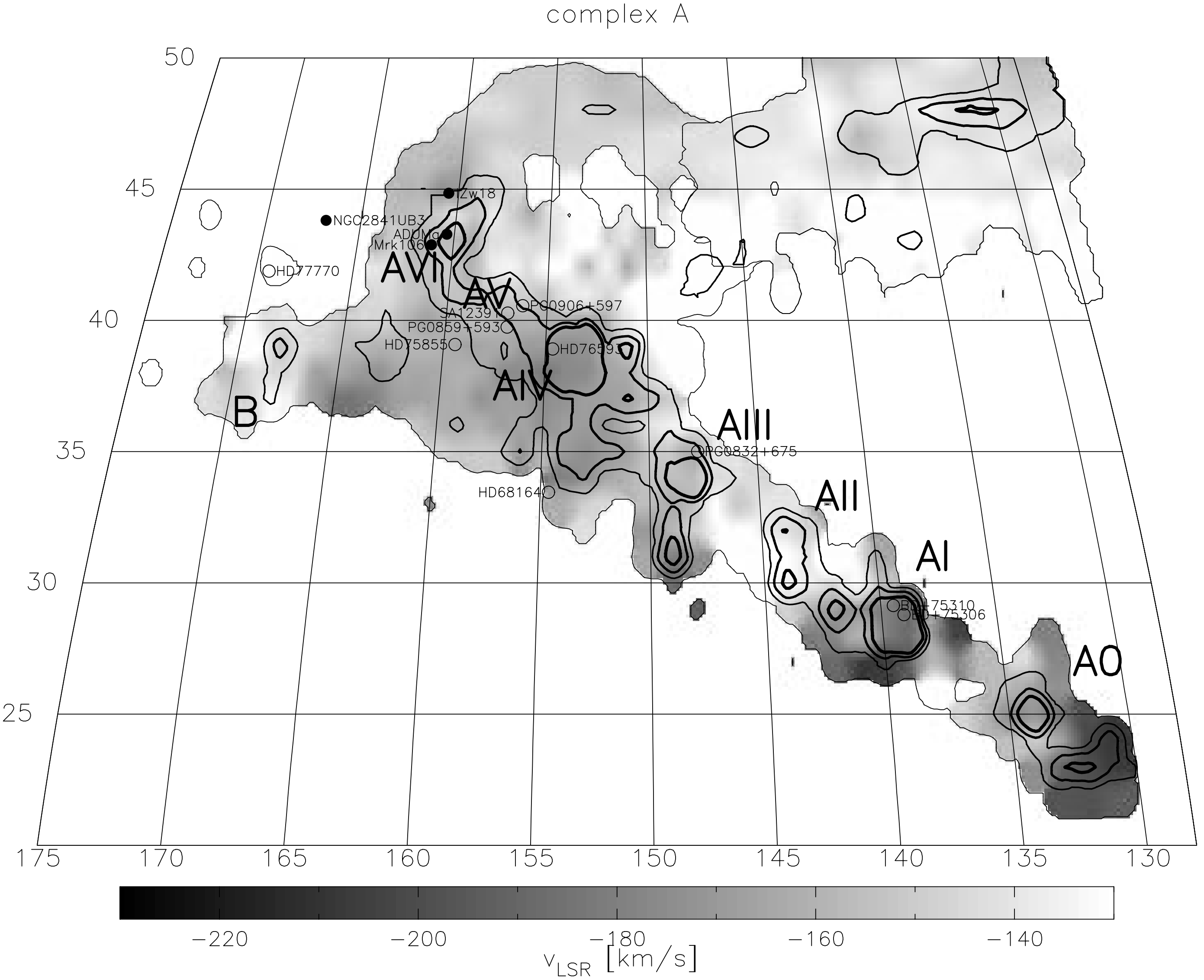

FIG. 4.—Map of HVC complex A, from Hulsbosch & Wakker (1988). Contours indicate brightness temperature levels of 0.05, 0.3, 0.6, and 1 K. The gray scale shows velocities, as identified by the wedge. The core names are shown, as are the positions of probe stars. Closed symbols refer to detections, open symbols to nondetections. The structure in the upper right corner is HVC complex C.

abundance ratios (e.g., Ca II/Mn II = 0.08 in IV4, 0.16 in warm gas, and 0.79 in halo gas). Such abundances are consistent with the small distance of 0.6–0.8 kpc (z = 0.5–0.7 kpc) that can be derived by combining the detection of Si II toward BD +49°2137 with the nondetection of Si II toward HD 106420 (Kuntz & Danly 1996). Ryans et al. (1997a) did not detect Ca II toward BD +49°2137 nor toward PG 1213+456 (at 2.9 kpc), but the limits of <2.1 and <50 ppb are not inconsistent with the value of 3.3 ± 0.9 ppb found toward SN 1998S. Note also that the distance of BD +49°2137 was revised from 1.8 kpc (Kuntz & Danly 1996) to 0.8 kpc by Ryans et al. (1997a). It remains to be seen whether this distance bracket applies to the higher velocity part of cloud MI. The mass of IV4 is constrained to the range 1.5–2.5 × 10^3 $M_\odot$.

In the gap between clouds MII and MIII lie BD +38°2182 and HD 93521, which are just 3′ apart, C II, O I, Si II, and Ca II absorption at the velocity of MIII are clearly seen toward BD +38°2182, and clearly absent toward HD 93521 (Danly, Albert, & Kuntz 1993). Taking the distance to BD +38°2182 from Ryans et al. (1997a), this sets an upper limit on the distance of MII/MIII of 4.0 kpc and an upper limit on the mass of 6 × 10^4 $M_\odot$. However, no strong lower limit can be derived from HD 93521, as a 12′ beam H I spectrum shows no emission at the velocity of the absorption toward either star, down to a 5 σ limit of 0.5 × 10^{18} cm^{-2} (Ryans et al. 1997a). If H^+ were present, no O I absorption is expected, but C II and Si II should still be seen. It remains unclear whether the high-velocity absorption toward HD 93521 is absent because the cloud is behind the star or because there is no high-velocity material in the sight line. The position in the sky of MII/MIII and their velocity strongly suggest that these clouds are part of the IV Arch. A lower distance limit of 1.9 kpc would then be at odds with the other distance brackets derived for the IV Arch (see § 4.24).

Ryans et al. (1997b) and Lehner et al. (1999a) reported Ca II absorption at a velocity of −108 km s^{-1} in the spec-

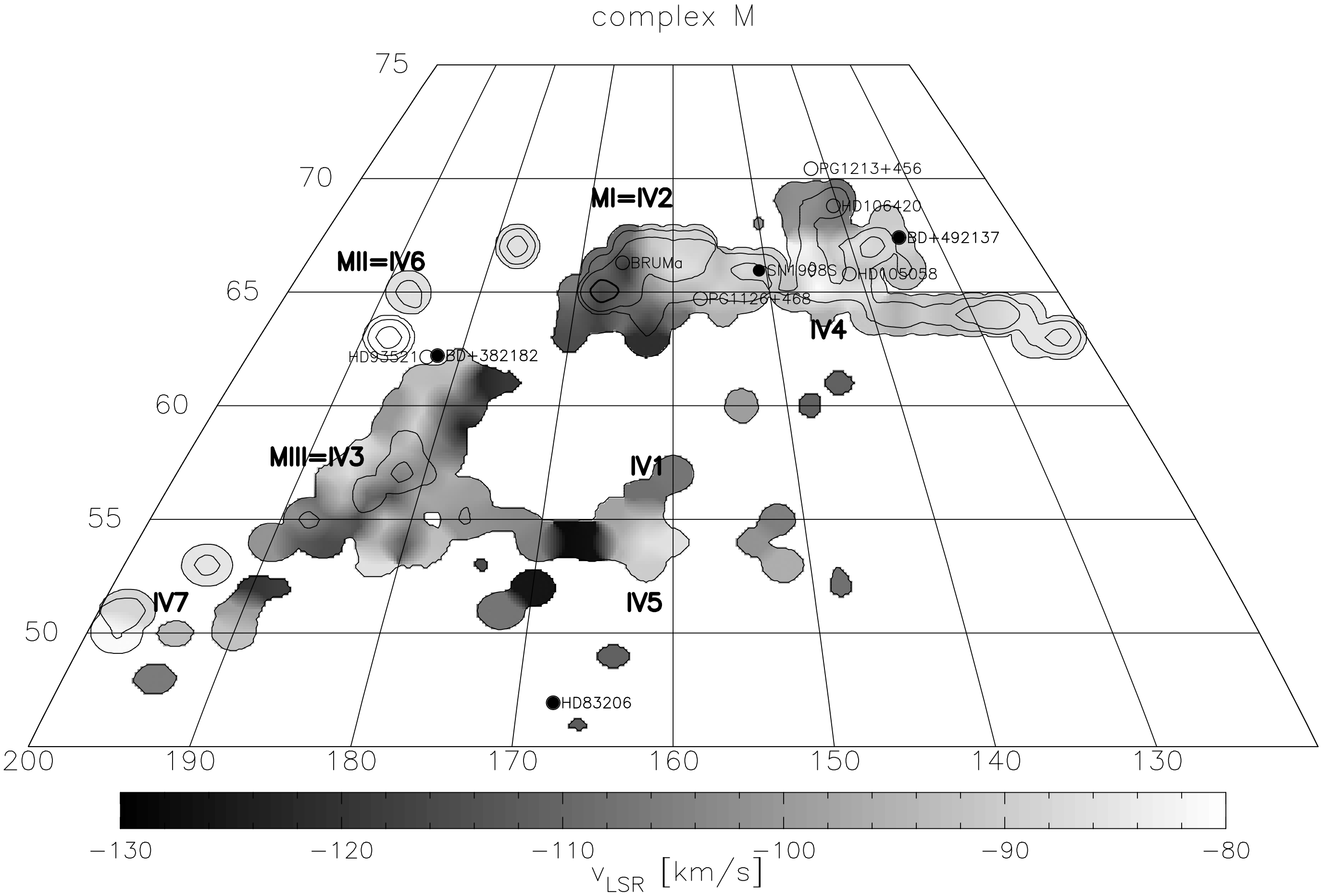

FIG. 5.—Map of HVC complex M, from Hulsbosch & Wakker (1988). Contours indicate brightness temperature levels of 0.05, 0.3, 0.8, and 2.5 K. The gray scale shows velocities, as identified by the wedge. The core names are shown, as defined by Wakker & van Woerden (1991) and Kuntz & Danly (1996). Closed symbols refer to detections, open symbols to nondetections.

trum of HD 83206. No H I is seen at this velocity down to a limit of 2×10^{18} cm^{-2}. The nearest H I cloud with similar velocity in the HVC survey of Hulsbosch & Wakker (1988) is 1°.5 away (cloud WW63; $v_{\rm LSR} = -112$ km s^{-1}; $l = 166°$, $b = 46°$), although this faint cloud cannot be discerned in the Leiden-Dwingeloo Survey. Just north of this position are the southernmost clouds of complex M (specifically WW51 and WW39, as well as some uncataloged clouds, all with velocities ~ -120 to ~ -100 km s^{-1}). Lehner et al. (2001) revisit these lines and conclude that they are stellar S II.

4.3. *Complex C*

Since complex C covers a large area of the sky (1600 square degrees), and since it contains a number of well-defined cores, it was split into five parts in Table 2. CI-A,B,C and CIII-A,B,C were defined by Giovanelli, Verschuur, & Cram (1973). "C-south" refers to the lower latitude part of C at longitudes greater than 80° (for a precise specification see Note 30). The core at $l = 68°$, $b = 38°$ ("CeI") was previously named "C-extension" by Giovanelli et al. (1973). Here cores CeI through CeV are defined by analogy. Complex D was defined by Wakker & van Woerden (1991); core "CD" within complex C is defined here as the core at $l = 90°$, $b = 34°$, $v_{\rm LSR} < -150$ km s^{-1}, which is close to complex D and has similarly high-negative velocities. Finally, core C/K is defined as the core at $l = 75°$, $b = 37°$, $v_{\rm LSR} \sim -90$ km s^{-1}, which lies close in angle and velocity to IVC complex K and may be part of that complex, rather than a core of complex C. A detailed analysis of the spectra in this region is called for.

The distance to HVC complex C is not well known. Ca II absorption was measured toward Mrk 290 and PG 1351+640, so that good abundance comparisons can be made for distance-determination purposes. However, toward both of these the component structure is slightly complicated. A best-guess fit yields two components toward Mrk 290 with Ca II abundances of 12 ± 3 and 22 ± 1 ppb, while toward PG 1351+640 abundances of 18 ± 2 and 110 ± 50 ppb are found. The last value is for a low-column density component with uncertain N(H I), and thus the fact that it differs from the other three is probably not significant.

Figure 6 shows the positions of the probes. Most observations of stellar probes lead to a nondetection but do not give significant distance information, usually because N(H I) is small. Most of the few significant nondetections are toward rather nearby stars, giving a strong lower distance limit of 1.2 kpc. Limits were set on A(Ca II) for seven distant (>3 kpc) stars. However, only one of these is significant (BS

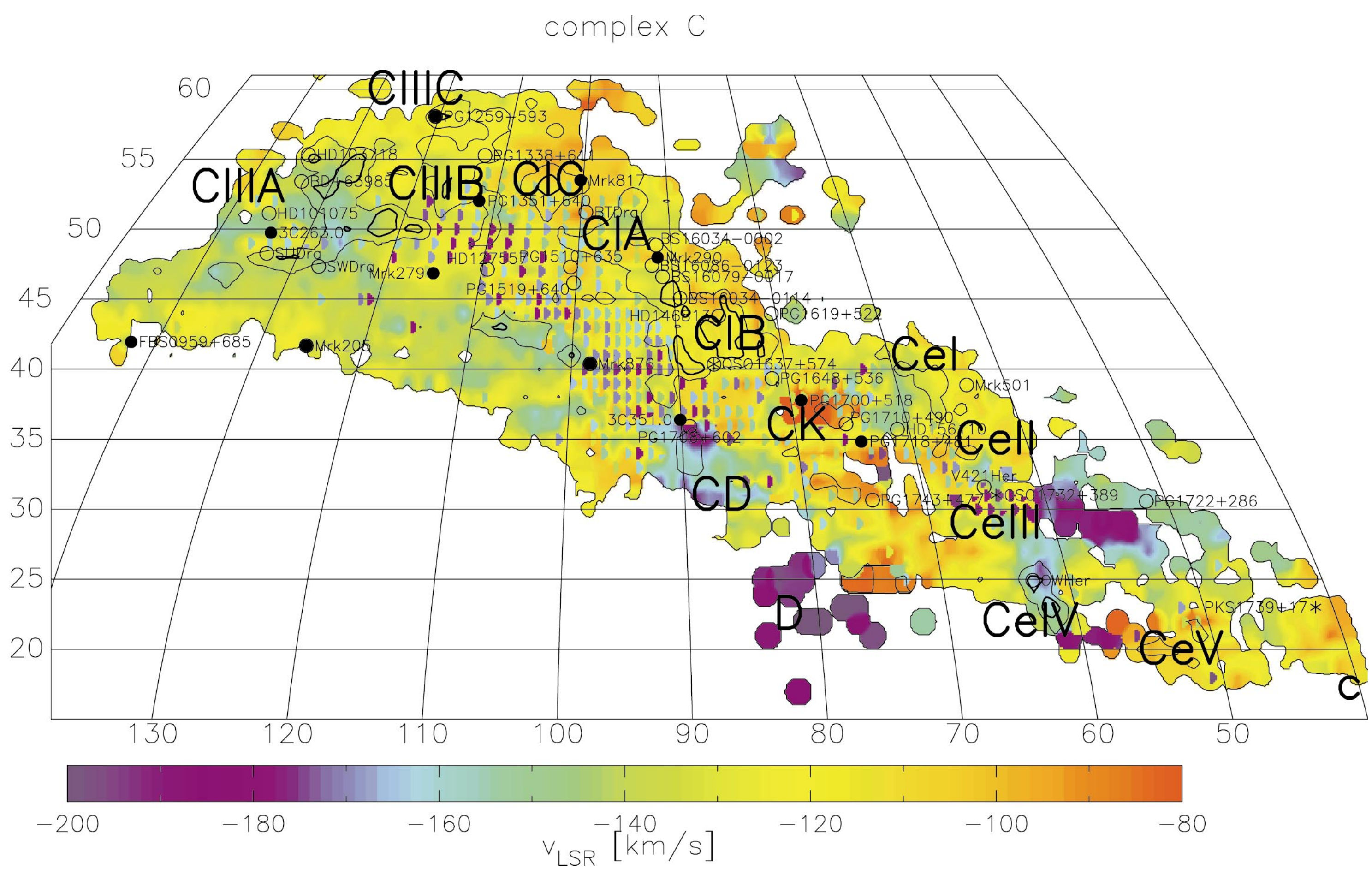

FIG. 6.—Map of HVC complex C, from Hulsbosch & Wakker (1988). Contours indicate brightness temperature levels of 0.05, 0.4, and 1.0 K. Colors indicate velocities, as identified by the wedge. At many positions along the central ridge emission is seen at two velocities. In these directions a half-circle is shown for the second component. Core names are also given, as are the positions of probe stars. CI-A, B and CIII-A, B were defined by Giovanelli et al. (1973), as was CeI, which they named C-extension. CeII–V are defined here by analogy. Giovanelli et al. (1973) also define a core CIIIC, which is named CIC here, while CIIIC is used for a core not observed by Giovanelli et al. (1973). Complex D was defined by Wakker & van Woerden (1991), core "CD" is defined here, as is core "C/K" (see text). Closed symbols refer to detections, open symbols to nondetections.

16034−0114 at 6.1 kpc), although a better analysis of these spectra is still needed. For BS 16034−0114 the ratio (expected)/(observed) is ∼10, which thus yields a (weak) lower limit of 6.1 kpc to the distance of core CIA. The strong lower distance limit gives a mass for complex C of more than $10^5\ M_\odot$, but the probable lower limit of 6.1 kpc yields $M > 3 \times 10^6\ M_\odot$.

Complex C is the only cloud for which several different metallicity measurements have been made, although in all cases there are some special considerations or special problems to be solved. S II λ1250 and/or 1253 and/or 1259 have been measured toward three AGNs projected onto complex C: Mrk 290 (Wakker et al. 1999b) and Mrk 817, Mrk 279 (Gibson et al. 2001). N I was measured toward Mrk 876 (Gibson et al. 2001; Murphy et al. 2000) and PG 1259+593 (Richter et al. 2001b), while O I/H I has been measured toward PG 1259+593 (Richter et al. 2001b).

The best determination is the one using Mrk 290, where N(H I) is measured at 2′ resolution and Hα was detected. The result is $N(\mathrm{S})/N(\mathrm{H}) = 0.09 \pm 0.02$ times solar, with a small dependence on the assumed distance and geometry. The measurement toward Mrk 817 yields $N(\mathrm{S\ II})/N(\mathrm{H\ I}) = 0.33 \pm 0.02$ solar, while that toward Mrk 279 gives 0.43 ± 0.10 solar. In both cases the (unknown) ionization correction may be high, as N(H I) in these directions is much lower than toward Mrk 290, whereas $N(\mathrm{H}^+)$ is expected to be more or less constant if the hydrogen is photoionized. High-resolution H I maps are also imperative to understand the difference between the Mrk 290 and Mrk 817/279 sight lines.

One other sight line with high N(H I) has been studied: PG 1259+593 (Richter et al. 2001b). Here O I/H I = $0.11^{+0.13}_{-0.08}$ solar. Richter et al. (2001b) also find that N I/H I = < 0.046 solar, as well as Si II/O I ∼ 1, but Fe II/O I ∼ 0.4. No H_2 was detected (fraction $<10^{-5}$), but this is not unexpected considering the relatively low total hydrogen column density and the relatively small amount of dust expected to go with the low metallicity. If there is no or little dust, the N I, O I, Si II, and Fe II abundances are consistent with an enhancement in the α elements (Si/O > 1), combined with a relatively low amount in the iron peak elements (Fe/O < 1) and no secondary nitrogen (N/O < 0.5). This is consistent with the idea that the heavy elements in complex C were created in Type II supernovae and that there has been no subsequent star formation.

The sight line toward Mrk 876 was analyzed by Murphy et al. (2000). It shows unusual abundances. Nominally undepleted elements have low abundances relative to H I [A(N I) ∼ 0.08 solar, A(P II) < 0.8, A(Ar I) < 0.1 solar], consistent with the values found using the other probes. However, the usually depleted Fe II has a high abundance [A(Fe II) = 0.5]. The probable interpretation in this case is that in the region around the sight line toward Mrk 876 the gas is partially photoionized throughout by a soft radiation field, so that H I is a ∼25% contaminant. Then Ar and N can become overionized relative to H, unlike Fe, which remains in the form of Fe II (Sofia & Jenkins 1998).

Nevertheless, the maximum ionization correction consistent with the absorption line and Hα data in the direction of Mrk 876 seems to be on the order of a factor 3–5. Since S/H = 0.1, this implies Fe/S ∼ 1–2. Such a ratio is very unlike the typical ratio of 0.2 seen in halo gas (Sembach & Savage 1996) or in other HVCs and IVCs (this paper). The implication is that complex C appears to have low dust content. This is further supported by the Si II/O I and Fe II/O I ratio toward PG 1259+593 (Richter et al. 2001b).

From the results described above, it has become clear that in order to derive reliable abundances and abundance ratios, it will be necessary to observe Hα emission for every probe, to pay close attention to ionization corrections and unusual circumstances, and to combine the absorption and emission data with modeling.

4.4. *Complex G*

This HVC has velocities that deviate only slightly from those allowed by differential galactic rotation, especially at the lowest latitudes. A better definition is needed. The nondetections of several elements with strong lines in the spectrum of 4 Lac are not commented upon by Bates et al. (1990), but they do set a (not unsurprising) lower limit of 1.3 kpc, and thus a mass limit of more than $5 \times 10^4\ M_\odot$.

4.5. *Complex H*

This HVC complex lies in the Galactic plane, which allows the use of luminous O and B stars as probes. So far, only a lower distance limit has been set, using the nondetection of Mg II, C II, and O I in *IUE* spectra (Wakker et al. 1998). Centurión et al. (1994) did not see Ca II absorption in seven stars projected onto complex H, but only one of the nondetections can be considered significant (assuming complex H has a Ca II abundance similar to that seen in other HVCs).

Figure 7 shows the positions of the probes. The HVC can be subdivided into several parts, although these are probably all spatially connected, as there are no clear boundaries. The distance limit for the brightest, central, core is $d > 5$ kpc, which implies a mass for the whole complex of more than $10^6\ M_\odot$.

4.6. *Anti-Center Shell*

The Anti-Center Shell (Fig. 8) was first delineated by Heiles (1984). Tamanaha (1997) made a detailed study of the region and argued that the Shell as such does not exist but is an artifact of the data display being based on channels at constant v_{LSR}. He rather sees it as the point of impact of a stream of HVCs falling toward the plane—the Anti-Center HVCs (§§ 4.8 and 4.9) being the rest of that stream.

Kulkarni & Mathieu (1986) failed to find Ca II absorption toward 6 OB stars in the direction of the Shell. They put the most distant star (HDE 248894) at 2.7 kpc (recalculated here as 3.0 kpc). The abundance of Ca II has not yet been measured, so although A(Ca II) is less than 15% of the "normal" value, the nondetection is not considered significant.

Kulkarni & Mathieu (1986) also observed HDE 256725, classified as an O star at $d < 2.5$ kpc. The nondetection of Ca II is not significant (a factor 5 below the expected value, rather than a factor greater than 20). According to SIMBAD, this is a B star, but Garmany, Conti, & Massey (1987) classified it as O5 V and gave a distance of 8.0 kpc. If confirmed and reobserved with higher S/N, this star might set an upper/lower distance limit of 8.0 kpc.

4.7. *Cloud AC0*

Cloud AC0 was defined by Tamanaha (1997), by analogy with the chain of cores ACIII, ACII, ACI (see Fig. 9). It is

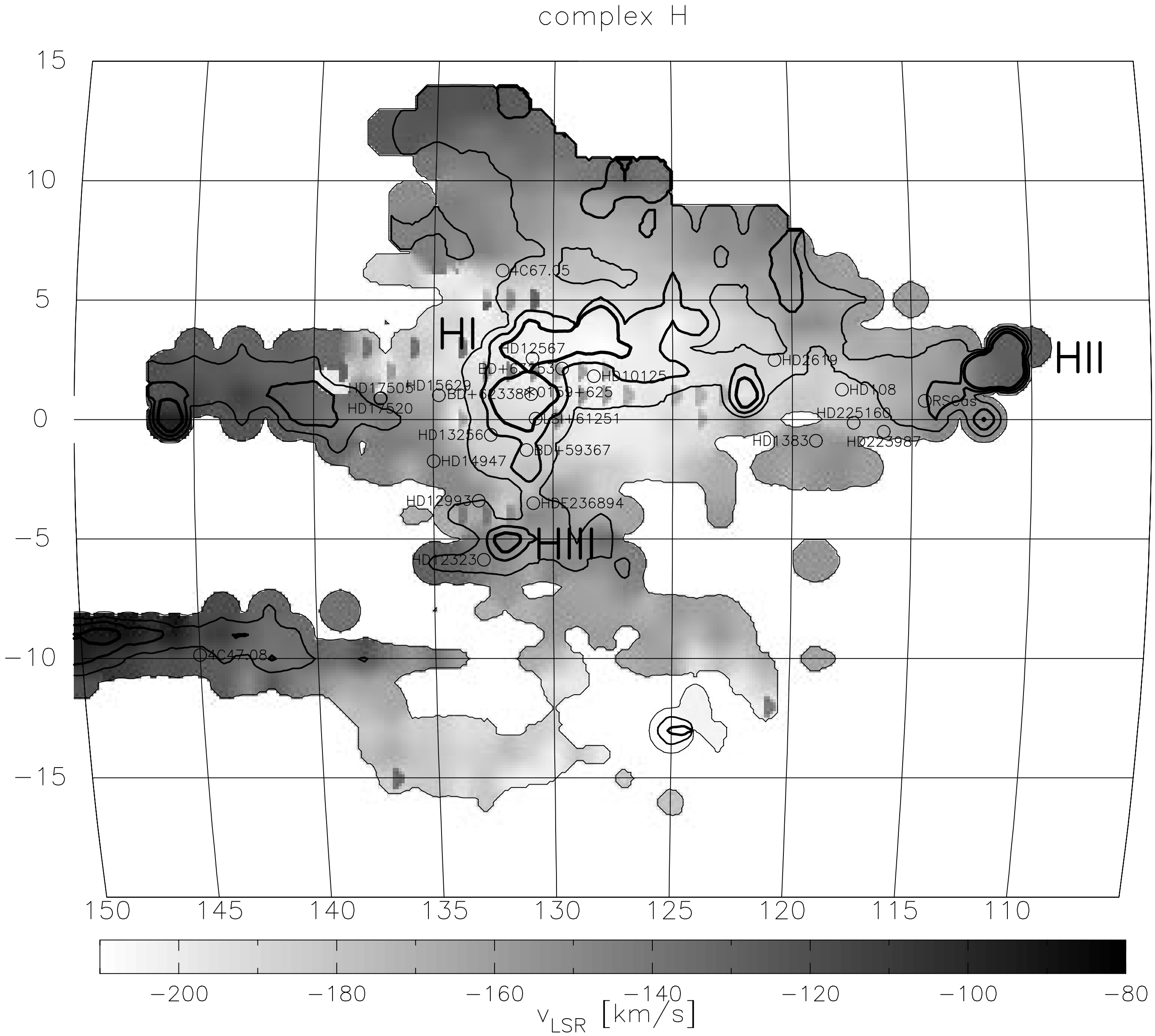

FIG. 7.—Map of HVC complex H, from Hulsbosch & Wakker (1988). Contours indicate brightness temperature levels of 0.05, 0.3, 0.6, and 1 K. The gray scale shows velocities, as identified by the wedge. The core names are shown, as are the positions of probe stars.

embedded in the Anti-Center Shell, but it stands out in velocity space. Tamanaha (1996) failed to find Ca II and Na I absorption toward four stars. None of the Na I nondetections are significant, however (the best being only a factor 9 below the average expected value), but the Ca II nondetection sets a weak lower limit of just 0.3 kpc. Note that Tamanaha (1996) includes LS V+30°31 as a probe of AC0, but the Effelsberg H I spectrum shows that this star lies just off the core.

4.8. *Clouds ACI and ACII*

Two studies of Na I and Ca II absorption were made for these two clouds, using bright ($V < 10$) B and A stars (Songaila et al. 1988; Tamanaha 1996). See Figure 9 for the positions of the probes. Again, none of the Na I nondetections contains distance information, whereas the Ca II nondetections toward ACI are mostly significant, setting a lower limit of 0.4 kpc to the distance. This is a not very interesting limit, as the expected distance is on the order of several to tens of kpc, if indeed the AC clouds are infalling intergalactic clouds, as proposed by Mirabel (1982) and Tamanaha (1995, 1997).

The same set of stars probes H I components assigned to ACII, which partly overlaps with ACI. However, since the column densities associated with ACII are lower, most nondetections are not considered significant.

4.9. *Cohen Stream and HVC 168−43+280 (Cloud WW507)*

Two studies of absorption were made for these two clouds, using bright ($V < 10$) B and A stars (Kemp et al. 1994; Tamanaha 1996, see Fig. 9). None of the Na I nondetections and only one of the Ca II nondetections are significant. However, from Mg II nondetections a lower distance limit of 0.3 kpc is set. Weiner, Vogel, & Williams (2001) detect Hα emission from three directions in cloud WW507,

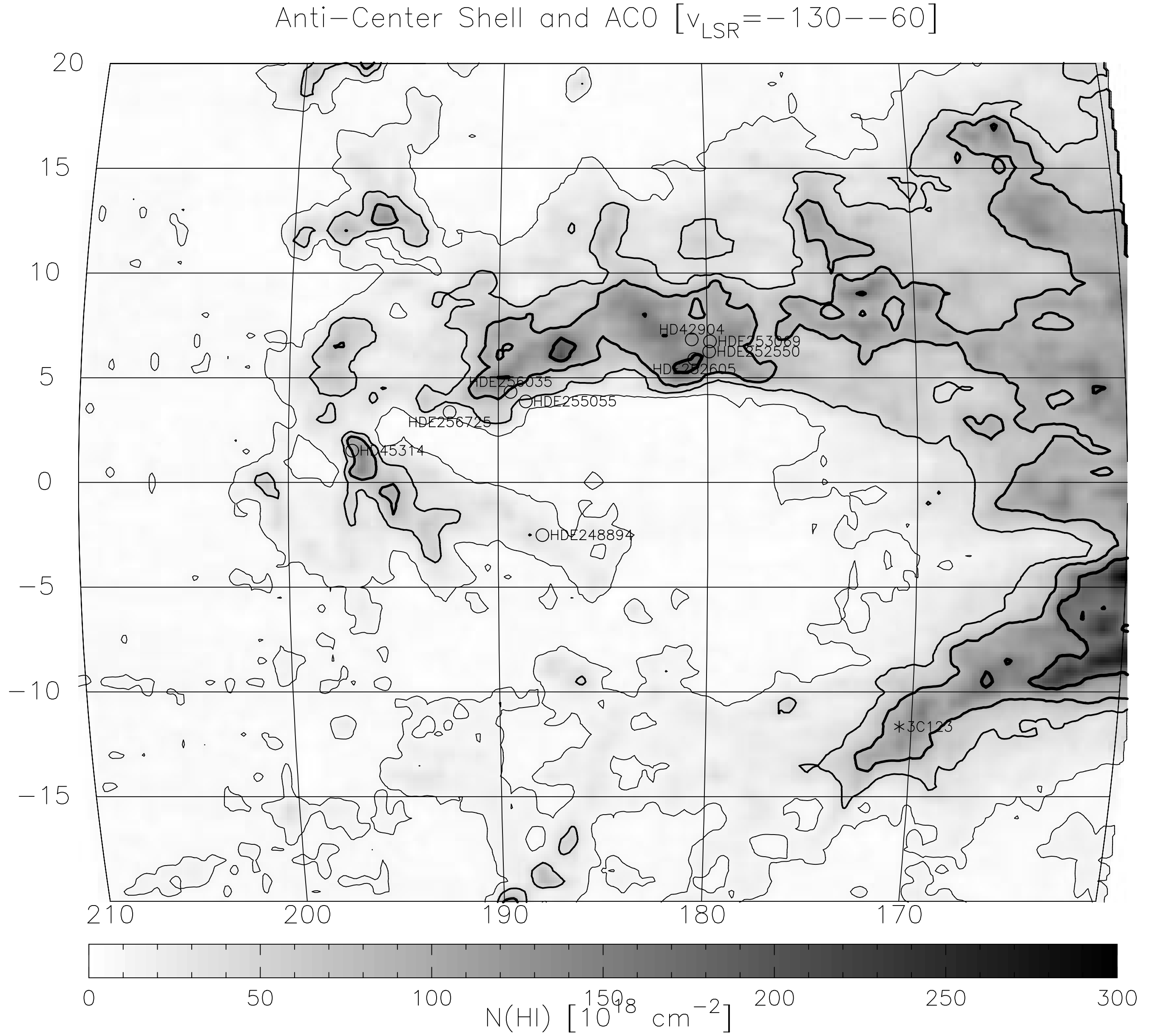

FIG. 8.—Map of the Anti-Center shell, from Hartmann & Burton (1997). Contours indicate column densities of 10, 40, 80, and 160 × 10^{18} cm^{-2} for gas in the velocity range −130 to −60 km s^{-1}. The open symbols show the positions of the probes with nondetections. The structure at $l = 180°$, $b = +6°$ is cloud AC0.

with intensities of 50–250 mR (1 rayleigh is $10/4\pi$ photons cm^{-2} s^{-1} sr^{-1}). Applying a model for the distribution of ionizing radiation (Bland-Hawthorn & Maloney 1999) then suggests distances on the order of 10–20 kpc.

Kemp & Bates (1998) searched for but did not detect Na I absorption toward the Seyfert galaxy Mrk 595. They calculated an expected value for EW(Na I) of ∼30 mÅ (1.3 × 10^{11} cm^{-2}), assuming that the Na I abundance is similar to that seen in low-velocity gas. Since their detection limit is 21 mÅ, and considering the large observed variations in A(Na I) (see § 3), this nondetection contains no information about the conditions in the Anti-Center clouds.

4.10. *Complex GCN*

These widely scattered, faint clouds have high negative velocities. High-ionization C IV and Si IV absorption was seen in the spectra of Mrk 509 and PKS 2155−304 by Sembach et al. (1995b, 1999), as was O VI (Sembach et al. 2001). Sembach et al. (1999) proposed that (a) the gas is photoionized by the extragalactic background radiation, (b) the thermal pressure in the sight lines is ∼1–5 K cm^{-3}, and (c) the distance of the gas is 10–100 kpc (depending on the metallicity, which was assumed to lie between 0.1 and 1 times solar). If it is assumed that the H I clouds in complex GCN are the denser and cooler tips of the iceberg of a large, coherent, mostly ionized cloud, then the implied cloud size is 8–80 kpc. These parameters are consistent with this (group of) clouds being a low-metallicity, tenuous, extragalactic cloud.

If the metallicity is eventually found to be ∼0.1 solar, complex GCN may represent an early stage in the process proposed by Oort (1970), in which hot gas at the outskirts

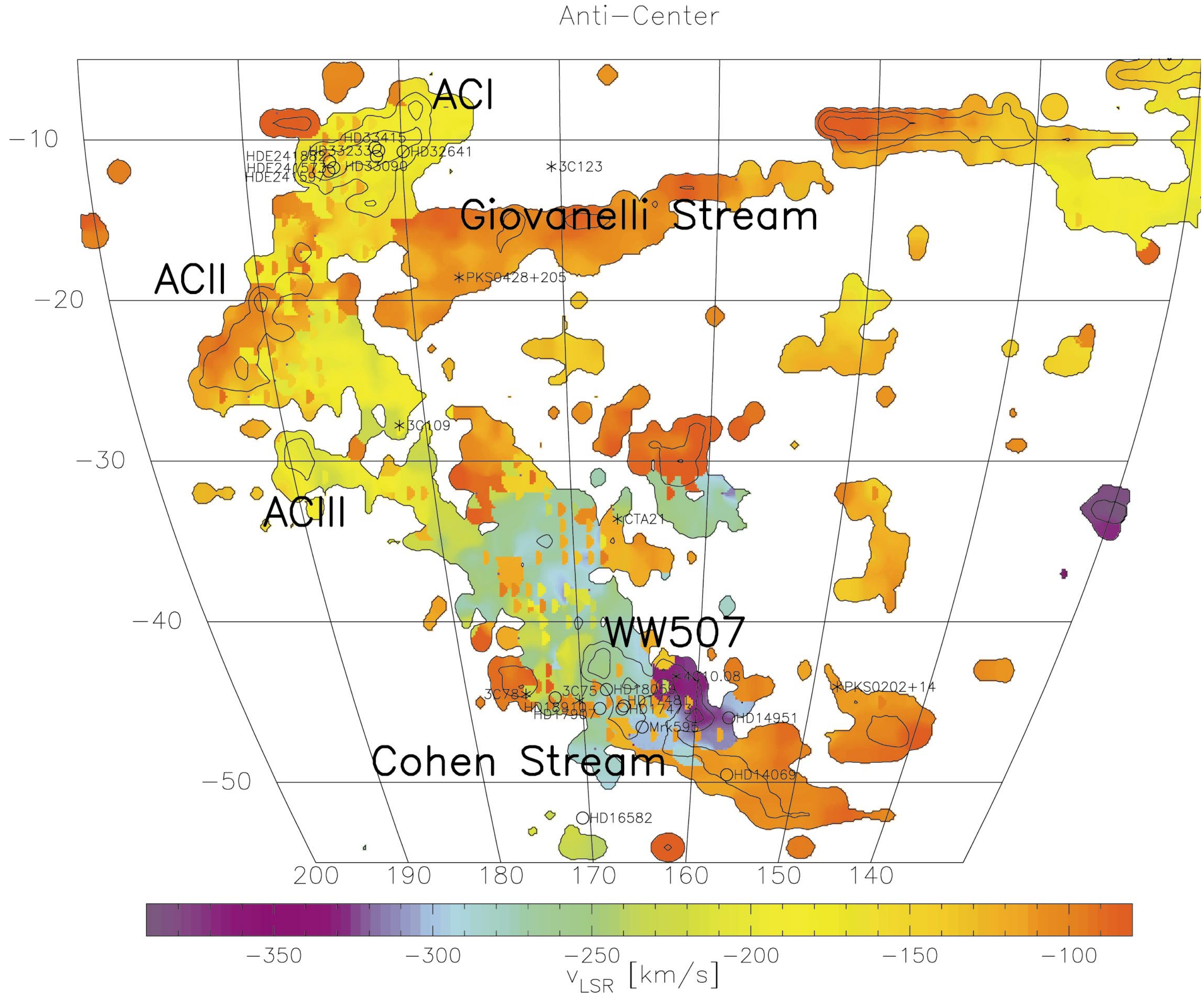

FIG. 9.—Map of the Anti-Center HVCs, from Hulsbosch & Wakker (1988). Contours indicate brightness temperature levels of 0.05, 0.3, 0.8, and 1.5 K. Colors indicate velocities, as identified by the wedge. At many positions along the central ridge emission is seen at two velocities. In these directions two half-circles are shown, with separate colors for each component. Core names are also shown, as are the positions of probe stars.

of the sphere of influence of the Milky Way condenses and then accretes. Complex C may be a late stage.

4.11. *Complex GCP*

Although there are many bright stars as well as distant RR Lyrae stars projected on this cloud, the only published data are from the first-ever paper concerning HVC absorption lines (Prata & Wallerstein 1967). The nondetection toward HD 187350 sets a lower distance limit of 0.3 kpc (and thus a lower mass limit of $10^3\ M_\odot$). Bland-Hawthorn et al. (1998) detected Hα emission associated with complex GCP and argued that it is related to the Sagittarius dwarf, at a distance of $\sim$25 kpc. However, if this cloud is related to lower velocity gas that seems connected to it, its distance can be no more than a few kpc (see § 4.29 for further discussion).

4.12. *Outer Arm*

The Outer Arm was first recognized as a separate, distant spiral arm by Habing (1966). It was further analyzed by Kepner (1970) and Haud (1992). The velocities are only 20–30 km s^{-1} higher than expected from a flat rotation curve for gas at galactocentric radii of 15–25 kpc. Toward $l \sim 90^\circ$ a large kinematical leverage is provided, allowing one to study the outer Galaxy. In the direction to H 1821+643, high-ionization C IV absorption was found by Savage et al. (1995), while O VI was reported by Oegerle et al. (2000) and Sembach et al. (2000).

4.13. *Cloud R*

This feature was defined by Kepner (1970) and may be associated with the Outer Arm, or it may be a separate, distant HVC.

4.14. *Magellanic Stream*

The Magellanic Stream is most likely a tidal tail torn out of the SMC during the tidal interaction between the Milky Way, LMC and SMC one orbit (2 Gyr) ago (Gardiner & Noguchi 1996). Some of the gas has been decelerated, forming the well-known Stream, and some of it has been accelerated ahead of the SMC system. Most of the latter fell on the LMC, but some has gotten past, forming a scattered leading arm. Lu et al. (1998) identified the extreme-positive-velocity clouds of Wakker & van Woerden (1991) as part of this leading arm. Figure 10 shows the Stream and these clouds in a projection that has galactic longitude 270° along the equator. Overlaid is the model of Gardiner & Noguchi (1996).

This projection was chosen as the simplest way to make the Magellanic Stream lie as near the equator as possible. This is basically done by turning the great circle $l = 90°$ and $l = 270°$ into the equator. Formally, the pole lies at galactic longitude $l = 180°$, galactic latitude $b = 0°$, and it is further rotated by 33.°42779 so that the current position of the LMC has new longitude $L = 0$.

The distances to the trailing and leading parts of the stream are not well known. If 50 kpc is assumed, the mass of the trailing part of the stream is about $1.5 \times 10^8\ M_\odot$ (not counting the gas in the Magellanic Bridge, at galactic latitudes greater than −45°). For the leading part, all clouds in complex EP of Wakker & van Woerden (1991) add up to about $5 \times 10^7\ M_\odot$ at an assumed distance of 50 kpc. The model predicts distances ranging from 50 to 100 kpc for this gas.

Also added in Figure 10 are some small positive-velocity clouds in the northern Galactic hemisphere that were not considered part of HVC complexes WA and WB by Wakker & van Woerden (1991). These appear to line up ahead of the curve defined by the SMC orbit and the EP clouds near $l = 290°$, $b = +20°$ (60°, −20° in Fig. 10), although they are not in the orbital plane of the Magellanic Clouds. For further discussion of these small clouds, see § 4.22.

The tidal model predicts a metallicity similar to that of the SMC. For sulfur that means S/H ~ 0.2–0.3 solar (Russel & Dopita 1992). Indeed, such values are found toward Fairall 9 in the tail (0.33 ± 0.05 solar, Gibson et al. 2000) and NGC 3783 in the leading arm (0.25 ± 0.08 solar, Lu et al. 1998). For NGC 3783 N(H I) was measured at 1′ resolution by combining ATCA and Parkes data. No high-resolution H I map has yet been made for the field around Fairall 9; a 25% correction is easily possible. In both directions a measurement of Hα will be needed to account for H^+, although N(H I) is high enough and the radiation field is expected to be low enough that only a small correction is expected.

Although the distance to different parts of the Stream is expected to be 30–80 kpc, no formal limit can be set, as only

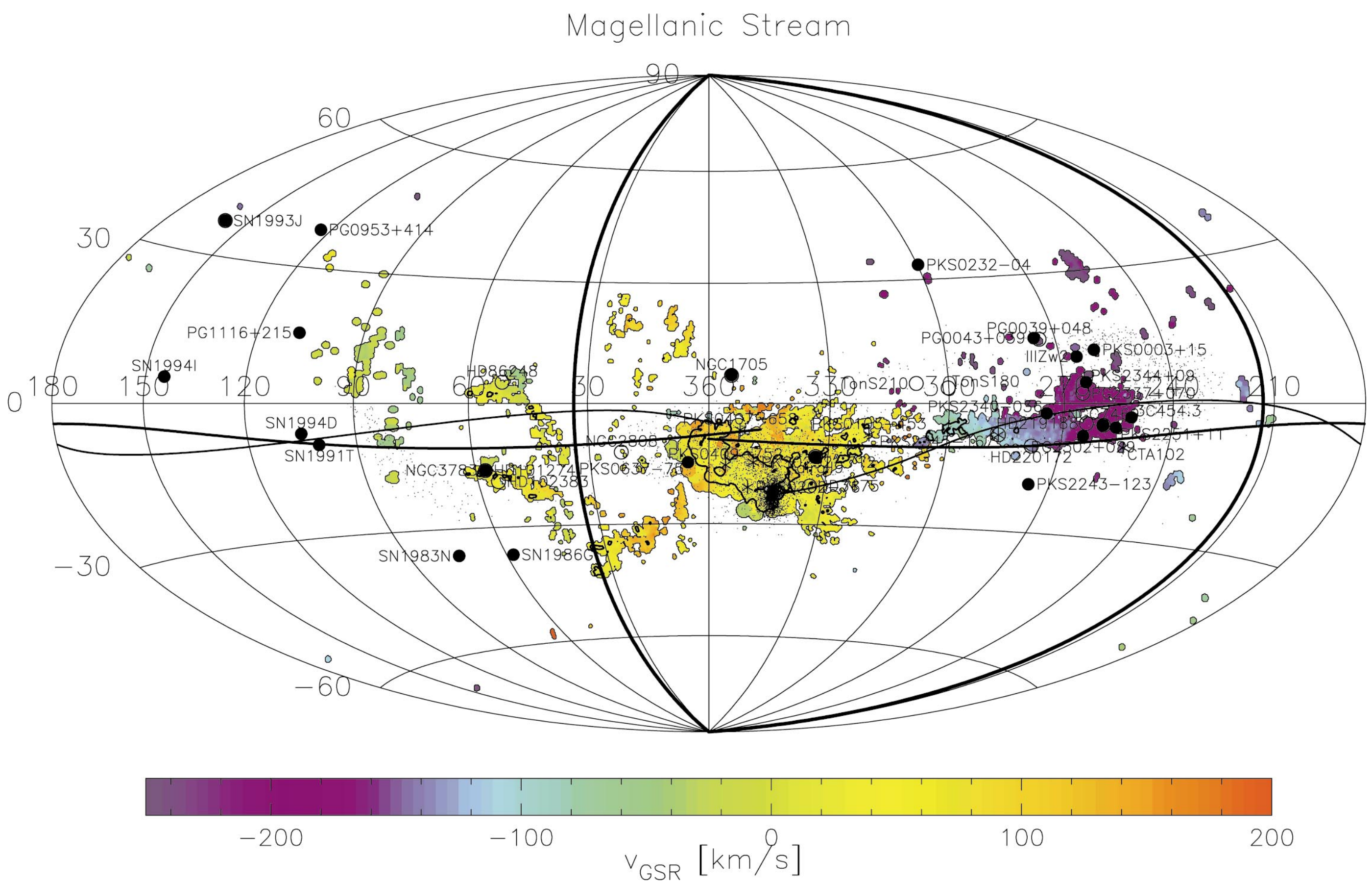

FIG. 10.—Map of the Magellanic Stream, using data from Hulsbosch & Wakker (1988) and Morras et al. (2000). Added are the clouds in populations EN and EP of Wakker & van Woerden (1991), as well as scattered small positive-velocity clouds in the northern Galactic hemisphere. Contour levels are at brightness temperatures of 0.05 and 1 K. Colors indicate velocities as identified by the wedge. The projection has galactic longitude 270° along the middle and the LMC near the center. The thick solid line crossing the poles represents the Galactic equator. The curved lines are the orbits of the LMC and SMC in the model of Gardiner & Noguchi (1996); the small dots are the present-day positions of the particles in that model. Labeled probes are those of the Magellanic Stream, clouds WW187, WW211, and WW487, as well as the extragalactic objects in which Na I or Ca II absorption is seen without associated H I (see § 4.22). Filled symbols indicate detections, open symbols nondetections.

nonsignificant nondetections have been found toward a few nearby stars. Considering the large sky area covered by the Magellanic Stream, it is possible that more nondetections lie hidden in the literature, in papers not aimed at studying the ISM, and therefore not noted.

Several AGNs behind the Magellanic Stream were observed with the FOS. Savage et al. (2000a) report equivalent widths for detections of Mg II; Jannuzi et al. (1998) give the wavelength offsets, from which velocities are calculated. Although the velocity resolution is only 220 km s^{-1}, this is sufficient to separate absorption by the Magellanic Stream from that by disk gas. As the H I profiles are broad (30–50 km s^{-1}; see Paper II), the estimated Mg II optical depths are 0.2–3, allowing to convert the equivalent widths to column densities. Figure 1*a* shows the resulting correlation between *N*(H I) and *A*(Mg II). For $N(\mathrm{H\ I}) > 2 \times 10^{18}$ cm^{-2}, *A*(Mg II) is nearly constant (average 3600 ppb, or 0.10 times solar). At lower *N*(H I) much higher values and lower limits are found. The most likely explanation for this change is that the hydrogen becomes mostly ionized, as the ionization potential of Mg II is higher than that of hydrogen, while its depletion seems to be independent of *N*(H I) (Wakker & Mathis 2000). The average abundance of 0.10 times solar implies an Mg II depletion of 0.3–0.4 for the Magellanic Stream, i.e., similar to the value in halo gas.

Abundances in the Stream can also be derived for Ca II, Fe II, and Si II, see Figure 3*c*. The table in Jannuzi et al. (1998) gives Fe II toward PKS 0637−75 near the SMC, which yields $A(\mathrm{Fe\ II}) = 0.062 \pm 0.025$ times solar. In the leading arm, NGC 3783 gives $A(\mathrm{Fe\ II}) = 0.033 \pm 0.006$ times solar. The implied ratios of $\mathrm{Fe/S} = 0.18 \pm 0.06$ and 0.13 ± 0.05 times solar are similar to the typical ratio in halo-like gas (0.23). The Mg II and Fe II abundances both imply that there is dust in the Magellanic Stream and that it has properties similar to the dust in the Galactic Halo.

4.15. *Population EP*

Several of the extreme-positive velocity clouds have been studied. Cloud WW187 was discussed above, in the context of it being part of the leading arm of the Magellanic Stream.

Sahu & Blades (1997) and Sahu (1998) observed NGC 1705 with a velocity resolution of 140 km s^{-1} and found absorption at $v_{\mathrm{LSR}} \sim +260$ km s^{-1} in several Si II lines. This was interpreted as being associated with HVC WW487, which has $v_{\mathrm{LSR}} = +240$ km s^{-1} and is 2 degrees away from NGC 1705; it is probably a shred of the Magellanic Stream (see Fig. 10). A map of this area was made by M. E. Putman (2000, private communication) using *HIPASS* data, after reprocessing in order to extract extended structure. This clearly shows WW487, but no other HVCs in the area. Faint (1.7×10^{18} cm^{-2}) high-velocity H I is detected directly in the sight line toward NGC 1705 (Paper II). Si II λ1190, Si II λ1304, and Si II λ1526 absorption are clearly seen, but the listed equivalent widths are inconsistent. The derived abundances are 0.48 ± 0.14, 2.9 ± 1.5, and 2.9 ± 1.5, respectively. This poses an unsolved problem. However, the result does suggest that most of the gas in this direction is in the form of H^+.

Sahu (1998) also lists an equivalent width for N I λ1199, but at 140 km s^{-1} resolution this absorption is a hopeless blend of λ1199.55 and λ1200.22 absorption due to the Galaxy, the HVC and NGC 1705.

The only cloud in population EP for which a formal distance limit exists is cloud WW187. HD 101274 is a few arcmin from NGC 3783 and sets a lower limit of 0.4 kpc. Wakker & van Woerden (1997) listed a lower limit of 6.2 kpc to the distance of the extreme-positive velocity cloud WW211, based on the nondetection of Si II toward HD 86248 by Danly et al. (1993). The revised distance of this star is 7.6 ± 3.0 kpc. Since WW211 is part of the leading arm of the Magellanic Stream, the expected Si II abundance is a factor 4 below the standard halo value of 19,000 ppb, i.e., $\sim$5000 ppb. The observed limit of 3300 ppb may therefore not be significant, and the nondetection does not set a lower limit to the distance of cloud WW211 after all.

4.16. *Very High-velocity Clouds*

The sight line to Mrk 205 passes through HVC WW84, which has $v_{\mathrm{LSR}} = -202$ km s^{-1}. Bowen et al. (1991a, 1991b) detected weak Mg II absorption from this cloud. The H I column density has not yet been properly measured toward this object. In the 9$'$.1 Effelsberg beam it appears to be 15×10^{18} cm^{-2}. However, as the high-resolution (1$'$) WSRT map presented by Braun & Burton (2000) shows, such a beam picks up some of the very bright small-scale structure that lies nearby. A proper correction requires to combine the WSRT map with a grid of single-dish data to produce a fully sampled interferometer map. This has not yet been done. In the meantime, the best guess for *N*(H I) is $8 \pm 5 \times 10^{18}$ cm^{-2}. This yields an Mg II abundance of 0.020 ± 0.014 times solar.

This value is much lower than usual in halo gas (0.4 solar is typical for gas with intrinsically solar abundance), and even lower than is found in cool disk gas with large amounts of dust (0.03 times solar). A value near 0.02 solar can also be found in a low-metallicity cloud. If there is some dust, the intrinsic metallicity could be $\sim$0.05–0.1 solar. Confirmation using other absorption lines is needed, as well as an improved value for the H I column density and an assessment of the ionization correction.

Combes & Charmandaris (2000) report a possible detection of HCO^+ at -198 km s^{-1} in the spectrum of the radio continuum source 1923+210 in a direction lying between the VHVCs WW274 ($v_{\mathrm{LSR}} = -200$ km s^{-1}) and WW283 ($v_{\mathrm{LSR}} = -198$ km s^{-1}). If the ratio of HCO^+ to H_2 were similar to that found in low-velocity gas (6×10^{-9}, Lucas & Liszt 1996), this would imply $N(H_2) = 7 \times 10^{19}$ cm^{-2}, whereas the observed limit to *N*(H I) is less than 2×10^{18} cm^{-2}. Clearly, this cloud is unusual in that it either has large molecular content, or relatively high HCO^+ abundance. These VHVCs may be outliers of the GCN complex, outliers of the Magellanic Stream, or genuine isolated VHVCs; their position in the sky does not allow an unambiguous identification.

4.17. *Complex L*

Albert et al. (1993) reported Ca II absorption components at -98 and -127 km s^{-1} in the spectrum of HD 135485, thought to be a B5 IIp star at a distance of 2.5 kpc. Van Woerden (1993) suggested that this absorption is due to complex L, but Danly, Lee, & Albert (1995) showed that interstellar C II, O I, and Si II absorption are absent at these velocities, implying that the Ca II components are circumstellar. They also reclassified HD 135485 and revised the distance down to 0.8 kpc. According to *Hipparcos*, the parallax is 5.52 ± 1.13 mas, which gives an even lower distance of 0.18 ± 0.04 kpc. Thus, in spite of earlier suggestions, all that is known for complex L through HD 135485 is a lower limit to its distance of 0.2 kpc.

Weiner et al. (2001) find that complex L shines brightly in Hα emission, with detections of 0.3–1.7 rayleigh ($=10^6/4\pi$ photons cm^{-2} s^{-1} sr^{-1}). [N II] λ6583 emission is similarly strong, with [N II]/Hα = 1.1. Applying a model for the distribution of ionizing radiation (Bland-Hawthorn & Maloney 1999) then suggests that complex L lies at a distance of 8–15 kpc, and 2–10 kpc above the galactic plane, either near the Galactic center or at the other side of the center. Of course, because of individual features such as spiral arms, the radiation model is least accurate close to the Galactic plane and close to the Galactic center. Nevertheless, the bright Hα emission associated with complex L shows that this HVC must lie in the lower Galactic Halo.

4.18. *Complex WB*

Only one resolved detection is known for a previously cataloged HVC complex with positive velocities: Ca II absorption associated with cloud WW225 is seen in the spectrum of PKS 0837−12 (Robertson et al. 1991). This gives the highest measured Ca II abundance for any HVC (280 ppb). The published value of 160 ppb was based on N(H I) = 14 × 10^{18} cm^{-2} as measured with the Parkes telescope (15′ beam) whereas with the 9′.1 Effelsberg beam N(H I) = 7.9 × 10^{18} cm^{-2}. Since N(H I) is low, and no other measurements exist for cloud WW225, it is unclear whether the high A(Ca II) is due to hydrogen ionization, to anomalously low calcium depletion, or to low H I column density (the latter effect is discussed by Wakker & Mathis 2000).

4.19. *Complex WE*

In the sight line to HD 156359 Sembach et al. (1991) found C II, Mg II, Si II, and Fe II absorption at a velocity of +110 km s^{-1}, while Sembach & Savage (1996) reported N V at +128 km s^{-1}. Differential galactic rotation predicts velocities between 0 and −100 km s^{-1} in this direction.

At the position of HD 156359 no H I is found in the list of Morras et al. (2000), but many small, faint HVCs with similar velocities exist nearby (Fig. 11). These include some clouds previously cataloged on a 2° × 2° grid (WW356, WW364, WW373, WW412). With the better view provided by the Morras et al. (2000) list, these clouds were swept together into "complex WE," by analogy with the positive-velocity complexes WA through WD defined by Wakker & van Woerden (1991).

It is now clear that HD 156359 lies less than 1° away from one of the brighter cores of this complex, which has a velocity of +110 km s^{-1}. The star thus sets an upper limit to the distance of the HVC of 12.8 kpc (z < 3.2 kpc). Most likely, the star samples the faint outer envelope of this cloud. Assuming solar abundance and halo-like depletion, the implied value of N(H) is about 10^{17} cm^{-2}. The mass of the

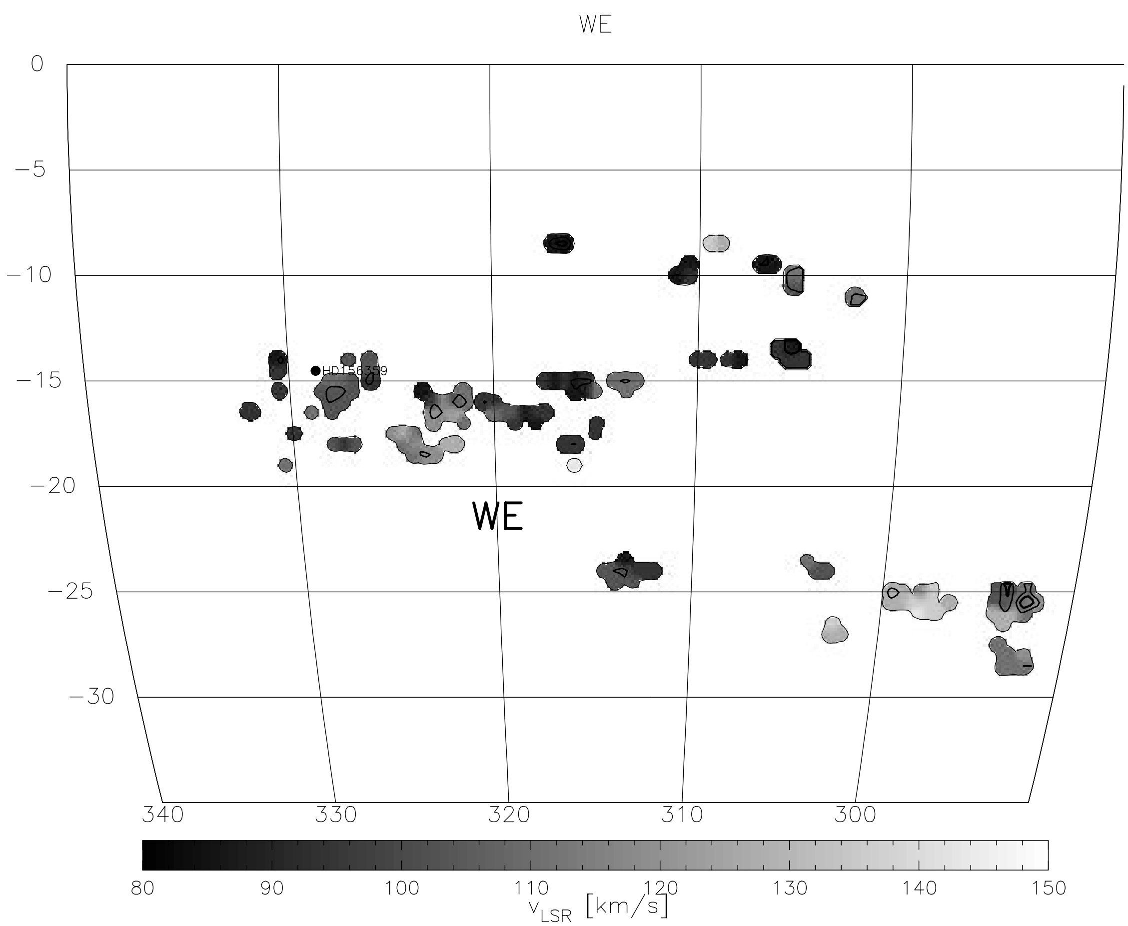

FIG. 11.—Map of complex WE, based on the data of Morras et al. (2000). The gray scale indicates velocities as identified by the wedge. Contours are at brightness temperatures of 0.05 and 0.3 K. The position of HD 156359 is indicated.

collection of clouds forming complex WE is limited to be less than $2.5 \times 10^5 M_\odot$.

4.20. *Small Positive-velocity Clouds*

The sight line to the star BD $+10°2179$ crosses a small (1 square degree) cloud, WW29. Danly et al. (1993) give a distance for this star of 4.0 kpc, with spectral type "Bp." SIMBAD does not provide a better type, so this distance is rather uncertain. The nondetection of Si II is only a factor 3 below the expected value, so it may not be significant.

The presence of heavy elements in some of the small positive-velocity clouds is suggested by wide Mg II lines toward 4C 06.41 and PKS 1136−13 (Savage et al. 2000a).

4.21. *HVC 100−7+110*

In HVC 100−7+110 (probed by 4 Lac) several elements were detected, giving an abundance pattern. Its velocity of $+106$ km s^{-1} is opposite to that expected from differential galactic rotation at a longitude of 100°. The cloud appears to be small and is within 200 pc of the Galactic plane. It is not seen in the Leiden-Dwingeloo Survey, but it is clearly detected in spectra taken with the Jodrell Bank telescope (12′ beam) and in a high-angular resolution map made at Westerbork (Stoppelenburg, Schwarz, & van Woerden 1998). The upper limit on its mass is 1 $M_\odot$, making it a very unusual low-z solar-metallicity blob moving away from the plane.

Bates et al. (1990) measured equivalent widths for several elements and converted these to column densities. For this step they quoted a b-value of 6.5 ± 0.5 km s^{-1}, as derived from the Fe II lines. This b-value is then used to convert the equivalent widths of the strongly saturated O I, Mg II, and Al II lines to a column density. For a range of 1 km s^{-1} in b, and using the listed equivalent width errors, this implies optical depths of more than 10 for the O I and Mg II lines and more than 3 for Al II. Thus, all one can say is that A(O I) lies in the range 0.2–2.2 times solar, A(Mg II) in the range 0.6–8.4 times solar, and A(Al II) in the range 0.3–0.8 times solar, with a most likely value for Al II of 0.42 solar (1300 ppb). The Fe II abundance is slightly more reliable and is 0.25 ± 0.06 times solar (8000 ppb). The Al II and Fe II abundances are comparable to the expected values for a cloud with intrinsically solar abundance and halo-like depletion (1600 and 7800 ppb, respectively).

4.22. *HVCs with Weak* H I

In eight extragalactic probes absorption is detected at high velocities but without corresponding H I emission, even though the upper limits on N(H I) can be quite good (3×10^{17} cm^{-2} in the case of SN 1991T). Only toward SN 1986G is such high-velocity absorption accompanied by a weak H I component. Below, possible explanations are provided for all but two or three of these absorption components.

An absorption that remains unexplained is the $+250$ km s^{-1} Na I component toward SN 1994I (Ho & Filippenko 1995). No other positive-velocity IVCs are known in the neighborhood ($l = 104°$, $b = 68°$). Also mysterious are the components at $+125$, $+140$, and $+230$ km s^{-1} seen toward SN 1993J ($l = 142°$, $b = 41°$), if they are indeed unrelated to the galaxy M81, as de Boer et al. (1993) argued. Finally, the $+275$ km s^{-1} Mg II absorption seen toward PKS 0232−04 (Savage et al. 2000a, $l = 174°$, $b = -56°$) is strange. No high-positive velocity gas is known in this part of the sky (a few degrees from the edge of the Anti-Center HVCs, which have high-negative velocity). As PKS 0232−94 has a redshift of 1.434, it is possible that two Lyα absorbers at $z = 1.3$ mimic the Mg II doublet.

The C II, Si II, Si III, and Al II absorption at -150 km s^{-1} seen toward PG 0953+414 (Fabian et al. 2001) may be related to an extended low-column density tail of either HVC complex A or IV1. Both of these have velocities of -120 to -150 km s^{-1}. However, IV1 is about 8° distant, while the H I edge of complex A is about 10° away. The ionic column densities imply $N(\mathrm{H}) \sim 10^{18}$ cm^{-2} for gas with 0.1 solar abundance. However, considering that N(Si II) $\sim$ N(Si III), most of the hydrogen should be ionized, so that N(H I) is much lower. A possible counterargument is that toward PG 0804+761 absorption associated with complex A is not seen in any line (Richter et al. 2001a), even though that probe lies just 0°.5 off the H I edge of complex A. That would suggest a rather sharp edge. However, PG 0804+761 lies near the more constrained low-latitude part of complex A, rather than near the flared-out high-latitude end. This problem requires further observations of AGNs in the region between PG 0953+414 and the edge of complex A.

Three of the remaining H I–less absorptions are seen at a velocity greater than $+200$ km s^{-1} in Na I and Ca II (SN 1994D; King et al. 1995; Ho & Filippenko 1995) SN 1991T (Meyer & Roth 1991) and SN 1983N (d'Odorico et al. 1985). H I–less absorption is also seen at $v_{\rm LSR} = +130$ km s^{-1} toward PG 0953+414 (Fabian et al. 2001). Weak H I is detected at $v_{\rm LSR} > +200$ km s^{-1} toward SN 1986G (d'Odorico et al. 1989). Finally, $+200$ km s^{-1} C II and Si II absorption is seen toward PG 1116+215 (Tripp, Lu, & Savage 1998). In these directions the Na I/H I ratios are >57, >59, >20, 46 ± 20, and 60 ± 18 ppb. All of these are much higher than the average value in neutral gas (4.6 ppb). Ca II/H I ratios are >140, >500, >140, >250, >370, 150 ± 70, 150 ± 50, and >27 ppb, again much higher than the reference value of 22 ppb. These high values are consistent with the relation found between A(Ca II) and N(H I), which is discussed by Wakker & Mathis (2000), who show that high apparent abundances are correlated with low H I column density.

These six sight lines all lie in the region $l = 180°$–$320°$, $b = 20°$–$70°$. Many small positive-velocity clouds are also present in this region. Figure 10 shows that this region further lies in the extension of the curve defined by the SMC orbit and the EP clouds near $l = 290°$, $b = +20°$ (at 60°, $-20°$ in Fig. 10). Thus, it is suggested that these high-positive velocity absorptions and small positive-velocity clouds are associated with the tenuous leading edge of the leading arm of the Magellanic Stream.

A possible problem with this model is that it requires that the leading-arm gas no longer follows the SMC's orbit, deviating more as it gets farther ahead. However, since the gas had to pass the LMC first, it seems reasonable to suggest that it was given an additional nudge at that time. A more complete model is required to test this hypothesis.

In the Gardiner & Noguchi (1996) model, the tip of the leading arm gas is supposed to be at a distance of 30–80 kpc. As the clouds in the leading arm's tip cover about 20° on the sky, this corresponds to path lengths of more than 10 kpc. Then column densities of $\sim 10^{18}$ cm^{-2} correspond to a volume density of $\sim 5 \times 10^{-5}$ cm^{-3}, which implies Hα emission intensities less than 0.01 R, which is below the current detection limit (Reynolds et al. 1998). Not detecting Hα emission from the small positive-velocity HVCs would therefore not conclusively favor a Local Group over a Magellanic origin.

A further check would be to determine whether high-velocity absorption is not seen toward extragalactic supernovae that lie away from the orbits of the Magellanic Clouds.

4.23. *HVCs/IVC toward the LMC*

In the spectrum of many stars in the LMC absorption is seen at velocities of +165, +120, and +65 km s^{-1}. Ca II and Na I are the most-observed elements (Blades 1980; Songaila & York 1981; Songaila et al. 1981; Blades, Elliot, & Meaburn 1982; Songaila et al. 1986; Magain 1987; Vidal-Madjar et al. 1987; Molaro et al. 1989; Wayte 1990; Molaro et al. 1993; Caulet & Newell 1996; Welty et al. 1999). Other studies concentrate on dominant elements (Welty et al. 1999; Bluhm et al. 2001). In principle these results could be used to study abundance variations in the HVCs and IVC. However, in practice there are many problems: (a) the earlier spectra suffer from low signal-to-noise ratios and the measured equivalent widths are not very reliable; (b) in almost all cases only equivalent widths were published and line widths need to be assumed to convert to column densities; (c) toward all but a few stars N(H I) must be based on an interpolation between nearby observations, often with barely sufficient sensitivity; (d) the clouds have not been mapped in H I, as they have rather low column density (the Parkes Narrow Band Survey should make this possible, eventually). Section 3.6 presents a summary of the conclusions achievable with these caveats in mind.

From the spectrum of SN 1987A in the LMC, a large set of accurate ion column densities was derived by Welty et al. (1999) for all three H I components. However, a good, directly measured, value for N(H I) was not obtained, and instead N(H I) was inferred from the abundance patterns (see item "AB" in description of col. [10]). The absolute abundance therefore remains uncertain. However, for the two HVCs the abundance pattern is similar to the halo pattern (Sembach & Savage 1996). The pattern for the IVC would suggest zero depletion. These matters are discussed in more detail by Welty et al. (1999).

For the +120 km s^{-1} HVC a notable detection is that of H_2 toward Sk −68°82 by Richter et al. (1999), showing the presence of molecular hydrogen. Bluhm et al. (2001) also find H_2 toward Sk −68°82 in the IVC with $v_{LSR} = +60$ km s^{-1}.

Fe II absorption in the +120 km s^{-1} HVC has been seen in five probes, but with uncertain results. A(Fe II) = 0.28 ± 0.07 solar toward SN 1987A (Welty et al. 1999), 0.8 ± 0.6 solar toward Sk −67°104 (Bluhm et al. 2001), 1.3 ± 0.9 solar toward Sk −67°166 (Bluhm et al. 2001), 0.6 ± 0.4 solar Sk −68°82 (Bluhm et al. 2001), and 0.16 solar toward Sk −69°246 (Savage & de Boer 1981). N(H I) is uncertain toward SN 1987A (based on the depletion pattern), Sk −67°104, Sk −67°166, and Sk −69°246 (based on an interpolation), and better measurements are needed to reconcile the factor 8 range. On the other hand, Bluhm et al. (2001) argue that the high S II, Si II, and Fe II abundances in this cloud combined with the low O I abundance (~0.5 solar) argues in favor of substantial ionization, possibly as high as 90%. In this case variations in N(Fe II)/N(H I) are due to variations in the ionized fraction.

4.24. *Intermediate-velocity Arch*

This structure was first studied by Wesselius & Fejes (1973). Kuntz & Danly (1996) presented a catalog of cores. These designations were used here to sort the many observed probes. At many positions, a higher- (< −60 km s^{-1}) and a lower- (> −60 km s^{-1}) velocity component overlap, so the IV Arch is further divided into two parts, one consisting of cores IV5 through IV17, the other containing cores IV18 through IV26 (IV1–4 are identical with HVC complex M). Within each part the cores are sorted along the Arch by decreasing galactic longitude. Figures 12 and 13 show the structure, with the probe positions overlaid.

Kuntz & Danly (1996) derived a z-height of 0.8–1.5 kpc for the IV Arch, and brackets for IV17 and IV26. The distance limits derived here are consistent with their results, and they are graphically shown in Figure 14. The horizontal axis in this figures shows an approximate "angle along the Arch," with 0 degrees at the highest-longitude core. As the IV Arch lies at high galactic latitudes, it is more useful to discuss z-heights than distances. A fuller discussion now follows.

For the *higher velocity part of the IV Arch*, z-height brackets can be set for three cores: $z = 0.4$–1.7 kpc for IV6, $z = 0.5$–0.7 kpc for IV17, and $z = 0.2$–1.6 kpc for IV9. These are consistent with the upper limit of 3.9 kpc for IV7 and the lower limit of 0.7 kpc for IV11. The upper limit for IV17 is based on the horizontal branch (HB) star BD +49°2137, for which Kuntz & Danly (1996) gave a z-height of 1.7 kpc, which is correct for the spectral type given in SIMBAD (B7 V). Ryans et al. (1997a) did a more detailed spectroscopic analysis and argue that it is a HB star at $z = 0.7$ kpc, although the final number is somewhat model dependent. The distance bracket for IV17 is set by the same stars as those that bracket IV4, suggesting that these two clouds are close together in space, even though they differ in velocity by 30 km s^{-1}.

For the *lower velocity part of the IV Arch, at angles along the Arch less than 50°* ($l > 150°$), a z-height bracket of 0.4–2.6 kpc can be set for IV26, as well as a lower limit for IV24 of 0.4 kpc. Off cores HD 93521 is the only star with $z < 2.6$ kpc, and it reduces the upper limit to 1.7 kpc.

For the *lower velocity part of the IV Arch, at angles along the Arch greater than 50°* IV19 sets an upper limit to the z-height of 1.6 kpc. The limits toward HDE 233791 and PG 1255+546 are in apparent conflict. However, the classification of HDE 233791 is uncertain (Ryans et al. 1997a) and instead of an HB star at 0.5 kpc distance it could be a B9 V star at 0.9 kpc distance ($z = 0.8$ kpc). For PG 1255+546 the 1 σ uncertainty in the distance is 0.3 kpc, so that this star could be at $z = 0.4$ kpc, rather than $z = 0.7$ kpc. If these uncertainties are taken into account, combining the lower limit for PG 1255+456 with the upper limit for HDE 233791 yields a possible z-height bracket for this part of the Arch of 0.4–0.8 kpc. HDE 233791 may even reduce the upper limit to 0.4 kpc.

A final complication is the low upper limit of 0.3 kpc derived from *core IV21*. This core is slightly off the main axis of the IV Arch and is further unusual in that CO and 100 μm emission have been detected in it (Weiss et al. 1999). These authors study the cloud as an example of a high-z molecular cloud. Benjamin et al. (1996) claimed a distance bracket of 0.3–0.4 kpc. However, the lower limit is based on

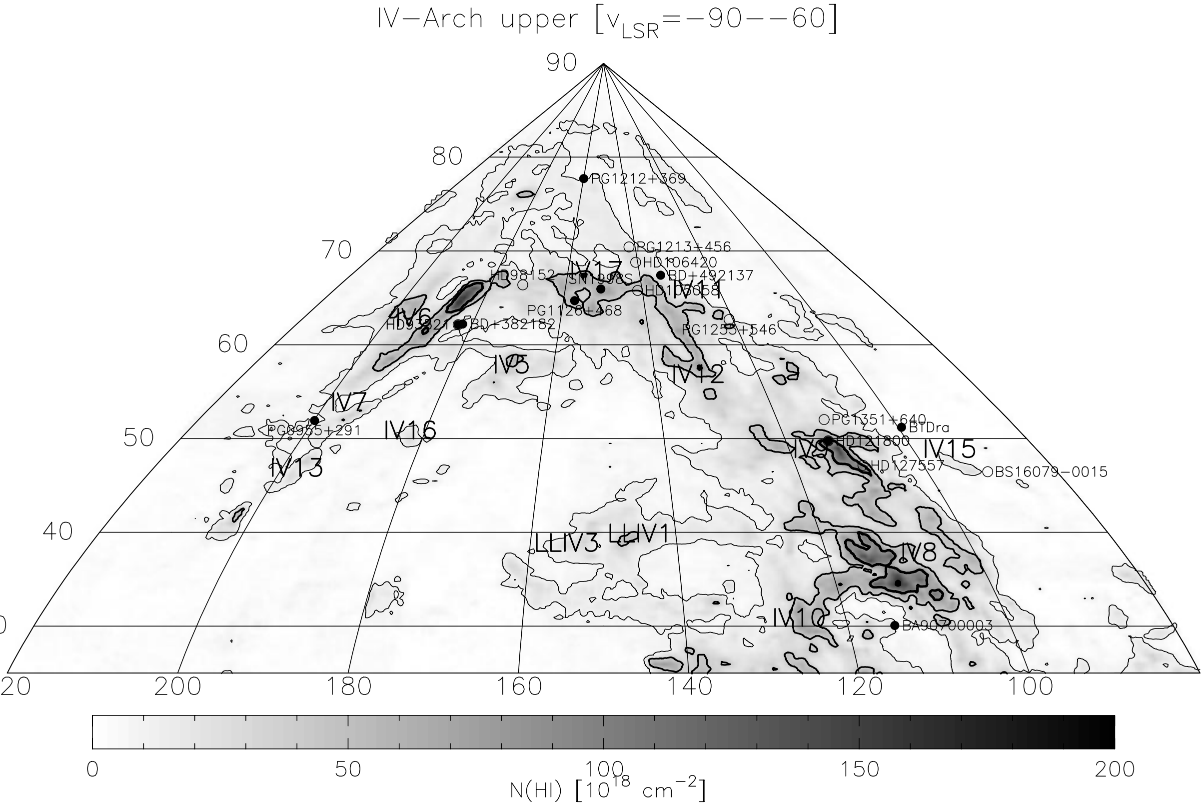

FIG. 12*a*

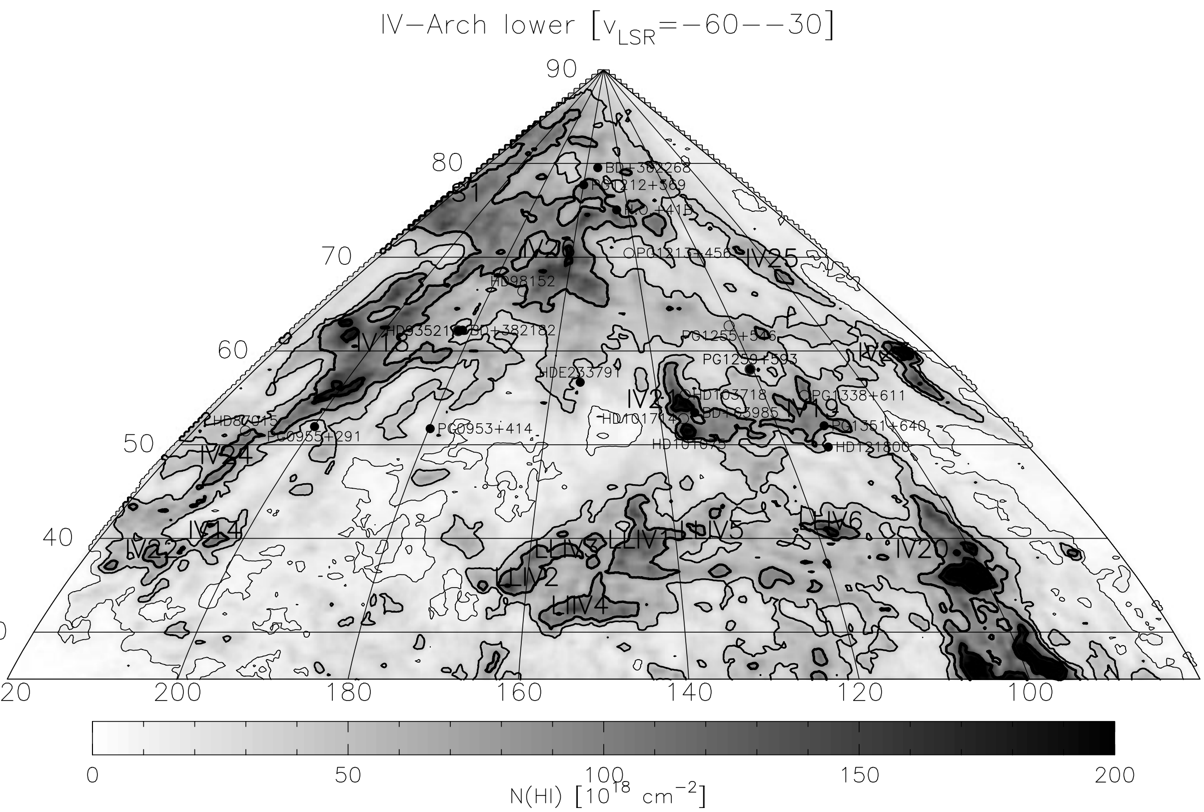

FIG. 12*b*

FIG. 12.—(*a*) Map of the intermediate-velocity arch at velocities between -90 and -60 km s^{-1}, from Hartmann & Burton (1997). The gray scale and contours indicate the column density in this velocity range, with contour levels at 10, 40, and 80 $\times$ 10^{18} cm^{-2}. The names of the cores defined by Kuntz & Danly (1996) are indicated. The positions of the probes are shown, with closed circles representing detections; open circles are nondetections. Map of the intermediate-velocity arch at velocities between -60 and -30 km s^{-1}, from Hartmann & Burton (1997). (*b*) Same as (*a*), except that there is an additional contour at 160 $\times$ 10^{18} cm^{-2}.

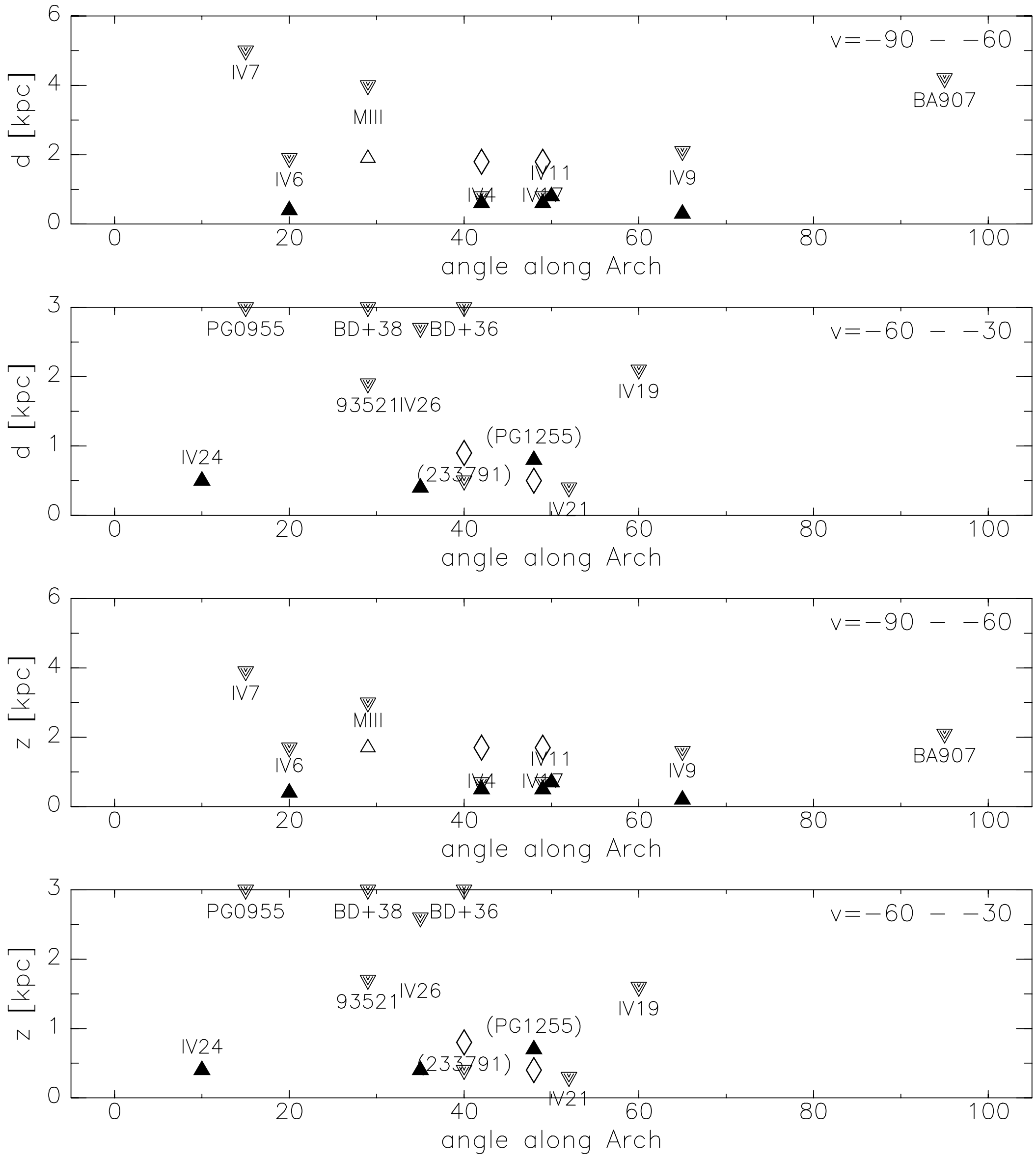

FIG. 13.—Summary of upper and lower distance limits for the IV Arch. The x-axis shows an approximate "angle along the Arch," with the origin at $l = 210°$, $b = 30°$. The top two panels show the distances, the bottom two the z-heights. Core names are indicated, as are the stars outside cores, for which just the beginning part of the name is shown. Three stars in the second and fourth panel are plotted at y-max, but they are more distant than that. Downward-pointing triangles are upper limits, upward-pointing triangles are lower limits. The open triangle for MIII refers to the possible lower limit from HD 93521. Diamond shapes are for the possible alternative distance for three stars with uncertain distances (BD +49°2137 toward IV4 and IV17, HDE 233791, and PG 1255+546).

Na I nondetections that are not significant, as they are only a factor ~6 below the measured Na I abundance. Therefore, the distance may be less than 0.3 kpc ($z < 0.2$ kpc). More observations, preferably using Ca II are required to settle this question.

In summary, for the higher velocity part of the IV Arch a strong bracket of $z = 0.7$–1.7 kpc can be derived. The upper limit depends mostly on the z-height of BD +49°2137, which may be as low as 0.7 kpc. For the lower velocity IV Arch the strong bracket is $z = 0.4$–1.6 kpc for the part with $l > 150°$. At lower longitudes the situation is slightly confusing, but a possible z-height is 0.4 kpc, although the strong bracket is 0.4–1.6 kpc.

Using these distance brackets, the mass of the IV Arch was estimated from the Leiden-Dwingeloo Survey to be 1–4.5 × 10^5 $M_\odot$ for velocities less than −60 km s^{-1}, and 1–8 × 10^5 $M_\odot$ for lower velocities. If the lower distances are used for BD +49°2137 and HDE 233791, the implied total mass of the IV Arch is about 2 × 10^5 $M_\odot$.

The metallicity of the IV Arch has not yet been well determined. Sulfur was observed to have near solar abundance toward HD 93521 (Fitzpatrick & Spitzer 1997); PG 0953+414 (Fabian et al. 2001) and HD 121800 (IV9/IV19—Howk et al. 2001). Similarly, oxygen is found to have an abundance of ~1 solar toward PG 1259+593 (Richter et al. 2001b).

Toward HD 93521 absorption components are seen at several velocities (−65, −57, −51, and −36 km s^{-1}), even though the H I profile just shows a 20.8 km s^{-1} wide component centered at −56 km s^{-1}. The component at −65

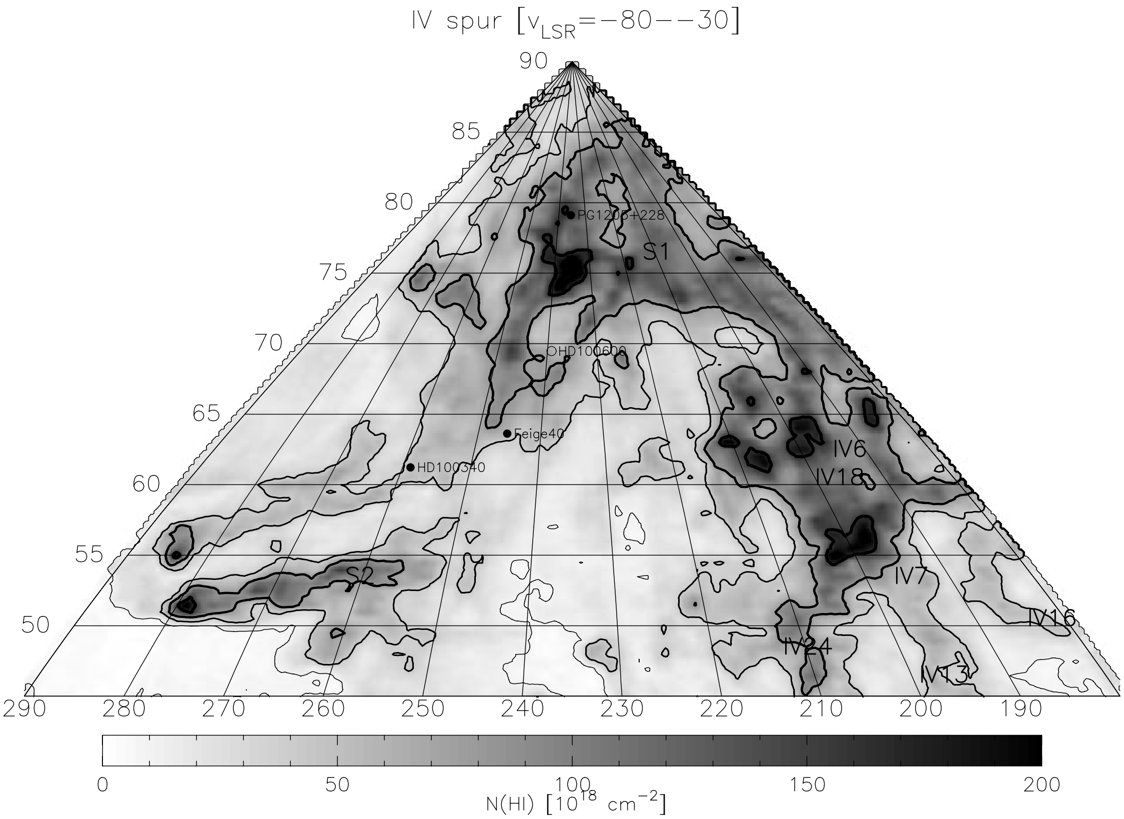

FIG. 14.—Map of the IV spur, from Hartmann & Burton (1997). Contours are at 10, 40, and 80 $\times$ 10^{18} cm^{-2}. The core names are shown, as are the positions of probe stars. Closed symbols refer to detections, open symbols to nondetections.

km s^{-1} is probably related to IV6. Applying a component analysis to the H I spectrum observed at Green Bank (21′ beam), Fitzpatrick & Spitzer (1997) derived S II/H I ratios of 2.1 $\pm$ 2, 0.78 $\pm$ 0.12, 1.2 $\pm$ 0.25 and 0.74 $\pm$ 0.31 times solar (0.97 $\pm$ 0.06 when summing all components). They further determine n_e and use the result to argue that hydrogen ionization is unimportant. Toward HD 121800 two H I and two S II components occur, which are not well separated. The average S II/H I ratio is 0.8 solar. In the sight line to PG 0953+414 Fabian et al. (2001) find S II/H I = 1.1 $\pm$ 0.2 times solar, but N(H I) is low (23 $\times$ 10^{18} cm^{-2}), so the ionization correction is potentially large. In general, these results suggest near-solar abundance for the IV Arch, although more work is needed on component structure, H I small-scale structure, and ionization corrections.

The abundance patterns toward HD 93521 were used by Savage & Sembach (1996a) to *define* the reference for halo gas. These patterns are shown in Figures 3*f* and 3*k*.

4.25. *Intermediate-velocity Spur*

These cores form an extension to the IV Arch, at somewhat lower velocities and higher longitudes and latitudes, and were defined by Kuntz & Danly (1996). These authors also derived the distance bracket of 0.3–2.1 kpc based on the Si II lines in *IUE* spectra. The implied mass bracket is 0.2–8 $\times$ 10^5 $M_\odot$. The positions of the probes are shown in Figure 15.

4.26. *Low-Latitude Intermediate-Velocity Arch*

This structure was named by Kuntz & Danly (1996). It crosses over complex A, resulting in a relatively large number of observed probes (see Fig. 16). The distance can be constrained to lie in the range 0.9–1.8 kpc (z = 0.6–1.2 kpc). The implied mass is 1.5–6 $\times$ 10^5 $M_\odot$. In the Galactic plane at these longitudes lies the Perseus Arm, a spiral arm that is 2.5 kpc distant (Reynolds et al. 1995). The LLIV Arch thus appears to be high-z interarm gas.

Several probes lie off the main structure and are collected under the heading "LLIV Arch extension." This gas has velocities similar to that in the LLIV Arch proper, and most likely is spatially close to it. If so, an upper distance limit of 0.9 kpc is set by HD 83206, equal to the lower distance limit for the main part of the LLIV Arch.

The metallicity and depletion pattern can be determined from the spectra of SN 1993J (de Boer et al. 1993), PG 0804+761 (Richter et al. 2001a) and HDE 233622 (Ryans et al. 1997b). The metallicity follows from N(O I)/N(H I) = 1.0 $\pm$ 0.5 solar and N(N I)/N(H I) = 0.55 $\pm$ 0.14 solar, as O and N are undepleted, and (especially O I) tied to H I. If hydrogen ionization were ignored, this would be inconsistent with the apparently supersolar abundance of P II (1.3 $\pm$ 0.6 solar) and Zn II (1.6 $\pm$ 0.4 solar). However, both these elements can coexist with both H I and H$^+$. The degree of ionization can be estimated by assuming that O I and H I go together. Then N(P II)/N(O I) $\sim$ [N(H I)+N(H$^+$)]/N(H I). This yields an ionization fraction of $\sim$20%.

The depletions of some refractory elements are typical for warm disk gas: δ(Si II) $\sim$ 0.3 (typical is 0.15), δ(Al II) = 0.09 (typical is 0.15), δ(Ti II) = 0.11 (typical is 0.05), and δ(Fe II) = 0.1–0.3 (typical is 0.1). See Figure 3*d* for a graphical representation.

Ca II abundances in the LLIV Arch are remarkable for their constancy. Out of 10 determinations 7 are in the range

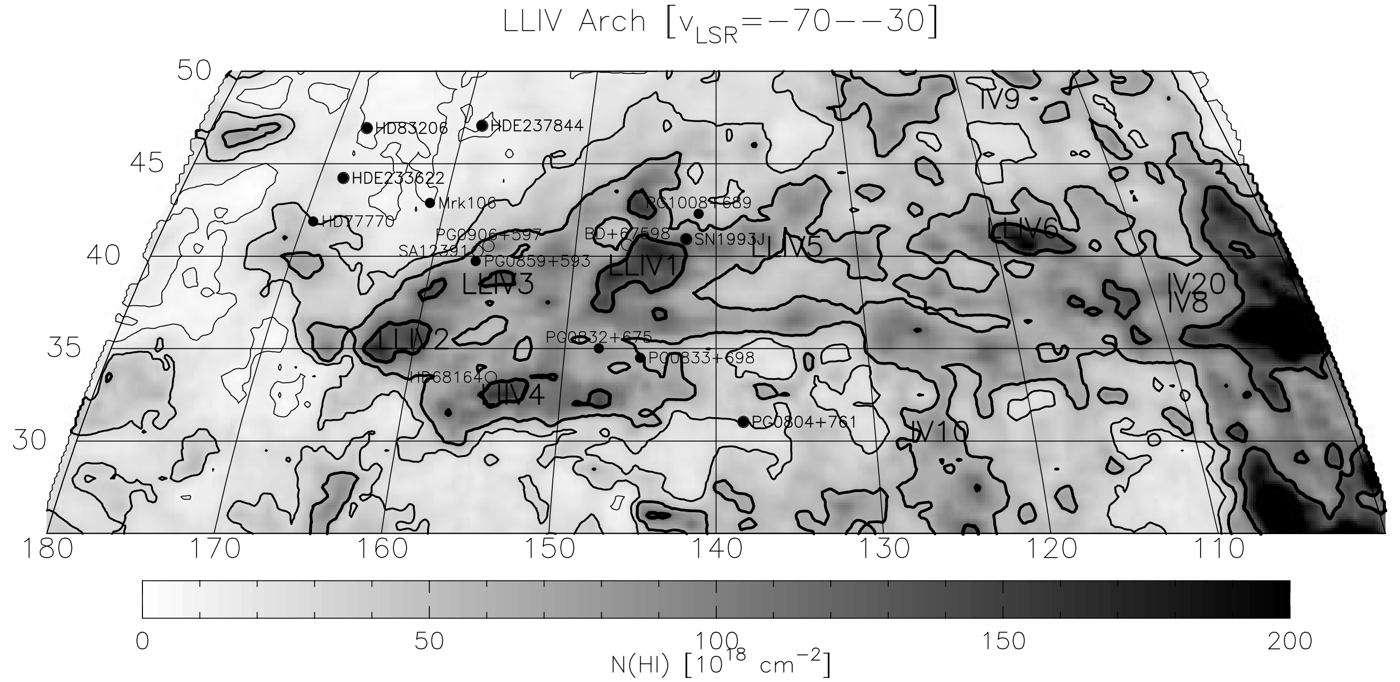

FIG. 15.—Map of the low-latitude intermediate-velocity arch, from Hartmann & Burton (1997). Contours are at 10, 40, and 80 × 10^{18} cm^{-2}. The core names are shown, as are the positions of probe stars. Closed symbols refer to detections, open symbols to nondetections. Note that HVC complex A lies between the probes Mrk 106 and PG 0804+761.

12–14 ppb, while "outliers" are 17 and 9.1 ppb. The only really deviating value is 2.5 ppb for the weaker component in the spectrum of PG 0833+698. However, for this probe the decomposition of the H I spectrum is somewhat suspect.

Intermediate-velocity O VI and C IV are also found toward PG 0804+762 and SN 1993J, respectively (Richter et al. 2001a; de Boer et al. 1993). Thus, the LLIV Arch appears to be a near-solar metallicity cloud, with a substantial H^+ fraction, disklike dust, embedded in hot gas, and located in the interarm region between the Local and Perseus spiral arms. Its velocity is 20–30 km s^{-1} more negative than expected from differential galactic rotation.

All these characteristics are typically those expected for a cloud that is part of the return flow of the Galactic Fountain. That is, gas that was ejected into the Galactic Halo from inside the solar radius is expected to have a metallicity slightly above that in the local ISM, the dust is expected to survive in the hot phase, the rotational velocity is expected to decrease as the gas rises and moves outward (because of conservation of angular momentum; Bregman 1980), and after condensations grow they will remain embedded in the as-yet uncooled part of the gas.

4.27. *Complex K*

This object was first seen in 21 cm emission by Kerr & Knapp (1972) in the direction of M13. De Boer & Savage (1983) detected Mg II toward the star Barnard 29 in M13. Figure 17 shows the gas between velocities of −95 and −60 km s^{-1} in this region of the sky, based on the Leiden-Dwingeloo Survey (Hartmann & Burton 1997). Below latitudes of 45°, the velocity of the peak is less than −70 km s^{-1}, and those components were included in the survey of Hulsbosch & Wakker (1988), and considered part of complex C. However, they stand out from the main body of C, although near $l \sim 80°$ the components merge and it is difficult to assign them to either C or K. Here complex K is defined as the intermediate-velocity gas with $-95 < v_{LSR} < -60$ km s^{-1} in this region of the sky. A better definition requires detailed component fitting.

From differential galactic rotation, velocities in the range from 0 to +30 km s^{-1} are expected, whereas complex K has $v_{LSR} \sim -80$ km s^{-1}. Thus, it rotates too slowly by about 100 km s^{-1}. A metallicity measurement is required to determine whether this is an infalling cloud, such as complex C, or whether it is a Galactic Fountain-type cloud.

Haffner, Reynolds, & Tufte (2001) detect faint Hα emission (0.1–0.2 R) associated with complex K. The Hα emission map correlates very well with the H I column density map for the fainter extended part and for the minor cores. However, in the brightest core (near $l = 55°$, $b = 38°$) the Hα peaks east of the H I.

Shaw et al. (1996) mapped the H I at high angular resolution (3′ × 2′) in the direction of the globular cluster M13, using a combination of Jodrell Bank and DRAO data. They found variations of a factor 2 on arcminute scales. They also observed Na I toward several stars, giving three detections (at 45, 14, and 13 ppb) and six upper limits (<5 ppb). Clearly, there are large variations in the Na I abundance on arcminute scales.

The Mg II and Na I, detections toward stars in M13 set an upper limit to the distance of K of 6.8 kpc, and a mass limit of less than 7.5 × 10^5 $M_\odot$.

Toward Mrk 501 the abundance of Ca II is found to be 89 ppb, although with large errors. There are 31 PG stars with a range of distances that lie projected onto the main core of complex K at $l = 55°$, $b = 35°$, but for none of these has a

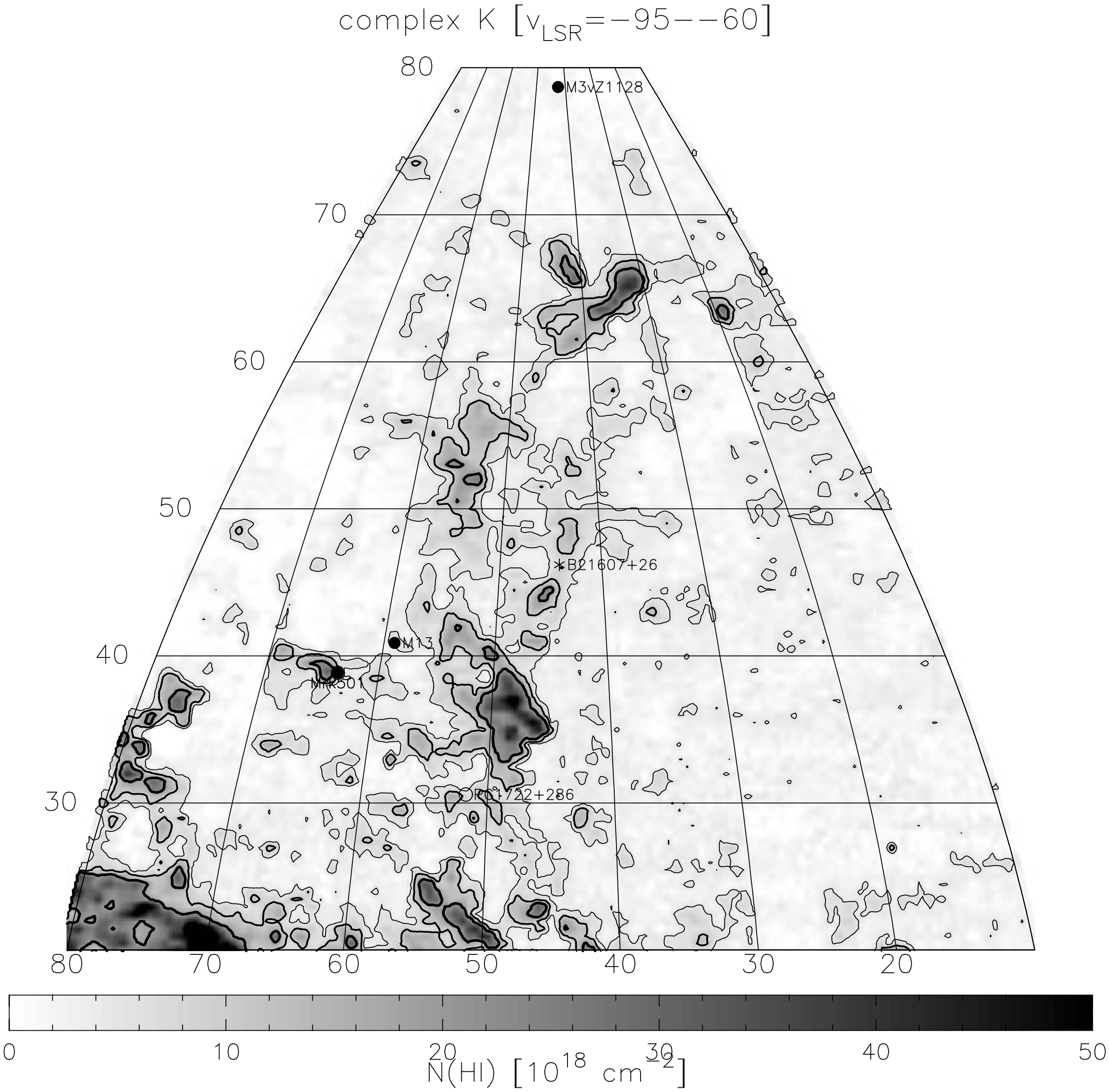

FIG. 16.—Map of complex K, from Hartmann & Burton (1997). Contours indicate column densities of 5, 10, and 20 × 10^{18} cm^{-2} for gas in the velocity range −95 to −60 km s^{-1}. The open symbols show the positions of the probes with nondetections, closed symbols refer to detections.

Ca II spectrum yet been taken. Clearly, a good distance determination is possible. However, since N(H I) is low, spectra with high signal-to-noise ratio will be necessary.

For the star M3 vz1128 ($l = 42°$, $b = 79°$, shown on Fig. 17) de Boer & Savage (1984) claimed strong C II absorption at a velocity of −70 km s^{-1}, although no associated H I is seen. Recent data from *FUSE* do not show this absorption in the C II λ1036 and other strong lines (J. C. Howk 2000, private communication). Thus, the claim by de Boer & Savage (1984) turns out to have been spurious.

4.28. *Southern Intermediate-Velocity Clouds*

At velocities between −85 and −45 km s^{-1} the southern Galactic sky contains a number of IVCs in the region between galactic longitudes 60° and 150°, as shown in Figure 18. Note that by placing the gas in the outer Galaxy, velocities up to −40 km s^{-1} can still be understood within the framework of differential galactic rotation for latitudes greater than −40°, and longitudes 90°–150°. High-velocity gas with $v_{LSR} < -100$ km s^{-1} also occurs in this area, as shown by the thick solid outlines (see figure caption for details).

These southern IVCs have not been studied, with the exception of the HD 215733 sight line, which was analyzed in great detail by Fitzpatrick & Spitzer (1997). This sight line shows intermediate-velocity absorption at −92, −56, and −43 km s^{-1}. The first of these is very weak in H I. The H I spectrum shows a single component centered at −44 km s^{-1}. Fitzpatrick & Spitzer (1997) decomposed it based on the UV absorption lines. The components can be associated with an Arch running through the constellations Pegasus and Pisces ($l = 90°$, $b = -40°$ to $l = 130°$, $b = -60°$). Here and elsewhere in the paper this structure is referred to as the Pegasus-Pisces Arch, or the PP Arch. Although much weaker, this is the closest southern counterpart to the IV Arch in the north.

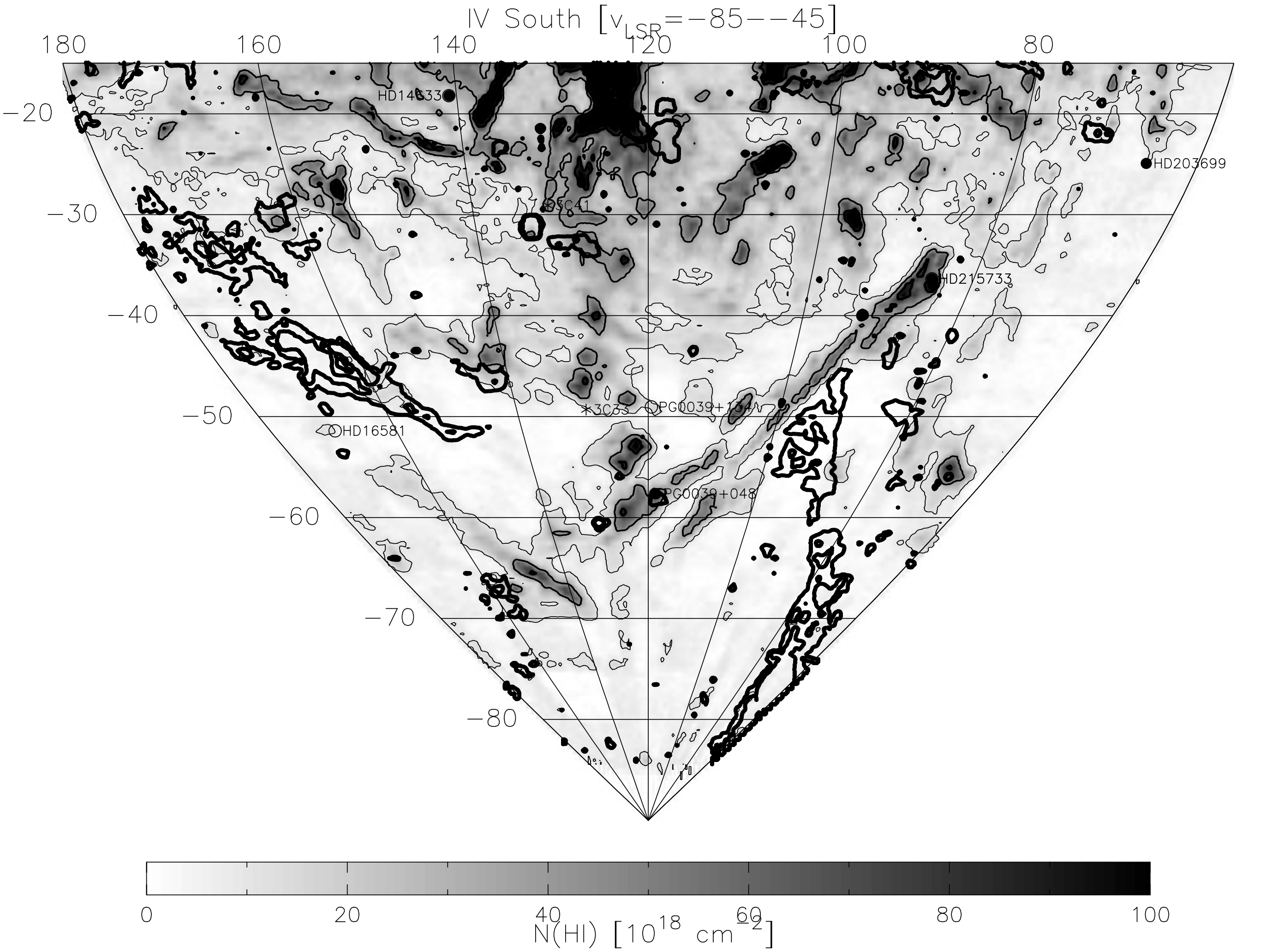

FIG. 17.—Map of southern IVCs, from Hartmann & Burton (1997). Contour levels are at 10, 40, and 80 × 10^{18} cm^{-2} for the gas with velocities relative to the LSR between −85 and −45 km s^{-1}. Closed symbols refer to detections, open symbols to nondetections. Thick solid lines outline the gas with $v_{LSR} < -85$ km s^{-1} and are contour levels at 15 and 40 × 10^{18} cm^{-2}. The following HVCs can be seen: the Cohen Stream and WW507 at $l = 160°$, $b = -45°$, the Magellanic Stream ($l \sim 80°$, $b < -50°$), the VHVC near M33 ($l = 125°$, $b = -30°$), and complex G ($l = 90°$, $b = -15°$). The features at $l = 120°$, $b = -20°$ and $l = 134°$, $b = -31°$ are M31 and M33.

Individually, the absorption components toward HD 215733 have S II/H I ratios of 0.17, 0.32, and 1.2 times solar, but when combined this is 0.54 ± 0.04 times solar. As Fitzpatrick & Spitzer exclude a large ionization correction, this is clearly subsolar. Together with HD 93521, the depletion pattern in these two components (see Figs. 3*n*, 3*p*, and 3*r*) *defines* the halo pattern.

From HD 215733 an upper distance limit of 2.7 kpc can be set to the northern knot of the Pegasus-Pisces Arch, or $z < 1.6$ kpc. For the southern part, PG 0039+048 seems to set an upper limit of 1.1 kpc, as Na I absorption is seen in its spectrum (Centurión et al. 1994). However, this component is only seen in the line wing and a more accurate measurement is needed.

Using the distance limit implied by PG 0039+048 and integrating the LDS data in the velocity range between −85 and −45 km s^{-1} sets an upper mass limit of about 0.5 × 10^5 $M_\odot$.

4.29. *Complex gp*

The IVC centered on $l = 65°$, $b = -27°$ was the first IVC detected in absorption, against the globular cluster M15 (Cohen 1979). A Leiden-Dwingeloo Survey map of the intermediate-velocity gas in this area shows a large number of scattered, faint IVCs (see Table 2). These seem to be an extension toward lower velocities of HVC 40−15+100, which is also known as the Smith cloud (Smith 1963), or as the main cloud in complex GP (Wakker & van Woerden 1991). This shows up prominently at $l = 35°$–$50°$, $b > -25°$. The IVCs between +60 and +90 km s^{-1} seem to extend complex GP toward more negative latitudes and velocities. Hence, these IVCs will be collectively referred to as "complex gp." Here it is worthwhile to note that at velocities between +30 and +60 km s^{-1} there are no coherent structures in this region of the sky. Differential galactic rotation can account for about 20–40 km s^{-1} of the observed radial velocity.

The detection of the IVC toward HD 203664 sets an upper distance limit of 4.3 kpc ($z < 2.0$ kpc), while the nondetection of the IVC toward HD 203699 sets a lower limit of 0.8 kpc ($z > 0.3$ kpc) (Albert et al. 1993; Little et al. 1994; Ryans et al. 1996; Kennedy et al. 1998). A rough integration of the LDS data in the velocity range between +55 and +100 km s^{-1} then gives a mass range of 0.1–3 × 10^5 $M_\odot$

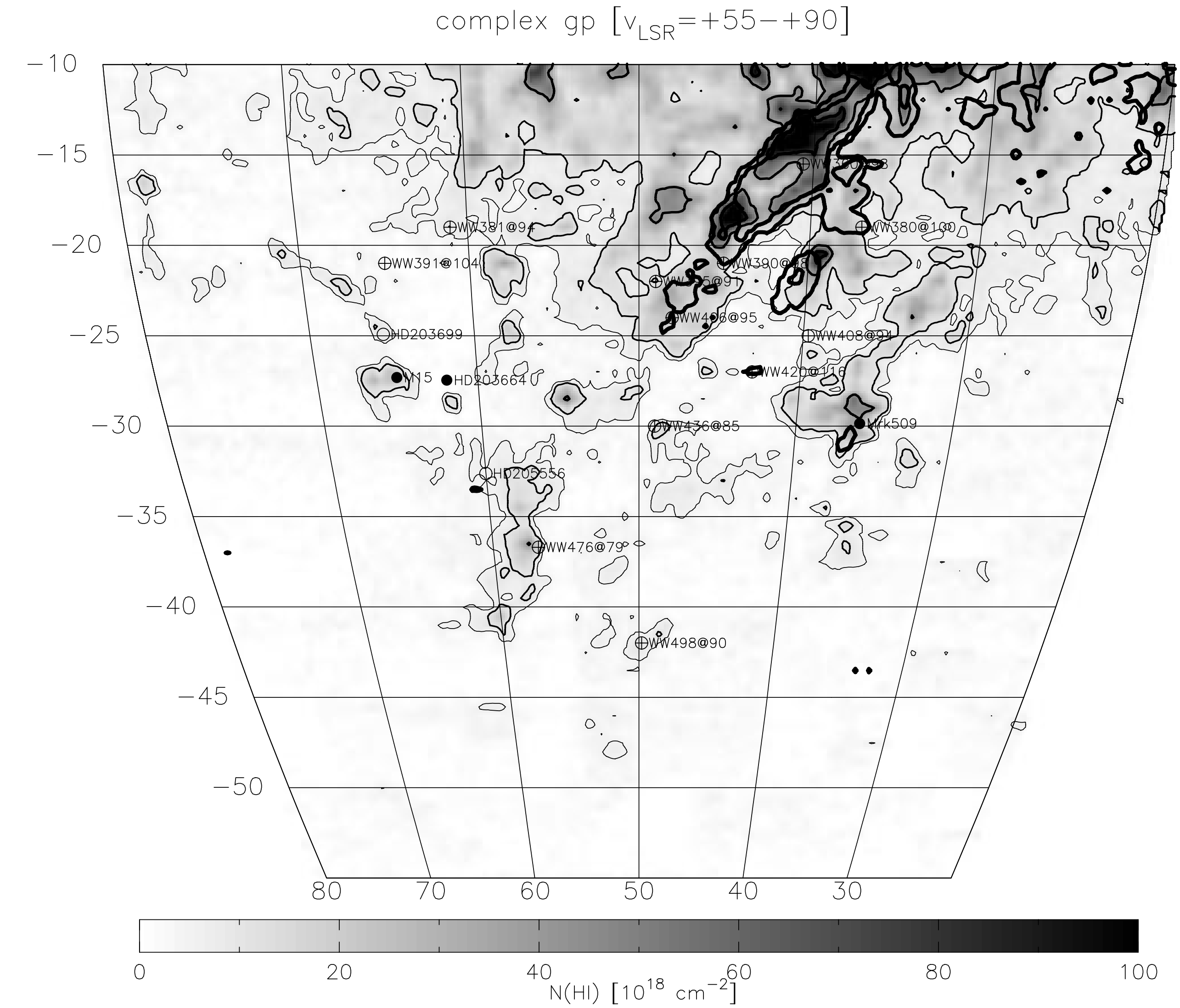

FIG. 18.—Map of the positive-intermediate-velocity gas in the region near HVC complex GP, from Hartmann & Burton (1997). The gray scale and contours show the gas with velocities between +50 and +200 km s^{-1}, with contour levels at 5, 10, 40, and 80 × 10^{18} cm^{-2}. The positions of probes are show. Closed symbols refer to detections, open symbols to nondetections. The thick contours show the gas with $v_{LSR} > +90$ km s^{-1}, i.e., HVC 40−15+100 (also known as the "Smith cloud"). The positions of the other WW clouds within complex GP are also shown, with a label of the form "WW#@v," where "WW#" is the catalog number of Wakker & van Woerden (1991) and "v" the velocity in that catalog.

for the intermediate-velocity gas. Compare this to the mass of the higher velocity gas (i.e., complex GP, § 4.11), which for the same distance limits would have a mass of 0.3–8 × 10^5 $M_\odot$. Thus, if they are related, the high-velocity gas has about twice the mass of the intermediate-velocity gas.

An detailed study of the metallicity of this cloud has not yet been made. However, Penton et al. (2000) list equivalent widths for S II $\lambda\lambda$1250, 1253 in the direction toward Mrk 509. These imply an S II/H I ratio of 2.0 solar. Sembach et al. (1999) show the spectrum in more detail, and from this it is clear that the numbers given by Penton et al. (2000) are a factor 2 too high and that a better abundance estimate is 0.8 solar. Since N(H I) for the +60 km s^{-1} component toward Mrk 509 is only about 24.5 × 10^{18} cm^{-2}, it seems likely that a substantial ionization correction is needed. However, even if that is a factor 2, a near-solar metallicity is implied. As Mrk 509 is one of the brightest AGNs in the UV, a good study of abundances and ionization will be possible with *FUSE*. Na I, Si II, and Ca II toward Mrk 509 were already measured by York et al. (1982), Blades & Morton (1983), and Morton & Blades (1986).

Bland-Hawthorn et al. (1998) detected Hα emission from two positions within the Smith cloud, and they proposed that complex GP is a tidal stream related to the Sagittarius dwarf galaxy, at a distance on the order of 25 kpc. This is difficult to reconcile with the upper distance limit of 4.3 kpc for the IVC, unless the apparent spatial relation between complex GP and the IVCs is accidental.

The intermediate-velocity gas is seen in the spectrum of many stars in the globular cluster M15, the sight line to which intersects one of the four cores of complex gp. Lehner et al. (1999b) measure Ca II toward 12 stars (see § 3.6), finding values in the range 14–79 ppb. Na I was measured by Langer et al. (1990) toward seven stars and was found to be in the range 6–21 ppb. However, Meyer & Lauroesch

(1999) find that Na I varies by a factor 15 across the face of M15. Toward HD 203664 (a few degrees from M15), the Ca II/H I ratio is much higher (440 ppb). However, at the very low N(H I) seen in that direction (2.2×10^{18} cm^{-2}) high Ca II/H I ratios are to be expected (see Wakker & Mathis 2000).

4.30. *Other IVCs*

In 23 sight lines, observations of a probe of an identified HVC or IVC also show absorption and/or H I emission associated with another IVC, usually small and/or faint clouds. These are collected under the heading "Other Negative- (Positive-) velocity IVCs." The data are usually too sparse to learn useful things about these IVCs, except that the abundances tend to be normal.

5. SUMMARY

Table 4 summarizes the distances, masses, metallicities, and depletion patterns discussed in the previous section. The main new conclusions that can be drawn from this table are the following.

1. HVC complex A is the only HVC for which a distance bracket is known, which is 4.0–9.9 kpc ($z = 2.6$–6.8 kpc). It may have a metallicity of about 0.1 solar.
2. Complex M is a grab-bag collection of clouds, which may or may not be physically related. The most likely metallicity of cloud MI is near-solar. Cloud IV4 (or MI-extension) lies at $z = 0.5$–0.7 kpc and has a warm-disk–like depletion pattern. Cloud MII/MIII lies at $z < 3.5$ kpc; a possible lower limit of 1.7 kpc remains controversial.
3. Complex C appears to have a metallicity of $\sim$0.1 solar, based on S II absorption toward Mrk 290 and N I toward Mrk 876. Richter et al. (2001b) report O I/H I = 0.1 solar toward PG 1259+593. S II/H I ratios of 0.3–0.4 solar that have been reported toward two other probes are uncorrected for ionization and H I small-scale structure. The Mrk 876 sight line gives some anomalous abundances, which are most likely due to high partial ionization.

TABLE 4

Summary of Distances and Abundances

Cloud	Distance (kpc)	z-Height (kpc)	Mass ($M_\odot$)	Abundance (Relative to Solar)	A(Ca II) (ppb)	Depletion Pattern
			HVCs			
Complex A	4.0–9.9	2.6–6.8	0.3–2×10^6	0.02–0.4	19 ± 5	Halo??
Core IV4	0.6–0.8(1.8)[a]	0.5–0.7(1.7)[a]	1.5–$2.5(13) \times 10^3$	$\sim$1	3.3 ± 0.9	Warm disk
Cloud MII/MIII	<4.0	<3.5	$<6 \times 10^4$			
Complex C	>1.2(>6.1)[b]	>0.8(>4.3)[b]	$>10^5(>3 \times 10^6)$	$0.089 \pm 0.024^{+0.020}_{-0.005}$	17 ± 5[c]	Halo?
G	>1.3		$5> \times 10^4$			
H	>5.0		$>10^6$			
AC Shell	(>1.5)[d]		$>2 \times 10^5$			
Cloud ACI	(>0.4)		$>1 \times 10^3$			
Cloud ACII	(>0.3)		$>5 \times 10^2$			
Cohen Stream	>0.3	>0.2	$>3 \times 10^2$			
Cloud WW507	>0.3	>0.2	$>4 \times 10^2$			
Complex GP	>0.3	>0.1	$>10^3$			
Mag. Str. (tail)			$>1.5 \times 10^8$[e]	0.33 ± 0.05	27 ± 2	Warm-disk–halo
Mag. Str. (leading arm)			$>5 \times 10^7$[f]	0.25 ± 0.08	69 ± 10	Warm-disk–halo
Complex L	>0.2	>0.1	>20			
Complex WB (WW225)					(280 ± 120)[g]	
Complex WE	<12.8	<3.2	$<2.5 \times 10^5$			
HVC 100–7+110	<1.3	<0.2	<1	$\sim$1?		Halo?
			IVCs			
Upper IV Arch	0.8–1.8(0.8)[h]	0.7–1.7(0.7)[h]	1–$4.5(1) \times 10^5$	$\sim$1	20 ± 9[i]	
Lower IV Arch $l > 150$	0.4–1.9	0.4–1.7	0.4–7.0×10^5	$\sim$1	22 ± 16	Halo
Lower IV Arch $l < 150$[j]	(0.5–0.9)	(0.4–0.8)	0.4–1.2×10^5		23 ± 13	
IV spur	0.3–2.1	0.3–2.1	0.2–8×10^5		22	
LLIV Arch	0.9–1.8(0.9)[k]	0.6–1.2(0.6)[k]	1.5–$6(1.5) \times 10^5$	1.0 ± 0.5	13 ± 1	Warm disk
Complex K	<6.8	<4.5	$<7.5 \times 10^5$	<2.0	(89)[l]	
Pegasus-Pisces Arch	<1.1	<0.9	$<0.5 \times 10^5$	0.54 ± 0.04	24 ± 10	Halo
Complex gp	0.8–4.3	0.3–2.0	0.1–3×10^5	1–2	38 ± 17	

[a] The value in parentheses is valid if the distance to BD +49°2137 is 1.8 kpc, rather than 0.8 kpc (see text).
[b] The value in parentheses is from the weak limit toward BS 16034−0114.
[c] Average of components seen toward Mrk 290 and PG 1351+640.
[d] This limit requires that the Ca II abundance is greater than 20 ppb.
[e] Mass excludes the bridge region ($b > -45°$) near the Magellanic Clouds, and assumes a distance of 50 kpc.
[f] Mass of population EP clouds, assuming a distance of 50 kpc.
[g] From PKS 0837−12, where N(H I) is low, so that A(Ca II) tends to be high.
[h] The upper limit (1.8 or 0.8 kpc) depends on the distance to BD +49°2137.
[i] Average does not include 4.3 ppb toward BD +49°2137 and 150 ppb toward BT Dra.
[j] Excluding IV21, using the lower distance for PG 1255+546 and the higher distance for HDE 233791.
[k] The upper limit depends on whether the gas probed by HD 77770 ($d = 1.2$ kpc) and HD 83206 ($d = 0.9$ kpc) is part of the LLIV Arch or not.
[l] From Mrk 501, where N(H I) is low, so that A(Ca II) tends to be high.

However, N I/H I is consistent with S II/H I. There seems to be little dust in complex C. In that case, the N I, O I, Si II, and Fe II abundance pattern toward PG 1259+593 is consistent with the idea that the heavy elements were produced in Type II supernovae, with no subsequent star formation. Finally, complex C shows the importance and necessity of corrections for ionization and H I fine structure.

4. The strong limit to the distance to complex C is greater than 1.2 kpc, but the distance is probably more than 6 kpc.

5. For the trailing and leading part of the Magellanic Stream S II abundances of 0.33 ± 0.05 and 0.25 ± 0.08 solar are found toward Fairall 9 (Gibson et al. 2000) and NGC 3783 (Lu et al. 1998), consistent with the idea that the Stream is a tidal feature extracted from the SMC (Gardiner & Noguchi 1996).

6. Using the FOS, Savage et al. (2000a) found Mg II absorptions associated with the Magellanic Stream, showing a nearly constant abundance of 0.1 solar when $N(\text{H I}) > 2 \times 10^{18}$ cm^{-2}, but showing larger Mg II/H I ratios at lower N(H I), suggesting increasing ionization.

7. Fe/S was determined for the trailing and leading parts of the Stream, giving values of 0.18 ± 0.06 and 0.13 ± 0.05 times solar. This is comparable to the value in SMC gas and indicates the presence of dust in the Stream.

8. Mg II absorption due to cloud WW84 is seen in the spectrum of Mrk 205. The Mg II abundance remains uncertain, however, due to H I small-scale structure. A(Mg II) could possibly be as low as 0.02 solar.

9. A second upper limit was set to the distance of a HVC: complex WE (which is identified and named in this paper) has $d < 12.8$ kpc, $z < 3.2$ kpc, based on the detection of absorption in the star HD 156359.

10. It is suggested that many small positive-velocity HVCs and the high-positive velocity absorptions without associated H I in the region $l = 180°$–$320°$, $b = 20°$–$70°$ are due to a spread-out leading edge to the leading arm of the Magellanic Stream. These occur in the extension of the curve defined by the SMC orbit and the EP clouds (Fig. 10).

11. For the higher velocity part of the IV Arch a strong bracket of $z = 0.7$–1.7 kpc can be derived. The upper limit depends mostly on the distance to BD $+49°2137$, which may be as low as 0.7 kpc. For the lower velocity IV Arch the strong bracket is $z = 0.4$–1.7 kpc for the part with $l > 150°$. At lower longitudes the situation is confusing, but a possible z-height is 0.4 kpc.

12. The IV Arch appears to have near solar abundances, based on S II/H I ratios of 0.97 ± 0.06, 0.8 ± 0.1, and 1.1 ± 0.2 found toward HD 93521, HD 121800, and PG 0953+414, respectively.

13. A metallicity of $\sim$0.7 solar and a distance of 0.9 kpc ($z = 0.6$ kpc) are known for the LLIV Arch. This object appears to be a prime example of the return flow of a Galactic Fountain: it lies at high z in an interarm region, it is rotating somewhat slower than expected from differential galactic rotation, it has a metallicity similar to that in the local ISM, the depletion pattern is similar to that in warm disk gas, and it is embedded in hot gas.

14. IVC complex K is newly defined in this paper, as IVC components with $v_{\text{LSR}} \sim -80$ km s^{-1} near $l = 50°$. It has a distance less than 6.8 kpc ($z < 4.5$ kpc), and many potentially useful targets exist. It is notable for a strong correlation between Hα emission and H I column density (Haffner et al. 2001).

15. The PP Arch is the best southern counterpart to the IV Arch in the northern Galactic hemisphere. An upper distance limit of 2.7 kpc ($z < 1.6$ kpc) can be set for the northern part, and of 1.1 kpc ($z < 0.9$ kpc) for the southern part. A metallicity of 0.5 solar is derived. This object deserves further study.

16. Positive-velocity IVCs near $l = 50°$, $b = -25°$ may be related to HVC complex GP (also known as HVC 40−15+100 or as the "Smith cloud"). Some of the IVCs lie in the distance range 0.8–4.3 kpc ($z = 0.3$–2.0 kpc) If the IVCs and complex GP are related, this excludes the suggestion by Bland-Hawthorn et al. (1998) that complex GP is a tidal stream connected to the Sagittarius dwarf. Complex gp is probed by the bright UV probe Mrk 509, toward which S II absorption suggests an abundance of 1–2 times solar.

17. The metallicity of HVCs and IVCs ranges from 0.1 to 1 solar. The most accurate value (0.089 times solar) is for complex C. For complex A $\sim$0.1 solar is suggested. The Magellanic Stream (both the trailing and the leading arms) has Magellanic-like abundances (0.25 solar for sulfur). IVCs tend to have higher metallicities: the PP Arch has $Z \sim 0.5$ solar, the LLIV Arch has $Z \sim 0.8$ solar, while the IV Arch has $Z \sim 1$ solar. Thus, the classical HVCs A and C most likely represent material that has never before been part of the Milky Way and is now being accreted (see Wakker et al. 1999a, 1999b for more discussion). The IVCs, on the other hand, consist of Galactic gas. It is an open question which clouds are previously hot halo gas compressed by infalling material, and which are part of the return flow of a Galactic Fountain. For the LLIV Arch the second possibility is preferred.

18. Very little information exists on dust in HVCs. The Magellanic Stream shows the pattern typical for halo gas. In complex C there are indications for a lack of dust, based on the ratio Fe II/H I = 0.5 solar toward Mrk 876. Since S/H = 0.1, a halo-like ratio of Fe/S = 0.25 would require $N(\text{H}^+)/N(\text{H I}) > 20$, which is incompatible with the other absorption lines and the nondetection of Hα emission (Murphy et al. 2000).

19. The IVC depletion pattern varies from that typical for warm disk gas (IV4, LLIV Arch) to that typical of halo gas (IV Arch, PP Arch).

20. Only one HVC distance bracket is known (4–10 kpc for complex A). An upper limit of $<$12.8 kpc was set for complex WE, and lower limits of $>$6 and $>$5 kpc exist for complexes C and H. In contrast, several IVC distance brackets were set. Expressed as z-heights, these tend to be about 0.5–1.5 kpc. Thus, the major IVCs appear to be a rather local phenomenon, whereas the major HVCs appear to be large clouds away from the Galactic plane.

21. For the large IVCs (IV Arch, LLIV Arch, PP Arch), mass limits typically are 0.1–8×10^5 $M_\odot$, whereas for the larger HVCs mass limits typically are greater than 10^6 $M_\odot$ (with an upper limit of 2×10^6 $M_\odot$ for complex A). The Magellanic Stream is the most massive HVC, having $M > 10^8$ $M_\odot$. Thus, the major HVCs (A, C, H, MS) appear to be more massive than the major IVCs.

22. The abundance of Ca II tends to vary by a factor 2–5 within clouds and by a factor 5–10 between clouds. At any given value of N(H I), N(Ca II) can vary by a factor 10. Nevertheless, a strong correlation is found between the Ca II abundance and N(H I), which is discussed in more detail by Wakker & Mathis (2000).

23. The abundance of Na I varies by a factor 100 for a given N(H I), and by a factor of more than 10 within a single cloud. No correlation is seen between log N(Na I) and log N(H I), showing that for HVCs and IVCs N(Na I) is an even worse predictor of N(H I) than it is for low-velocity gas.

24. It is possible to use Ca II to set lower limits to cloud distances, but this requires (a) knowledge of the Ca II abundance in the cloud, (b) sight lines with sufficiently high N(H I) ($>5 \times 10^{18}$ cm^{-2}), and (c) sufficiently sensitive observations of the Ca II lines. For Na I the safety factor required to interpret a nondetection as a lower limit is prohibitively large and in practice nondetection of Na I should not be considered significant.

This research has made extensive use of the SIMBAD database, operated at CDS, Strasbourg, France.

APPENDIX

DESCRIPTION OF THE COLUMNS

A1. COLUMN (1)

Column (1) gives the name of the stellar or extragalactic probe. In most cases this is the name given in the publication (see col. [19]). In a few cases the HD, BD, or PG number is substituted, most notably for the SAO stars in Lilienthal, Meyerdierks, & de Boer (1990) and Tamanaha (1997), for HZ 22 (=PG 1212+369), HZ 25 (=BD +36°2268), and AG +53 783 (=HDE 233791) in Ryans et al. (1997a), and for H.O. +23B (=PG 1205+228) in Kuntz & Danly (1996) (a revised distance was also determined for the latter star by Quinn et al. 1991). In the case of extragalactic objects, an effort was made to use the names in the Véron-Cetty & Véron (1996) catalog of QSOs and Seyfert galaxies, even if a different name was used in the absorption-line publication.

A2. COLUMNS (2) AND (3)

Columns (2) and (3) give the galactic longitude and latitude of the probe, rounded to 1/100th of a degree. For more accurate values, see SIMBAD or the original publication.

A3. COLUMNS (4) AND (5)

Column (4) gives the distance to the star and the distance error, in kiloparsec. This is followed by a flag that indicates the method used to make the estimate. Column (5) shows the z-height in kiloparsec, derived as d sin (b). The following flags are used.

"p".—Distance is 1/parallax, as measured by *Hipparcos*, and as given in SIMBAD. This is used if the parallax is known to better than about 30%. The distance error is calculated from the given parallax error, using $\Delta d/d = \Delta p/p$. Usually, the resulting distance is consistent with the spectroscopic distance (see below, under flag "t") to within 0.1 kpc. The most notable exception is HD 135485 (type B5 IIp), which was estimated to be at 2.5 kpc by Albert et al. (1993) and at 0.8 kpc by Danly et al. (1995), but whose parallax puts it at 0.18 kpc.

"a".—Distance determined from a detailed atmospheric analysis based on intermediate-resolution spectroscopy. For 22 PG stars, the distance values are taken from Moehler et al. (1990), Theissen et al. (1995), Wakker et al. (1996a), and Ryans et al. (1997a, 1997b). In the latter paper three non-PG stars were also analyzed (BD +38°2182, BD +49°2137, and HDE 233781). The nominal errors (as given in the publications above) are typically 0.3–0.4 kpc. In some cases the spectral analysis is difficult because the star may be either a HB or a post-AGB star. In this case, the actual uncertainty is much larger than the formal uncertainty. In particular, PG 0832+675 was at some point thought to be a main-sequence B1 V star at 31 kpc (Brown et al. 1989), but Hambly et al. (1996) found it to be an evolved star at 8.1 kpc, which is what is used here.

"g".—For stars in globular clusters and in the LMC, the distance is the distance to the cluster or to the LMC. Globular cluster distances are taken from Harris (1996). The LMC is assumed to be at a distance of 50 kpc.

"s".—Distance determined from the spectral type, which yields the absolute magnitude of the star. An extinction correction is applied, using the map of Lucke (1978), which gives the average A_V out to 2 kpc in mag kpc^{-1} for 5° × 5° regions on the sky. Except for stars on complex H and clouds AC0 and ACI, the extinction estimates always are below 0.2 mag. A distance calculation is done even if the original reference gives a spectroscopic distance, so that all distances are calculated on the same absolute-magnitude system. The differences between published and recalculated values are usually less than 10%.

For RR Lyrae stars, $M_V = 0.58$ is assumed, based on recent calibrations of their absolute magnitude (Fernley et al. 1998). A 10% error is assumed, which corresponds to 0.2 mag.

For confirmed horizontal branch stars that have not been subjected to a detailed analysis (PG 1126+468, PG 1510+635, PG 1008+689, and PG 1343+577) it is assumed that M_V is in the range 0.55–1.15 (Preston, Shectman, & Beers 1991). The average of these two values gives the most likely distance. The distance error is found as half of the range implied by the range in M_V. Five probes of complex C are probably also horizontal branch stars, and the M_V-values above are also used; better classifications are needed to confirm their status.

For stars with an MK classification the table of Straizys & Kurilene (1981) is used to convert from spectral type to M_V. The resulting distances are normally within 0.2 kpc of estimates made for the same star by other authors. The (1 σ) distance error is estimated by also calculating the distance using a classification that differs by one subtype and one luminosity class. This gives a maximum range for the distance, which is assumed to be equivalent to $\pm 3\ \sigma$. For main-sequence stars, as well as for all

O-type stars, the typical error is less than 10%. Large relative errors (10%–100%) occur for (super)giant A and B stars, where a difference of one luminosity class can make a difference of 2 mag in the estimated absolute magnitude.

"t".—The spectroscopic distance is given, even though the parallax was measured by *Hipparcos*. However, the measured parallax is more uncertain than the spectroscopic distance.

"r".—Distance given is value quoted in reference, as the spectral type is not well specified in SIMBAD or the reference, and thus the distance cannot be recalculated on the same system as for other stars. This is the case for BD $+10°2179$ and H.O. $+41$B.

A4. COLUMN (6)

Column (6) gives the classification of the probe. This can be an MK spectral type, "sd" for subdwarfs (sometimes with subtype), "HB" for confirmed horizontal branch stars, "(HB)" for suspected horizontal branch stars, "PAGB" for post–asymptotic giant branch, "SN" for extragalactic supernovae, as well as the obvious "RR Lyr," "QSO," "BL Lac," "Sey," or "Gal." "radio" is used for 21 cm or 3 mm continuum sources where high-velocity H I absorption has been searched for.

A5. COLUMN (7)

Column (7) gives the name or number of the HVC/IVC on which the probe is projected. For IVCs in the IV and LLIV Arch, the core numbers in the catalog of Kuntz & Danly (1996) are used. For stars that probe the IV Arch away from its cores "IVa" is given. The HVC names and numbers are from the catalog of Wakker & Woerden (1991). For clouds outside complexes the catalog number is preceded by the acronym "WW." One new HVC complex and three new IVC complexes are introduced in this paper: "WE," "K," the "PP Arch," and "gp"—see §§ 4.19, 4.27, 4.28, and 4.29.

A6. COLUMNS (8) AND (9)

Columns (8) and (9) show the best value for the H I velocity and column density in the direction of the probe. The velocity is given in km s^{-1}, relative to the LSR. The column density and its error are given in units of 10^{18} cm^{-2}. Upper limits are 5 σ. If there is absorption, but no corresponding H I component was detected, the value within parentheses refers to the velocity at which an upper limit to the H I column density is set. For all probes, the H I spectrum and Gaussian fits to the components are shown in Paper II.

For a few probes the Ca II and/or Na I absorption spectra show multiple components, although only one H I component can be discerned, When these are closer together than half the FWHM of the H I spectrum, the H I column density is split in two, assuming that the ion abundance in both components is the same. This results in two H I components listed at the same velocity, suffixed by "a" and "b" for BD $+49°2137$ (IV17), BD $+38°2182$ and BD $+36°2268$ (Lower IV Arch), PG 1008+689 (LLIV Arch), HD 203664 (complex gp), as well as for seven stars in the LMC.

A7. COLUMN (10)

Column (10) shows a code that shows the telescope used to measure the H I column density. In general, the value determined at the highest available resolution is used, as (especially in cores) H I fine structure can produce variations of a factor of a few at arcminute scales (Wakker & Schwarz 1991; Wakker et al. 1996a). The following codes are used.

We.—*N*(H I) from a combination of Westerbork and Effelsberg data (1′ or 2′ beam), derived as described by Wakker et al. (1996a). This was done for 5 probes (Mrk 106, PG 0832+675, PG 0859+593, PG 0906+597, Mrk 290).

Ws.—*N*(H I) from a Westerbork map only (0159+625 in complex H).

AP.—*N*(H I) from a combination of ATCA and Parkes data (1′ beam). This was done for NGC 3783 and HD 101274 (Lu et al. 1998).

WJ.—*N*(H I) from a combination of Westerbork and Jodrell Bank data (2′ beam). This was done for HD 135485 and 4 Lac by Stoppelenburg et al. (1998).

JD.—*N*(H I) from a combination of Jodrell Bank and DRAO (2′) data. This was done for the stars in M13 (Shaw et al. 1996).

Ar.—*N*(H I) from a spectrum taken at Arecibo (3′ beam). This is the case for 20 probes in the H I absorption studies of Payne et al. (1980), Colgan et al. (1990), and Akeson & Blitz (1999).

Ef, ef.—*N*(H I) derived from a spectrum taken at Effelsberg (9$'.$1 beam). For 9 probes in complexes A, C, H, and K this is a published value (code "ef") (Lilienthal et al. 1990; de Boer et al. 1994; Centurión et al. 1994). For 113 other probes new spectra were taken with Effelsberg (code "Ef"; see Paper II).

JB.—*N*(H I) derived from a published spectrum taken with the Jodrell Bank Mark III telescope (12′ beam). New Gaussian fits were made to six of the probes in Ryans et al. (1997a, 1997b), for which no Effelsberg spectrum was obtained (see Paper II). These usually agree with the published values, except when the intermediate-velocity H I component is in the line wing.

Pk.—*N*(H I) based on an observation at Parkes (15′ beam). This is the case for 112 stars.

PN.—*N*(H I) from a fit to a spectrum extracted from the Parkes Narrow Band Survey (Haynes et al. 1999, 10 sight lines). These spectra are presented in Paper II.

PK.—*N*(H I) from a fit to a spectrum extracted from the Parkes Multibeam Survey (HIPASS) (Staveley-Smith 1997). These four spectra are presented in Paper II.

GB.—*N*(H I) derived from an observation with the Green Bank 140 foot telescope (21′ beam). For 14 extragalactic sources this is a deep observation done by Murphy (detection limit $\sim 3 \times 10^{17}$ cm^{-2}), see summary in Savage et al. (2000a). For three stars (HD 86248, HD 137569, and HD 100340) values were taken from Danly et al. (1992) and Albert et al. (1993). Finally, for HD 93521 and HD 215733 the component fits of Spitzer & Fitzpatrick (1993) and Fitzpatrick & Spitzer (1997) were used.

PI.—For some LMC stars, N(H I) is found from an interpolation between the value toward SN 1987A (see code "AB" below) and Parkes observations toward Sk $-69°246$ and position JM43 in McGee & Newton (1986).

PR.—For some LMC stars, N(H I) in the $+165$, $+120$, and $+65$ km s^{-1} clouds was found by using a ruler on the plot of Wayte (1990). These numbers are therefore not very reliable.

HC.—For SN 1991T a special 24 hour integration was done at Hat Creek (see Paper II), in order to achieve a 5 σ upper limit of 3×10^{17} cm^{-2}.

Dw.—For 67 sight lines, N(H I) is based on an interpolation between gridpoints in the LDS (Hartmann & Burton 1997) (36′ beam). That atlas gives the spectrum on every half degree in galactic longitude and latitude. Therefore, for each velocity channel a weighted average was constructed using the four gridpoints surrounding the direction to the probe; the weights are given by max $(0, 0.5-R)$, where R is the distance to the nearest gridpoint in degrees.

VE.—For HD 156359 the limit of 2×10^{18} cm^{-2} is based on the fact that Morras et al. (2000) do not list a component at this position, as determined from observations with the IAR telescope at Villa Elisa.

AB.—No H I observation directly centered on SN 1987A has been published. Welty et al. (1999) derived the value of N(H I) for each spectral component from the abundance pattern of absorption, combined with the likely abundance of undepleted elements. In particular, if solar abundance (from Anders & Grevesse 1989) and standard halo depletion (from Savage & Sembach 1996a) are assumed, an implied N(H I) can be derived from the column densities of Mg II, Al II, Si II, Mn II, and Fe II. This yields column densities of 8.0 ± 2.5 and $5.4 \pm 1.9 \times 10^{18}$ cm^{-2} for the components at $+120$ and $+165$ km s^{-1}, respectively, which are consistent with the N(H I) measured half a degree away by McGee & Newton (1986) in the directions toward Sk $-69°246$ and their position "JM43." Using this method for the IVC yields $N(\text{H I}) = 31 \pm 6 \times 10^{18}$ cm^{-2}, a factor 5 higher than the H I spectrum would suggest, indicating either no depletion, low abundance or a high ionization fraction in this cloud. The analysis of Welty et al. (1999) does not definitively allow a choice between these three possibilities. Here a column density of 6.5×10^{18} cm^{-2} will be used, which is the average of the 6.1 and 7.1×10^{18} cm^{-2} observed half a degree away.

ab.—In the H I spectrum of 3C 123 three absorption components are seen, but only one emission component. Except for the main component, the absorption column density is therefore given in column (13).

md.—For Mrk 509 and PKS 2155$-$304, Sembach et al. (1999) use the Green Bank 140 foot telescope and find that N(H I) is less than 6×10^{17} cm^{-2}. A photoionization model is used to convert the observed column densities of several ions (C IV, C II, Si III) to a most likely value for $N(\text{H}) = N(\text{H I}) + N(\text{H}^{+})$. This depends on the assumed metallicity, which may be in the range 0.1–1 times solar. For these two exceptional sight lines, the value in column (9) therefore is the total hydrogen column density, with an "error" expressing the possible range.

A8. COLUMN (11)

Column (11) shows the ion observed in absorption. Some entries between "(" (in col. [11]) and ")" (in col. [19]) refer to measurements superseded by a more recent reference.

A9. COLUMN (12)

Column (12) gives the velocity (relative to the LSR) of the measured absorption line.

A10. COLUMN (13)

Column (13) gives the column density (and error or upper/lower limit) for the observed ion, in units of 10^{11} cm^{-2}.

A11. COLUMN (14)

Column (14) shows a code showing how the column density was derived.

"N".—Column density quoted in reference. This is sometimes derived from assuming a linear relation between equivalent width and column density, but in many cases from a fit to the apparent optical depth profile or a curve of growth.

"L".—The logarithm of the column density was given in the reference. In this case the errors are usually given as logarithmic errors. These are converted to a linear error by calculating $[\text{dexp}\,(L+\delta) - \text{dexp}\,(L-\delta)]/2$, where L is the logarithmic column density and δ the logarithmic error. For example, $\log(N) = 11.25 \pm 0.15$ indicates a range of 1.3–2.5×10^{11} and becomes $N = 1.8 \pm 0.6 \times 10^{11}$.

"W".—The equivalent width is given in the reference. This is converted to a column density by assuming that the gas temperature is 7000 K and using this to calculate the turbulent width from the observed H I line width $[W(\text{H I})]$: $v_{\text{turb}} = [W(\text{H I})^2 - W(T)^2]^{1/2}$, where W(T) is given by $[8 \ln 2kT/m(\text{H})]^{1/2}$. The width of the absorption line for the ion is then found as $W(\text{ion}) = \{W[T, m(\text{ion})]^2 + v_{\text{turb}}^2\}^{1/2}$. Then the formula for the equivalent width ($EW = \int 1 - \exp[-\tau(v)]$) is inverted, assuming $\tau(v)$ is Gaussian. If the H I line width is less than $W(7000) = 17.9$ km s^{-1}, $v_{\text{turb}} = 0$ and a lower temperature are assumed and a "V" is added to the notes column (this happens in eight directions). If the H I line width was not measured (four directions as well as all LMC sight lines), a value of 30 km s^{-1} is assumed, and a "W" is added to the notes column. Note that the derived column density is not very sensitive to the assumed temperature for weak lines.

"E".—Detection inferred from large equivalent width. This is the case for 21 extragalactic sources observed with the FOS (Burks et al. 1994; Savage et al. 2000a). That is, when expressed as a velocity width, the equivalent width of the Mg II or C II absorption line is as large or larger than the total width of the H I 21 cm line, including the HVC.

"S".—Upper limit to column density derived from a quoted signal-to-noise (S/N) level, which is converted to an equivalent error using the error formula for fitting a Gaussian given by Kaper et al. (1966): $\sigma(W) = (\lambda/c)[3(\pi/8 \ln 2)^{1/2}]^{1/2}(Wh)^{1/2}(1/\text{SN})$, where the observed line width, W, and a grid spacing $h = 8$ km s^{-1} are used.

"τ".—This happens for observations of 21 cm absorption, and the optical depth of the absorption is given. The ion column density column then contains the column density of the absorbing cool H I (but in units of 10^{18} cm^{-2} rather than 10^{11} cm^{-2}).

Note that for rows giving a summary of cloud parameters, this column may give, within square brackets a reference value for the column density of highly ionized atoms (C IV, N V, O VI, and Si IV).

A12. COLUMN (15)

Column (15) shows the ratio N(ion)/N(H I), in units of 10^{-9} (i.e., parts per billion or ppb). In the case of H I absorption the ratio N(H I,absorption)/N(H I, emission) is given. These values should be compared to the expected abundance of the ion, which is given in column (16) in the cloud overview (see § 3).

A13. COLUMN (16)

For rows giving an overview of abundances for a particular cloud, column (16) shows the expected abundance values (see § 3), in square brackets. In the case of complexes A and C all expected abundances are scaled down by a factor 10, as an abundance of 0.089 times solar was found for sulfur in complex C (Wakker et al. 1999a), and an oxygen abundance of $\sim$0.06 times solar was suggested for complex A (Kunth et al. 1994, § 4.1. Both sulfur and oxygen are not or lightly depleted onto dust. For directions toward the Magellanic Stream (both the trailing and leading arms), the expected abundances are scaled down by a factor 4, as indicated by the sulfur abundances found toward NGC 3783 and Fairall 9.

A14. COLUMN (17)

Column (17) gives the derived abundance relative to the solar abundance, given by Anders & Grevesse (1989), with updates for C, N, and O from Grevesse & Noels (1993).

A15. COLUMN (18)

Column (18) shows a flag indicating whether the result gives an upper or lower distance limit. Detections toward stellar probes yield an upper limit (flag "U"). Nondetections may set a lower limit (flags "1" and "L"; see below), but only if it can be shown that the line should have been seen if the probe were behind the cloud. To get to that point, there are several effects to consider.

Fine structure in the H I distribution can lead to variations of up to a factor 5 on arcminute scales in HVC cores (Wakker & Schwarz 1991; Wakker et al. 2001b), although the variations may be less outside cores (Wakker et al. 1996a). For eight probes N(H I) has been observed at 35′, 9′, and 2′ resolution (see Paper II). As the covering factor of the very bright spots is low ($\sim$10% of the surface area of the cloud), an observation with a 10′–20′ beam will usually give a column density accurate to within 50%, i.e., a factor 2. This factor of less than 2 is supported by the results of Savage et al. (2000a). They compared N(H I) measured using Lyα with the value measured in 21 cm emission toward 12 extragalactic probes. The Lyα values are 60%–90% of those measured at 21 cm. A more detailed discussion of the comparison between values of N(H I) derived with different beams is presented in Paper II.

The gaseous abundance of an ion may also vary within a cloud, as both the depletion and ionization can vary. For dominant ions, variations are expected to be small if the H I column density is high, say above 10^{19} cm^{-2}, while for nondominant ions (e.g., Ca II and especially Na I), ionization variations are expected to be large. As discussed in § 3, multiple measurements in the same cloud exist for several ions (mainly Na I, Mg II, S II, Ca II, Fe II). As the quality of these measurements is not always the same, and the H I values are usually derived using different telescopes, no systematic study can be made. Yet, it is clear that for $N(\text{H I}) > 5 \times 10^{18}$ cm^{-2} most ions show variations of at most a factor 3–5 within a single cloud, whereas Na I can vary by a factor 20 for different sight lines through the same cloud (Meyer & Lauroesch 1999; § 3.5).

Thus, to determine whether a nondetection is significant and sets a lower limit to the distance of a cloud, the observed limit is compared with an expected value. This is done in terms of optical depths, since the absorption has to be deep enough to be recognizable. The expected optical depth is calculated by combining the expected column density for the ion in question with the measured H I line width. The expected column density is found as the product of the H I column density and either the measured or the reference abundance (see § 3 and col. [16]).

The expected optical depth is then divided by a safety factor, to account for possible H I small-scale structure and depletion and/or ionization variations. H I small-scale structure introduces a safety factor of 2. For Na I and for strongly depleted elements (atomic numbers >18, except Zn), the depletion safety factor is 2.5; for other elements it is 1.5. The ionization safety factor is 5 for Na I, 2 for other elements, except for C II, Mg II, and O I, where it is 1. For C II this is because the ionization potential of the next ionization stage is high, and C III will only occur where H is (almost) fully ionized. In the case of O I, ionization is not a problem, as O I and H I are coupled through a strong charge-exchange reaction (Osterbrock 1989). A final safety factor of 2 is introduced if the ion abundance had to be assumed. The combined safety factor ranges from 3 for O I, C II, and Mg II for clouds where their abundance has been measured, to typical factors of 10 for Ca II in clouds with known abundance, 12 for Si II and 20 for Fe II for clouds with assumed abundance, and a factor of 50 for Na I if its abundance has not been measured in the cloud.

If the safety-factor–multiplied expected optical depth is larger than the observed lower limit, the nondetection is considered significant enough to set a lower limit to the cloud's distance (flag "1"). If the expected value is more than 3 times larger than the observed limit, the distance limit is considered strong (flag "L").

For HVC complex H and the Anti-Center clouds, no direct abundance measurement exists, but in the framework of the "Local Group model" (Blitz et al. 1999) an abundance of 0.1 times solar is predicted. Therefore, the safety factor needs to be calculated as if the abundance were 1/10th solar.

A16. COLUMN (19)—REFERENCES

(1) Prata & Wallerstein (1967); (2) Wesselius & Fejes (1973); (3) Savage & de Boer (1979); (4) Cohen (1979); (5) Payne et al. (1978, 1980); (6) Blades (1980), Meaburn & Blades (1980); (7) Meaburn (1980); (8) Songaila & York (1981); (9) Songaila (1981); (10) Savage & de Boer (1981); (11) Savage & Jeske (1981); (12) Songaila et al. (1981); (13) York et al. (1982); (14) Blades et al. (1982); (15) de Boer & Savage (1983); (16) Albert (1983); (17) de Boer & Savage (1984); (18) Ferlet et al. (1985a); (19) Songaila et al. (1985); (20) d'Odorico et al. (1985); (21) Kulkarni et al. (1985); (22) West et al. (1985); (23) Songaila et al. (1986); (24) Kulkarni & Mathieu (1986); (25) Morton & Blades (1986); (26) Magain (1987); (27) Vidal-Madjar et al. (1987), Andreani et al. (1987); (28) de Boer et al. (1987); (29) Dupree et al. (1987); (30) Keenan et al. (1988); (31) d'Odorico et al. (1989); (32) Conlon et al. (1988); (33) Songaila et al. (1988); (34) Blades et al. (1988); (35) Meaburn et al. (1989); (36) Molaro et al. (1989); (37) Savage et al. (1989); (38) Lilienthal et al. (1990); (39) Colgan et al. (1990); (40) Wayte (1990); (41) Langer et al. (1990); (42) Bates et al. (1990, 1991); (43) Wakker et al. (1991); (44) Mebold et al. (1991); (45) Sembach et al. (1991); (46) Quin et al. (1991); (47) Meyer & Roth (1991); (48) Robertson et al. (1991); (49) Bowen et al. (1991a, 1991b); (50) Danly et al. (1992); (51) Spitzer & Fitzpatrick (1992); (52) Molaro et al. (1993); (53) de Boer et al. (1993); (54) Sembach et al. (1993); (55) Bruhweiler et al. (1993); (56) Spitzer & Fitzpatrick (1993); (57) Danly et al. (1993); (58) Albert et al. (1993); (59) Kunth et al. (1994); (60) de Boer et al. (1994); (61) Vladilo et al. (1993, 1994); (62) Centurión et al. (1994); (63) Bowen et al. (1994); (64) Lu et al. (1994a); (65) Little et al. (1994); (66) Lu et al. (1994b); (67) Burks et al. (1994); (68) Kemp et al. (1994); (69) King et al. (1995); (70) Schwarz et al. (1995); (71) Sembach et al. (1995a); (72) Lipman & Pettini (1995); (73) Ho & Filippenko (1995, 1996); (74) Bowen et al. (1995a); (75) Bowen & Blades (1993), Bowen et al. (1995b); (76) Savage et al. (1995); (77) Keenan et al. (1995); (78) Danly et al. (1995); (79) Wakker et al. (1996b); (80) Welsh et al. (1996); (81) Bomans et al. (1996); (82) Ryans et al. (1996); (83) Kuntz & Danly (1996); (84) Benjamin et al. (1996); (85) Caulet & Newell (1996); (86) Savage & Sembach (1996b); (87) Wakker et al. (1996a); (88) Shaw et al. (1996); (89) Lockman & Savage (1995); (90) Fitzpatrick & Spitzer (1997); (91) Sahu & Blades (1997); (92) Tamanaha (1997); (93) Ryans et al. (1997a); (94) Ryans et al. (1997b); (95) Stoppelenburg et al. (1998); (96) Wakker et al. (1998); (97) Tufte et al. (1998); (98) Tripp et al. (1998); (99) Jannuzi et al. (1998); (100) Lu et al. (1998); (101) Sahu (1998); (102) Kennedy et al. (1998); (103) Kemp & Bates (1998); (104) van Woerden et al. (1999a); (105) Richter et al. (1999); (106) Wakker et al. (1999b); (107) Lehner et al. (1999a); (108) Lehner et al. (1999b); (109) Welty et al. (1999); (110) Sembach et al. (1995b, 1999); (111) Meyer & Lauroesch (1999); (112) Akeson & Blitz (1999); (113) Ryans et al. (1999); (114) van Woerden et al. (1999b); (115) Combes & Charmandaris (2000); (116) Gringel et al. (2000); (117) Bowen et al. (2000); (118) Sembach et al. (2000); (119) Murphy et al. (2000); (120) Penton et al. (2000); (121) Savage et al. (1993, 2000a); (122) Gibson et al. (2000); (123) Richter et al. (2001a); (124) Bluhm et al. (2001); (125) Gibson et al. (2001); (126) Richter et al. (2001b); (127) Sembach et al. (2001); (128) Fabian et al. (2001); (129) Howk et al. (2001).

A17. COLUMN (20)—NOTES

τ.—With the measured FWHM of the H I profile, the column density or equivalent width implies $\tau > 10$.

W.—For the conversion of equivalent width to column density, the H I line width is assumed to be 30 km s^{-1}.

V.—H I line width is less than 17.9 km s^{-1}, implying $T < 7000$ K; $v_{\rm turb} = 0$ is assumed.

T.—Last two data columns give spin temperature and width of absorption feature; the N(ion) column gives N(H I) of the cold, absorbing gas, in units of 10^{18} cm^{-2} ; the abundance column is N(abs)/N(em).

s.—Approximate limit for N(Si II), assuming S/N = 10 in the line; also: N(C II) $< 10^{13}$ cm^{-2}.

S.—Based on *IUE* spectra in which Si II is the strongest uncontaminated line; spectra for HD 100600, HD 97991, and HD 121800 in Danly et al. (1992), others unpublished.

f.—Low-velocity resolution (220 km s^{-1}) FOS spectrum, HVC absorption implied by large equivalent width; H I spectrum in Lockman & Savage (1995).

1.—Also known as Mrk 116; the measurement has a very large error.

2.—Distance estimate of star has changed a lot. Brown et al. (1989) found it had type B1 V, and $z = 18$ kpc. Hambly et al. (1996) find $z = 4.6$ kpc.

3.—Error visually estimated from spectrum and quoted typical S/N.

4.—Parallax is 2.19 $\pm$ 0.92 mas, or $d = 0.45$ kpc; 1.2 kpc is 1.5 σ off; $d = 0.45$ kpc would imply type B6 IV or B5 V.

5.—Na limit not given, but estimated from S/N = 50.

6.—Is SAO 6225 in Lilienthal et al. (1990).

7.—Is SAO 6253 in Lilienthal et al. (1990).

8.—Is SAO 14733 in Songaila et al. (1988).

9.—Definitively shown to be stellar by Lilienthal et al. (1990).

10.—In NGC 3877, which has $v_{\rm LSR} = +910$ km s^{-1}.

11.—Kuntz & Danly (1996) give the distance to this star as 1.8 kpc.

12.—The *Hipparcos* parallax is 3.86 $\pm$ 1.17 mas, which gives $d = 250$ pc, with 1.6 kpc at 2.5 σ; Lehner et al. (1999a) argue for a spectroscopic distance of 1.2 kpc.

13.—Cloud 63 is $\sim 1°$ away, while cloud 51, at the southern edge of complex M, is $\sim 2°$ away; Ryans et al. (1997a) do not list this component in H I; it could be in the IV Arch.

14.—5 σ upper limits for N(H I) with 12′ beam, (Ryans et al. 1997a); with a 20′ beam N(H I) = 3.5 $\times$ 10^{18} cm^{-2} for BD +38°2182 and 4.1 $\times$ 10^{18} cm^{-2} for HD 93521 (Danly et al. 1993).

15.—Limits for N(Na I) and for N(Ca II) toward HD 93521 are implied but not actually given, the errors for BD +38°2182 are used as estimate.

16.—Limit to N(C II), N(O I), and N(Si II) from assuming S/N = 20 in the continuum.

17.—Complex C in region $\ell = 80°–90°$, $b = 37°–43°$, and $v_{\rm LSR} > -140$; distance limit assumes HB classifications are correct for the BS stars.
18.—Corrected for S^{+2} and H^+ (i.e., $[N(S^+) + N(S^{+2})]/[N(H^0) + N(H^+)]$), the S abundance is 0.089 solar.
19.—The N I spectrum is noisy and was fitted by a single component; half of this was assigned to each H I component.
20.—Total O VI column density split evenly between the two H I components.
21.—Limit to N(CO) from nondetection of absorption (3 σ significance), assuming excitation temperature of 10 K.
22.—Danly et al. (1992) classify HD 146813 as B1.5 at $d = 2.4$ kpc, Diplas & Savage (1994) give 2.6 kpc, I would find 3.3 kpc; the SIMBAD type B8 V is consistent with the *Hipparcos* parallax of 2.41 ± 0.78 mas, implying $d = 0.4$ kpc.
23.—A nonexistent Na I detection at -133 km s^{-1} was also claimed.
24.—Disputed, very high probability that the line is stellar; moreover, there is no H I at -136 km s^{-1}, the velocity of the claimed absorption.
25.—Complex C at $\ell > 109°$ and $b > 49°$.
26.—Detection not mentioned in paper (Burks et al. 1994), but equivalent widths are 280 km s^{-1} for C II and 160 km s^{-1} for Si II.
27.—H I also has component at -118 km s^{-1} ($2.7 \pm 0.3 \times 10^{18}$ cm^{-2}).
28.—Is HD 100971.
29.—Is Feige 87 in Schwarz et al. (1995).
30.—Complex C at $\ell > 101°$, $b < 48°$, and $\ell = 80° –100°$, $b < 43°$, plus $v_{\rm LSR} < -140$ in region of overlap with C I.
31.—This is a very doubtful S II component; H I has two components of 19.1 and 11.6×10^{18} cm^{-2} at -137 and -102 km s^{-1}.
32.—Revised equivalent widths from Bowen et al. 1995b.
33.—Source name is 0959+68W1 in FOS Key Project; H I has tail to -175 km s^{-1}.
34.—Complex C at $\ell < 80°$.
35.—Is "1749+096" in Akeson & Blitz (1999).
36.—4 Lac sets a distance limit on complex G, although this is not commented upon by Bates et al. (1991).
37.—Components with $T_B > 0.5$ K in the region $\ell = 123°–133°$, $b = -3°$ to $+5°$.
38.—Continuum source in Westerbork map of core of complex H.
39.—Centurión et al. (1994) give a distance of 1.1 kpc for HD 10125 and 4.1 kpc for HD 13256.
40.—Is Hiltner 198 in Centurión et al. (1994).
41.—Is Hiltner 190 in Centurión et al. (1994).
42.—Components in the region $\ell = 110°$ to 120°.
43.—Components within a few degrees of the core at $\ell = 132°$, $b = -5°$.
44.—The spectral type would suggest a distance of 3.4 kpc, if the extinction is assumed to be 1.6 mag, it may be 5 mag.
45.—Complex H components outside the three cores.
46.—Is "0224+671" in Akeson & Blitz (1999).
47.—Is "0300+470" in Akeson & Blitz (1999).
48.—The spectral type would suggest a distance of 2.1 kpc, if the extinction is indeed 2.4 mag, it may be 5 mag.
49.—This star was erroneously called BD $+61°2619$ by Centurión et al.
50.—In the H I emission profile only a single, broad component at ~ -60 km s^{-1} can be discerned, listed on the first line. The -73 and -58 km s^{-1} components are only clearly seen in absorption; the listed H I column densities are those of the absorption.
51.—Kulkarni & Mathieu (1986) classify this as an O star at 2.5 kpc. According to SIMBAD it is a B star. According to Garmany et al. (1987) it is O5 V at 8.0 kpc.
52.—Error assumed from quoted S/N of 100, width 15 km s^{-1} and grid 6 km s^{-1}.
53.—Is SAO 76016 in Songaila et al. (1988).
54.—Is SAO 76994 in Songaila et al. (1988).
55.—Is SAO 76980 in Songaila et al. (1988).
56.—Is SAO 76954 in Songaila et al. (1988).
57.—Estimated S/N = 20 for the *IUE* spectra.
58.—A general 5 mÅ detection limit is given.
59.—Is "0239+108" in Akeson & Blitz (1999).
60.—Cloud 363 is the "Giovanelli Stream," is "0428+20" in Akeson & Blitz (1999).
61.—Cloud 525 ($v = -231$) is 1 degree away in the Dwingeloo survey.
62.—Cloud 419 in pop. GCN $\sim 1°$ away.
63.—N(H,total) based on photoionization models; N(H I) $< 0.6 \times 10^{18}$ cm^{-2} from Green Bank data.
64.—Total O VI column density split in ratio 1:2 between the two components.
65.—About 10° away from nearest GCN cloud; an unclassified H I HVC at -133 km s^{-1} is detected 15′ away.
66.—Is "1829+29" in Akeson & Blitz (1999).
67.—Is "1901+319" in Akeson & Blitz (1999).
68.—Is "1828+487" in Akeson & Blitz (1999).
69.—Is "2037+511" in Akeson & Blitz (1999).
70.—A deeper STIS spectrum suggests that the CIV component at -213 km s^{-1} may not be real.
71.—Lockman & Savage (1995) give a 72 km s^{-1} wide component from -150 to -78 km s^{-1}; this was split in two.
72.—Is "1928+738" in Akeson & Blitz (1999); H I has tail to -161 km s^{-1}.

73.—H I has tail to -128 km s^{-1}.
74.—Is "0538+498" in Akeson & Blitz (1999).
75.—Average of values toward 5 probes with N(H I) > 2.5×10^{18} cm^{-2}.
76.—Low-velocity resolution (220 km s^{-1}) FOS spectrum, but HVC component is separately seen; the actual EW values and velocities are from Jannuzi et al. (1998).
77.—Is PG 0007+106.
78.—N(H I) from single-component fit, although there are two H I components: at $+194$ km s^{-1}, N(H I) = $75.3 \pm 0.8 \times 10^{18}$, width 45.0 km s^{-1}, and $+140$ km s^{-1}, N(H I) = 13.7 ± 0.6 km s^{-1}, width 27.7 km s^{-1} ; in absorption usually only one component can be discerned.
79.—The Na I and Ca II absorptions toward Fairall 9 found by Songaila & York (1981) were published again by Songaila (1981).
80.—Lu et al. (1994a) give EW(Si II λ1260) = 368 mÅ, but this is for absorption from $+160$ to $+300$ km s^{-1} and is larger than possible for the observed H I line width of 37 km s^{-1}. Possibly there is an extra component at $v \sim +200$ km s^{-1}. The EW listed here is the maximum possible given the observed W(H I).
81.—Lu et al. (1994a) use a linear conversion from equivalent width.
82.—Parallax measured as 1.84 ± 1.22 mas; distance given as 6.2 kpc by Danly et al. (1992), as 6.6 kpc by Diplas & Savage (1994).
83.—Cloud WW84 is very centrally condensated, and a 10′ Effelsberg beam centered on Mrk 205 picks up some of the very bright emission from the cloud center. WSRT observations have not yet been properly combined with single-dish data. The tabulated value is the current best guess.
84.—Parallax measured as 5.52 ± 1.13 mas, revising distance down from 0.8 kpc in Danly et al. (1995), or 2.5 kpc in Albert et al. (1993); N(H I) from Stoppelenburg et al. (1998).
85.—Probably circumstellar (Danly et al. 1995). Albert et al. (1993) do not actually claim this as a detection.
86.—Is 3C 206.
87.—Nearest HVC (WW364, $v = +120$) is 6° away, but the region was only sampled on a $2° \times 2°$ grid.
88.—In NGC 4527, which has $v_{LSR} = +1733$ km s^{-1}.
89.—HVC 100-7+100; N(H I) from Stoppelenburg et al. (1998); parallax is 1.54 ± 0.52 mas, giving $d < 1.0$ kpc (1 σ).
90.—In NGC 5194, which has $v_{LSR} = +463$ km s^{-1} ; paper assumes a ratio N(Na I)/N(H I), but the implied N(H I) then is much larger than limit from the Dwingeloo profile.
91.—In M81, which has $v_{LSR} = -130$ km s^{-1}, -40 km s^{-1} at position of SN 1993J.
92.—In NGC 4526, which has $v_{LSR} = +625$ km s^{-1}, 880 km s^{-1} at position of SN 1994D; faint H I found at Arecibo; the erratum corrects the misconception that this originates inside NGC 4526.
93.—In NGC 5128, which has $v_{LSR} \sim +400$ km s^{-1} ; HVCs 219 and 208 are 1° and 3° away.
94.—In M83, which has v_{LSR} = 320–620 km s^{-1}.
95.—Average of values toward SN 1987A and Sk $-69°243$. These are consistent with the values for other probes, for which N(H I) is uncertain and low.
96.—*IUE* spectra without measurements are presented by de Boer et al. (1987) and Dupree et al. (1987).
97.—Ca II profile was published, but not the measurements; estimated equivalent widths.
98.—N(H I) from McGee & Newton (1986).
99.—Average of the values found toward Sk $-67°104$, Sk $-67°166$, and Sk $-68°82$.
100.—Average of the values found toward SN 1987A, Sk $-67°104$, Sk $-67°166$, and Sk $-68°82$.
101.—Average of the values found toward Sk $-67°104$, Sk $-67°166$, and Sk $-68°82$.
102.—Average of the best determinations, toward SN 1987A, Sk $-69°243$, Sk $-69°246$, Sk $-69°247$, Sk $-71°41$, Sk $-71°42$, and Sk $-71°45$.
103.—Average of the values found toward SN 1987A, Sk $-67°104$, Sk $-67°166$, Sk $-68°82$, and Sk $-69°246$.
104.—Absorption occurs at all velocities between 0 and $+300$ km s^{-1} ; results given for velocity range 120–190 km s^{-1} ; for Al III the 1854 line gives log $N = 11.64$, the 1862 line has log $N = 12.08$.
105.—HDE 268605.
106.—N(H I) from McGee & Newton (1986), position JM43; also has component at $+182$ (5.9×10^{18}).
107.—Value toward SN 1987A, which is the only reliable one; equivalent widths toward Sk $-67°05$, Sk $-68°82$, and Sk $-71°3$ are only rough values; Molaro et al. (1993) find an upper limit of 5.2 ppb toward Sk $-69°246$.
108.—Average of the values toward Sk $-67°05$ and Sk $-67°104$; Blades et al. (1988) imply 2.6 solar toward SN 1987A, but that column density is very uncertain and was not measured by Welty et al. (1999).
109.—The three measurements are very discrepant: 0.08 solar toward Sk $-69°246$ (Savage & de Boer 1981), 0.85 solar toward Sk $-67°104$ (Savage & Jeske 1981), and 2.1 solar toward SN 1987A (Welty et al. 1999).
110.—Average of values toward SN 1987A, R 139, R 140, Sk $-69°243$, Sk $-69°246$, Sk $-69°248$, Sk $-69°255$, Sk $-71°41$, Sk $-71°42$, and Sk $-71°45$. For other measurements N(H I) is based on interpolation or reading off plots.
111.—Value toward SN 1987A; toward Sk $-69°246$ Savage & de Boer (1981) found 0.2 solar, but this is uncertain; the values toward Sk $-67°05$ and Sk $-67°104$ are for the combined $+65$ and $+120$ km s^{-1} components.
112.—In absorption components are seen at -64, -45, and -30 km s^{-1}, but in the H I spectrum these are blended. The fit was forced to have components at -65 and -45 km s^{-1}.
113.—At the edge of IV6, which is not separately visible in the H I emission spectrum.
114.—Mg II column densities determined from the 1239/1240 lines are corrected downward by 0.67 dex, see Savage & Sembach (1996a).

115.—In the paper, the fits to these components are shown, but no numbers are given—they were provided by Bowen.

116.—Mixture of IV17 and IV26; IVC absorption not listed in Schwarz et al. (1995).

117.—Ca absorption does not resolve IV9 ($v = -73$, $T_B = 0.56$ K) and IV19 ($v = -48$, $T_B = 2.36$ K); column densities are combined values.

118.—In the GHRS absorption spectrum IV9 and IV19 are hard to separate, the combined S II column density was proportionally divided between the two H I components.

119.—Spectrum analyzed by Conlon et al. (1988); coordinates differ from those quoted by Kuntz & Danly (1996), who also confuse z and d.

120.—Is HZ 22 in Ryans et al. (1997a).

121.—The discrepancy between the "normal" value for the Ca II of IV15 abundance measured toward Mrk 290 and the unusually high (by a factor 10) value toward BT Dra suggests that the -83 km s^{-1} absorption toward BT Dra may be stellar (its b-value is also unusually low).

122.—Is HZ 25 in ref.

123.—Ryans et al. (1997a) call this star AG $+53°783$ and give $\ell = 154\overset{\circ}{.}4$, $b = 56\overset{\circ}{.}6$; is this the same star? Possibly it is a B9 V star at 1.1 kpc; the identification of AG $+53°783$ with HDE 233791 is based on SIMBAD.

124.—O I λ1304, C II λ1334, Si II are seen in the line wing.

125.—Is HIP55461.

126.—In reference as H.O. +23B, to which SIMBAD has 11 references with coordinates differing by up to 5″; z determined by Quin et al. (1991).

127.—N(H I) fitted to a spectrum in which M81 was taken out by means of a third order polynomial fit; the uncertainty reflects the uncertainty in the zero level at $v = -50$ km s^{-1}

128.—Assuming S/N = 30.

129.—BD names given in paper: HDE 237844 = BD $+56°1411$, HDE 233622 = BD $+50°1631$.

130.—Combined component groups 1–2, 3–5, and 6–9 to form -92, -56, and -43 km s^{-1} components.

131.—For the -56 and -43 km s^{-1} components, the (logarithmic) ionization fraction has been determined to be -3.6 to -1.3 and -3.6 to -1.9, respectively.

132.—Penton et al. (2000) fit a component at $+60$ km s^{-1} to the S II $\lambda\lambda$1250, 1253, and 1259 lines, with EWs of 58, 85, and 30 mÅ; S II λ1259 is blended with Si II λ1260. The weaker lines are shown by Sembach et al. (1999), and this shows that they are half as strong. The listed column density is based on the lower EWs.

133.—Originally found by York et al. (1982), analyzed by Blades & Morton (1983), and improved by Morton & Blades (1986).

134.—N(H I) determined by interpolating between the values on a 3×3 grid with 9′ spacing.

135.—M15 NW/SE core refer to the positions with the highest and lowest Na I abundance measured using a 7×13 ($27'' \times 43''$) array of 3″ fibers.

136.—In NGC 1316, which has $v_{\rm LSR} = +1521$ km s^{-1}.

137.—de Boer & Savage (1984) claimed to have found this C II absorption line; however, recent *FUSE* data (J. C. Howk 2000, private communication) do not show the absorption in the C II λ1036 and other strong lines.

REFERENCES

Akeson, R. L., & Blitz, L. 1999, ApJ, 523, 163
Albert, C. E. 1983, ApJ, 272, 509
Albert, C. E., Blades, J. C., Morton, D. C., Lockman, F. J., Proulx, M., & Ferrarese, L. 1993, ApJS, 88, 81
Anders, E., & Grevesse, N. 1989, Geochim. Cosmochim. Acta, 53, 197
Andreani, P., Ferlet, R., & Vidal-Madjar, A. 1987, Nature, 326, 770
Bajaja, E., Cappa de Nicolau, C. E., Cersosimo, J. C., Martin, M. C., Loiseau, N., Morras, R., Olano, C. A., & Pöppel, W. G. L. 1985, ApJS, 58, 143
Bajaja, E., Cappa de Nicolau, C. E., Martin, M. C., Morras, R., & Olano, C. A. 1989, A&AS, 78, 345
Bates, B., Catney, M. G., Gilheany, S., Keenan, F. P., Davies, R. D., & Hummel, E. 1991, MNRAS, 249, 282
Bates, B., Catney, M. G., & Keenan, F. P. 1990, MNRAS, 242, 267
Benjamin, R. A., Venn, K. A., Hiltgen, D. D., & Sneden, C. 1996, ApJ, 464, 836
Blades, J. C. 1980, MNRAS, 190, 33
Blades, J. C., Elliot, K. H., & Meaburn, J. C. 1982, MNRAS, 192, 101
Blades, J. C., & Meaburn, J. 1980, MNRAS, 190, 59P
Blades, J. C., & Morton, D. C. 1983, MNRAS, 204, 317
Blades, J. C., Wheatley, J. M., Panagia, N., Grewing, M., Pettini, M., & Wamsteker, W. 1988, ApJ, 332, L75
Bland-Hawthorn, J., & Maloney, P. R. 1999, ApJ, 510, L33
Bland-Hawthorn, J., Veilleux, S., Cecil, G. N., Putman, M. E., Gibson, B. K., & Maloney, P. R. 1998, MNRAS, 299, 611
Blitz, L., Spergel, D., Teuben, P., Hartmann, D., & Burton, W. B. 1999, ApJ, 514, 818
Bluhm, H., de Boer, K. S., Marggraf, O., & Richter, P. 2001, A&A, 367, 299
Bomans, D. J., de Boer, K. S., Koornneef, J., & Grebel, E. K. 1996, A&A, 313, 101
Bowen, D. V., & Blades, J. C. 1993, ApJ, 403, L55
Bowen, D. V., Blades, J. C., & Pettini, M. 1995a, ApJ, 448, 634
———. 1995b, ApJ, 448, 662
Bowen, D. V., Pettini, M., Penston, M. V., & Blades, J. C. 1991a, MNRAS, 248, 153
———. C. 1991b, MNRAS, 249, 145
Bowen, D. V., Roth, K. C., Blades, J. C., & Meyer, D. M. 1994, ApJ, 420, L71
Bowen, D. V., Roth, K. C., Meyer, D. M., & Blades, J. C. 2000, ApJ, 536, 225
Braun, R., & Burton, W. B. 1999, A&A, 351, 437
———. 2000, A&A, 354, 853
Bregman, J. N. 1980, ApJ, 237, 280
Brown, P. J. F., Dufton, P. L., Keenan, F. P., Boksenberg, A., King, D. L., & Pettini, M. 1989, ApJ, 339, 397
Bruhweiler, F. C., Boggess, A., Norman, D. J., Grady, C. A., Urry, C. M., & Kondo, Y. 1993, ApJ, 409, 199
Brüns, C., Kerp, J., & Staveley-Smith, L. 2001, in ASP Conf. Ser., Mapping the Hidden Universe, ed. (San Francisco: ASP), in press
Burks, G. S., et al. 1994, ApJ, 437, 630
Caulet, A., & Newell, R. 1996, ApJ, 465, 205
Centurión, M., Vladilo, G., de Boer, K. S., Herbstmeier, U., & Schwarz, U. J. 1994, A&A, 292, 261
Cohen, J. G. 1979, ApJ, 231, 751
Colgan, S. W. J., Salpeter, E. E., & Terzian, Y. 1990, ApJ, 351, 503
Combes, F., & Charmandaris, V. 2000, A&A, 357, 75
Conlon, E. S., Brown, P. J. F., Dufton, P. L., & Keenan, F. P. 1988, A&A, 200, 168
Crinklaw, G., Federman, S. R., & Joseph, C. L. 1994, ApJ, 440, 241
d'Odorico, S., di Serego Alighieri, S., Pettini, M., Magain, P., Nissen, P. E., & Panagia, N. 1989, A&A, 215, 21
d'Odorico, S., Pettini, M., & Ponz, D. 1985, ApJ, 299, 852
Danly, L., Albert, C. E., & Kuntz, K. D. 1993, ApJ, 416, L29
Danly, L., Lee, Y. P., & Albert, C. E. 1995, BAAS, 27, 860
Danly, L., Lockman, F. J., Meade, M. R., & Savage, B. D. 1992, ApJS, 81, 125

de Boer, K. S., Altan, A., Bomans, D., Lilienthal, D., Moehler, S., van Woerden, H., Wakker, B., & Bregman, J. 1994, A&A, 286, 925
de Boer, K. S., Grewing, M., Richtler, T., Wamsteker, W., Gry, C., & Panagia, N. 1987, A&A, 177, L37
de Boer, K. S., Rodriguez Pascual, P., Wamsteker, W., Sonneborn, G., Fransson, C., Bomans, D. J., & Kirshner, R. P. 1993, A&A, 280, L15
de Boer, K. S., & Savage, B. D. 1983, ApJ, 265, 210
———. 1984, A&A, 136, L7
Diplas, A., & Savage, B. D. 1994, ApJS, 93, 211
Dupree, A. K., Kirshner, R. P., Nassiopoulos, G. E., Raymond, J. C., & Sonneborn, G. 1987, ApJ, 320, 597
Fabian, D., Tripp, T. M., Savage, B. D., & Wakker, B. P. 2001, ApJ, submitted
Ferlet, R., Dennefeld, M., & Maurice, E. 1985a, A&A, 152, 151
Ferlet, R., Vidal-Madjar, A., & Gry, C. 1985b, ApJ, 298, 838
Fernley, I., et al. 1998, A&A, 330, 515
Fitzpatrick, E. L., & Spitzer, L. 1997, ApJ, 475, 623
Gardiner, L. T., & Noguchi, M. 1996, MNRAS, 278, 191
Garmany, C. D., Conti, P. S., & Massey, P. 1987, AJ, 93, 1070
Gibson, B. K., Giroux, M. L., Penton, S. V., Putman, M. E., Stocke, J. T., & Shull, M. J. 2000, AJ, 120, 1830
Gibson, B. K., Penton, S. V., Giroux, M. L., Stocke, J. T., Shull, M. J., & Putman, M. E. 2001, ApJ, submitted
Giovanelli, R., Verschuur, G. L., & Cram, T. R. 1973, A&AS, 12, 209
Grevesse, N., & Noels, A. 1993, in Origin of the Elements, ed. N. Prantzos, E. Vangioni-Flam, & M. Cassé (Cambridge: Cambridge Univ. Press), 15
Gringel, W., Barnstedt, J., de Boer, K. S., Grewing, M., Kappelmann, N., & Richter, P. 2000, A&A, 358, L37
Habing, H. J. 1966, Bull. Astron. Inst. Netherlands, 18, 323
Haffner, L. M., Reynolds, R. J., & Tufte, S. L. 1999, ApJ, 523, 223
———. 2001, ApJ, in press
Hambly, N. C., Keenan, F. P., Dufton, P. L., Brown, P. J. F., Saffer, R. A., & Peterson, R. C. 1996, ApJ, 466, 1018
Harris, W. E. 1996, AJ, 112, 1487
Hartmann, D., & Burton, W. B. 1997, Atlas of Galactic Neutral Hydrogen (Cambridge: Cambridge Univ. Press)
Haud, U. 1992, MNRAS, 257, 707
Haynes, R., et al. 1999, IAU Symp. 190, New Views of the Magellanic Clouds, ed. Y.-H. Chu, N. Suntzeff, J. Hesser, & D. Bohlender (Dordrecht: Kluwer), 108
Heiles, C. 1984, ApJS, 55, 585
Ho L. C., & Filippenko, A. V. 1995, ApJ, 444, 165
———. 1996, ApJ, 463, 818
Howk, J. C., Savage, B. D., & Fabian, D. 1999, ApJ, 525, 253
Howk, J. C., Sembach, K. R., Roth, K. C., & Kruk, J. W. 2000, ApJ, 544, 867
Hulsbosch, A. N. M., & Wakker, B. P. 1988, A&AS, 75, 191
Jannuzi, B. T., et al. 1998, ApJS, 118, 1
Jenkins, E. B., Savage, B. D., & Spitzer, L. 1986, ApJ, 301, 355 1986
Kaper, H. G., Smits, D. W., Schwarz, U. J., & Takakubo, K., & van Woerden, H. 1966, Bull. Astron. Inst. Netherlands, 18, 465
Keenan, F. P., Conlon, E. S., Brown, P. J. F., & Dufton, P. L. 1988, A&A, 192, 295
Keenan, F. P., Shaw, C. R., Bates, B., Dufton, P. L., & Kemp, S. N. 1995, MNRAS, 272, 599
Kemp, S. N., & Bates, B. 1998, MNRAS, 301, 1095
Kemp, S. N., Bates, B., Dufton, P. L., Keenan, F. P., & Montgomery, A. S. 1994, MNRAS, 270, 597
Kennedy, D. C., Bates, B., Keenan, F. P., Kemp, S. N., Ryans, R. S. I., Davies, R. D., & Sembach, K. R. 1998, MNRAS, 297, 849
Kepner, M. E. 1970, A&A, 5, 444
Kerr, F. J., & Knapp, G. R. 1972, AJ, 77, 354
King, D. L., Vladilo, G., Lipman, K., de Boer, K. S., Centurión M., Moritz, P., & Walton, N. A. 1995, A&A, 300, 881
Kulkarni, S. R., Dickey, J. M., & Heiles, C. 1985, ApJ, 291, 716
Kulkarni, S. R., & Mathieu, R. 1986, Ap&SS, 118, 531
Kunth, D., Lequeux, J., Sargent, W. L. W., & Viallefond, F. 1994, A&A, 282, 709
Kuntz, K. D., & Danly, L. 1996, ApJ, 457, 703
Langer, G. E., Prosser, C. F., & Sneden, C. 1990, AJ, 100, 216
Lehner, N., Rolleston, W. R. J., Ryans, R. S. I., Keenan, F. P., Bates, B., Pollacco, D. L., & Sembach, K. R. 1999b, A&AS, 134, 257
Lehner, N., Sembach, K. R., Lambert, D. L., Ryans, R. S. I., & Keenan, F. P. 1999a, A&A, 352, 257
Lehner, N., Trundle, C., Keenan, F. P., Sembach, K. R., & Lambert, D. L. 2001, A&A, 370, 996
Lilienthal, D., Meyerdierks, H., & de Boer, K. S. 1990, A&A, 240, 487
Lipman, K., & Pettini, M. 1995, ApJ, 442, 628
Little, J. E., Dufton, P. L., Keenan, F. P., & Conlon, E. S. 1994, ApJ, 427, 267
Lockman, F. J., & Savage, B. D. 1995, ApJS, 97, 1
Lu, L., Savage, B. D., & Sembach, K. R. 1994a, ApJ, 426, 563
———. 1994b, ApJ, 437, L119
Lu, L., Savage, B. D., Sembach, K. R., Wakker, B. P., Sargent, W. L. W., & Oosterloo, T. A. 1998, AJ, 115, 162
Lucas, R., & Liszt, H. S. 1996, A&A, 282, 237
Lucke, P. B. 1978, A&A, 64, 367
Magain, P. 1987, Nature, 329, 606
McGee, R. X., & Newton, L. M. 1986, Proc. Astron. Soc. Australia, 6, 358
Meaburn, J., & Blades, J. C. 1980, MNRAS, 190, 403
Meaburn, J., Solomos, N., Laspias, V., & Goudis, C. 1989, A&A, 225, 497
Mebold, U., Greisen, E. W., Wilson, W., Haynes, R. F., Herbstmeier, U., & Kalberla, P. M. W. 1991, A&A, 251, L1
Meyer, D. M., Jura, M., & Cardelli, J. A. 1998, ApJ, 493, 222
Meyer, D. M., & Lauroesch, J. T. 1999, ApJ, 520, L103
Meyer, D. M., & Roth, K. C. 1991, ApJ, 383, L41
Mirabel, I. F. 1982, ApJ, 256, 112
Moehler, S., Heber, U., & de Boer, K. S. 1990, A&A, 239, 265
Molaro, P., Vladilo, G., Avila, G., & d'Odorico, S. 1989, ApJ, 339, L63
Molaro, P., Vladilo, G., Monai, S., d'Odorico, S., Ferlet, R., Vidal-Madjar, A., & Dennefeld, M. 1993, A&A, 274, 505
Morras, R., Bajaja, E., Arnal, E. M., & Pöppel, W. G. L. 2000, A&AS, 142, 25
Morton, D. C. 1991, ApJS, 77, 119
Morton, D. C., & Blades, J. C. 1986, MNRAS, 220, 927
Morton, D. C. 2001, ApJS, 130, 403
Muller, C. A., Oort, J. H., & Raimond, E. 1963, CR Acad. Sci. Paris, 257, 1661
Murphy, E. M., et al. 2000, ApJ, 538, L35
Oegerle, W. R., et al. 2000, ApJ, 538, L23
Oort, J. H. 1970, A&A, 7, 381
Osterbrock, D. P. 1989, Astrophysics of Gaseous Nebulae and Active Galactic Nuclei (Mill Valley: University Science Books)
Payne, H. E., Dickey, J. M., Salpeter, E. E., & Terzian, Y. 1978, ApJ, 221, L95
Payne, H. E., Salpeter, E. E., & Terzian, Y. 1980, ApJ, 240, 499
Penton, S. V., Stocke, J. T., & Shull, J. M. 2000, ApJS, 130, 121
Prata, S., & Wallerstein, G. 1967, PASP, 79, 202
Preston, G. W., Shectman, S. A., & Beers, T. C. 1991, ApJS, 76, 1001
Putman, M. E., et al. 1998, Nature, 394, 752
Quin, D. A., Brown, P. J. F., Conlon, E. S., Dufton, P. L., & Keenan, F. P. 1991, ApJ, 375, 342
Reynolds, R. J., Tufte, S. L., Haffner, L. M., Jaehnig, K., & Percival, J. W. 1998, Proc. Astron. Soc. Australia, 15, 14
Reynolds, R. J., Tufte, S. L., Kung, D. T., McCullough, P. R., & Heiles, C. 1995, ApJ, 448, 715
Richter, P., de Boer, K. S., Widmann, H., Kappelmann, N., Gringel, W., Grewing, M., & Barnstedt, J. 1999, Nature, 400, 382
Richter, P., Savage, B. D., Wakker, B. P., & Kalberla, P. M. W. 2001a, ApJ, in press
Richter, P., Sembach, K. R., Savage, B. D., Murphy, E. M., & Wakker, B. P. 2001b, ApJ, submitted
Robertson, J. G., Schwarz, U. J., van Woerden, H., Murray, J. D., Morton, D. C., & Hulsbosch, A. N. M. 1991, MNRAS, 248, 508
Routly, P. M., & Spitzer, L. 1952, ApJ, 115, 227
Russel, S. C., & Dopita, M. A. 1992, ApJ, 384, 508
Ryans, R. S. I., Keenan, F. P., Rolleston, W. R. J., Sembach, K. R., & Davies, R. D. 1999, MNRAS, 304, 947
Ryans, R. S. I., Keenan, F. P., Sembach, K. R., & Davies, R. D. 1997a, MNRAS, 289, 83
———. 1997b, MNRAS, 289, 986
Ryans, R. S. I., Sembach, K. R., & Keenan, F. P. 1996, A&A, 314, 609
Sahu, M. S. 1998, AJ, 116, 1205
Sahu, M. S., & Blades, J. C. 1997, ApJ, 484, L125
Savage, B. D., & de Boer, K. S. 1979, ApJ, 230, L77
———. 1981, ApJ, 243, 460
Savage, B. D., Jenkins, E. B., & Joseph, C. L., & de Boer, K. S. 1989, ApJ, 345, 393
Savage, B. D., & Jeske, N. A. 1981, ApJ, 244, 768
Savage, B. D., et al. 1993, ApJ, 413, 116
Savage, B. D., & Sembach, K. R. 1996a, ARA&A, 34, 279
———. 1996b, ApJ, 470, 893
Savage, B. D., et al. 2000a, ApJS, 129, 563
Savage, B. D., et al. 2000b, ApJ, 538, L27
Savage, B. D., Sembach, K. R., & Lu L. 1995, ApJ, 449, 145
Schwarz, U. J., Wakker, B. P., & van Woerden, H. 1995, A&A, 302, 364
Sembach, K. R., & Danks, A. C. 1994, A&A, 289, 539
Sembach, K. R., Danks, A. C., & Savage, B. D. 1993, A&AS, 100, 107
Sembach, K. R., Howk, J. C., Savage, B. D., & Shull, J. M. 2001, AJ, 121, 992
Sembach, K. R., & Savage, B. D. 1992, ApJS, 83, 147
———. 1996, ApJ, 457, 211
Sembach, K. R., Savage, B. D., & Lu, L. 1995a, ApJ, 439, 672
Sembach, K. R., Savage, B. D., Lu, L., & Murphy, E. M. 1995b, ApJ, 415, 616
———. 1999, ApJ, 515, 108
Sembach, K. R., Savage, B. D., & Massa, D. 1991, ApJ, 372, 81
Sembach, K. R., et al. 2000, ApJ, 538, L31
Shaw, C. R., Bates, B., Kemp, S. N., Keenan, F. P., Davies, R. D., & Roger, R. S. 1996, ApJ, 473, 849
Smith, G. P. 1963, Bull. Astron. Inst. Netherlands, 17, 203
Sofia, U. J., & Jenkins, E. B. 1998, ApJ, 499, 951
Songaila, A. 1981, ApJ, 243, L19
Songaila, A., Blades, J. C., Hu E. M., & Cowie, L. L. 1986, ApJ, 303, 198
Songaila, A., Cowie, L. L., & Weaver, H. F. 1988, ApJ, 329, 580

Songaila, A., Cowie, L. L., & York, D. G. 1981, ApJ, 248, 956
Songaila, A., & York, D. G. 1981, ApJ, 242, 976
Songaila, A., York, D. G., Cowie, L. L., & Blades, J. C. 1985, ApJ, 293, L15
Spitzer, L., & Fitzpatrick, E. L. 1992, ApJ, 391, L41
———. 1993, ApJ, 409, 299
Stark, A. A., Gammse, C. F., Wilson, R. W., Bally, J., Linke, R. A., Heiles, C., & Hurwitz, M. 1992, ApJS, 79, 77
Staveley-Smith, L. 1997, Proc. Astron. Soc. Australia, 14, 111
Stoppelenburg, P. S., Schwarz, U. J., & van Woerden, H. 1998, A&A, 338, 200
Straizys, V., & Kurilene, G. 1981, Ap&SS, 80, 353
Tamanaha, C. M. 1995, ApJ, 450, 638
———. 1996, ApJS, 104, 81
———. 1997, ApJS, 109, 139
Theissen, A., Moehler, S., Heber, U., Schmidt, J. H. K., & de Boer, K. S. 1995, A&A, 298, 577
Tripp, T. M., Lu, L., & Savage, B. D. 1998, ApJ, 508, 200
Tufte, S. L., Reynolds, R. J., & Haffner, L. M. 1998, ApJ, 504, 773
Vallerga, J. V., Vedder, P. W., Craig, N., & Welsh, B. Y. 1993, ApJ, 411, 729
van Woerden, H. 1993, in ASP Conf. Ser. 45, Luminous High-Latitude Stars, ed. D. Sasselov (San Francisco: ASP), 11
van Woerden, H., Peletier, R. F., Schwarz, U. J., Wakker, B. P., & Kalberla, P. M. W. 1999b, in ASP Conf. Ser. 166, Stromlo Workshop on High-Velocity Clouds, ed. B. K. Gibson & M. E. Putman (San Francisco: ASP), 1
van Woerden, H., Schwarz, U. J., Peletier, R. F., Wakker, B. P., & Kalberla, P. M. W. 1999a, Nature, 400, 138
Verner, D. A., Barthel, P. D., & Tytler, D. 1994, A&A, 108, 287
Véron-Cetty, M. P., & Véron, P. 1996, ESO Sci. Rep. 17, A Catalogue of Quasars and Active Nuclei (7th ed.; Garching: ESO)
Vidal-Madjar, A., Andreani, P., Christiani, S., Ferlet, R., Lanz, T., & Vladilo, G. 1987, A&A, 177, L17
Vladilo, G., Centurión M., de Boer, K. S., King, D. L., Lipman, K., Stegert, J. S. W., Unger, S. W., & Walton, N. A. 1993, A&A, 280, L11
———. 1994, A&A, 291, 425
Wakker, B. P. 1991, A&A, 250, 499
Wakker, B. P., Howk, C., van Woerden, H., Schwarz, U. J., Beers, T. C., Wilhelm, R., Kalberla, P. M. W., & Danly, L. 1996a, ApJ, 473, 834
Wakker, B. P., Kalberla, P. M. W., van Woerden, H., de Boer, K. S. 2001a, ApJS, in press (Paper II)
Wakker, B. P., & Mathis, J. S. 2000, ApJ, 544, L107
Wakker, B. P., Oosterloo, T. A., Putman, M. E. 2001b, AJ, submitted
Wakker, B. P., & Schwarz, U. J. 1991, A&A, 250, 484
Wakker, B. P., & van Woerden, H. 1991, A&A, 250, 509
———. 1997, ARA&A, 5, 217
Wakker, B. P., van Woerden, H., de Boer, K. S., & Kalberla, P. M. W. 1998, ApJ, 493, 762
Wakker, B. P., et al. 1999a, Nature, 400, 388
Wakker, B. P., van Woerden, H., & Gibson, B. K. 1999b, in ASP Conf. Ser. 166, Stromlo Workshop on High-Velocity Clouds, ed. B. K. Gibson & M. E. Putman (San Francisco: ASP), 311
Wakker, B. P., van Woerden, H., Schwarz, U. J., Peletier, R. F., & Douglas, N. G. 1996b, A&A, 306, L25
Wakker, B. P., Vijfschaft, B., & Schwarz, U. J. 1991, A&A, 249, 233
Wayte, S. R. 1990, ApJ, 355, 473
Weiner, B. J., Vogel, S. N., Williams, T. B. 2001, in ASP Conf. Ser., Gas and Galaxy Evolution, ed. J. E. Hibbard, M. P. Rupen, & J. H. van Gorkom (San Francisco: ASP), in press
Weiss, A., Heithausen, A., Herbstmeier, U., & Mebold, U. 1999, A&A, 344, 955
Welsh, B. Y., Craig, N., & Roberts, B. 1996, A&A, 308, 428
Welty, D. E., Frisch, P. C., Sonneborn, G., & York, D. G. 1999, ApJ, 512, 636
Welty, D. E., Hobbs, L. M., & Kulkarni, V. P. 1994, ApJ, 436, 152
Wesselius, P. R., & Fejes, I. 1973, A&A, 24, 15
West, K. A., Pettini, M., Penston, M. V., Blades, J. C., & Morton, D. C. 1985, MNRAS, 215, 481
York, D. G., Songaila, A., Blades, J. C., Cowie, L. L., Morton, D. C., & Wu, C. C. 1982, ApJ, 255, 467